The Paleobiology of South African Therocephalian Therapsids (Amniota, Synapsida) and the Effects of the End-Permian Extinction on Size, Growth, and Bone Microstructure

Adam Keith Huttenlocker

A dissertation

submitted in partial fulfillment of the

requirements for the degree of

Doctor of Philosophy

University of Washington

2013

Reading Committee:

Christian A. Sidor, Chair

Jennifer Botha-Brink

Susan W. Herring

Gregory P. Wilson

Program Authorized to Offer Degree:

Department of Biology

University of Washington

Abstract

The Paleobiology of South African Therocephalian Therapsids (Amniota, Synapsida) and the Effects of the End-Permian Extinction on Size, Growth, and Bone Microstructure

Adam Keith Huttenlocker

Chair of the Supervisory Committee:
Professor Christian A. Sidor
Department of Biology

Despite their relative diversity in terrestrial Permian and Triassic rocks, the fossil record of therocephalian therapsids (Eutheriodontia) and their utility for understanding evolutionary patterns in the therapsid forerunners of mammals remains poorly understood. In this study, I investigate the extent to which body size reductions and shifts in growth patterns in Triassic therocephalians were influenced by the end-Permian mass extinction (ca. 252.3 Ma) (rather than the culmination of longer-term phylogenetic trends traceable to their Permian predecessors). Specifically, I examine whether body size reductions observed in earliest Triassic therocephalians ('Lilliput phenomena') were the product of within-lineage size reductions, differential extinctions, or rapid diversifications of new small-bodied clades. To address this question, I first review the global diversity and taxonomic composition of therocephalians from the Middle Permian through early-Middle Triassic (Chapter 1). I then present a paleobiological investigation of the Permo-Triassic therocephalian *Moschorhinus* as a case study on within-lineage patterns of growth and body size evolution during the end-Permian mass extinction (Chapter 2). Finally, I examine clade-wide (among-taxon) size patterns by evaluating the stratigraphic and phylogenetic components of body size evolution (Chapter 3) and the underlying influences of bone histology and growth (Chapter 4).

To examine within-lineage patterns, I studied cranial sizes and limb bone histology in Permian and Triassic specimens of *Moschorhinus*, the largest therapsid predator found both before and after the end-Permian mass extinction. Triassic specimens were found to have significantly decreased basal skull lengths compared to Permian specimens. Histological analysis indicated that variations in body size were associated with differences in subadult growth rate and duration (traits that are highly variable in environmentally stressed extant reptile species). Small Triassic individuals tended to display limb bones with fewer growth marks and more richly vascularized bone tissues than similarly sized Permian individuals, with an abundance of radially-oriented vascular canals, corroborating the hypothesis that conditions of the earliest Triassic favored rapid growth to a minimum body size requirement in *Moschorhinus* and, consequently, shortened developmental times.

Broader-scale 'Lilliput-type' patterns were examined in a large sample of therocephalians and compared with that of their sister clade, Cynodontia, in both geologic and phylogenetic contexts. Using a museum collections-based approach, I evaluated temporal and phylogenetic distributions of body size in Permo-Triassic eutheriodonts by time series analysis, rank order correlations, and phylogenetic model fitting. Results supported significant size reductions in earliest Triassic eutheriodonts, but suggested a pattern that was underscored largely by Brownian processes and constructive selectivity (a more general tendency to evolve smaller body sizes as in background intervals). Geologically brief size reductions were likely accomplished by the ecological removal of large-bodied species without rapid originations of new small-bodied clades or shifts from long-term evolutionary patterns. Finally, a survey of growth patterns and histomorphology in limb bones of Karoo therocephalians indicated that long-term changes in bone tissue vascularization (and thus growth) correlated with evolutionary changes in body size (e.g., smaller-bodied descendants tended to have less vascularized bone tissues than their larger-bodied ancestors). Results support a synergistic model of size reductions for Triassic therocephalians, influenced both by within-lineage

heterochronic shifts in survivor taxa (e.g., *Moschorhinus*) and cladistically inferred survival of small-bodied taxa with short growth durations (e.g., baurioids). These findings mirror the multi-causal Lilliput patterns described in marine faunas, but contrast with skeletochronologic studies that suggest slowed, prolonged shell secretion in marine benthos. Subjecting new histologic data to phylogenetic comparative methods, as in these therocephalians, will improve our understanding of the generality of growth and size shifts in Lilliput faunas and interplay between macroevolution and extinction during this and other major geologic transitions.

Table of Contents

List of Figures

List of Tables

Preface

This dissertation represents the culmination of a decade of research on therocephalian synapsids (literally 'beast-heads'). I first embarked on this journey during my undergraduate studies in the Department of Geology, University of Colorado at Boulder, which later unfolded with my inspiring trips to South Africa both before and during my PhD studies at University of Washington. This work would have been impossible without the coaching I received from friends and mentors during my early years at University of Colorado. My interests in the interface between ontogeny and evolution were cultivated by many debates with my partner in Permian paleontology, Jason Pardo, who also correctly predicted I would oneday slide down the slippery trunk of the tetrapod tree and author several papers on anamniotes and lungfish. Fortunately, our mentor, Bryan Small, and my advisors at University of Colorado, Karen Chin, Toni Culver, Jaelyn Eberle, Peter Robinson, and Dena Smith, as well as my Master's advisor, Stuart Sumida, helped to keep me on my chosen path.

My early work was enhanced greatly by helpful discussions with my colleagues in synapsid paleontology. First and foremost, James Hopson kindly relinquished specimens for me to research as early as my undergraduate studies, and we have had a few impactful encounters since. Although I have not had the pleasure of collaborating directly with Tom Kemp, I have benefitted from his reflections on the state of the field at professional conferences and on field excursions in South Africa, and his book 'Mammal-like Reptiles and the Origins of Mammals' (1982) was the reason I became a synapsid paleontologist. I have also benefited from many discussions and debates with my close coauthors and collaborators: Fernando Abdala, Kenneth Angielczyk, Jeffrey Benca, Jennifer Botha-Brink, Christian Kammerer, Sean Modesto, Trond Sigurdsen, and Roger Smith. For access to specimens and museum collections, I acknowledge Billy de Klerk (AM); Carl Mehling and Mark Norell (AMNH); Fernando Abdala, Bruce Rubidge, Michael Raath, and Bernhard Zipfel (BP); Ellen De Kock and Johann Neveling (CGS); Angela Milner (NHMUK); Jennifer Botha-Brink and Elize Butler (NMQR); Robert Rubidge (RC); Sheena Kaal and Roger Smith (SAM); Anusuya Chinsamy-Turan (University of Cape Town); Toni Culver and Jaelyn Eberle (UCM); and Patricia Holroyd and Kevin Padian (UCMP). Roger Smith and Bruce Rubidge also provided enlightening discussions on the biostratigraphy of *Moschorhinus* (Chapter 2) and other therocephalians, as well as helpful locality information.

My doctoral committee at University of Washington (UW) provided guidance and helpful suggestions on various aspects of this project: Christian Sidor (supervisory committee chair), Jennifer Botha-Brink, Sue Herring, Elizabeth Nesbitt, and Gregory Wilson. In particular, Dr. Botha-Brink oversaw many aspects of this work abroad, in the lab, and in the field, and I thank her for the critical role she played in getting this research off the ground. In addition to Drs. Sidor, Nesbitt, and Wilson, I also thank the other paleobiology faculty in the Department of Biology with whom I've interacted for their

resourcefulness, insights, and support: Caroline Strömberg and Peter Ward. For my continuing support by the UW Department of Biology I also acknowledge department chair(s) Toby Bradshaw and Ray Huey, as well as Judy Farrow and the rest of the UW Department of Biology administrative staff. Additionally, Karen Petersen supplied me with much needed vertebrate biology teaching assistantships when research funds were unavailable, and, in the process, instilled me with a deep appreciation for the wildlife of the Pacific Northwest. Each of these mentors has supported my scholarly endeavors in some way, and fostered my academic growth both as a researcher and a teacher.

I am deeply indebted to my fellow Sidor Lab underlings, both past and present: Charles Beightol, Emmanuel 'Noli' Ergas, Sterling Nesbitt, Brandon Peecook, and Linda Tsuji. The UW Paleograds and Biology graduate student faculty have also been a constant source of support. From day one, I was treated like a neighbor. I also acknowledge the support of the UW Burke Museum staff and volunteers: Bruce Crowley, Ron Eng, Don Hopkins, Gary Livingston, and Jude Swales. Bruce Crowley mechanically prepared some study specimens, whereas Jude Swales prepared some illustrations and casts. Histological processing in Seattle was assisted by Jacqueline Lungmus, who also helped with data collection and some digitization. The National Museum (Bloemfontein) preparator staff also provided assistance and preparation of some specimens for histological processing: John Nyaphuli, Joël Mohoi, Nthaopa Ntheri, Sam Stuurman, Sharon Ledibane, Sina Chaka, and William Molehe. Alex Brink provided helpful comments and suggestions on some of the statistical methods (Chapters 2 and 3). Max Maliska and Daril Vilhena provided help with some of the 'R' scripts, and Gene Hunt helped with time series analysis and the 'paleoTS' package (Chapter 3).

Finally, the love and moral support of my friends, family, and loved ones got me through tough times and occasional long nights. I am thankful for my aunt and uncle, Linda and Pat Mulcahy, who took me under their wings, and to my father Joseph, mother Nila, and my siblings Lisa, David, and Joe, who encouraged me to work hard and pursue my lifelong dream of becoming a professional student. Of course, because it takes one to know one, Lindsay Walker always displayed such understanding for which I am forever grateful and downright awestruck. I hope she gives me the opportunity to return the favor.

Funding was provided through several generous sources: National Science Foundation (NSF-DDIG 1209018); Tad Dillhoff, Rick Dillhoff and the Evolving Earth Foundation; University of Washington Department of Biology WRF-Hall Fellowship, Burke Museum of Natural History and Culture Vertebrate Paleontology Fellowship, and the Society of Vertebrate Paleontology Richard Estes Memorial Grant for fellowship and international travel funds. I also thank Christian Sidor and Jennifer Botha-Brink for partial funding during research and travel phases (NSF-ANT 0838762 to C.S.; NRF-65244 to J.B.-B.).

This work is dedicated to my ‘ohana.

Chapter 1—Introduction: Systematic Review of Permian and Triassic Therocephalians (Therapsida, Eutheriodontia)

Summary—Therocephalians were an ecologically diverse group of nonmammalian synapsids whose evolutionary history spanned the Middle Permian through Middle Triassic, ca. 268–241 million years ago (Ma). Their phylogenetic proximity to nonmammmlian cynodonts and rich fossil record during the Permian-Triassic transition, as well as their survival of the end-Permian extinction, have sparked interest in their evolutionary diversification and paleobiology. Here, I review the global diversity and systematic composition of Therocephalia, with an updated phylogenetic analysis incorporating 56 therapsid taxa (including 49 therocephalians) and 135 morphological characters. Therocephalia is demonstrated to be monophyletic and the sister clade to Cynodontia, and contains several diverse subclades whose diagnostic characters and proposed taxonomic composition are also reviewed. Lastly, I describe observed and phylogenetically-inferred diversity patterns of therocephalians in the context of their survivorship during the end-Permian extinction. In general, therocephalians were successful before and after the Permo-Triassic extinction boundary, but turnover rates were relatively depressed during the Triassic and the group went extinct during the early-

---

Includes excerpts published as: Huttenlocker, A. K. 2009. An investigation into the cladistic relationships and monophyly of therocephalian therapsids (Amniota: Synapsida). Zoological Journal of the Linnean Society 157:865–891; *and* Huttenlocker, A. K., C. A. Sidor, and R. M. H. Smith. 2011b. A new specimen of *Promoschorhynchus* (Therapsida: Therocephalia: Akidnognathidae) from the Lower Triassic of South Africa and its implications for theriodont survivorship across the Permo-Triassic boundary. Journal of Vertebrate Paleontology 31:405–421.

Middle Triassic (Anisian). The reasons for their initial success and ultimate extinction are unclear, but an improved phylogeny and stratigraphic framework will promote a better understanding of large-scale evolutionary patterns before and after the end-Permian extinction.

Introduction

The fossil record of nonmammalian synapsids (colloquially known as 'mammal-like reptiles') has played a key role in our understanding of macroevolution and the origins of mammalian structure and physiology (Romer and Price, 1940; Kemp, 1982, 2005; Hopson and Barghusen, 1986; Hopson, 1991, 1994; Sidor and Hopson, 1998; Rubidge and Sidor, 2001). Historically, their remains were recorded extensively in Permian and Triassic-aged rocks of North America, Eastern Europe, and especially sub-Saharan Africa (Owen, 1845a, b, 1859, 1876; Huxley, 1859; Cope, 1870, 1877, 1878; Seeley, 1889, 1894, 1895; Osborn, 1903). The nonmammalian therapsids, a subgroup of the earlier sphenacodontian 'pelycosaurs' (or pelycosaur-grade synapsids) (Fig. 1.1), are best documented by a continuous record from Middle Permian to Middle Triassic rocks of the Karoo Basin of South Africa, although their fossilized remains have also been recovered from contemporaneous basins on all other continents (Rubidge, 1995, 2005; Rubidge and Sidor, 2001; Catuneanu et al., 2005; Smith et al., 2012). Consequently, this rich fossil record has lended itself to recent applications of cladistic methodology, presenting opportunities to study large-scale evolutionary patterns during a major

geologic transition (e.g., Sidor and Hopson, 1998; Sidor, 2001, 2003; Angielczyk, 2004). The end-Permian extinction, for example, had profound effects on ecological interactions and biodiversity (Erwin, 1998, 2003, 2006; Twitchett et al., 2001; Ward et al., 2005; Smith and Botha, 2005; Botha and Smith, 2006; Roopnarine et al., 2007; Sahney and Benton, 2008; Chen and Benton, 2012), but its influences on morphological evolution and other macroevolutionary patterns in Permo-Triassic vertebrates are only beginning to be investigated using cladistics and phylogenetic comparative methods (Angielczyk and Walsh, 2008; Botha-Brink and Angielczyk, 2010; Sookias et al., 2012a, b).

Among the major groups of Permo-Triassic therapsids, evolutionary patterns have been investigated in dicynodonts (due to their relative abundances and their resulting biostratigraphic utility) and nonmammalian cynodonts (due to their phylogenetic proximity to the origin of mammals) (Hopson and Kitching, 1972; Rowe, 1986, 1988; Hopson, 1991; Sidor and Hopson, 1998; Rubidge and Sidor, 2001; Sidor, 2001, 2003; Angielczyk, 2004; Angielczyk and Walsh, 2008). Conversely, few studies have focused on the need to resolve systematic problems within the nearest relatives of the cynodonts: Therocephalia (Fig. 1.2). Therocephalians first appeared in the Middle Permian of South Africa as large-bodied predators with massive, triangular skulls and paired suborbital vacuities on the palate (Rubidge and Sidor, 2001). They later diversified into a variety of body sizes and ecological niches, with some losing their postcanine dentition (e.g., Late Permian whaitsiids; Fig. 1.2D) and others having broad, transversly expanded postcanine teeth with precise tooth-to-tooth occlusion (e.g., the late-Early-to-Middle Triassic

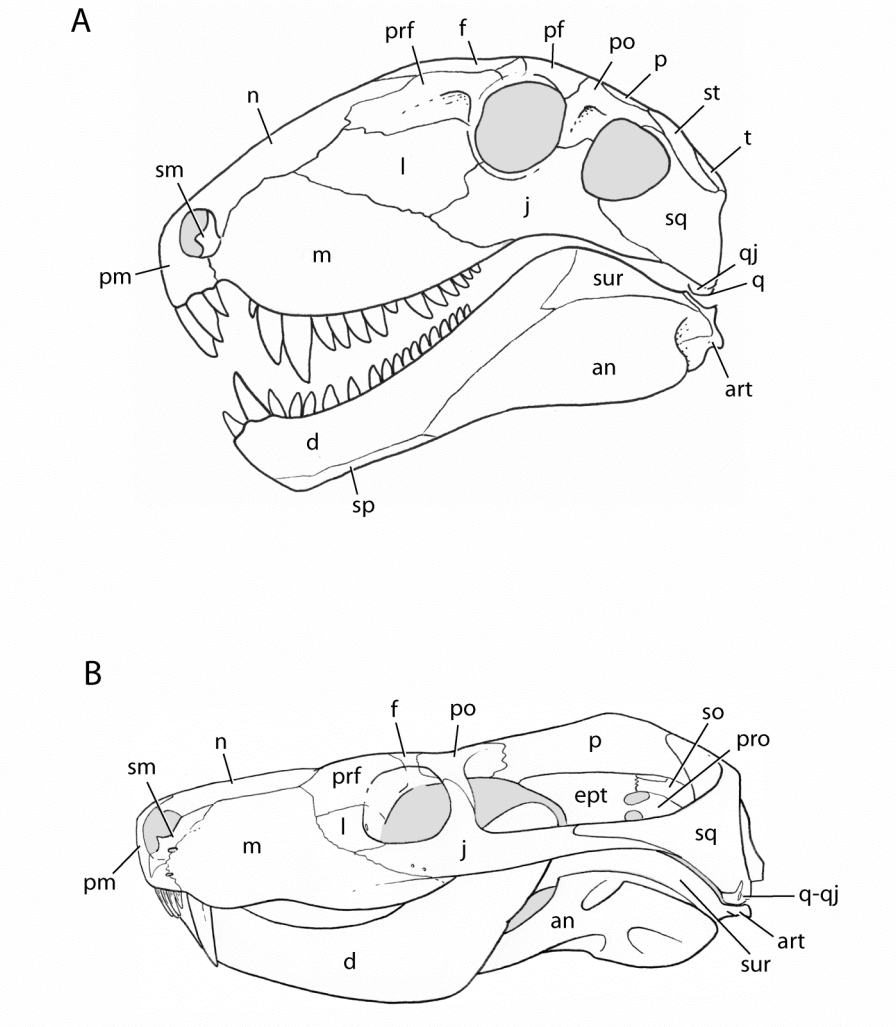

Figure 1.1. Comparison of skull anatomy in (**A**) a basal (pelycosaur-grade) synapsid, *Dimetrodon* Cope (redrawn from Romer and Price, 1940), and (**B**) a therocephalian therapsid, *Theriognathus* Owen. Skulls are not drawn to scale. Abbreviations: an, angular; art, articular; d, dentary; ept, epipterygoid; f, frontal; l, lacrimal; m, maxilla; n, nasal; p, parietal; pf, postfrontal; pm, premaxilla; po, postorbital; prf, prefrontal; pro, prootic; q, quadrate; q-qj; quadrate-quadratojugal complex; qj, quadratojugal; sm, septomaxilla; so, supraoccipital; sp, splenial; sq, squamosal; st, supratemporal; sur, surangular; t, tabular.

bauriids; Fig. 1.2F). Together, cynodonts and therocephalians have been demonstrated with robust character support to form a monophyletic clade: Eutheriodontia (Hopson and Barghusen 1986; Hopson 1991; Rubidge and Sidor, 2001; 'Therosauria' of Kemp 1982). Nevertheless, their particular intra-relationships have been the subject of debate, as earlier non-cladistic investigations (Kemp, 1972a) and more recent phylogenetic studies incorporating computer-assisted cladistic analysis have suggested that cynodonts may share a sister group relationship with at least some therocephalians (e.g., the whaitsiid *Theriognathus*; Abdala, 2007; Botha et al., 2007). This hypothesis deserves serious consideration because, if correct, it suggests that cynodonts represent a subgroup of a paraphyletic 'Therocephalia,' and that the origins of cynodont morphological structure may be encompassed by the evolution of early therocephalians.

Historical Review of Therocephalian Literature

Early discoveries: Karoo Basin, South Africa—Therocephalian therapsids were first described by Owen (1876) based on specimens that were discovered and donated by the prolific collector and geological engineer, A. G. Bain, during major roads projects in southern Africa. The specimens were described and illustrated in detail in Owen's "Catalogue of the Fossil Reptiles of South Africa in the Collections of the British Museum," and included *Theriognathus* (then considered a dicynodont), *Scaloposaurus*, and others primarily represented by poorly preserved, weathered snouts. Additional taxa from the same collections, including the basal therocephalian *Pristerognathus*, were described subsequently by Seeley (1895). The higher taxon 'Therocephalia' was

Figure 1.2. Selected skull reconstructions of therocephalian therapsids in left lateral view. **A**, akidnognathid eutherocephalian *Moschorhinus kitchingi* (modified from Durand, 1991). **B**, akidnognathid *Promoschorhynchus* (based on SAM-PK-K10014 and RC 116). **C**, hofmeyriid *Mirotenthes digitipes* (based on UCMP 40467). **D**, whaitsiid *Theriognathus microps*. **E**, basal ictidosuchid baurioid *Ictidosuchoides longiceps* (modified from Hopson, 1994). **F**, derived bauriid *Bauria cynops* (modified from Brink, 1963). Skulls are not drawn to scale. Abbreviations: d a, dentary angle; d v p, dentary ventral/mental protuberance; e m poc, edentulous postcanine region of maxilla; ept, epipterygoid; f l m, maxilla facial lamina/plate; m f, mandibular fenestra; m sob, maxillary portion of suborbital bar; mas p, mastoid process; mc poc, multi-cusped postcanines; p cr, parietal/sagittal crest; po p, postorbital process; poc, postcanine; prc, precanine; r p pm, premaxilla rostral process; ref lam, angular reflected lamina; sq v p, squamosal ventral process.

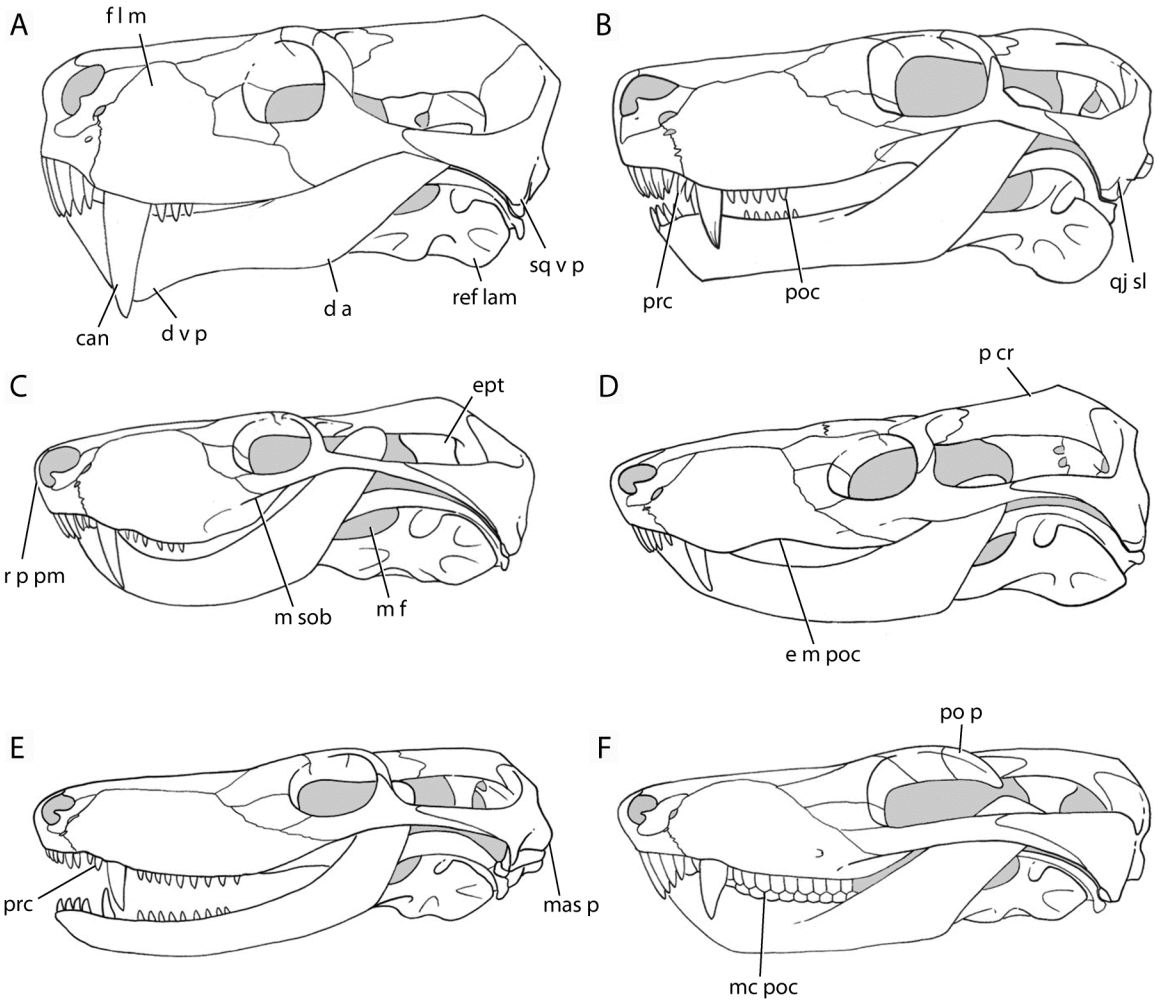
A
f l m
sq v p
d a
ref lam
can
d v p
B
prc
poc
qj sl
C
ept
r p pm
m sob
m f
D
p cr
e m poc
E
prc
mas p
F
po p
mc poc

established later by Broom (1903) to accommodate the early carnivorous families Scylacosauridae (e.g., *Scylacosaurus*, *Pristerognathus*), the diminutive Ictidosuchidae (e.g., *Ictidosuchus*), and some other therapsids that are no longer regarded as therocephalians (i.e. the gorgonopsians *Aelurosaurus* and *Gorgonops*, and the dinocephalians *Deuterosaurus*, *Rhopalodon*, and *Titanosuchus*).

Major expansions on therocephalian taxonomy followed this initial period of discovery, with notable contributions by Haughton (1918, 1924), Broom (1920, 1925, 1931, 1932, 1935, 1936a,b, 1948; Broom and Robinson, 1948), Nopsca (1923, 1928), Watson (1931; Watson and Romer, 1956), and Boonstra (1934, 1935, 1936, 1938, 1953, 1954a,b). Haughton described the whaitsiid *Whaitsia platyceps* (syn. *Theriognathus*) and *Akidnognathus parvus* (1918), as well as the bizarre, ornamented *Choerosaurus* (1929). Nopsca (1923) expanded the family-level taxonomy of early therocephalians, including Lycosuchidae (for *Lycosuchus* Broom, 1903) and Scylacosauridae, but Haughton (1924) combined the former two families into Pristerognathidae, which would dominate the literature for decades (likely because he regarded *Pristerognathus* Seeley as the oldest described member of the group). Later, Nopsca (1928) established five major therocephalian groups, including Lycosuchidae, Scylacosauridae, Whaitsidae (sic), Akidognathinae (sic), and Scaloposaurinae (although he regarded the last two as subgroups of Gorgonopsidae). Broom published several contributions, with redescription of *Whaitsia* Haughton (Broom 1920), descriptions of new whaitsiid taxa (1920, 1925, 1931, 1935, 1936b), and new basal (‘pristerognathids’) and derived forms of

therocephalians (1932, 1935, 1936a, b). The later works of Broom (1936b, 1948) synthesized diversity patterns in Karoo therapsid faunas, recognizing the dominance of dinocephalians and large, basal therocephalians from what is now known as the Middle Permian *Tapinocephalus* Assemblage Zone, and describing stratigraphic patterns of reduction and loss of postcanine dentition in some later Permian therocephalians, such as *Cerdosuchoides* and *Moschorhinus*. Brink (1954, 1965) and Mendrez (1974a, b) subsequently described other specimens of carnivorous therocephalians having affinities with Broom's *Cerdosuchoides* and *Moschorhinus*, including Permo-Triassic boundary representatives like *Promoschorhynchus* (Fig. 1.3) and '*Olivieria'* (now *Olivierosuchus*; Kammerer and Sidor, 2002).

Broom (1932, 1936b, 1948) also identified the prevalence of small baurioids in the Triassic *Lystrosaurus* Assemblage Zone. Watson (1931) and Broom (1932) initially recognized these small Triassic forms as having therocephalian affinities, but distinguished them from therocephalians in a separate group termed 'Bauriamorpha.' Soon after, Boonstra (1934) published his restudy of specimens in the collection of the Natural History Museum, London. He recognized seven families, including Pristerognathidae, Euchambersidae (sic), Alopecopsidae, Whaitsidae (sic), Ictidosuchidae, Lycideopsidae (sic), and Scaloposauridae. Later, Boonstra (1953) divided Therocephalia into two major subgroups: Pristerosauria and Scaloposauria. The Scaloposauria included the single family Scaloposauridae, which, according to Boonstra, "flow[ed] directly into the Bauriamorpha" (1953:605).

Figure 1.3. Interpretive drawings of a disarticulated akidnognathid therocephalian, *Promoschorhynchus* cf. *P. platyrhinus* (SAM-PK-K10014), from the earliest Triassic *Lystrosaurus* Assemblage Zone, Bethulie District, South Africa (from Huttenlocker et al., 2011b:fig. 3). Specimen in right (**A**) and left (**B**) lateral views. Scale bar equals 20 mm. Abbreviations: art, articular; c vert, caudal vertebra; can, canine tooth; co, coracoid; d, dentary; d vert, dorsal vertebra; fi, fibula; hu, humerus; icl, interclavicle; mtp, metapodial; pco, procoracoid; ph, phalanx; pra, prearticular; ra, radius; sc, scapula; sq, squamosal; st, sternum; sur, surangular; ti, tibia; to, tooth; u, ulna; un, ungual.

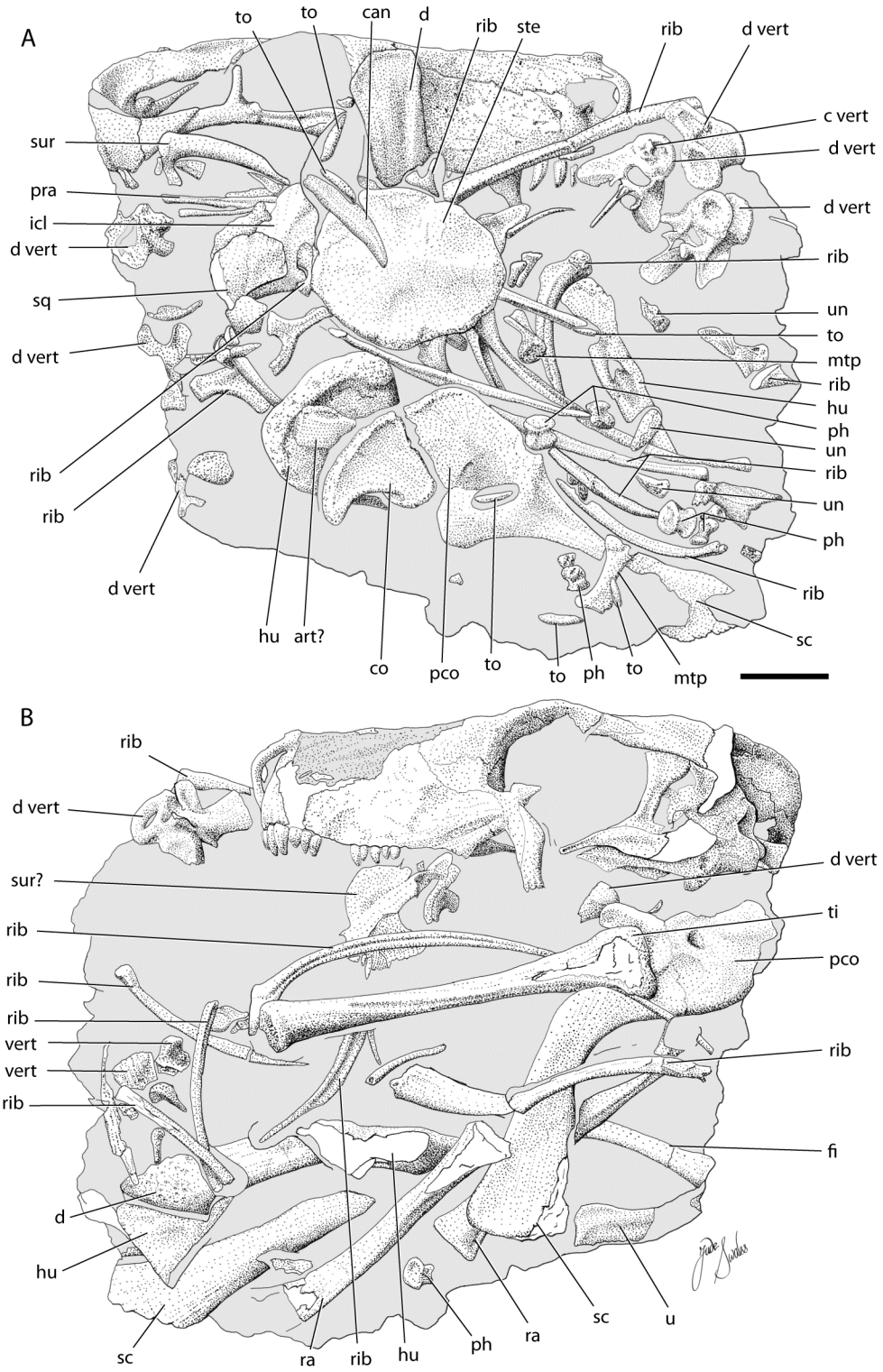
A
to
to
can
d
rib
ste
rib
d vert
c vert
d vert
d vert
rib
un
to
mtp
rib
hu
ph
un
rib
un
ph
rib
sc
sur
pra
icl
d vert
sq
d vert
rib
rib
d vert
hu
art?
co
pco
to
to
ph
to
mtp
B
rib
d vert
sur?
rib
rib
rib
d vert
d vert
rib
d
hu
sc
ra
rib
hu
ph
ra
sc
u
d vert
ti
pco
rib
fi

Non-Karoo records—As taxonomic revisions and new discoveries boomed in South Africa by mid-20th century, with new contributions by Boonstra (1934, 1935, 1938, 1953, 1954a,b) and Brink (1954, 1956, 1958, 1960, 1963, 1965), records also emerged from outside the Karoo Basin (Fig. 1.4). Von Huene (1950) reported two skulls that he attributed to the whaitsiids *Notosollasia* and *Notaelurops* (jun. syn. *Theriognathus*) along with small ictidosuchids (*Silphoictidoides*) from the Upper Permian Ruhuhu Basin of Tanzania. Additional whaitsiid material collected by Parrington was later described and illustrated by Kemp (1972a, b). Other undescribed specimens from the Upper Permian Madumabisa mudstone of the neighboring Luangwa Basin, Zambia were briefly reported by Drysdall and Kitching (1963) and reside in the collections of the Evolutionary Studies Institute (previously Bernard Price Institute for Palaeontological Research). Other African records include unidentified postcranial remains from the Busi Valley, Zimbabwe (Boonstra, 1969), the bauriid *Herpetogale* (jun. syn. *Microgomphodon*) from the Middle Triassic Omingonde Formation, Namibia (Keyser and Brink, 1979), and an undescribed jaw of a probable akidnognathid from the Upper Permian lower Sakamena Formation, Madagascar (SAM-PK-K8293; R. M. H. Smith and A. Huttenlocker, personal observations).

Though mostly fragmentary and represented by few specimens, therocephalians were also well known from Eastern Europe, first documented by the basal akidnognathid *Annatherapsidus* (previously '*Anna' petri*; Amalitzky, 1922). These taxa were reviewed

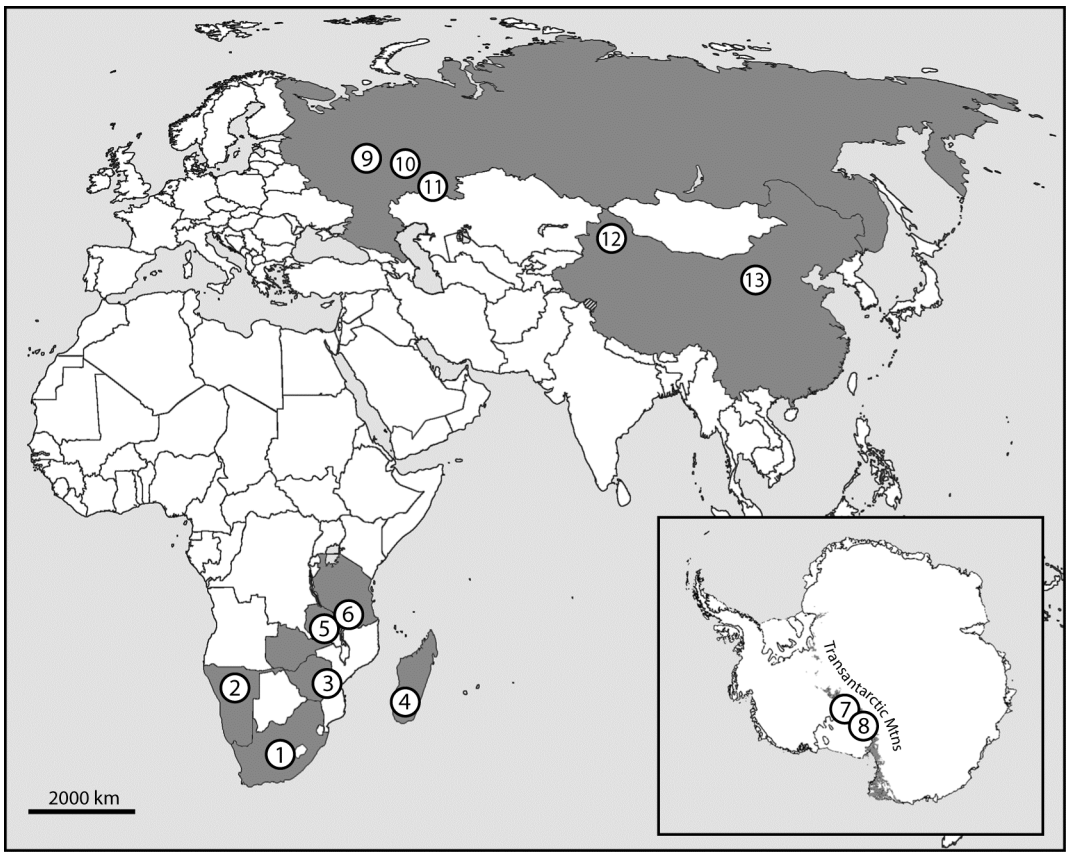

Figure 1.4. Geographic distributions of therocephalian-bearing localities. Dark gray indicates countries/regions having known therocephalian occurrences, whereas numbers (1-13) indicate specific basins. **1**, Karoo Basin, South Africa; **2**, Waterberg region, Namibia; **3**, Busi Valley, Zimbabwe; **4**, Ihorombe region, Madagascar; **5**, Luagwa Basin, Zambia; **6**, Ruhuhu Basin, Tanzania; **7**, Shackleton Glacier, Transantarctic Mountains; **8**, Beardmore Glacier, Transantarctic Mountains; **9**, Vyazniki, Vladimir region, Russia; **10**, Kotelnich, Kirov region, Russia; **11**, Orenburg region, Russia; **12**, Junggar Basin, northwest China; **13**, Ordos (Shanganning) Basin, northern China.

recently by Ivakhnenko (2011) and are summarized only briefly here. Several Upper Permian forms likely represent aberrant groups or basal members of known southern African families, including the eutherocephalians *Chthonosaurus* (Vjuschkov, 1955), *Scylacosuchus* (Tatarinov, 1968), and *Perplexisaurus* (Tatarinov, 1997); the basal whaitsiids *Moschowhaitsia* (Tatarinov, 1963) and *Viatkosuchus* (Tatarinov, 1995a); and the baurioid *Karenites* (Tatarinov, 1995b). Triassic taxa from Russia include *Antecosuchus* (= *Neotrirachodon*) (Tatarinov, 1973, 1974), *Nothogomphodon* (Tatarinov, 1974), and *Silphedosuchus* (Tatarinov, 1977). Notably, no genera are shared between the Eastern European and African therocephalian faunas, although recent collections from the upper Madumabisa mudstone of Zambia include undescribed taxa having apparent affinities with *Chthonosaurus* and *Karenites* (Sidor et al., 2013). Records have also been documented from the Lower Triassic of China, including *Urumchia* (Young, 1952), *Ordosiodon* (Young, 1961; Hou, 1979), *Traversodontoides* (Young, 1974), *Hazhenia* (Sun and Hou, 1981), and *Yikezhaogia* (Li, 1984). Lastly, records from the Triassic of Antarctica near Shackleton Glacier included small indeterminate baurioids, an akidnognathid, and a fragmentary specimen attributed to the baurioid *Ericiolacerta* (Colbert and Kitching, 1981; Huttenlocker and Sidor, 2012), as well as an indeterminate ilium from the Middle Triassic upper Fremouw Formation of Fremouw Peak near Beardmore Glacier, collected and prepared by the present author (Sidor et al., in press).

Systematic and phylogenetic renaissance—The resulting taxic diversity that accompanied these prolific discoveries, both regionally in the Karoo Basin and globally,

inspired a need to carefully describe and revise therocephalian anatomy, especially in the case of poorly preserved or non-diagnostic material that may have been oversplit by Broom and earlier workers. The detailed anatomical descriptions of Mendrez (1972, 1974a, 1974b, 1975; Mendrez-Carroll, 1979) permitted more precise inferences of their intra-relationships and the taxonomic compositions of major subgroups, as well as stratophenetic patterns during the Permian-Triassic transition (e.g., the parallel development of a bony secondary palate in some groups, as in dicynodonts and cynodonts; see Mendrez, 1975). These and more recent studies have emphasized their structural evolution with increasing emphasis on internal anatomy and fine structure (e.g., Maier, 1996; Sigurdsen, 2006; Sigurdsen et al., 2012), but have not fully integrated comparative morphological and cladistic data.

The systematic studies of Hopson and Barghusen (1986) and van den Heever (1994) offered the first higher-level cladistic frameworks for studying therocephalian evolution prior to the era of computer-assisted parsimony analysis and tree-searching algorithms (Fig. 1.5). Hopson and Barghusen (1986) examined the phylogenetic relationships of the major families of Therocephalia in detail, building on the studies of Mendrez (1975 and unpublished). The authors were the first to demonstrate the probable monophyly of Therocephalia with a list of proposed synapomorphies, and also distinguished between basal therocephalians (‘Pristerosauria,’ which included lycosuchids and scylacosaurids in a single group) and the newly recognized Eutherocephalia. Van den Heever (1994) emphasized the diversity of basal

Figure 1.5. Previously published hypotheses of the cladistic relationships of therocephalian therapsids. **A**, Hopson and Barghusen (1986). **B**, van den Heever (1994). **C**, Abdala (2007) and Botha et al. (2007). **D**, Huttenlocker (2009) and Huttenlocker et al. (2011b). **E**, Botha-Brink and Modesto (2011). **F**, Sigurdsen et al. (2012).

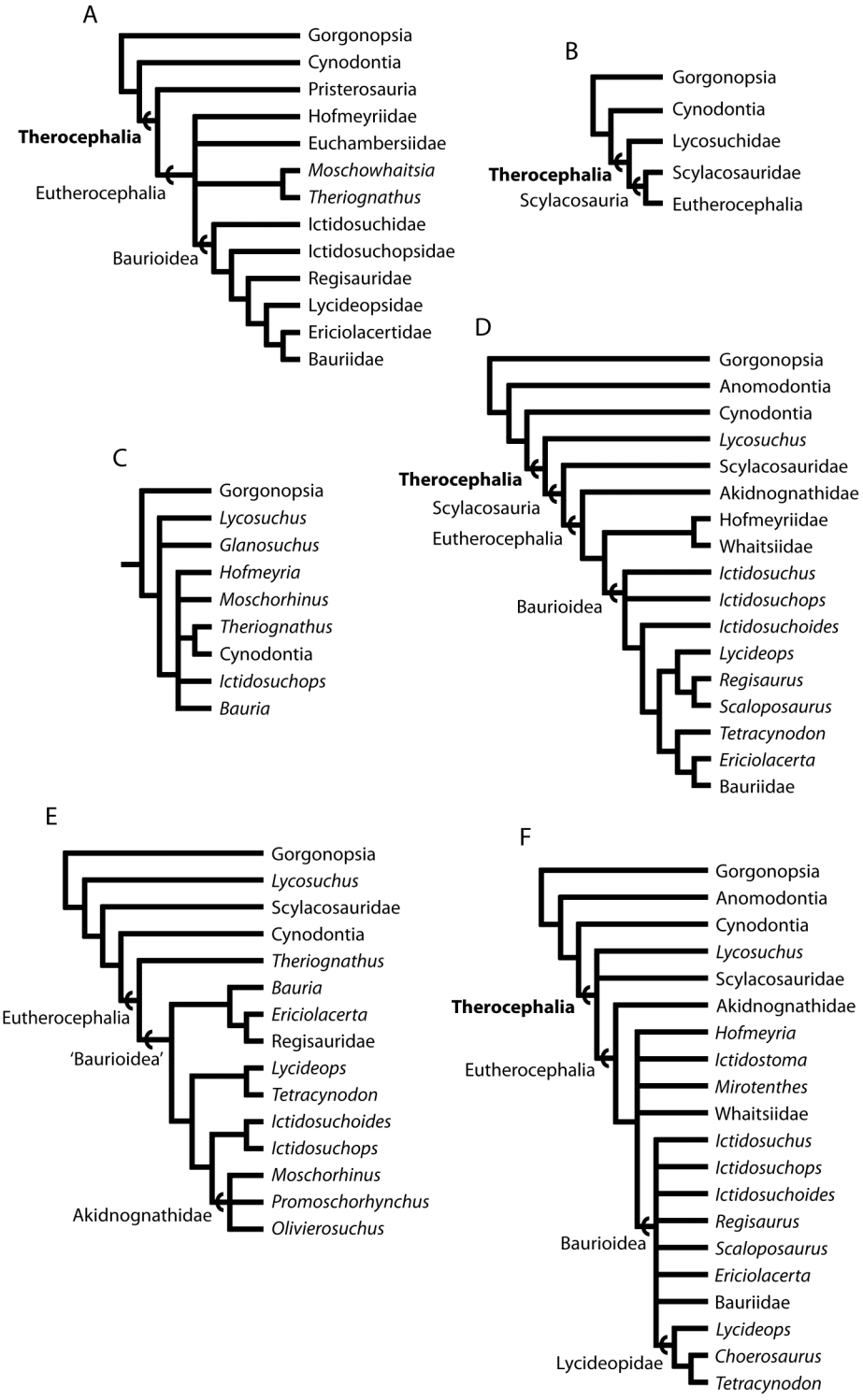
A
Gorgonopsia
Cynodontia
Pristerosauria
Hofmeyriidae
Therocephalia
Euchambersiidae
Moschowhaitsia
Eutherocephalia
Theriognathus
Ictidosuchidae
Ictidosuchopsidae
Baurioidea
Regisauridae
Lycideopsidae
Ericiolacertidae
Bauriidae
B
Gorgonopsia
Cynodontia
Lycosuchidae
Therocephalia
Scylacosauridae
Scylacosauria
Eutherocephalia
C
Gorgonopsia
Lycosuchus
Glanosuchus
Hofmeyria
Moschorhinus
Theriognathus
Cynodontia
Ictidosuchops
Bauria
D
Gorgonopsia
Anomodontia
Cynodontia
Lycosuchus
Scylacosauridae
Therocephalia
Akidnognathidae
Scylacosauria
Hofmeyriidae
Eutherocephalia
Whaitsiidae
Ictidosuchus
Baurioidea
Ictidosuchops
Ictidosuchoides
Lycideops
Regisaurus
Scaloposaurus
Tetracynodon
Ericiolacerta
Bauriidae
E
Gorgonopsia
Lycosuchus
Scylacosauridae
Cynodontia
Theriognathus
Bauria
Eutherocephalia
Ericiolacerta
Regisauridae
'Baurioidea'
Lycideops
Tetracynodon
Ictidosuchoides
Ictidosuchops
Moschorhinus
Akidnognathidae
Promoschorhynchus
Olivierosuchus
F
Gorgonopsia
Anomodontia
Cynodontia
Lycosuchus
Scylacosauridae
Therocephalia
Akidnognathidae
Hofmeyria
Eutherocephalia
Ictidostoma
Mirotenthes
Whaitsiidae
Ictidosuchus
Ictidosuchops
Ictidosuchoides
Baurioidea
Regisaurus
Scaloposaurus
Ericiolacerta
Bauriidae
Lycideops
Lycideopidae
Choerosaurus
Tetracynodon

therocephalians, re-establishing and revising the families Lycosuchidae and Scylacosauridae, and uniting scylacosaurids with the more derived eutherocephalians in a more inclusive group called Scylacosauria (though this was not the only hypothesis presented in that study). Though van den Heever's work advanced what was known about the cranial morphology of early therocephalians, little remains known about the patterns that characterized and shaped early eutheriodont evolution. This lack of progress is partly a result of limited taxon and character sampling among eutherocephalians and, by extension, an incomplete understanding of eutheriodont phylogeny.

Recent efforts have helped to clarify the cladistic relationships of therocephalians and eutheriodonts more generally, but results vary according to the taxon and character sampling of each author (Abdala, 2007; Botha et al., 2007; Huttenlocker, 2009; Huttenlocker et al., 2011b; Botha-Brink and Modesto, 2011; Sigurdsen et al., 2012). The discovery of a basal cynodont, *Charassognathus gracilis*, from the Late Permian *Tropidostoma* Assemblage Zone, South Africa, prompted a re-examination of early eutheriodont phylogeny, necessitating a cladistic analysis that incorporated both therocephalian and basal cynodont taxa (Botha et al., 2007). Results supported Kemp's concept of a paraphyletic 'Therocephalia,' nesting Cynodontia as the sister taxon to the whaitsiid *Theriognathus* (e.g., Kemp, 1972a), although the primary objective of the study was to assess the relative position of *Charassognathus* among basal cynodonts and reveal the order of acquisition of 'cynodont' characters during the course of eutheriodont evolution. As such, only seven therocephalian taxa were selected for the study, but

subsequent analysis using increased taxon sampling yielded similar results (Fig. 1.5C; Abdala, 2007). A later study on the anatomy and relationships of *Olivierosuchus* found a monophyletic Eutherocephalia with Lycosuchidae, Scylacosauridae, and Cynodontia positioned as successive outgroups (Fig 1.5E; Botha-Brink and Modesto, 2011). The studies of Huttenlocker (2009), Huttenlocker et al. (2011b), and Sigurdsen et al. (2012) have offered the most complete taxon and character sampling (including a number of postcranial characters) and generally support van den Heever's hypothesis of a monophyletic Therocephalia, with Lycosuchidae as the basal sister taxon to a monophyletic Scylacosauria (including Eutherocephalia) (Fig. 1.5D, F). Importantly, none of the recent studies have attempted a comprehensive analysis of all known therocephalian genera, a prospect previously hindered by the need for taxonomic revisions and restudy of historic specimens.

Present Study

Therocephalians offer great potential to investigate evolutionary patterns during the Permian-Triassic transition given their ecological diversity and relative species richness during the Middle Permian through Middle Triassic (surpassing dicynodont therapsids in generic diversity during the earliest Triassic). Here, I review the systematics and compositions of major therocephalian groups and present a comprehensive re-analysis of their cladistic relationships. A clearer understanding of their systematic compositions and evolutionary histories is critical to address hypotheses of morphological and physiological evolution in the group during the Permo-Triassic. The

following sections include (1) a brief discussion of Karoo biostratigraphy (upon which the biochronology of Permo-Triassic tetrapods is largely based); (2) a comprehensive Systematic Paleontology of Therocephalia with a discussion of the major subgroups and proposed taxonomic compositions; (3) an updated phylogenetic analysis of Therocephalia with a discussion of proposed synapomorphies; and (4) a review of therocephalian diversity during the Permian-Triassic transition. The present discussion establishes the temporal and cladistic contexts for this dissertation, including the reference phylogeny used for phylogenetic comparative methods explored in later chapters (Chapters 3 and 4).

Geologic and Stratigraphic Context

Stratigraphic Correlations and Dating

Given their abundance and stratigraphic variation in Middle Permian through Middle Triassic rocks of the Beaufort Group (Karoo Supergroup), fossil therapsids have provided the basis for the temporal succession and subdivisions of the Permian-Triassic Beaufort Series in southern Africa (Watson, 1914; Kitching, 1970, 1977). This has led to the designation of distinct vertebrate assemblage zones in the main Karoo and neighboring basins: *Eodicynodon*, *Tapinocephalus*, *Pristerognathus*, *Tropidostoma*, *Cistecephalus*, *Dicynodon*, *Lystrosaurus*, and *Cynognathus* assemblage zones (herein 'AZs') (Fig. 1.6). The stratigraphic conventions and dates used herein follow Rubidge (1995, 2005), Hancox et al. (1995), Hancox and Rubidge (2001), Neveling (2004), Smith and Botha (2005), Ward et al. (2005), Botha and Smith (2006, 2007), Abdala et al.

(2008), Abdala and Ribeiro (2010), Retallack et al. (2011), Smith et al. (2012), and Rubidge et al. (2013). Correlations have been established with other Karoo-aged basins elsewhere in Africa, Central and Eastern Europe, and China, and here follow Lucas (1998, 2001, 2005, 2009), Benton et al. (2004), Neveling (2004), Catuneanu et al. (2005), Rubidge (2005), Tverdokhlebov et al. (2005), Abdala and Ribeiro (2010), Retallack et al. (2011), Smith et al. (2012), and Retallack (2013). Absolute dates for global standard stratigraphy are updated from Mundil et al. (1996, 2001, 2004), Gradstein and Ogg (2004), Gradstein et al. (2004), Muttoni et al. (2004), Lehrmann et al. (2006), and Shen et al. (2011), while absolute dates for the Beaufort Series are based on Coney et al. (2007) and Rubidge et al. (2013).

The basal two biozones representing the Middle Permian include the *Eodicynodon* and *Tapinocephalus* AZ. The discovery of two species of scylacosaurid therocephalians (viz. *Glanosuchus macrops* and *Ictidosaurus angusticeps*) in the *Eodicynodon* AZ near the Ecca-Beaufort Group contact indicates that therocephalians were present among the earliest therapsid faunas of the Karoo, ca. 268–265.8 Ma (Rubidge et al., 1983; Rubidge, 1988; Abdala et al., 2008). An abundance of large-bodied pareiasaurs, dinocephalians, and scylacosaurid therocephalians, and the paucity of dicynodont therapsids in the younger *Tapinocephalus* AZ mirrors the Capitanian (late Middle Permian) tetrapod faunas of Eastern Europe (Smith et al., 2012). The younger *Pristerognathus* AZ records a relatively higher abundance of scylacosaurids and small dicynodonts, such as *Diictodon*, and is largely correlated with Russian Zones II and III (Capitanian). However, the

Figure 1.6. Stratigraphic framework for the present study. Selected non-Karoo basins represent regions/units having published therocephalian records. Based on Rubidge (1995), Hancox et al. (1995), Hancox and Rubidge (2001), Lucas (2001), Rubidge (2005), and Smith et al. (2012). Absolute dates (Ma) from Shen et al. (2011), Smith et al. (2012), and Rubidge et al. (2013). Dates in parentheses represent U/Pb dates from within the Beaufort Group, Karoo Basin (from Rubidge et al., 2013). PTB = Permian-Triassic boundary.

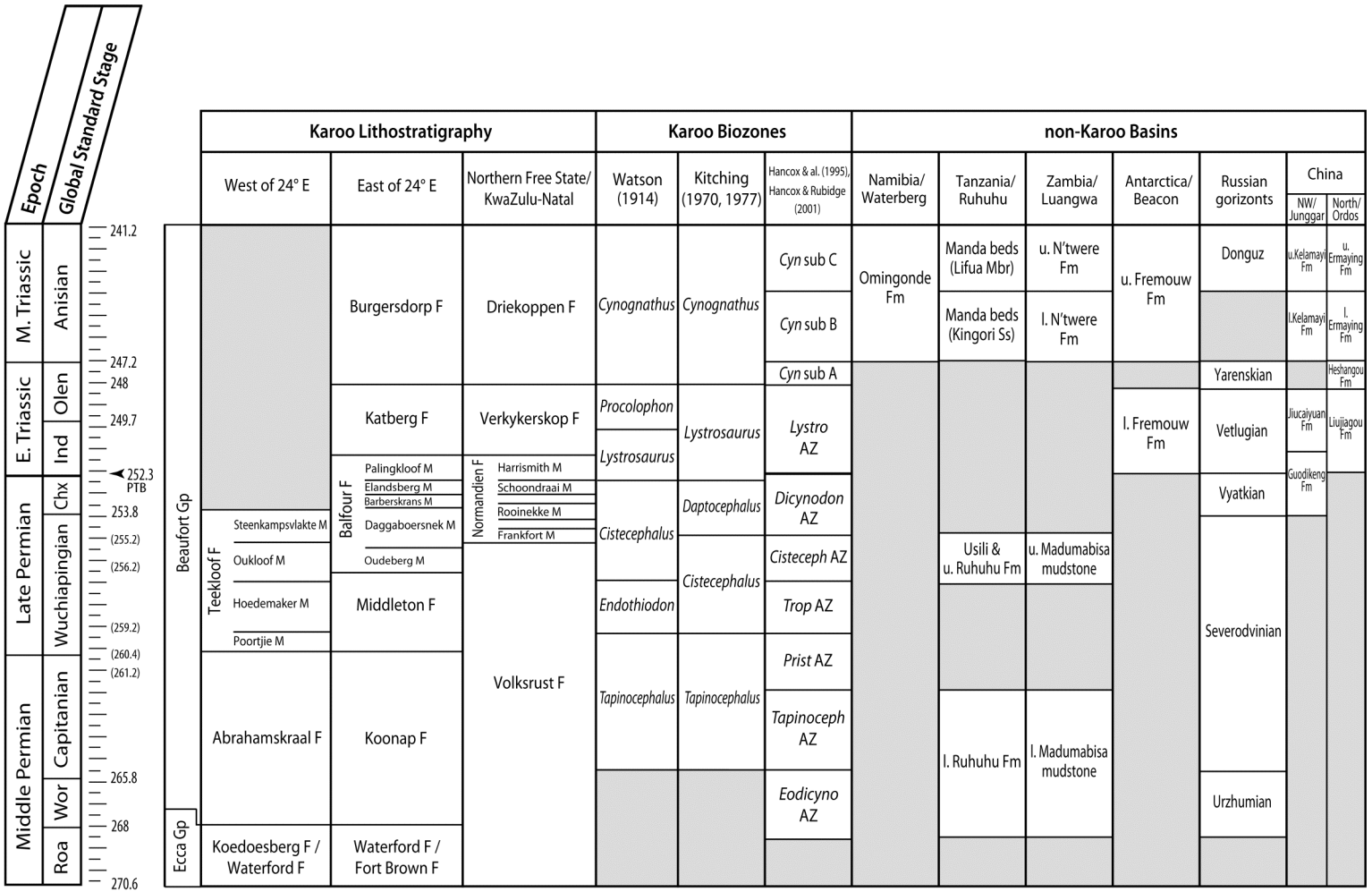
Epoch
Global Standard Stage
Middle Permian
Late Permian
E. Triassic
M. Triassic
Roa
Wor
Capitanian
Wuchiapingian
Chx
Ind
Olen
Anisian
241.2
247.2
248
249.7
252.3
PTB
253.8
(255.2)
(256.2)
(259.2)
(260.4)
(261.2)
265.8
268
270.6
Karoo Lithostratigraphy
Karoo Biozones
non-Karoo Basins
West of 24° E
East of 24° E
Northern Free State/ KwaZulu-Natal
Watson (1914)
Kitching (1970, 1977)
Hancox & al. (1995), Hancox & Rubidge (2001)
Namibia/ Waterberg
Tanzania/ Ruhuhu
Zambia/ Luangwa
Antarctica/ Beacon
Russian gorizonts
China
NW/ Junggar
North/ Ordos
Beaufort Gp
Ecca Gp
Burgersdorp F
Driekoppen F
Katberg F
Verkykerskop F
Balfour F
Palingkloof M
Elandsberg M
Barberskrans M
Daggaboersnek M
Oudeberg M
Normandien F
Harrismith M
Schoondraai M
Rooinekke M
Frankfort M
Teekloof F
Steenkampsvlakte M
Oukloof M
Hoedemaker M
Poortjie M
Middleton F
Volksrust F
Abrahamskraal F
Koonap F
Koedoesberg F / Waterford F
Waterford F / Fort Brown F
Cynognathus
Procolophon
Lystrosaurus
Cistecephalus
Endothiodon
Tapinocephalus
Cynognathus
Lystrosaurus
Daptocephalus
Cistecephalus
Tapinocephalus
Cyn sub C
Cyn sub B
Cyn sub A
Lystro AZ
Dicynodon AZ
Cisteceph AZ
Trop AZ
Prist AZ
Tapinoceph AZ
Eodicyno AZ
Omingonde Fm
Manda beds (Lifua Mbr)
Manda beds (Kingori Ss)
Usili & u. Ruhuhu Fm
l. Ruhuhu Fm
u. N'twere Fm
l. N'twere Fm
u. Madumabisa mudstone
l. Madumabisa mudstone
u. Fremouw Fm
l. Fremouw Fm
Donguz
Yarenskian
Vetlugian
Vyatkian
Severodvinian
Urzhumian
u.Kelamayi Fm
l.Kelamayi Fm
Jiucaiyuan Fm
Guodikeng Fm
u. Ermaying Fm
l. Ermaying Fm
Heshangou Fm
Liujiagou Fm

position of the Middle-to-Late Permian (Capitanian-Wuchiapingian) boundary is held to be present within the upper portion of the *Pristerognathus* AZ, a hypothesis that is recently supported by new U-Pb dates from the Koonap and Middleton formations which bound this transition, ca. 260.4 Ma (Rubidge et al., 2013). The subsequent early-Late Permian (Wuchiapingian) biozonation therefore includes the uppermost *Pristerognathus*, *Tropidostoma*, *Cistecephalus*, and lowermost *Dicynodon* AZ.

Based on a combination of biostratigraphy, paleomagnetic and carbon-isotope evidence, the Permian-Triassic boundary (PTB) has been traced to a rhythmically bedded maroon mudrock unit (approximately 8–10 meters thick) demarcating the transition between the lower and upper portions of the Palingkloof Member of the Balfour Formation (Beaufort Group). At several localities, this unit includes the last occurrences of the dicynodonts *Lystrosaurus maccaigi* and *Daptocephalus leoniceps*, defining the top of the *Dicynodon* AZ (MacLeod, 2000; Ward et al., 2005; Botha and Smith, 2007). Therocephalians and cynodonts are less notable biostratigraphic markers of this transition, but their fossils are common in boundary sections and record greater diversity in the *Lystrosaurus* AZ compared to sympatric dicynodonts (which are represented by only four species in two genera locally in the *Lystrosaurus* AZ; Fröbisch, 2008). In addition to well-documented negative carbon-isotope excursions linked to perturbations in the global carbon cycle (MacLeod et al., 2000; Ward et al., 2005; Retallack et al., 2011; Retallack, in press), a single zircon recovered from boundary beds at the Commando Drift Dam in Eastern Cape Province has placed a maximum (lower) age of

252.5 Ma on the boundary beds (Coney et al., 2007). This is consistent with the currently accepted age of 252.3 Ma for both terrestrial and marine PTB stratotype sections in South China (Shen et al., 2011).

The uppermost portion of the *Lystrosaurus* AZ ("*Procolophon* abundance zone" of Neveling, 2004) is correlated to the Smithian substage of the Olenekian in Eastern Europe and China, whereas the lowermost portion of the threefold *Cynognathus* AZ (subzone A) is correlative to the Spathian substage (based mainly on the presence of a capitosauroid temnospondyl (*Kestrosaurus*) and trematosaurids, as in the Triassic basins of Central and Eastern Europe) (Neveling, 2004; Smith et al., 2012). The age of the Smithian-Spathian boundary within the Olenekian is approximately 248 Ma (Gradstein et al., 2004). The Olenekian-Anisian (Early-to-Middle Triassic) boundary is variably dated to 245 (Gradstein and Ogg, 2004) and more recently 247.2 Ma (Lehrmann et al., 2006). Here, I follow the more recent analysis of Lehrmann et al. in assigning the Olenekian-Anisian boundary a date of 247.2 Ma with the preceding interval (Olenekian) therefore spanning approximately 2.5 million years, just under the average duration of assemblage zones sampled in this and other recent studies using Karoo-based time series (e.g., Fröbisch, 2008, 2013; Abdala and Ribeiro, 2010). Stratigraphic nomenclature and dates for Middle-to-Late Triassic Gondwanan basins used in later chapters follow Abdala et al. (2006), Abdala and Ribeiro (2010), Irmis et al. (2010) and references cited therein.

Systematic Paleontology

SYNAPSIDA Osborn, 1903

THERAPSIDA Broom, 1905

EUTHERIODONTIA Hopson and Barghusen, 1986

THEROCEPHALIA Broom, 1903

Lycosuchidae Nopsca, 1923

Composition—*Lycosuchus vanderrieti* Broom, 1903.

Definition—All therocephalians sharing a more recent common ancestry with *Lycosuchus vanderrieti* than with *Scylacosaurus sclateri* or *Theriognathus microps*.

Revised diagnosis—Large therocephalians with V-shaped frontal-nasal suture, pointing toward occiput; basal tubera enlarged, approximating one-quarter to one-third of the occipital breadth; upper incisors number five (shared with some eutherocephalians); upper postcanines reduced to three to four (also in some eutherocephalians); upper postcanines situated in special ventral maxillary flange; short, tall dentary with strong dentary angle; lower incisors number three (also in scylacosaurids); pterygoid boss teeth absent (also in some eutherocephalians).

Occurrence—Middle Permian *Tapinocephalus* AZ, Karoo Basin, South Africa.

Remarks—Van den Heever (1980) temporarily abandoned usage of Lycosuchidae (= Trochosauridae, Trochosuchidae) based on the dubious diagnostic character of two functional maxillary canines (interpreted instead as replacement dentition). Subsequent study, however, supported the group's validity based on additional characters (listed above), but condensed its diversity within *Lycosuchus* Broom, with *Hyaenosuchus* and *Zinnosaurus* regarded as synonyms of the former genus (van den Heever, 1987, 1994). *Scymnosaurus* (regarded as "Lycosuchidae incertae sedis") as well as *Trochorhinus, Trochosaurus* and *Trochosuchus* (regarded as nomena dubia) may also represent synonyms of *Lycosuchus* given a lack of their own unique autapomorphies (van den Heever, 1987, 1994). A large, possible lycosuchid may also be present in the *Pristerognathus* AZ, although this record is currently under investigation by other workers (F. Abdala, personal communication, 2010).

SCYLACOSAURIA van den Heever, 1994

(= SCYLACOSAUROIDEA sensu Tatarinov, 1974)

Scylacosauridae Broom, 1903

Composition—*Pristerognathus polyodon* Seeley, 1895; *Ictidosaurus angusticeps* Broom, 1903; *Scylacosaurus sclateri* Broom, 1903; *Glanosuchus macrops* Broom, 1904; *Alopecodon priscus* Broom, 1908; *Pardosuchus whaitsi* Broom, 1908.

Definition—All therocephalians sharing a more recent common ancestry with *Scylacosaurus sclateri* than with *Lycosuchus vanderrieti* or *Theriognathus microps*.

Revised diagnosis—Medium-to-large therocephalians with rostrum moderately elongated and bearing long, shallow antorbital fossa; upper incisors number six to seven (also in some baurioids); lower incisors number three (but shared with *Lycosuchus*).

Additional combinations of symplesiomorphic characters in the group include suborbital bar shallow; interpterygoid vacuity narrow/reduced; basal tubera small; pterygoid boss teeth present; incisors and caniniform teeth bear serrations; dentary angle sharply pronounced (van den Heever, 1994; Abdala et al., 2008).

Occurrence—Middle Permian *Eodicynodon*, *Tapinocephalus,* and *Pristerognathus* AZs in southern Africa (Abdala et al., 2008).

Remarks—Though initially established by Broom (1903), Nopsca (1923) expanded the family-level taxonomy of the early therocephalians into two families: Lycosuchidae (for *Lycosuchus*) and Scylacosauridae. Haughton (1924), however, compressed the diversity of these groups into a single family, Pristerognathidae, which became the accepted name for several years. Van den Heever (1987, 1994) most recently revised the diversity of early therocephalians. He followed Nopsca's (1923) concept of two major groups, Lycosuchidae and Scylacosauridae, and recognized only six valid genera in the latter group based on variations in their dental formula: *Pristerognathus* (= *Ptomalestes*), *Ictidosaurus*, *Scylacosaurus* (= *Scylacorhinus*, *Therioides*), *Glanosuchus* (= *Alopecognathus*, *Pristerognathoides*, *Walteria*, *Karroowalteria*), *Alopecodon*, and

Pardosuchus. This scheme was followed by Abdala et al. (2008) in their biostratigraphic review of early therocephalians (which included the first records of *Ictidosaurus* and *Glanosuchus* in the *Eodicynodon* AZ of the Karoo Basin).

EUTHEROCEPHALIA Hopson and Barghusen, 1986

Scylacosuchidae Ivakhnenko, 2011

Composition—*Scylacosuchus orenburgensis* Tatarinov, 1968.

Definition—All eutherocephalians sharing a more recent common ancestry with *Scylacosuchus orenburgensis* than with *Akidnognathus parvus* or *Theriognathus microps*.

Revised diagnosis—Medium-to-large eutherocephalian with anteroposteriorly short postorbital region (less than half of the skull breadth); nasals extremely narrow and elongated; upper dental formula includes five incisors, one to two precanines, one canine, and six postcanines; lower incisors number five (also in some karenitid and lycideopid baurioids). Synapomorphic features shared with other eutherocephalians but absent in lycosuchids and scylacosaurids include upper incisors with longitudinal fluting/striae; incisor cutting margins smooth and unserrated. A plesiomorphic feature retained in Scylacosuchidae but lost in most other eutherocephalians is the presence of the postfrontal.

Occurrence—Wuchiapingian, Upper Permian, Orenburg region, Russia.

Remarks—*Scylacosuchus* was previously regarded by Tatarinov (1968, 1974) and Battail and Surkov (2000) as an aberrant member of Scylacosauridae (making it the only Russian representative of what was largely a southern African group). However, its late geologic occurrence in Wuchiapingian-aged rocks (Upper Permian) and aspects of its dentition, including a lack of serrations on the incisors and canines and presence of fluted antecanine teeth, suggest affinities to the Late Permian eutherocephalians. Van den Heever (1994) excluded *Scylacosuchus* from the basal lycosuchids and scylacosaurids based on the dentition, but did not offer an alternative designation. Ivakhnenko (2011) consequently established a separate monotypic family, Scylacosuchidae, which is followed here.

Perplexisauridae Tatarinov, 2000

Composition—*Perplexisaurus foveatus* Tatarinov, 1997; *Perplexisaurus lepusculus?* Ivakhnenko, 2011.

Definition—All eutherocephalians sharing a more recent common ancestry with *Perplexisaurus foveatus* than with *Scylacosuchus orenburgensis, Chthonosaurus velocidens, Akidnognathus parvus,* or *Theriognathus microps*.

Revised diagnosis—Small eutherocephalians with short rostrum and relatively large orbits; maxilla facial lamina pitted with row of foramina arranged along the alveolar

margin; pterygoid boss teeth present; long row of ten to eleven upper postcanines; upper postcanines mediolaterally flattened (not rounded in section) and bear coarse denticles.

Occurrence—Wuchiapingian, Upper Permian, Kotelnich, Kirov region, Russia.

Remarks—Tatarinov (2000) recognized two genera, *Perplexisaurus* and *Chlynovia*, which comprised a distinct family of therocephalians having a characteristic "porous sensory system" in the maxilla: Perplexisauridae. The two genera were later synonymized (Ivakhnenko, 2011). *Perplexisaurus lepusculus* was also added as a new species (Ivakhnenko, 2011). However, the material (PIN 520/23) was based on a very fragmentary maxilla with six preserved teeth from much older (Middle Permian) deposits. *P. foveatus* is restricted to the Wuchiapingian (Upper Permian) Kotelnich locality in Russia.

Chthonosauridae Tatarinov, 1974

Composition—*Chthonosaurus velocidens* Vjuschkov, 1955.

Definition—All eutherocephalians sharing a more recent common ancestry with *Chthonosaurus velocidens* than with *Scylacosuchus orenburgensis, Perplexisaurus foveatus, Akidnognathus parvus,* or *Theriognathus microps*.

Revised diagnosis—Small eutherocephalians with short intertemporal region lacking a pineal foramen; median frontonasal crest (also in akidnognathids and some

whaitsiids); palatal surface of maxilla and palatines bear deep furrows; medial process of maxilla may be present anteriorly near canine, contacting vomer (incompletely preserved in *Chthonosaurus*); suborbital vacuities anteroposteriorly short and broad with a scalloped anterior margin; pterygoid 'webbing' connecting transverse flanges and quadrate ramus bears scalloped edge; pterygoid boss teeth present; upper postcanines number six; massive, conical postcanines decrease in size posteriorly; postcanines bear a non-denticulated carina on posterior (distal) cutting edge (also in some akidnognathids).

Occurrence—Wuchiapingian, Upper Permian, Kotelnich, Kirov region, Russia; late Wuchiapingian or Changxingian (Vyatkian gorizont), Upper Permian, Orenburg region, Russia; Wuchiapingian (*Cistecephalus* AZ-equivalent), Upper Permian, Luangwa Basin, Zambia.

Remarks—Tatarinov (1974) established the family Chthonosauridae to accommodate *Chthonosaurus velocidens*. Mendrez (1974a) designated *Chthonosaurus* and *Annatherapsidus* together in a separately family, Annatherapsididae (= Annidae), and later expanded this group to include two additional subfamilies, Moschorhininae and Euchambersiinae (Mendrez, 1975). This scheme was followed by Battail and Surkov (2000) and Ivakhnenko (2011). Additional material from the Upper Permian Madumabisa mudstone of Zambia (Sidor et al., 2013) represents the first record of Chthonosauridae outside Russia. These specimens exhibit a furrowed palatal surface of the maxilla and palatines, medial projection of the anterior maxilla which contacts the vomer, and six massive, conical postcanines which decrease in size posteriorly and bear an unserrated

posterior (distal) carina (resembling the fragmentary '*Kotelcephalon'* from the Kirov region of Russia). The Zambian specimens are designated only by their voucher numbers in this dissertation (NHCC LB36, LB38; see Figs. 1.7, 1.8) as they are undergoing formal description.

Akidnognathidae Nopsca, 1928

Composition—*Akidnognathus parvus* Haughton, 1918; *Moschorhinus kitchingi* Broom, 1920; *Annatherapsidus petri* (Amalitzky, 1922); *Euchambersia mirabilis* Broom, 1931; *Cerdosuchoides brevidens* Broom, 1936b; *Promoschorhynchus platyrhinus* Brink, 1954; *Olivierosuchus parringtoni* (Brink, 1965).

Definition—All eutherocephalians sharing a more recent common ancestry with *Akidnognathus parvus* than with *Theriognathus microps* or *Bauria cynops* (sensu Huttenlocker and Sidor, 2012).

Revised diagnosis—Medium-to-large eutherocephalians with median frontonasal crest (also in *Chthonosaurus* and some whaitsiids); maxillary postcanine alveolar margin in ventral view buccally convex, bowing outward away from midline; upper postcanine diastema immediately behind canine absent such that postcanine row is pressed tightly against canine; dentary symphysis anteroposteriorly thickened with strong suture; palatal

housing for lower caniniform formed as a separate fossa by premaxillary and maxillary extensions of the primary palate (except in *Annatherapsidus*).

Occurrence—late Wuchiapingian or Changxingian (Vyatkian gorizont), Upper Permian, Arkhangelsk region, Russia; *Cistecephalus*, *Dicynodon* (Upper Permian), and *Lystrosaurus* (Lower Triassic) AZs, Karoo Basin, South Africa; Lower Triassic lower Fremouw Formation, Shackleton Glacier, Transantarctic Mountains.

Remarks—Nopsca (1928) initially regarded Akidnognathidae (or 'Akidognathinae' sic) as a subgroup of Gorgonopsidae. *Promoschorhynchus* was initially described as a basal whaitsiid (Brink, 1954) and *Olivierosuchus* (=*Olivieria*) as an ictidosuchid baurioid (Brink, 1965). Mendrez (1974a,b) correctly established these genera under a single family with *Moschorhinus*: Moschorhinidae (borrowing the family name used by Brink, 1958). Hopson and Barghusen (1986) preferred the name Euchambersiidae Boonstra (1934), but most subsequent authors have recognized Akidnognathidae Nopsca (1928) as having priority (e.g., Sigurdsen, 2006; Huttenlocker, 2009; Huttenlocker et al., 2011b; Botha-Brink and Modesto, 2011). Synonymy between *Moschorhinus* and *Tigrisuchus* (based on a weathered snout) has been proposed (Mendrez 1974 a, b), although others have referred *Tigrisuchus* to Gorgonopsia (e.g., Sigogneau, 1970 and van den Heever, 1987). A formalized synonymy awaits adequate redescription of *Tigrisuchus*. *Annatherapsidus* from Russia is a basal representative of this group, although additional undescribed material from the *Cistecephalus* AZ of South Africa (USNM PAL 412421) also occupies a relatively basal position in the group

(Kammerer, 2008) indicating a relatively widespread geographic distribution early in their evolutionary history. Huttenlocker and Sidor (2012) have also identified a partial skull assignable to Akidnognathidae from the Lower Triassic Fremouw Formation of Antarctica (originally described by Colbert and Kitching, 1981). A fragmentary specimen from the Anisian Ermaying Formation of China, *Yikezhaogia megafenestrala*, compares closely to *Olivierosuchus* (Li, 1984; Sun, 1991). The specimen, however, would be the youngest akidnognathid, having a lineage that survived until the Anisian (Middle Triassic). The group therefore ranges from the Upper Permian *Cistecephalus* through Lower Triassic *Lystrosaurus* AZs in southern Africa (and possibly as late as the Anisian in China, depending on proper identification of *Yikezhaogia*).

UNNAMED CLADE (NON-AKIDNOGNATHID 'WHAITSIOIDS')

Hofmeyriidae Hopson and Barghusen, 1986

Composition— *Ictidostoma hemburyi* (Broom, 1911); *Hofmeyria atavus* Broom, 1935; *Mirotenthes digitipes* Attridge, 1956.

Definition—All eutherocephalians sharing a more recent common ancestry with *Ictidostoma hemburyi* than with *Theriognathus microps* or *Bauria cynops*.

Revised diagnosis—Small-to-medium sized eutherocephalians with prefrontal-postorbital sutural contact ventrally on dorsomedial wall of orbit; epipterygoid

anteroposteriorly expanded, having broad dorsal contact with parietal (shared with whaitsiids and cynodonts); pterygoid boss teeth present; dentary slender and boomerang- or banana-shaped (shared with whaitsiids); dentary lateral surface smooth, lacking longitudinal furrow or trough (shared with whaitsiids, regisaurids, and *Lycideops*); with the exception of *Ictidostoma*, lower postcanines often reduced in number (three to four as in *Hofmeyria*) or absent.

Occurrence—Wuchiapingian *Pristerognathus* through lower *Dicynodon* AZs, Upper Permian, Karoo Basin, South Africa.

Remarks—Hofmeyriidae was established by Hopson and Barghusen (1986) to include *Ictidostoma* and *Hofmeyria* together as a basal family of eutherocephalians. *Mirotenthes* was soon added to this list (van den Heever, 1987). The relatively basal position of hofmeyriids among eutherocephalians was supported originally by the primitive retention of paired vomers and a postfrontal, although later investigation failed to recognize these features in most specimens (Hopson and Barghusen, 1986). For example, the postfrontal is present on one side of the skull of the holotype of *Hofmeyria*, but is absent in referred specimens and is therefore polymorphic. An undescribed specimen (SAM-PK-K8516) from the Teekloof Formation of South Africa (lower *Cistecephalus* AZ) likely represents a new, aberrant species belonging to this family (Sidor et al., 2013) and was included in the present phylogenetic analysis.

Whaitsiidae Haughton, 1918

Composition—*Theriognathus microps* Owen, 1876; *Ictidochampsa platyceps* Broom, 1948; *Moschowhaitsia vjuschkovi* Tatarinov, 1963; *Viatkosuchus sumini* Tatarinov, 1995a.

Definition—All eutherocephalians sharing a more recent common ancestry with *Theriognathus microps* than with *Ictidostoma hemburyi* or *Bauria cynops*.

Revised diagnosis—Medium-to-large eutherocephalians with median frontonasal crest (also in *Chthonosaurus* and akidnognathids); specialized vomer anterolateral processes sutured to maxillary crista choanalis at level of canine, dividing choana into anterior and posterior portions; suborbital vacuities reduced in size or absent; prefrontal and postorbital nearly contact, restricting contribution of frontal to dorsal border of orbit; epipterygoid extremely expanded anteroposteriorly (more so than hofmeyriids); epipterygoid posterior apophysis forms specialized "trigeminal notch"; pterygoid boss teeth may be absent (but present in *Viatkosuchus*); dentary lateral surface smooth, lacking longitudinal furrow or trough (condition uncertain in *Ictidochampsa*).

Occurrence—Wuchiapingian upper *Tropidostoma*, *Cistecephalus*, and lower *Dicynodon* AZs, Upper Permian, Karoo Basin, South Africa; Wuchiapingian *Cistecephalus* AZ-equivalent, Upper Permian, Ruhuhu Basin, Tanzania; Wuchiapingian *Cistecephalus* AZ-equivalent, Upper Permian, Luangwa Basin, Zambia; Wuchiapingian, Upper Permian, Kotelnich, Kirov region, Russia; Changxingian *Archosaurus* AZ, Upper Permian, Vladimir region, Russia.

Remarks—Whaitsiidae Haughton (1918) was a diverse group that also previously accommodated several forms now recognized as akidnognathids (e.g., *Promoschorhynchus*; Brink, 1954). Several southern African genera from the *Cistecephalus* and *Dicynodon* AZs lacking postcanine teeth have since been synonymized with *Theriognathus* Owen (= *Whaitsia*, *Alopecopsis*, *Notosollasia*, *Hyenosaurus*, *Moschorhynchus*, *Notaelurops*, *Aneugomphius*) (e.g., Mendrez, 1974b; Brink, 1980). *Theriognathus* is thusly the best-represented genus, with abundant occurrences in South Africa and isolated records in Tanzania and, more recently, Zambia (Sidor et al., 2013). To this family can be added two Russian forms previously placed in Moschowhaitsiidae (Tatarinov, 1995a): *Viatkosuchus* from the Wuchiapingian Kotelnich locality, Russia, and *Moschowhaitsia* from the Changxingian Vyazniki-1 locality (*Archosaurus* AZ), Russia. The existence of Russian and South African forms mirrors the geographically widespread pattern seen in other groups by the Wuchiapingian (e.g., akidnognathids). Other South African forms may represent early diverging members of this group, including *Ictidochampsa* Broom (1948) and a new, undescribed whaitsiid represented by two partial skulls (SAM-PK-K10984 and K10990) from the Teekloof Formation of South Africa (upper *Tropidostoma* AZ).

BAURIOIDEA Broom, 1911

Ictidosuchidae Broom, 1903

Composition—*Ictidosuchus primaevus* Broom, 1900; *Ictidosuchoides longiceps* (Broom, 1920)

Definition—All eutherocephalians sharing a more recent common ancestry with *Ictidosuchus primaevus* than with *Theriognathus microps* or *Bauria cynops*.

Revised diagnosis—Medium sized eutherocephalians with a long, narrow rostrum; pterygoid boss teeth present; one to two diminutive upper precanine teeth, anteriorly-tilted and situated in a sinuous, concave precanine 'step'; postcanines eight to ten in number; postcanines short and conical with faint longitudinal striations (deep striae in *Ictidosuchus*; also present in *Akidnognathus*); dentary coronoid process tall, extending at least to mid- to upper portion of orbit. A plesiomorphic feature shared by *Ictidosuchus* and *Ictidosuchoides* but lost in other baurioids is the moderately developed crista choanalis lacking a connection to the vomer.

Occurrence—Wuchiapingian *Pristerognathus*, *Tropidostoma*, *Cistecephalus*, and lower *Dicynodon* AZs, and Changxingian upper *Dicynodon* AZ, Upper Permian, Karoo Basin, South Africa.

Remarks—Only two species are herein recognized within the Ictidosuchidae: *Ictidosuchus primaevus*, which was restricted to the Wuchiapingian *Tropidostoma* AZ in South Africa, and *Ictidosuchoides longiceps* (originally *'Ictidosuchus' longiceps*; Broom, 1920) which is the most common baurioid throughout the Upper Permian of South Africa, spanning *Pristerognathus* through *Dicynodon* AZs. *I. longiceps* was moved to the

genus *Ictidosuchoides* by Broom (1931). Both are distinguished from *Ictidosuchops* by the few diagnostic characters listed above and shared plesiomorphies, including a continuous, undivided choana that is unobstructed by adjoining vomerine processes of the secondary palate. *Olivierosuchus parringtoni* (previously *Olivieria*) was originally considered an ictidosuchid (Brink, 1965), but has since been allied with the Akidnognathidae (Kitching, 1977; Sidor, 2001; Kammerer and Sidor, 2002; Huttenlocker, 2009; Huttenlocker et al., 2011b; Botha-Brink and Modesto, 2011). *Karenites* was also originally considered an ictidosuchid (Tatarinov, 1995b), but has since been moved to its own monotypic family (Tatarinov, 1997; Ivakhnenko, 2011). *Silphoictidoides ruhuhuensis* (von Huene, 1950) from the Upper Permian Ruhuhu Basin in Tanzania might belong to Ictidosuchidae or may be conspecific with one of its existing species (e.g., *Ictidosuchoides longiceps*), but apomorphic features are uncertain and the material has not been restudied since its original description in 1950.

Ictidosuchopidae Hopson and Barghusen, 1986

Composition—*Ictidosuchops rubidgei* Broom, 1938.

Definition—All eutherocephalians sharing a more recent common ancestry with *Ictidosuchops rubidgei* than with *Ictidosuchus primaevus* or *Bauria cynops*.

Revised diagnosis—Small-to-medium sized eutherocephalians with stout rostrum; continued expansion of the crista choanalis, just contacting the anterior process

of the vomer without sutural connection and dividing the choana into anterior and posterior portions; pterygoid boss teeth present; six fluted upper incisors; upper precanines one to two in number; upper postcanines seven to eight in number.

Occurrence—Wuchiapingian upper *Cistecephalus* and lower *Dicynodon* AZs, Upper Permian, Karoo Basin, South Africa.

Remarks—*Ictidosuchops rubidgei* was initially described as a new species of *Ictidosuchoides* (Broom, 1937), but later moved to a new genus, *Ictidosuchops*, by Broom (1938). Other forms were subsequently added to the genus *Ictidosuchops*, including *I. intermedius* (Crompton, 1955; Brink, 1960) and *I. baurioides* (Broom, 1940; Brink, 1960). These specimens are predominantly dorsoventrally compressed, thereby giving their skulls a superficially broader appearance in dorsal view (personal observations). The rudimentary development of the crista choanalis and aspects of the dentition, including two small precanines situated within a concave diastema, suggest that "*Ictidosuchops" intermedius* is likely a junior synonym of *Ictidosuchoides longiceps*, and therefore invalid. The type species, *Ictidosuchops rubidgei*, can be differentiated from other small baurioids by the combination of six fluted upper incisors, one to two upper precanines, seven to eight postcanines, pterygoid boss teeth, and continued expansion of the crista choanalis which just contacts the anterior process of the vomer and divides the choana into anterior and posterior portions. Unlike the more derived non-ictidosuchopid baurioids, however, this connection is not sutural and the maxilla does not contact the premaxilla vomerine process along the medial border of the anterior choana/lower canine

fossa. The medial border of the lower canine fossa is therefore still partially formed by the vomer.

Regisauridae Hopson and Barghusen, 1986

Composition—*Urumchia lii* Young, 1952; *Regisaurus jacobi* Mendrez, 1972.

Definition—All eutherocephalians sharing a more recent common ancestry with *Regisaurus jacobi* than with *Ictidosuchops rubidgei* or *Bauria cynops*.

Revised diagnosis—Small-to-medium sized eutherocephalians with large, dorsally oriented orbits; interparietal region anteroposteriorly short; very sharp mastoid process formed by squamosal and opisthotic (also in karenitids and lycideopids); crista choanalis expanded, contacting the anterior process of the vomer with a short sutural connection (also in *Scaloposaurus* and *Nothogomphodon*); pterygoid teeth present on raised tuberosity; dentary lateral surface smooth, lacking longitudinal furrow or trough (also in hofmeyriids, whaitsiids, and *Lycideops*).

Occurrence—Induan *Lystrosaurus* AZ, Lower Triassic, Karoo Basin, South Africa; Induan or Olenekian *Lystrosaurus* AZ-equivalent Jiucaiyuan Formation, Lower Triassic, Junggar Basin, northwest China.

Remarks—*Urumchia* from the Lower Triassic Jiucaiyan Formation of China was originally placed in the family ‘Alopecopsidae’ (Young, 1952), but, following the discovery of *Regisaurus* Mendrez (1972), was later allied to Regisauridae of Hopson and

Barghusen (1986) based on the structure of the rudimentary secondary palate (Sun, 1991). The holotype of *Urumchia* is currently lost, replaced by a plastotype (Sun, 1991). *Regisaurus jacobi* was described by Mendrez (1972) based on a moderately-sized adult specimen, but other smaller presumably juvenile specimens have also been attributed to Regisauridae (Kemp, 1986). The holotype of *Scalopolacerta hoffmanni* may be one such example (Crompton, 1955; Mendrez-Carroll, 1979) as it lacks a pineal foramen as in *Regisaurus* (contrasting with *Scaloposaurus*) and the dentary bears a smooth lateral surface. Other small baurioids from the *Lystrosaurus* AZ may be allied to the Regisauridae as well (e.g., BP/1/5898 from Barendskraal, Eastern Cape, South Africa; Damiani et al., 2003). The group is restricted to the Lower Triassic *Lystrosaurus* AZ of South Africa and equivalent beds in China.

Karenitidae Tatarinov, 1997

Composition—*Karenites ornamentatus* Tatarinov, 1995b.

Definition—All eutherocephalians sharing a more recent common ancestry with *Karenites ornamentatus* than with *Lycideops longiceps* or *Bauria cynops*.

Revised diagnosis—Small-to-medium sized eutherocephalians with long, slender rostrum; slender upper canine; pineal foramen reduced, but usually present; pterygoid

boss teeth present; dentary angle boss present (‘supporting platform’ of Tatarinov, 1995b) (also present in *Choerosaurus* in modified form).

Occurrence—Wuchiapingian, Upper Permian, Kotelnich, Kirov region, Russia; Wuchiapingian *Cistecephalus* AZ-equivalent, Upper Permian, Luangwa Basin, Zambia.

Remarks—*Karenites* was described from the Wuchiapingian Kotelnich locality of Russia by Tatarinov (1995b) and recognized as an ictidosuchid baurioid. Later, Tatarinov (1999) described more complete specimens of a new taxon, *Scalopodon tenuisfrons,* from the same locality, and allied it to the Scaloposauridae. However, Ivakhnenko (2011) regarded *Scalopodon* as a junior synonym of *Karenites* and placed the revised taxon in its own monotypic family: Karenitidae (Tatarinov, 1997). Completeness of the material indicated a reduced pineal foramen and a unique dentary ‘platform’ or boss. A new specimen from the Upper Permian Madumabisa mudstone of the Luangwa Basin in Zambia (NHCC LB44) shares these features, suggesting the presence of the family in Gondwana (Sidor et al., 2013). The well-preserved specimen is included in the present phylogenetic analysis, but awaits formal description and is therefore designated only by its voucher number. The stratigraphic range of Karenitidae is restricted to the Wuchiapingian global standard stage in Russia and *Cistecephalus* AZ-equivalent deposits in the Luangwa Basin, Zambia.

Lycideopidae Boonstra, 1934

Composition—*Choerosaurus dejageri* Haughton, 1929; *Lycideops longiceps* Broom, 1931; *Tetracynodon tenuis* Broom and Robinson, 1948; *Tetracynodon darti* Sigogneau, 1963.

Definition—All eutherocephalians sharing a more recent common ancestry with *Lycideops longiceps* than with *Karenites ornamentatus* or *Bauria cynops*.

Revised diagnosis—Small-to-medium sized eutherocephalians with very long, narrow rostrum (anterior border of orbit being situated behind midline of skull); nasal-lacrimal suture present (as in cynodonts); zygomatic arch relatively straight and narrow (rather than strongly concave ventrally as in other therocephalians); long sutural connection between palatal processes of the maxilla and vomer forming an incipient secondary palate; parietal foramen absent throughout ontogeny (also in *Regisaurus*, *Ericiolacerta*, and *Bauria*); pterygoid boss teeth usually present (but absent in *Tetracynodon*); dentary long and gently curved, having a low coronoid process that extends dorsally only just above the surangular, and terminating below the middle of the orbit even in large individuals (also in *Scaloposaurus*); reflected lamina of angular reduced (also in *Ericiolacerta*); lower incisors number five or more.

Occurrence—Wuchiapingian *Tropidostoma*, and lower *Dicynodon* AZs (not currently known from the *Cistecephalus* AZ), Changxingian upper *Dicynodon* AZ (Upper Permian), and Induan *Lystrosaurus* AZ (Lower Triassic), Karoo Basin, South Africa.

Remarks—Kammerer (2008) considered the small-bodied *Tetracynodon tenuis* a subjective junior synonym of *Lycideops longiceps*, making the genus name *Tetracynodon* invalid. It was suggested that the Permian species of *Tetracynodon*, *T. tenuis,* was a juvenile of *Lycideops*, and that Triassic representatives of the genus (i.e., *T. darti*) were erroneously placed in this taxon due to shared juvenile characteristics or symplesiomorphies. Although *Lycideops* and *Tetracynodon* share several characteristics, including an elongated snout and nasal-lacrimal contact, the generality of these characters is only informative at the family-level (i.e., they are synapomorphies of Lycideopidae). Other features of the two *Tetracynodon* species include the relatively flat structure of the pterygoids (lacking parasagittal processes that usually contact the para-basisphenoid), absence of pterygoid boss teeth, and high antecanine tooth count, constituting a unique combination of features that conflict with assignment to *Lycideops* and instead support the traditional view (Sigurdsen et al., 2012). Four species of Lycideopidae are thus recognized: *Lycideops longiceps, Choerosaurus dejageri, T. tenuis,* and *T. darti*. *Tetracynodon* is consequently recognized here as a Permian-Triassic boundary-crossing lineage as is traditionally accepted.

Scaloposauridae Broom, 1914

Composition—*Scaloposaurus constrictus* Owen, 1876.

Definition—All eutherocephalians sharing a more recent common ancestry with *Scaloposaurus constrictus* than with *Lycideops longiceps* or *Bauria cynops*.

Revised diagnosis—Small baurioid eutherocephalians with constricted rostrum behind canine; pineal foramen present; short sutural connection between palatal processes of the maxilla and vomer forming an incipient secondary palate (also in regisaurids and *Nothogomphodon*); pterygoid boss teeth absent; upper canines well developed and usually two in number; lower canine bears longitudinal striations; upper postcanines nine to eleven in number; lower postcanines may be tricuspid toward back of row, bearing weak anterior and posterior accessory cusps.

Occurrence—Induan *Lystrosaurus* AZ, Lower Triassic, Karoo Basin, South Africa.

Remarks—Scaloposauridae is frequently regarded as a wastebasket taxon of juvenile therocephalians belonging to different groups (e.g., Hopson and Barghues, 1986; Kemp, 1986). *Scaloposaurus constrictus* was redescribed by Mendrez-Carroll (1979) who recognized it as a valid species. However, '*Scaloposaurus' hoffmani* Crompton (1955) was moved to a new genus, *Scalopolacerta*, based on differences in the palate and absence of the pineal foramen. '*S.' hoffmani* may be a juvenile *Regisaurus*, but a formalized synonymy awaits more complete material and better growth series. *Nanicticephalus* Broom (1940), also attributed to Scaloposauridae by Mendrez-Carroll (1979), is based on a small, crushed skull with little apomorphic information and should be regarded as a nomen dubium. The Scaloposauridae is herein revised to include only

the type genus *Scaloposaurus*, and is therefore monotypic. The provenance of the type specimen of *Scaloposaurus* (NHMUK R1723) has been sourced variably to the *Cistecephalus* or *Lystrosaurus* AZ of the Sneeuwberg Range, South Africa (e.g., Mendrez-Carroll, 1979), but subsequent collecting suggests that the taxon's range is restricted to the Lower Triassic Katberg Formation (*Lystrosaurus* AZ) in South Africa (Smith and Botha, 2005; Botha and Smith, 2006).

Ericiolacertidae Watson and Romer, 1956

Composition—*Ericiolacerta parva* Watson, 1931; *Silphedosuchus orenburgensis* Tatarinov, 1977.

Definition—All eutherocephalians sharing a more recent common ancestry with *Ericiolacerta parva* than with *Scaloposaurus constrictus* or *Bauria cynops*.

Revised diagnosis—Small baurioid eutherocephalians with short, stout rostrum; pineal foramen absent; maxillae joined anteriorly at midline on palatal surface, covering the anteriormost portion of the vomer in palatal view (also in ordosiids and to a greater extent in bauriids); pterygoid boss teeth absent; lower incisors highly procumbent; upper and lower caniniform teeth reduced or absent; upper and lower postcanines tall and cylindrical with accessory cuspules.

Occurrence—Induan *Lystrosaurus* AZ, Lower Triassic, Karoo Basin, South Africa; Induan *Lystrosaurus* AZ-equivalent, Lower Triassic, Shackleton Glacier, Transantarctic Mountains; Induan, Lower Triassic, Orenburg region, Russia.

Remarks—Watson (1931) originally allied *Ericiolacerta* with Scaloposauridae before placing it in a new family of its own, Ericiolacertidae Watson and Romer (1956). Ericiolacertidae has since been followed by other authors (Mendrez, 1975; Mendrez-Carroll, 1979; Hopson and Barghusen, 1986). Although it was long represented only by the type specimen from near Harrismith, South Africa (Lower Triassic *Lystrosaurus* AZ), Colbert and Kitching (1981) reported a new fragmentary specimen of *Ericiolacerta* from the lower Fremouw Formation of Antarctica. This assignment was supported by Huttenlocker and Sidor (2012) who reviewed the material using an apomorphy-based approach. *Silphedosuchus* Tatarinov (1977) from the Lower Triassic of the Orenburg region of Russia is also referable to this group (Battail and Surkov, 2000; Ivakhnenko, 2011). The stratigraphic range of Ericiolacertidae is restricted to the Lower Triassic *Lystrosaurus* AZ in South Africa and equivalent strata in Antarctica and Russia.

Nothogomphodontidae Tatarinov, 1974

Composition—*Nothogomphodon danilovi* Tatarinov, 1974.

Definition—All eutherocephalians sharing a more recent common ancestry with *Nothogomphodon danilovi* than with *Ericiolacerta parva* or *Bauria cynops*.

Revised diagnosis—Small baurioid eutherocephalians with short, stout rostrum; pineal foramen absent; short sutural connection between palatal processes of the maxilla and vomer forming an incipient secondary palate (also in regisaurids and *Scaloposaurus*); pterygoid boss teeth absent; upper and lower canines long, cylindrical; upper and lower postcanines mediolaterally compressed with narrow neck and denticulated cutting edges.

Occurrence—Anisian, Middle Triassic, Orenburg region, Russia.

Remarks—Tatarinov (1974) established Nothogomphodontidae, which he allied with Ericiolacertidae and Bauriidae. Its only representative was *Nothogomphodon danilovi,* a single specimen consisting of a partial skull and dentary from Middle Triassic (Anisian) rocks of the Orenburg region, Russia. Ivakhnenko (2011) recently reviewed the material and suggested affinities to *Microgomphodon* (although he retained usage of the term 'Nothogomphodontidae').

Ordosiidae Hou, 1979

Composition—*Ordosiodon lincheyuensis* Young, 1961; *Ordosiodon* (=*Ordosia*) *youngi* Hou, 1979; *Hazhenia concava* Sun and Hou, 1981.

Definition—All eutherocephalians sharing a more recent common ancestry with *Ordosiodon youngi* than with *Nothogomphodon danilovi* or *Bauria cynops*.

Revised diagnosis—Small-to-medium sized baurioid eutherocephalians with long, low skull; pineal foramen absent; maxillae joined anteriorly at the midline, covering the anteriormost portion of the vomer (also in ericiolacertids); pterygoid boss teeth absent; rear postcanines slightly expanded transversely; postcanines bear a single, central cusp ringed by smaller accessory cuspules.

Occurrence—Olenekian (Lower Triassic) through Anisian (Middle Triassic), Shanxi, Ordos Basin, northern China.

Remarks—*Ordosiodon* was originally described from a partial dentary with transversely expanded teeth recovered from the Middle Triassic of northwest Shanxi (Ordos Basin, China), and assigned to the cyndont group Diademodontidae (Young, 1961). More complete material collected from the red marl of the Middle Triassic Ermaying Formation (Anisian) was described as '*Ordosia' youngi* and placed in its own family: Ordosiidae Hou (1979). *Hazhenia* Sun and Hou (1981) was discovered approximately 30 kilometers from the type locality of '*Ordosia*' (though much lower in section where it co-occurred with the pseudosuchian *Xilousuchus*) and was added to the Ordosiidae. Most recently, Sun (1991) revised the composition of the group by recognizing *Ordosiodon* as a member and transferring '*Ordosia' youngi* to the former genus, thereby abandoning use of the name '*Ordosia'* (*Ordosia* Lu, 1954 was also preoccupied by a trilobite). The stratigraphic range of Ordosiidae spans from the Olenekian (Lower Triassic) through Anisian (Middle Triassic) of northern China.

Bauriidae Broom, 1911

Composition—*Microgomphodon oligocynus* Seeley, 1895; *Bauria cynops* Broom, 1909; *Antecosuchus ochevi* Tatarinov, 1973; *Traversodontoides wangwuensis* Young, 1974.

Definition—All eutherocephalians sharing a more recent common ancestry with *Bauria cynops* than with *Ordosiodon youngi* or *Nothogomphodon danilovi*.

Revised diagnosis—Small-to-medium sized baurioid eutherocephalians with short, stout rostrum; squamosal with posterior V-shaped notch in occipital view; pineal foramen may be present as in *Microgomphodon* and *Traversodontoides* (but absent in *Bauria*); maxillae joined broadly at the midline on the palatal surface, nearly covering the entire vomer in palatal view; pterygoid boss teeth absent; dentary strongly curved with a well-defined oblique line; dentary symphysis thickened with strong suture; dentary lateral surface bears marked constriction where upper canine rests behind lower canine (also in some akidnognathids); upper canines reduced in size; postcanines transversely expanded with broad grinding surface between two transversely arranged cusps; angular reflected lamina enlarged (also in some earlier baurioids).

Occurrence—Olenekian (Lower Triassic) through Anisian (Middle Triassic) *Cynognathus* AZ, Karoo Basin, South Africa; Anisian *Cynognathus* AZ-equivalent Omingonde Formation, Waterberg region, Namibia; Anisian, Middle Triassic, Orenburg region, Russia; Anisian, Middle Triassic, Henan, Ordos Basin, northern China.

Remarks—A number of Middle Triassic bauriid genera were recognized in southern Africa based on variations in size, postcanine number, build of the postorbital bar, and presence or absence of a pineal foramen (Broom, 1911; Brink, 1963, 1986). However, the species composition of southern African bauriids was revised by Abdala (in press), who recognized only two Gondwanan forms: *Microgomphodon oligocynus* Seeley (= *Herpetogale*, *Melinodon*, *Sesamodon*, *Watsoniella*) and *Bauria cynops* Broom (= *Aelurosuchus*, *Baurioides*, *Sesamodontoides*). The former is known from the Lower and Middle Triassic *Cynognathus* AZ of South Africa (Burgersdorp Formation) and Namibia (Omingonde Formation), whereas the latter is known only from the Middle Triassic *Cynognathus* subzone B of South Africa. Records outside southern Africa are more rare, but are documented in the Middle Triassic of Russia (*Antecosuchus*) and China (*Traversodontoides*). Both *Antecosuchus* (= *Neotrirachodon*) and *Traversodontoides* were originally misidentified as gomphont cynodonts (Tatarinov, 1973, 1974; Young, 1974). Battail and Surkov (2000) correctly placed *Antecosuchus* within Bauriidae, which was followed by Ivakhnenko (2011). *Traversodontoides* was originally regarded as a traversodontid (Young, 1974), but further preparation of the palate and exposure of suborbital vacuities revealed its identity as a bauriid therocephalian (Sun, 1981, 1991).

Table 1.1. Higher-level taxonomy of Therocephalia followed in this dissertation (based on Hopson and Barghusen, 1986; van den Heever, 1987, 1994; Huttenlocker, 2009; Huttenlocker et al., 2011b; and Sigurdsen et al., 2012).

THERAPSIDA Broom, 1905		
EUTHERIODONTIA Hopson and Barghusen, 1986		
THEROCEPHALIA Broom, 1903		
	Lycosuchidae Nopsca, 1923	
	Lycosuchus	(= *Hyaenosuchus, Scymnosaurus?, Trochorhinus?, Trochosaurus?, Trochosuchus?, Zinnosaurus*)
	SCYLACOSAURIA van den Heever, 1994	
	Scylacosauridae Broom, 1903	
	Alopecodon	
	Glanosuchus	(= *Alopecognathus, Pristerognathoides, Walteria, Karroowalteria*)
	Ictidosaurus	
	Pardosuchus	
	Pristerognathus	(= *Ptomalestes*)
	Scylacosaurus	(= *Scylacorhinus, Therioides*)
	EUTHEROCEPHALIA Hopson and Barghusen, 1986	
	Scylacosuchidae Ivakhnenko, 2011	
	Scylacosuchus	
	Perplexisauridae Tatarinov, 2000	
	Perplexisaurus	(= *Chlynovia*)
	Chthonosauridae Tatarinov, 1974	
	Chthonosaurus	
	Akidnognathidae Nopsca, 1928	
	Annatherapsidus	(= *Anna*)
	Akidnognathus	(= *Pelictosuchus, Proalopecopsis*)
	Promoschorhynchus	(= *Notaelurodon*?)
	Olivierosuchus	(= *Olivieria*)
	Euchambersia	
	Cerdosuchoides	(= *Cerdops, Hewittia*)
	Moschorhinus	(= *Tigrisuchus*?)
	UNNAMED CLADE	
	Hofmeyriidae Hopson and Barghusen, 1986	
	Hofmeyria	
	Ictidostoma	(= *Ictidognathus*)
	Mirotenthes	

Table 1.1. (Continued)

Whaitsiidae Haughton, 1918	
Ictidochampsa	
Viatkosuchus	
Moschowhaitsia	(= *Hexacynodon?*)
Theriognathus	(= *Whaitsia, Alopecopsis, Notosollasia, Hyenosaurus, Moschorhynchus, Notaelurops, Aneugomphius*)
BAURIOIDEA Broom, 1911 (= ICTIDOSUCHOIDEA Brink, 1963)	
Ictidosuchidae Broom, 1903	
Ictidosuchoides	(= *Ictidodraco*)
Ictidosuchus	
Ictidosuchopidae Hopson and Barghusen, 1986	
Ictidosuchops	
Regisauridae Hopson and Barghusen, 1986	
Regisaurus	
Urumchia	
Karenitidae Tatarinov, 1997	
Karenites	(= *Scalopodon*)
Lycideopidae Boonstra, 1934	
Choerosaurus	
Lycideops	
Tetracynodon	
Scaloposauridae Broom, 1914	
Scaloposaurus	
Ericiolacertidae Watson and Romer, 1956:	
Ericiolacerta	
Silphedosuchus	
Nothogomphodontidae Tatarinov, 1974:	
Nothogomphodon	
Ordosiidae Hou, 1979	
Hazhenia	
Ordosiodon	(= *Ordosia*)
Bauriidae Broom, 1911	
Antecosuchus	(= *Neotrirachodon*)
Bauria	(= *Aelurosuchus, Baurioides, Sesamodontoides*)
Microgomphodon	(= *Herpetogale, Melinodon, Sesamodon, Watsoniella*)
Traversodontoides	

Table 1.1. (Continued)

Therocephalia incertae sedis:	
Alopecorhinus	indet. basal therocephalian
Blattoidealestes	indet. scylacosaurid juvenile
Cerdodon	indet. basal therocephalian
Cerdosuchus	holotype lost
Crapartinella	indet. scylacosaurid juvenile?
Cynariognathus	indet. scylacosaurid
Dongusaurus	indet. ordosiid or bauriid?
Homodontosaurus	indet. lycideopid juvenile?
Hyorhynchus	indet. scylacosaurid
Icticephalus	indet. eutherocephalian
Ictidodon	indet. baurioid
Ictidoparia	holotype lost; scylacosaurid juvenile?
Kotelcephalon	indet. chthonosaurid?
Lycedops	indet. scylacosaurid
Macroscelesaurus	indet. baurioid
Malasaurus	invalid (not therocephalian?)
Maraisaurus	indet. scylacosaurid
Nanicticephalus	indet. lycideopid juvenile?
Nanictidops	indet. akidnognathid juvenile?
Pedaeosaurus	indet. baurioid juvenile
Polycynodon	indet. baurioid
Porosteognathus	indet. basal therocephalian?
Pristerosaurus	indet. scylacosaurid
Rhigosaurus	indet. baurioid juvenile
Scalopocephalus	indet. baurioid
Scalopodontes	indet. eutherocephalian (karenitid or chthonosaurid?)
Scalopognathus	indet. juvenile ordosiid or bauriid?
Scalopolacerta	baurioid juvenile (possible synonym of *Regisaurus*)
Scaloporhinus	indet. baurioid juvenile
Scaloposuchus	indet. baurioid juvenile
Silphoictidoides	Ictidosuchidae incertae sedis?
Simorhinella	indet. lycosuchid or scylacosaurid juvenile
Yikezhaogia	Akidnognathidae incertae sedis?
Zorillodontops	indet. akidnognathid juvenile?

* 119 named genera; 43 recognized as valid; ~36% taxonomic reduction

The stratigraphic range of Bauriidae spans from the Olenekian (Lower Triassic, *Cynognathus* subzone A and equivalent) through Anisian (Middle Triassic, *Cynognathus* subzone C and equivalent) global standard stages.

Phylogenetic Analysis

Rationale and Design

The proposed higher-level taxonomy is informed, at least in part, by a comprehensive reanalysis of the cladistic relationships of therocephalians (updated from Huttenlocker, 2009; Huttenlocker et al., 2011b; and Sigurdsen et al., 2012). I assembled a matrix of 135 craniodental and postcranial characters, and 56 taxa (54 ingroup taxa, including 49 therocephalians) with two outgroups (*Biarmosuchus* and *Titanophoneus*) chosen for the parsimony analysis. Following the method of Sereno (2007), previous character lists were corrected in some cases by arranging them into a set of individual "character statements" composed of an anatomical locator, variable and/or variable qualifier, and its respective character states. This formula was preferred to minimize ambiguity in character coding and improve data comparison. Six additional characters (chars. 130–135, Appendices 3, 4) and 22 new ingroup taxa were also analyzed. Previously studied therocephalian taxa included: *Lycosuchus vanderrieti*, *Glanosuchus macrops*, *Ictidosaurus angusticeps*, *Pristerognathus polyodon*, *Promoschorhynchus platyrhinus*, *Olivierosuchus parringtoni*, *Cerdosuchoides* (=*Cerdops*) *brevidens*, *Moschorhinus kitchingi*, *Hofmeyria atavus*, *Mirotenthes digitipes*, *Ictidostoma hemburyi*,

Viatkosuchus sumini, *Moschowhaitsia vjuschkovi*, *Theriognathus microps*, *Ictidosuchus primaevus*, *Ictidosuchoides longiceps*, *Ictidosuchops rubidgei*, *Regisaurus jacobi*, *Lycideops longiceps*, *Choerosaurus dejageri*, *Tetracynodon tenuis*, *Tetracynodon darti*, *Scaloposaurus constrictus*, *Ericiolacerta parva*, *Bauria cynops*, and *Microgomphodon oligocynus*.

New taxa analyzed to increase the breadth of phylogenetic and temporal sampling included: *Alopecodon priscus* (SAM-PK-920; AMNH 5569), *Pardosuchus whaitsi* (SAM-PK-1077), *Scylacosaurus sclateri* (SAM-PK-634; SAM-PK-11888), *Scylacosuchus orenburgensis* (Tatarinov, 1974; Ivakhnenko, 2011), *Perplexisaurus foveatus* (Tatarinov, 1997; Ivakhnenko, 2011), *Chthonosaurus velocidens* (PIN 521/1), a new Zambian chthonosaurid (NHCC LB36, 38), *Annatherapsidus petri* (Tatarinov, 1974; Ivakhnenko, 2011), a new *Cistecephalus* AZ akidnognathid (USNM PAL412421), *Akidnognathus parvus* (SAM-PK-4021; BP/1/499; BP/1/641), a new *Cistecephalus* AZ hofmeyriid (SAM-PK-K8516), *Ictidochampsa platyceps* (RC 69), a new *Tropidostoma* AZ whaitsiid (SAM-PK-K10990, K10984), *Urumchia lii* (Young, 1952; Sun, 1991), *Karenites ornamentatus* (Tatarinov, 1995b, 1999; Ivakhnenko, 2011), a new Zambian karenitid (NHCC LB44), *Silphedosuchus orenburgensis* (Battail and Surkov, 2000; Ivakhnekno, 2011), *Nothogomphodon danilovi* (Tatarinov, 1974; Ivakhnenko, 2011), *Hazhenia concava* (Sun and Hou, 1981; Sun, 1991), *Ordosiodon youngi* (Hou, 1979; Sun, 1991), *Antecosuchus ochevi* (Tatarinov, 1974; Ivakhnenko, 2011), and *Traversodontoides wangwuensis* (Sun, 1981; Sun, 1991).

The data were analyzed using the maximum parsimony criterion of PAUP 4.0 beta 10 (Swofford, 1999), and a Bayesian analysis in MrBayes v. 3.1.2 (Ronquist et al., 2009). In PAUP, I performed the analysis using the tree-bisection-reconnection branch-swapping algorithm with DELTRAN optimization. Initially, all characters were unordered and had equal weight. I then ran an ordered trial using the same parameters, but ordering characters 40, 43, and 57. In both unordered and ordered trials, multistate taxa were treated as polymorphisms. A heuristic search was performed using a random addition sequence with 100 replicates. A bootstrap analysis was also performed as an additional measure of clade support, using 1000 bootstrap replicates. The Bayesian analysis was performed using flat prior probabilities and standard settings (*Mk* model for morphological evolution; Lewis, 2001), running the analysis until the standard deviation of split frequencies fell below 0.01 (one million generations) and sampled every 100 generations. Analyses were ran with the gamma distribution parameter allowing variable character rates.

Phylogenetic Results

Results of ordered and unordered parsimony and Bayesian analyses agreed to large measure in their overall topology (Figs. 1.7, 1.8). The unordered parsimony analysis resulted in 90932 equally parsimonious trees of 412 steps (retention index = 0.788, consistency index = 0.487). Consensus trees showed support for monophyly of the traditional families recognized here and reviewed in the 'Systematic Paleontology,' although intra-relationships within some groups are not completely resolved (e.g.,

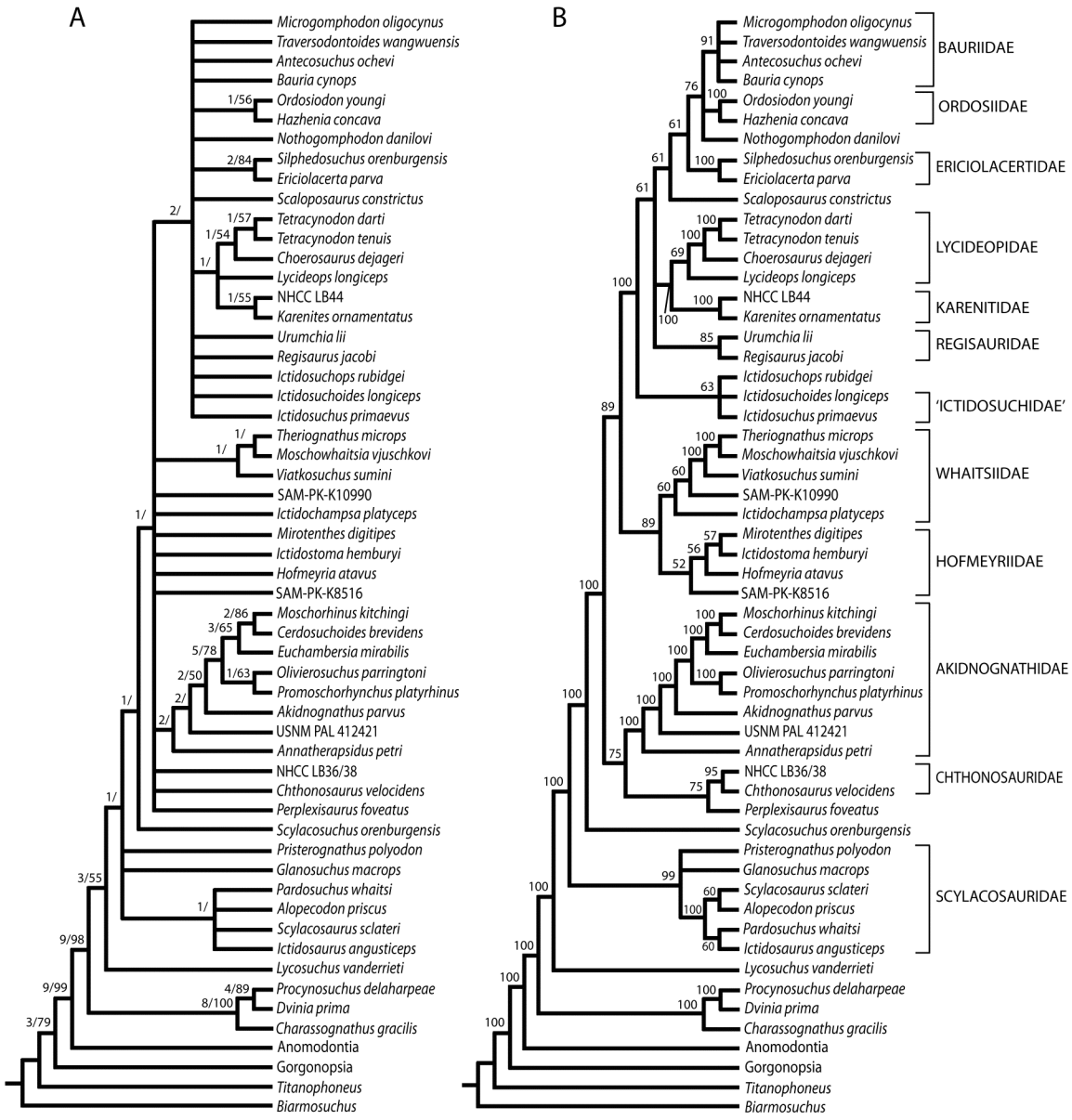

Figure 1.7. Hypothesis of the cladistic relationships of therocephalian eutheriodonts based on maximum parsimony. **A**, Strict consensus of most parsimonious trees. Numbers at nodes indicate Bremer support (left of virgule) and bootstrap values >50% (right of virgule). **B**, Majority rule consensus of most parsimonious trees. Numbers at nodes represent consensus indices. Tree length, 412 steps; retention index, 0.788; consistency index, 0.487.

scylacosaurids, bauriids) and the relative positions of other groups vary among subsampled trees (e.g., the inadequately known *Perplexisaurus* and chthonosaurids relative to other eutherocephalians). Nevertheless, higher-level groups are generally resolved with good character support (Appendix 5), including a monophyletic Therocephalia (sister to Cynodontia), Eutherocephalia, and Baurioidea. Within Baurioidea, subsampled trees varied in their polarities, with the positions of Lycideopidae and Bauriidae being somewhat volatile likely due to character state reversals in the latter group. Resolution within Baurioidea was therefore poor in the strict consensus, but the 50% majority rule consensus most frequently resolved bauriids in a deeply nested position within Baurioidea. This result was supported further by the ordered run, in which 156488 equally parsimonious trees of 421 steps (RI = 0.791, CI = 0.472) demonstrated a consensus topology in which the rudimentary crista choanalis (e.g., ictidosuchids) developed progressively toward a completely formed secondary palate in Triassic forms (e.g., ericiolacertids, ordosiids, and bauriids). This topology, in which bauriids occupy a deeply nested position within Baurioidea, has high stratigraphic congruence, as bauriids were also one of the last families to appear chronostratigraphically (late-Early to Middle Triassic).

Higher-Level Relationships of Therocephalia

Monophyly of Therocephalia—The concept of Therocephalia as a monophylum has been of great interest recently. Whereas some early authors (Brink, 1960a, 1965) suggested a link between ‘scaloposaurian’ therocephalians, ‘bauriamorphs’ and

Figure 1.8. Bayesian analysis of therocephalian eutheriodonts. One million generations were run, sampling every 100 generations, with the gamma distribution parameter for variable character rates. Numbered nodes (52-100) denote posterior probabilities.

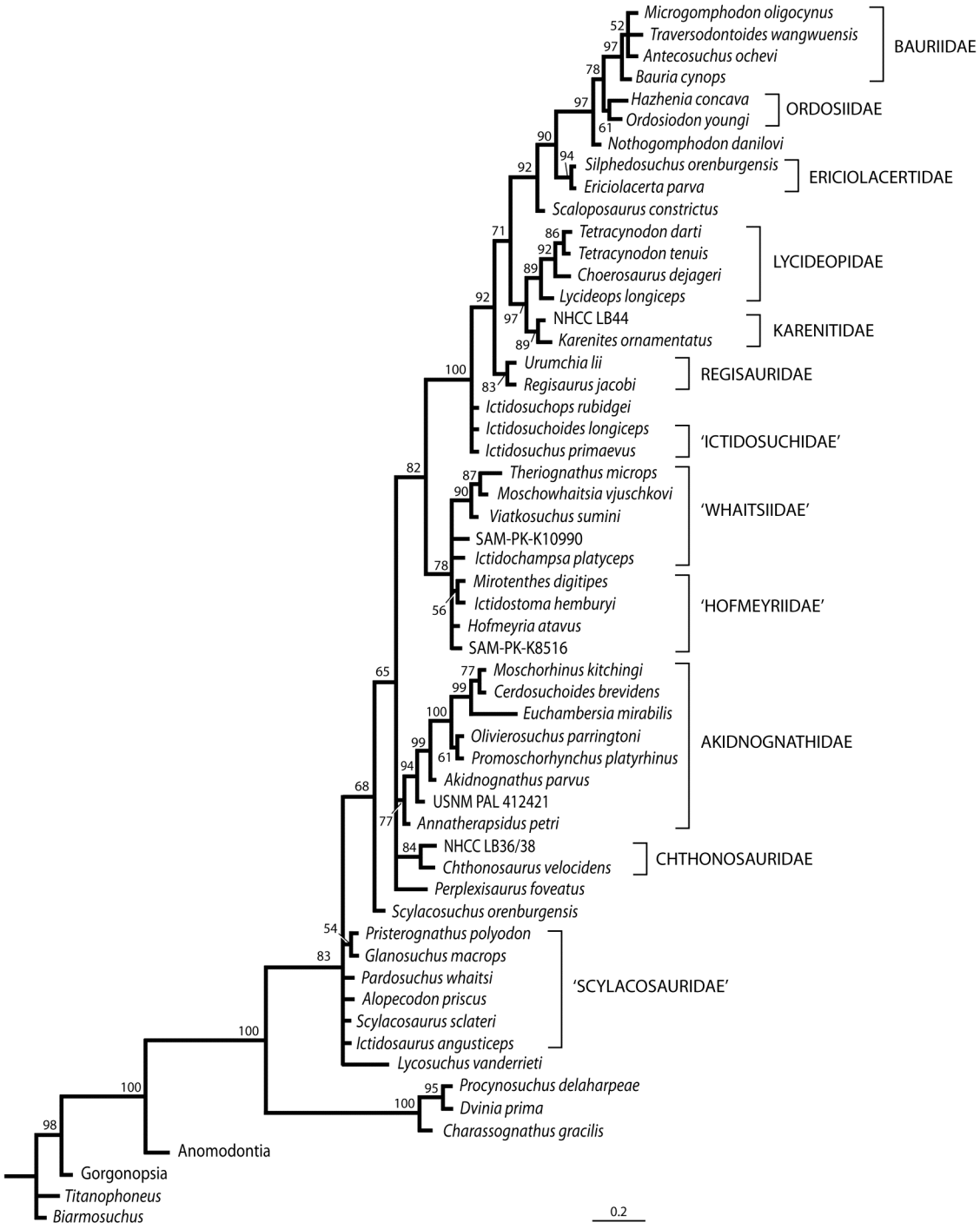
Microgomphodon oligocynus
Traversodontoides wangwuensis
Antecosuchus ochevi
Bauria cynops
BAURIIDAE
Hazhenia concava
Ordosiodon youngi
ORDOSIIDAE
Nothogomphodon danilovi
Silphedosuchus orenburgensis
Ericiolacerta parva
ERICIOLACERTIDAE
Scaloposaurus constrictus
Tetracynodon darti
Tetracynodon tenuis
Choerosaurus dejageri
Lycideops longiceps
LYCIDEOPIDAE
NHCC LB44
Karenites ornamentatus
KARENITIDAE
Urumchia lii
Regisaurus jacobi
REGISAURIDAE
Ictidosuchops rubidgei
Ictidosuchoides longiceps
Ictidosuchus primaevus
'ICTIDOSUCHIDAE'
Theriognathus microps
Moschowhaitsia vjuschkovi
Viatkosuchus sumini
SAM-PK-K10990
Ictidochampsa platyceps
'WHAITSIIDAE'
Mirotenthes digitipes
Ictidostoma hemburyi
Hofmeyria atavus
SAM-PK-K8516
'HOFMEYRIIDAE'
Moschorhinus kitchingi
Cerdosuchoides brevidens
Euchambersia mirabilis
Olivierosuchus parringtoni
Promoschorhynchus platyrhinus
Akidnognathus parvus
USNM PAL 412421
Annatherapsidus petri
AKIDNOGNATHIDAE
NHCC LB36/38
Chthonosaurus velocidens
CHTHONOSAURIDAE
Perplexisaurus foveatus
Scylacosuchus orenburgensis
Pristerognathus polyodon
Glanosuchus macrops
Pardosuchus whaitsi
Alopecodon priscus
Scylacosaurus sclateri
Ictidosaurus angusticeps
'SCYLACOSAURIDAE'
Lycosuchus vanderrieti
Procynosuchus delaharpeae
Dvinia prima
Charassognathus gracilis
Anomodontia
Gorgonopsia
Titanophoneus
Biarmosuchus
0.2

Figure 1.9. Summary cladogram of therocephalian relationships and names of major subclades followed in this study. Representative skulls shown to right of cladogram are drawn to scale.

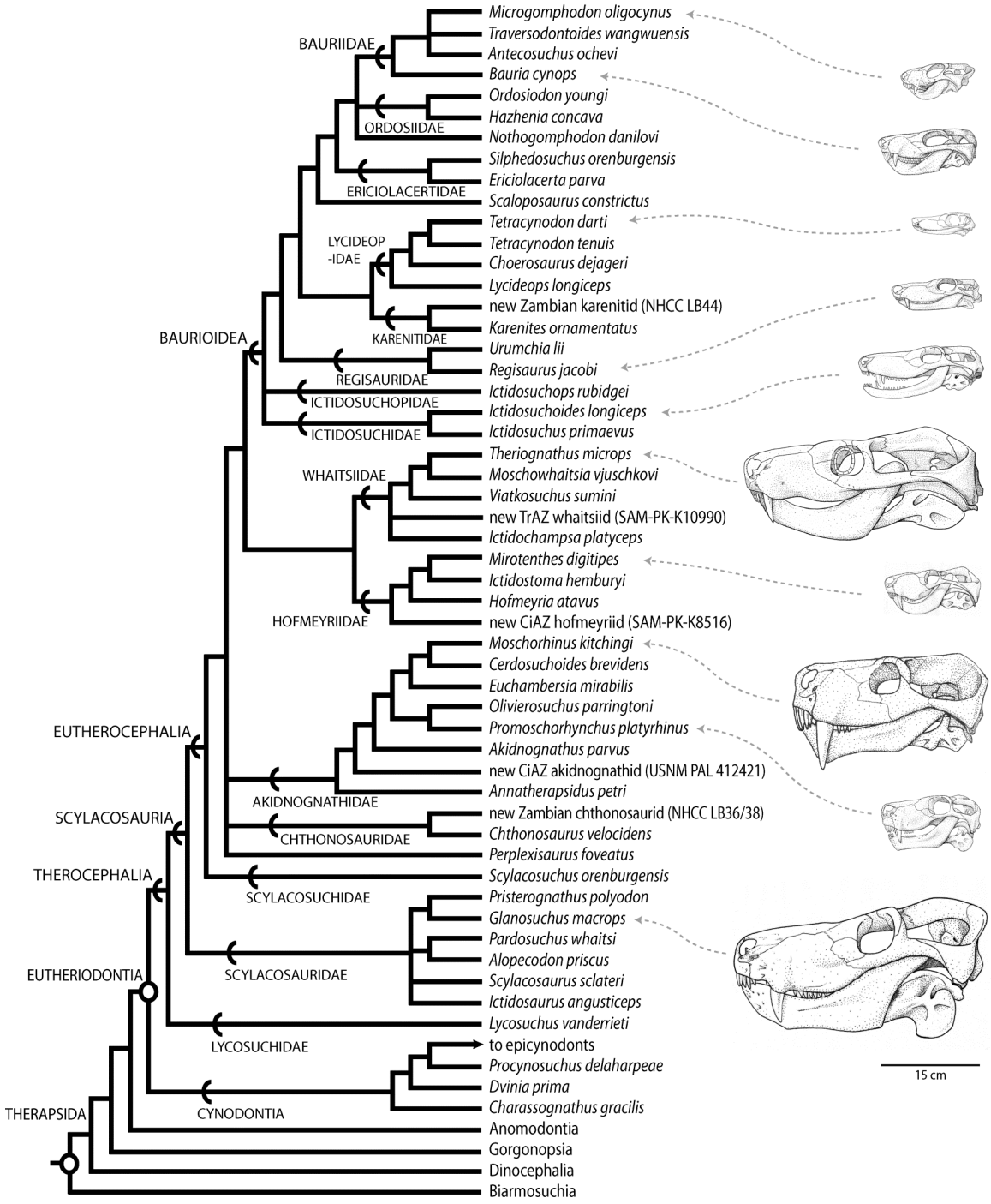
Microgomphodon oligocynus
Traversodontoides wangwuensis
Antecosuchus ochevi
Bauria cynops
Ordosiodon youngi
Hazhenia concava
Nothogomphodon danilovi
Silphedosuchus orenburgensis
Ericiolacerta parva
Scaloposaurus constrictus
Tetracynodon darti
Tetracynodon tenuis
Choerosaurus dejageri
Lycideops longiceps
new Zambian karenitid (NHCC LB44)
Karenites ornamentatus
Urumchia lii
Regisaurus jacobi
Ictidosuchops rubidgei
Ictidosuchoides longiceps
Ictidosuchus primaevus
Theriognathus microps
Moschowhaitsia vjuschkovi
Viatkosuchus sumini
new TrAZ whaitsiid (SAM-PK-K10990)
Ictidochampsa platyceps
Mirotenthes digitipes
Ictidostoma hemburyi
Hofmeyria atavus
new CiAZ hofmeyriid (SAM-PK-K8516)
Moschorhinus kitchingi
Cerdosuchoides brevidens
Euchambersia mirabilis
Olivierosuchus parringtoni
Promoschorhynchus platyrhinus
Akidnognathus parvus
new CiAZ akidnognathid (USNM PAL 412421)
Annatherapsidus petri
new Zambian chthonosaurid (NHCC LB36/38)
Chthonosaurus velocidens
Perplexisaurus foveatus
Scylacosuchus orenburgensis
Pristerognathus polyodon
Glanosuchus macrops
Pardosuchus whaitsi
Alopecodon priscus
Scylacosaurus sclateri
Ictidosaurus angusticeps
Lycosuchus vanderrieti
to epicynodonts
Procynosuchus delaharpeae
Dvinia prima
Charassognathus gracilis
Anomodontia
Gorgonopsia
Dinocephalia
Biarmosuchia
BAURIIDAE
ORDOSIIDAE
ERICIOLACERTIDAE
LYCIDEOP
-IDAE
KARENITIDAE
REGISAURIDAE
ICTIDOSUCHOPIDAE
ICTIDOSUCHIDAE
WHAITSIIDAE
HOFMEYRIIDAE
AKIDNOGNATHIDAE
CHTHONOSAURIDAE
SCYLACOSUCHIDAE
SCYLACOSAURIDAE
LYCOSUCHIDAE
CYNODONTIA
BAURIOIDEA
EUTHEROCEPHALIA
SCYLACOSAURIA
THEROCEPHALIA
EUTHERIODONTIA
THERAPSIDA
15 cm

cynodonts, thus nesting cynodonts within Therocephalia, Romer (1969) argued that the similarities between cynodonts and 'scaloposaurs' represent retentions of the plesiomorphic eutheriodont condition. Romer (1969) also argued that therocephalians possessed a number of shared derived features that exclude basal cynodonts from a therocephalian ancestry, a view that was adopted by Hopson and Barghusen (1986) in their cladistic analysis of Eutheriodontia. A few authors have advocated a sister group relationship between cynodonts and the whaitsiid therocephalian *Theriognathus*, largely based on the presence of an expanded epipterygoid ascending process and a quadrate notch in the squamosal (Kemp, 1972a; Abdala, 2007; Botha et al., 2007). The present analysis, however, supports a monophyletic Therocephalia with Cynodontia as its nearest sister group as represented frequently in the literature (Hopson and Barghusen, 1986; Hopson, 1991; van den Heever, 1994; Sidor and Hopson, 1998; Rubidge and Sidor, 2001).

Among therocephalians, *Lycosuchus* resolves as the basal sister group to all other taxa sampled in the analysis. Modest support from bootstrap resampling is likely due to the aberrant nature of *Lycosuchus* as well as homoplasic characters shared between cynodonts and scylacosaurians, rather than low character sampling for Therocephalia. *Lycosuchus* and other therocephalians share several unambiguous cranial synapomorphies, including: (1) zygomatic arch width greatest at back of arch (char. 35; Fig. 1.10); (2) vomer premaxillary process expands anteriorly and is widest at its contact with the premaxilla (char. 41); (3) suborbital vacuities bound by palatine, pterygoid, and

ectopterygoid (char. 46); (4) pterygoid ventromedian tubercle/crest present anterior to interpterygoid vacuity (char. 47); (5) pterygoid transverse flange expansion moderate with sharp posterolateral extension (char. 50); (6) opisthotic dorsolateral process present, contacting tabular/squamosal, thus excluding supraoccipital from post-temporal fenestra (char. 63); (7) stapes dorsal process reduced/absent (char. 74); (8) dentary ramus lateral groove present (char. 94); and (9) femur bears distinct trochanter minor (char. 122). The ilium anterior process and 'notch' (char. 118) has been cited as a diagnostic feature for Therocephalia (e.g., Kemp, 2005) and perhaps a useful synapomorphy (e.g., Huttenlocker, 2009; Huttenlocker et al., 2011b), but its presence is uncertain in *Lycosuchus*. As such, this feature should be considered a synapomorphy of the less inclusive group Scylacosauria (see below) until the hind limb girdle of *Lycosuchus* is more completely known.

Other Therocephalia synapomorphies are considered ambiguous due to their presence in other higher-level therapsid clades (and therefore ambiguous ancestral state optimizations at the split of major clades). These may include: concave ventral margin of suborbital and zygomatic arch (also present in anomodonts); palatal fenestra for lower caniniform confluent with internal naris (also present in gorgonopsians); splenial laterally obscured by dentary (either convergent in non-*Procynosuchus* cynodonts or plesiomorphic for Eutheriodontia with a reversal in *Procynosuchus*); and stapedial foramen absent (also in anomodonts). Additional postcranial characters were suggested as diagnostic by Fourie and Rubidge (2007) including: absence of an ectepicondylar

Figure 1.10. Dorsal skull roofs of selected therocephalians and other neotherapsids. **A**, gorgonopsian (modified from Kemp, 1969); **B**, basal cynodont *Procynosuchus* (modified from Kemp, 1979 and Hopson, 1991); **C**, akidnognathid eutherocephalian *Moschorhinus* (modified from Durand, 1991); **D**, hofmeyriid eutherocephalian *Mirotenthes* (based on UCMP 40467 and CGP-1-1264); **E**, baurioid eutherocephalian *Regisaurus* (modified from Mendrez, 1972). Skulls are not drawn to scale. Numbers represent important characters and character states from Appendices 3-5.

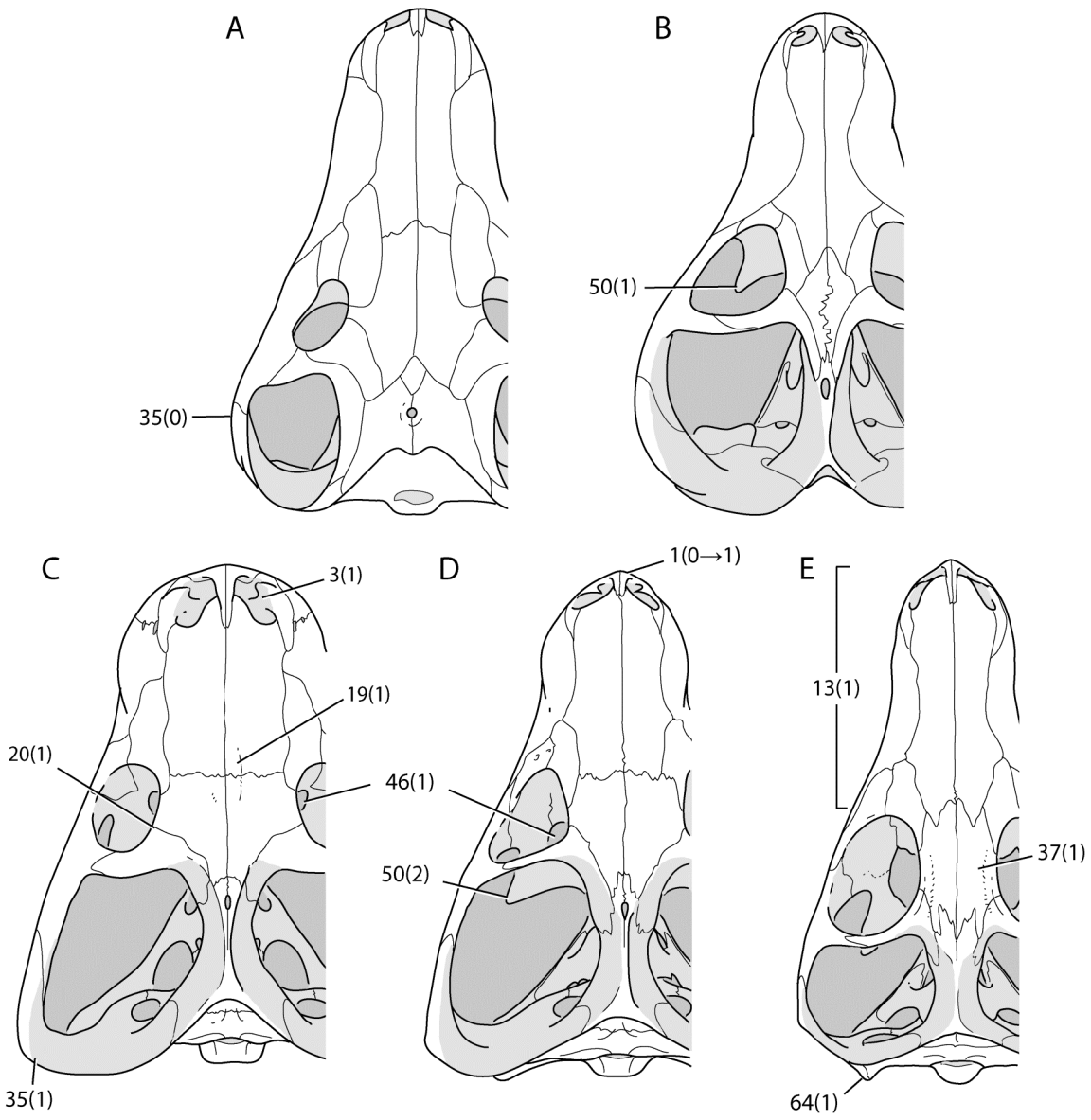
A
35(0)
B
50(1)
C
3(1)
19(1)
20(1)
35(1)
D
1(0→1)
46(1)
50(2)
E
13(1)
37(1)
64(1)

foramen of the humerus (present study, char. 115), although this does appear to be present in the basal Lycosuchidae (e.g., SAM-PK-12185, '*Zinnosaurus'* holotype); and caudal vertebra count reduced to less than fifteen (present study, char. 109). Consequently, as few as nine and as many as 14 osteological synapomorphies appropriately diagnose Therocephalia (Appendix 5).

Scylacosauria—The consensus of most parsimonious trees supported a monophyletic Scylacosauridae sister to Eutherocephalia supporting van den Heever's Scylacosauria hypothesis (Fig. 1.5B). These post-*Lycosuchus* therocephalians share the following synapomorphies: (1) anterior border of orbit located on transverse midline of skull (reversed in some akidnognathids, hofmeyriids, whaitsiids, and some baurioids) (char. 14; Fig. 1.10); (2) well-developed medial process of the squamosal contributing to the pterygo-paroccipital foramen (char. 31; Fig. 1.11), (3) premaxilla alveolar margin horizontal/straight (char. 36); (4) marked development of the crista choanalis anteriorly (char. 40); (5) narrow ventromedian crest on the posterior portion of the vomer (char. 44); (6) pterygoid transverse flange teeth absent (char. 48); (7) vomer anterior vault absent (char. 55); (8) functional upper precanine maxillary teeth (char. 99); (9) humerus ectepicondylar foramen absent (char. 115); (10) iliac dorsal plate bears sharp anterior process below an anterodorsal concavity (char. 118); and (11) pubis and ischium orientation more horizontal, forming a broad puboischiatic plate (char. 119). Within Scylacosauria, the Scylacosauridae resolves as a basal clade. Detailed discussions of basal therocephalians and characteristics of Scylacosauridae are provided by

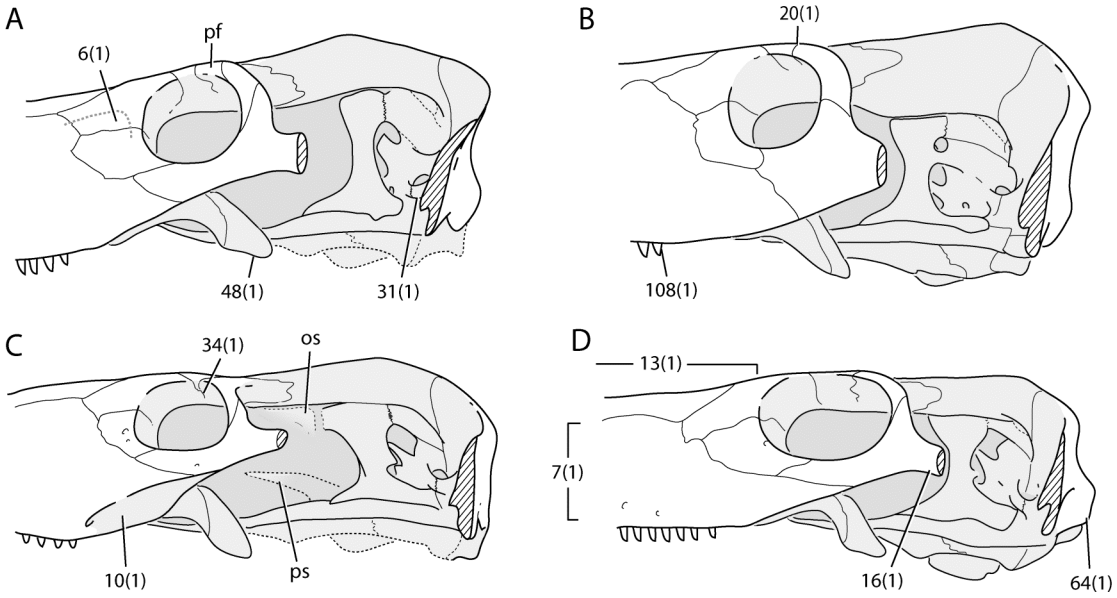

Figure 1.11. Posterior skull and braincase in left lateral view (left cheek removed). **A**, basal therocephalian *Glanosuchus* (modified from van den Heever, 1994); **B**, akidnognathid eutherocephalian *Moschorhinus* (modified from Durand, 1991); **C**, hofmeyriid eutherocephalian *Mirotenthes* (based on CGP-1-1264); **D**, baurioid eutherocephalian *Regisaurus* (based on BP/1/5394 and Mendrez, 1972). Skulls are not drawn to scale. Numbers represent important characters and character states from Appendices 3-5. Abbreviations: os, orbitosphenoid; pf, postfrontal; ps, presphenoid.

van den Heever (1994) and Abdala et al. (2008). Here, two diagnostic features provide potential synapomorphies for the group, including: (1) long, shallow antorbital depression anterior to a thickened ridge on the anterior margin of the orbit (char. 6; Fig. 1.11A); and (2) upper incisors number six or more (char. 96; Fig. 1.12A). Scylacosaurids also exhibit an ambiguous synapomorphy of three lower incisors (instead of four or more as in most other scylacosaurians) (char. 107).

Eutherocephalia—The sister group to Scylacosauridae is the scylacosaurian clade Eutherocephalia. A monophyletic Eutherocephalia was supported in the consensus of most parsimonious trees and Bayesian consensus and diagnosed by at least three synapomorphies: (1) anterodorsal most tip of premaxilla forms a rostral process, overhanging incisors (char. 1); (2) upper incisor longitudinal fluting/striae present (char. 97; Figs. 1.12, 1.13); and (3) incisor cutting margins unserrated (char. 105). Aside from *Scylacosuchus* and some specimens of *Hofmeyria*, all other eutherocephalians have lost the postfrontal (char. 20). Other synapomorphies may include: vomers unpaired (uncertain in *Scylacosuchus*; char. 43); paroccipital process dorsal surface deeply hollowed in floor of post-temporal fenestra (condition uncertain in *Scylacosuchus* and *Perplexisaurus*; char. 61); mandibular fenestra present, penetrating the mandible and visible laterally (condition uncertain in *Scylacosuchus*, *Perplexisaurus*, and Chthonosauridae; char. 89); lower incisors number four (modified in karenitids and lycideopids which may bear more than four, and some derived baurioids which may bear fewer than four; char. 107); interclavicle shape short and broad anterior to sternum

(condition uncertain in *Scylacosuchus*, *Perplexisaurus*, and Chthonosauridae; char. 113); and obturator foramen position bound by pubis and ischium (condition uncertain in *Scylacosuchus*, *Perplexisaurus*, and Chthonosauridae; char. 121).

Relationships within Eutherocephalia

Akidnognathidae and basal eutherocephalians—Haughton and Brink (1954) adopted Akidnognathidae Nopsca (1928) to include a mixture of valid akidnognathid taxa (e.g. *Akidnognathus parvus*) and some scylacosaurid taxa, probably due to shared plesiomorphies. Watson and Romer (1956), however, allied many recognized akidnognathids with the family Whaitsiidae, but Mendrez (1974a, b) and Durand (1991) contested this relationship. A more general interpretation might be that the akidnognathids are morphologically intermediate between basal therocephalians (e.g., scylacosaurids) and whaitsiid-like forms, a view that reconciles the hypotheses of the above authors. Accordingly, Tatarinov (1995a) placed representatives of the Akidnognathidae and Whaitsiidae within the superfamily 'Whaitsioidea,' although the ranking was arbitrary and the group is demonstrated here to be paraphyletic. Synapomorphies of Akidnognathidae include: (1) median frontonasal crest (also in *Chthonosaurus* and some whaitsiids; char. 19); (2) dentary symphysis anteroposteriorly thickened with strong suture (char. 80); (3) maxillary postcanine alveolar margin in ventral view buccally convex at anterior extent, bowing outward away from the midline (char. 131); and (4) upper postcanine diastema immediately behind dominant caniniform absent (char. 132). Aside from *Annatherapsidus*, all African akidnognathids exhibit a

Figure 1.12. Jaws and dentition of selected therocephalians in left lateral view. **A**, basal scylacosaurid therocephalian (top: *Glanosuchus*, SAM-PK-K7808; bottom: *Pristerognathus*, SAM-PK-11942). **B**, akidnognathid eutherocephalian (top: *Olivierosuchus*, NMQR 62; bottom: *Promoschorhynchus*, RC 116). **C**, hofmeyriid eutherocephalian *Mirotenthes* (top: CGP-1-1264; bottom: CGP-1-1264 and UCMP 40467). **D**, whaitsiid eutherocephalian *Theriognathus* (top: BP/1/724; bottom: BP/1/512 and 1/844). **E**, baurioid eutherocephalian *Ictidosuchoides* (top: SAM-PK-K10521; bottom: RC 106 and SAM-PK-K8659). **F**, bauriid eutherocephalian *Microgomphodon* (SAM-PK-K10160). Skulls are not drawn to scale. Numbers represent important characters and character states from Appendices 3-5.

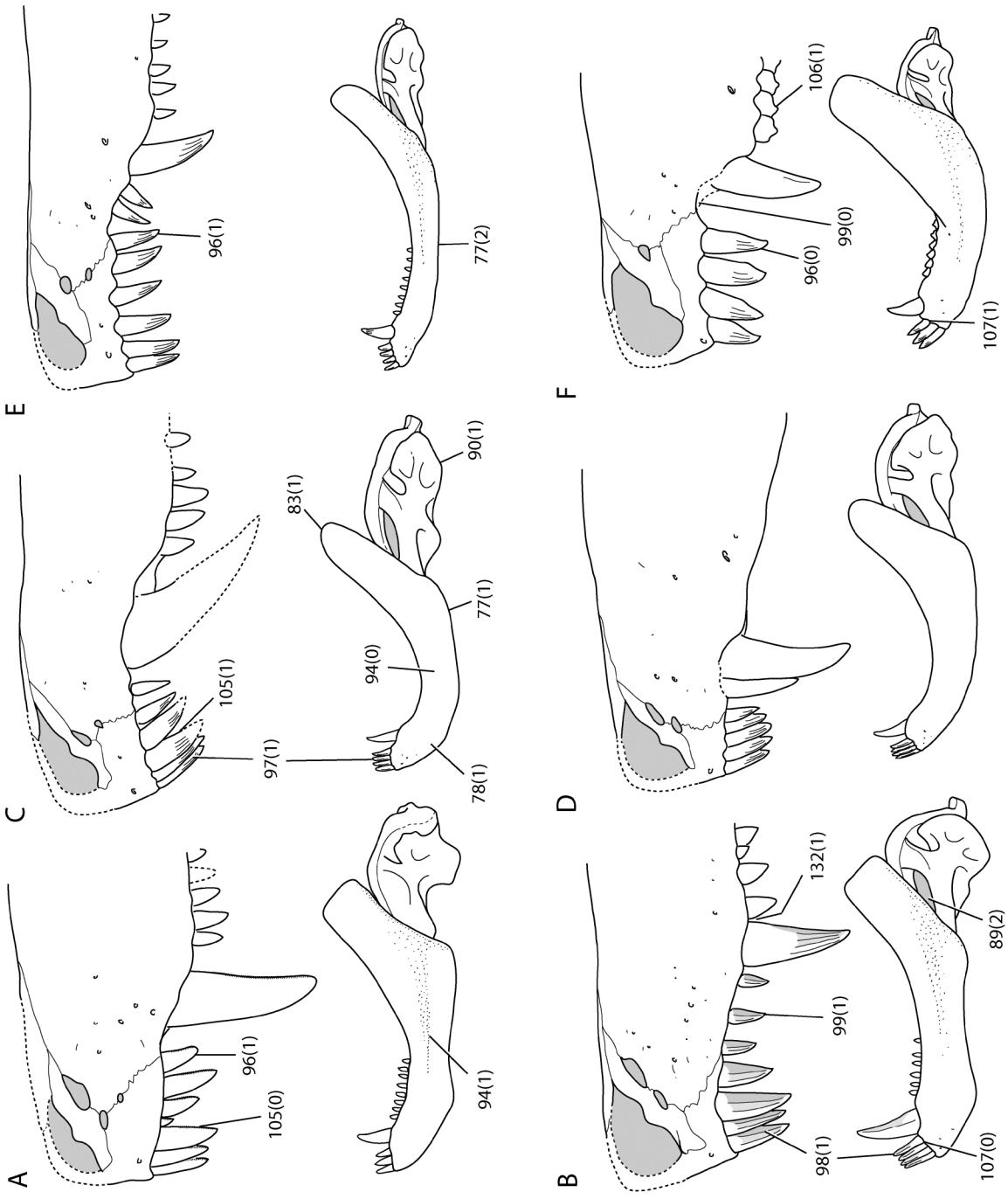
A
96(1)
105(0)
94(1)
C
105(1)
97(1)
83(1)
90(1)
94(0)
77(1)
78(1)
E
96(1)
77(2)
B
132(1)
99(1)
98(1)
89(2)
107(0)
D
F
96(0)
99(0)
106(1)
107(1)

Figure 1.13. Dental morphology of selected eutherocephalians. **A**, undescribed basal akidnognathid (USNM PAL 412421) left upper incisor (A1) and upper postcanine (A2) in lateral view. **B**, derived akidnognathid (SAM-PK-K10922) left upper second (B1) and third (B2) incisors in lingual view. **C**, akidnognathid *Promoschorhynchus* (SAM-PK-K10014) upper canine in lateral view. **D**, *Promoschorhynchus*-like akidnognathid (SAM-PK-K10697) right lower jaw in lateral view, showing grooved and faceted teeth. **E**, hofmeyriid *Mirotenthes* (CGP-1-1264) left upper incisor in lateral view, showing longitudinal fluting. **F**, whaitsiid *Theriognathus* (SAM-PK-K10981) right upper incisor in anterior view, showing longitudinal fluting. **G**, basal baurioid *Ictidosuchus primaevus* holotype (AMNH 5529) (from Broom, 1900:plate 26) left lower postcanines (G2-3) and referred specimen (SAM-PK-K10650) left upper postcanine (G4) in lateral view, showing pronounced postcanine striations. Numbers represent important characters and character states from Appendices 3-5. Abbreviations: f, flat facets; i fl, incisor longitudinal fluting; m-d c, mesio-distal carinae; poc str, postcanine striae.

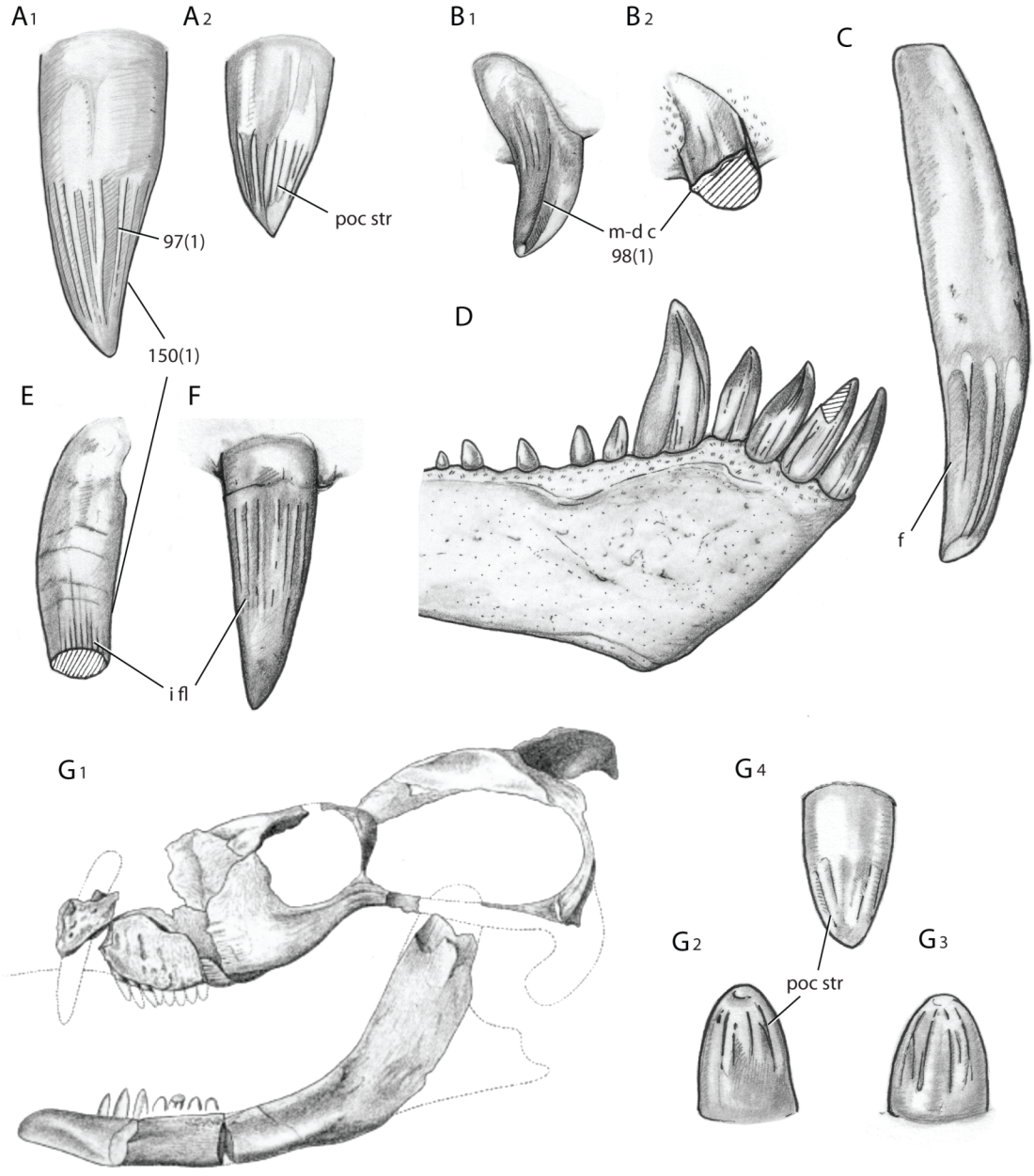
A1
A2
poc str
97(1)
150(1)
B1
B2
m-d c
98(1)
C
f
D
E
F
i fl
G1
G4
G2
G3
poc str

palatal housing for the lower canine formed as a separate fossa by premaxillary and maxillary extensions from the primary palate, and frequently have large forward-facing nares and lack pterygoid boss teeth (Fig. 1.14C). Akidnognathids also lack certain features of more derived eutherocephalians, such as the more gracile dentary that tapers rather than thickens anteriorly, a more rounded coronoid process, and a reflected lamina of the angular that is more elongate and spade-shaped (lacking the rounded margin that extends ventral to the dentary of more basal therocephalians and other therapsids). In more derived forms (e.g., *Promoschorhynchus*, *Olivierosuchus*, *Cerdosuchoides*, *Moschorhinus*), the incisors are spatulate with a bell-shaped cross-section, having smooth mesio-distal cutting edges (char. 98; Fig. 1.13B).

Non-akidnognathid 'whaitsioids'—Some akidnognathids mentioned above (e.g., *Promoschorhynchus*) were at one time placed among the Whaitsiidae (Huene, 1940; Watson and Romer, 1956; Romer, 1966). Tatarinov (1974, 1995a) included Annatherapsididae (= Akidnognathidae), Moschowhaitsiidae, and Whaitsiidae within the more inclusive 'Whaitsioidea.' Mendrez (1974a) separated akidnognathids from Whaitsiidae and removed other forms that she did not see fit in either of the two groups, such as *Hofmeyria* and *Mirotenthes*. Attridge (1956) regarded *Mirotenthes* as a possible whaitsiid based on the classification schemes of previous authors and Brink (1956) also included *Hofmeyria* within the Whaitsiidae. Two major clades of post-akidnognathid eutherocephalians are recognized here: an unnamed clade of non-akidnognathid 'whaitsioids' (including hofmeyriids and whaitsiids) and Baurioidea.

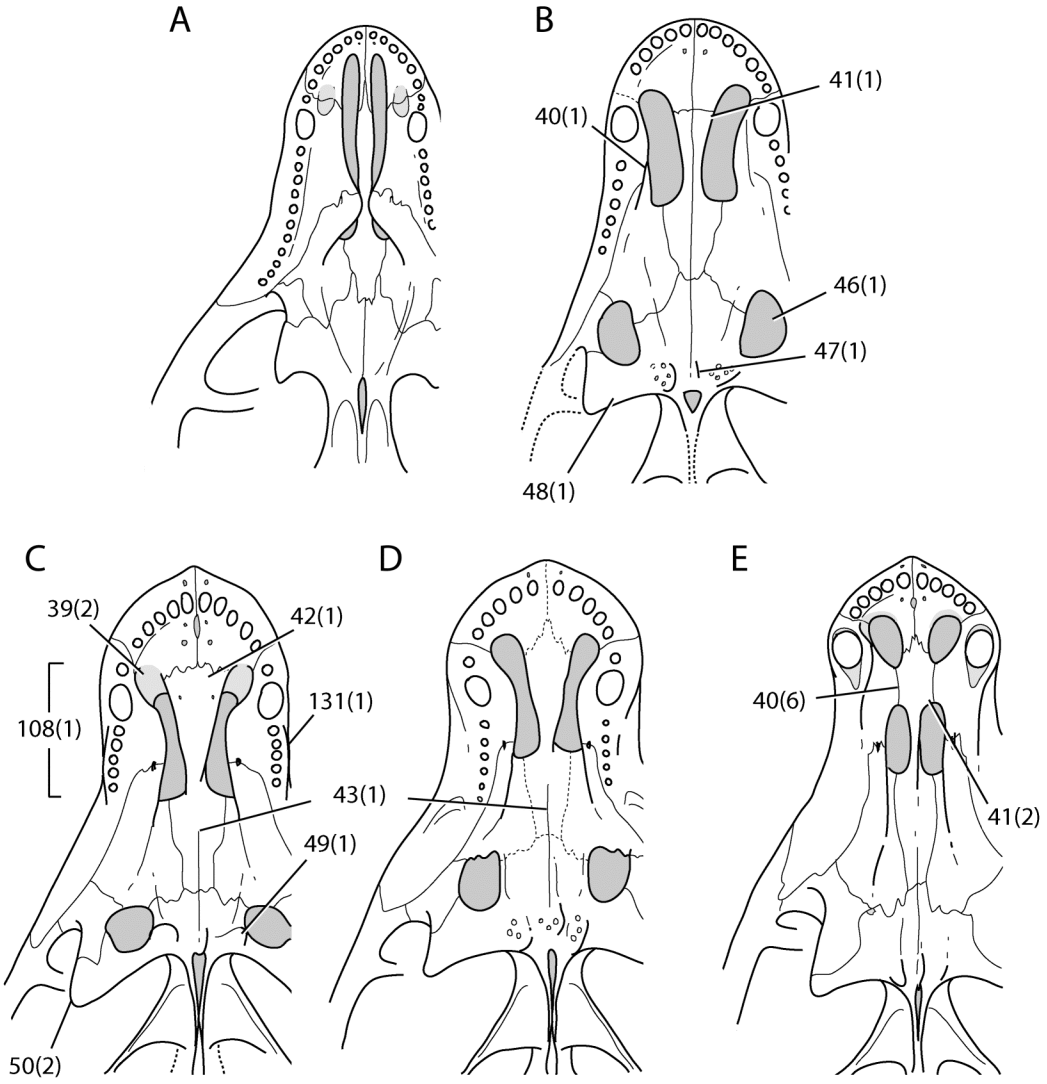

Figure 1.14. Palate morphology of a cynodont and selected non-baurioid therocephalians. **A**, basal cynodont *Procynosuchus* (modified from Hopson, 1991). **B**, scylacosaurid *Pristerognathus* (=*Ptomalestes*) (modified from van den Heever, 1994:fig. 8). **C**, akidnognathid *Promoschorhynchus* (modified from Mendrez, 1974b). **D**, hofmeyriid *Mirotenthes* (based on UCMP 40467 and CGP-1-1264). **E**, whaitsiid *Theriognathus* (based on Mendrez, 1975 and Brink, 1980). Skulls are not drawn to scale. Numbers represent important characters and character states from Appendices 3-5.

Proposed synapomorphies in support of a monophyletic grouping of all non-akidnognathid 'whaitsioids' include: (1) posterior region of the maxillary facial plate folded inward onto the palatal region, so that the maxilla is well exposed ventrally just anterior to the orbit (char. 10); (2) suborbital bar is laterally expanded, contributing to a pronounced degree of orbital convergence (i.e., orbits facing forward and appearing more triangular than oval in dorsal view) (char. 12); (3) anterior border of orbit located on anterior half of skull (char. 14); (4) jugal anterior extent restricted to anterior border of orbit (char. 38); (5) tabular extends below post-temporal fenestra (interpreted as a reversal) (char. 66); (6) tabular dorsal extent low and broad (char. 71); (7) dentary short and banana-shaped (char. 77); (8) area between left and right dentaries relatively long and narrow just posterior to symphyseal region (char. 93); (9) dentary ramus lateral groove absent (interpreted as a reversal) (char. 94). Postcanine dentary teeth are also often reduced in number or completely absent (e.g., *Mirotenthes*, *Theriognathus*). Postcanine dentary teeth are present in *Ictidostoma*, but they are reduced in size, number, and spacing. In *Hofmeyria*, postcanine dentary teeth are reduced in number and packed tightly against the lower canine on a raised platform.

Baurioidea—Hopson and Barghusen (1986) suggested a monophyletic grouping of Baurioidea based on extensive palatal exposure of the maxilla. Synapomorphies presented here include: (1) maxilla facial plate low with a height less than 40% its length (char. 7); (2) long, low rostrum just anterior to orbital region present (char. 13); interorbital width narrow, less than 20% basal skull length (char. 37); (3) maxilla palatal

processes present and contact or nearly contact the ventrally extending vomer at a shallow angle (char. 40; Fig. 1.15); (4) palatal exposure of maxilla behind canine greater than 20% distance from canine to posterior end of palatine (char. 52); (5) squamosal and opisthotic paroccipital process form a distinct, posteriorly projecting 'mastoid process' (char. 64); (6) dentary overall shape, long and slender with straight ventral edge (char. 77); dentary angle anterolateral to reflected lamina shallow, smoothly rounded (char. 82); (7) upper incisors number six or more (char. 96); and (8) calcaneal tuber (tuber calcis) present, oriented posteriorly (char. 127). Also, compared to more basal therocephalians, baurioids showed a general pattern toward smaller sizes and more gracile skulls and limb skeletons.

In derived baurioids such as the Lycideopidae, a long sutural connection is generally formed between the vomer and palatal processes of the maxilla (extensions of the crista choanalis). A recent study on the paleobiology of the lycideopid *Tetracynodon* found strong evidence for monophyly of Lycideopidae (Sigurdsen et al., 2012). Synapomorphies for the group include: (1) anterior border of orbit located on posterior half of skull (char. 14); (2) nasal-lacrimal contact present (char. 33); and (3) two enlarged premaxillary foramina on palate (char. 128). Post-lycideopid baurioids include a primarily Triassic clade formed by the most recent common ancestor of *Scaloposaurus* and *Microgomphodon* and all of its descendants. Synapomorphies include: (1) postcanines with two or more cusps in line (char. 106); and (2) lower incisors number less than four (also in lycosuchids and scylacosaurids) (char. 107). In post-*Scaloposaurus*

Figure 1.15. Palate morphology of baurioid eutherocephalians. **A**, basal baurioid *Ictidosuchops rubidgei* (based on RC 6 and CGP CM86-486). **B**, regisaurid *Regisaurus jacobi* (modified from Mendrez, 1972). **C**, lycideopid *Lycideops longiceps* (based on NHMUK R5695 and RC 646). **D**, lycideopid *Tetracynodon darti* (modified from Sigurdsen et al., 2012). **E**, ericiolacertid (based on CAMZM T369 and BP/1/4794; Mendrez, 1975). **F**, bauriid *Bauria cynops* (modified from Brink 1963). Skulls are not drawn to scale. Numbers represent important characters and character states from Appendices 3-5.

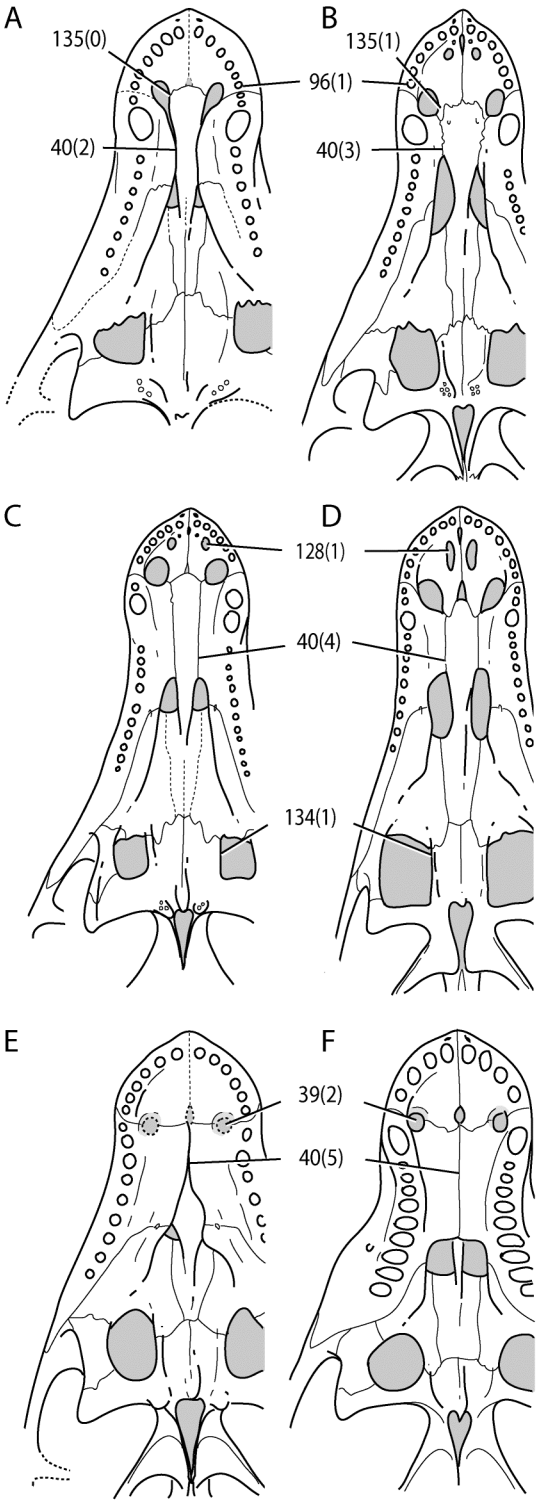
A
135(0)
40(2)
B
135(1)
96(1)
40(3)
C
128(1)
40(4)
134(1)
D
E
39(2)
40(5)
F

baurioids, the palatal processes of the maxillae meet on the midline ventral to the vomer, obscuring its anterior extent in ventral view (e.g., ericiolacertids, bauriids). The nature of the development of the secondary palate is one of the most notable features of baurioid evolution (Mendrez, 1975; Hopson and Barghusen, 1986; Maier, 1999). The presence of a complete, ossified secondary palate in advanced baurioids may have contributed to earlier classifications placing some cynodonts amongst therocephalians (Brink, 1960a; Romer, 1966). However, most authors agree that the secondary palate evolved multiple times in therapsids (Angielczyk, 2009). The independent acquisition of a complete secondary palate in baurioid therocephalians and cynodonts may imply similar developmental factors, but the most parsimonious representations of therapsid phylogeny and subtle morphological differences (e.g., absence of an incisive fissure and lack of contact between palatines at midline in baurioids) do not permit a common evolutionary origin for these structures in the two groups (see Maier, 1999 for more discussion).

Permian Diversifications

Figures 1.16 and 1.17 summarize observed and phylogeny-augmented stratigraphic ranges of therocephalian lineages from the Middle Permian through the Middle Triassic (updated and expanded from Huttenlocker et al., 2011b). Huttenlocker et al. (2011b) suggested as many as three ‘peaks’ in eutheriodont origination and extinction, which corresponded to traditional ‘stages of diversification’ discussed by Broom (1948), Hotton (1991), and recently by Abdala et al. (2008). However, more complete sampling and precise estimations of origination/extinction correcting for stratigraphic bin duration

indicates an initial diversification during the Middle Permian, followed by a later increase in origination/extinction rates with the proliferation of Eutherocephalia during the Late Permian (Fig. 1.17).

The study of Abdala et al. (2008) emphasized the Middle Permian diversification, which included the first appearance of the basal therocephalian families Lycosuchidae and Scylacosauridae, as well as the minimum divergence of Scylacosauria (scylacosaurids + eutherocephalians). Diversifications during the early-Late Permian are represented by the abundance of eutherocephalian genera in strata overlying the *Tapinocephalus* AZ of southern Africa (i.e., *Pristerognathus*, *Tropidostoma*, and *Cistecephalus* AZs). The diversity of early eutherocephalians in these strata suggests a divergence by the Middle-Late Permian transition (ca. 260.4 Ma). Moreover, akidnognathids, hofmeyriids, and basal baurioids are inferred to have diverged during this time, whereas whaitsiids likely diverged in Eastern Europe shortly thereafter (based on *Viatkosuchus* and *Moschowhaitsia*). However, it is possible that the temporal discordance between this and the initial diversification of therocephalians is due to coarse stratigraphic resolution and the poorly resolved systematics of *Tapinocephalus* AZ theriodont faunas in the Karoo. During the Late Permian, diversification was marked by increased richness of eutherocephalian groups in the *Cistecephalus* and *Dicynodon* AZs. It was during this time that some of the more derived and specialized genera, including *Theriognathus* and *Moschorhinus*, diverged from within pre-existing families that were

Figure 1.16. Stratigraphic ranges of therocephalian eutheriodonts. Absolute dates (Ma) follow boundary dates for global standard stratigraphy (Gradstein et al., 2004; Lehrmann et al., 2006; Shen et al., 2011; Smith et al., 2012) and new radiometric dates from within the Karoo sequence (parentheses) (Rubidge et al., 2013). Geographic provenance is indicated next to taxon name (An, Antarctica; Ch, China; Na, Namibia; Ru, Russia; SA, South Africa; Tz, Tanzania; Za, Zambia). Dark gray interval indicates approximate position of the earliest Triassic upper Palingkloof Member. PTB = Permian-Triassic boundary.

Middle Permian
Late Permian
E. Triassic
M. Triassic
Epoch
Roa
Wor
Capitanian
Wuchiapingian
Chx
Ind
Olen
Anisian
Global Standard Stage
Eodicyno AZ
Tapinoceph AZ
Prist AZ
Trop AZ
Cisteceph AZ
Dicynodon AZ
Lystro AZ
Cyn sub A
Cyn sub B
Cyn sub C
Karoo Biozone
270.6 Ma
268
265.8
(261.2)
(260.4)
(259.2)
(256.2)
(255.2)
253.8
252.3
249.7
247.2
241.2
PTB
Ictidosaurus angusticeps (SA)
Glanosuchus macrops (SA)
Alopecodon prisca (SA)
Pardosuchus whaitsi (SA)
Scylacosaurus sclateri (SA)
Lycosuchus vanderrieti (SA)
Pristerognathus polydon (SA)
Perplexisaurus foveatus (Ru)
Viatkosuchus sumini (Ru)
Karenites ornamentatus (Ru)
Ictidostoma hembury (SA)
Hofmeyria atavus (SA)
Ictidosuchoides longiceps (SA)
Scylacosuchus primaevus (SA)
Choerosaurus orenburgensis (Ru)
Choerosaurus dejageri (SA)
new TrAZ whaitsiid (SA)
new CisAZ hofmeyriid (SA)
new Zambian chthonosaurid (Za)
new Zambian karenitid (Za)
new CisAZ akidnognathid (Za)
Eucham bersia mirabilis (SA)
Mirotenthes digitipes (SA)
Annatherapsidus petri (Ru)
Chthonosaurus velocidens (Ru)
Theriognathus microps (SA, Ru)
Ictidosuchops rubidgei (SA)
Akidnognathus parvus (SA)
Cerdosuchoides brevidens (SA)
Lycideops longiceps (SA)
Tetracynodon tenuis (SA)
Promoschorhynchus platyrhinus (SA)
Moschorhinus kitchingi (SA)
Ictidochampsa platyceps (SA)
Moschowhaitsia vjuschkovi (Ru)
Fricioceria parva (SA, An)
Regisaurus hoffmani (SA)
Oliviersuchus parringtoni (SA)
Tetracynodon darti (SA)
Sliphedosuchus orenburgensis (Ru)
Urumchia lii (Ch)
Scaloposaurus constrictus (SA)
Hazhenia concava (Ch)
Microgomphodon oligocynus (SA, Na)
Yikezhaogia megafenestrata (Ch)
Ordosiodon linchevuensis (Ch)
Ordosiodon youngi (Ch)
Bauria cynops (SA)
Nothogomphodon daniloi (Ru)
Antecosuchus ochevi (Ru)
Traversodontoides wangwuensis (Ch)

established during the initial eutherocephalian diversification. It is also during this time that therocephalian species richness reached its zenith. Therocephalians from outside the Karoo Basin generally conformed to the pattern of diversification highlighted here.

Permo-Triassic Boundary-Crossing Lineages

The diversity of therocephalians and cynodonts during the Permian-Triassic transition has received some attention in recent years due to their apparent success and relative richness in Lower Triassic rocks of the *Lystrosaurus* AZ (Sidor and Smith, 2004; Huttenlocker, 2009; Huttenlocker et al., 2011b). Sidor and Smith (2004) suggested that at least two major cynodont lineages crossed the Permo-Triassic boundary, although no individual genus had been recorded from both Permian and Triassic strata in or outside of the Karoo. The results of the current study support that at least six eutherocephalian lineages crossed the Permo-Triassic boundary. Three of these lineages represent observed genera, whereas the remaining are ghost lineages inferred by cladistic methods (i.e., the lineage that includes *Olivierosuchus*, the lineage that includes Regisauridae, and a clade of derived Triassic baurioids that includes *Scaloposaurus*, ericiolacertids, and bauriids). In some cases, the latter examples may represent cryptic or undiscovered taxa from the underlying *Dicynodon* AZ fauna or new arrivals to the depositional basin (immigrants) following the extinction. Accordingly, many Triassic therocephalian genera found at Permo-Triassic boundary localities in the Karoo represent members of pre-existing Late Permian lineages rather than earliest Triassic diversifications (Fig. 1.17). More importantly, with regards to genus-level diversity, the recent identification of

Promoschorhynchus in the *Lystrosaurus* AZ (Huttenlocker et al., 2011b) suggests that fossils of at least three therocephalian genera span the Permo-Triassic boundary (viz. *Moschorhinus*, *Promoschorhynchus*, and *Tetracynodon*). Among other therapsids, only the dicynodont *Lystrosaurus* shows a comparable pattern (Botha and Smith, 2007).

Shifts in the relative diversities of cynodonts, which continued to diversify across the Permo-Triassic boundary, and therocephalians have long been documented (Abdala et al., 2008; Abdala and Ribeiro, 2010) although an explanation for this protracted wedge pattern has not been proposed. Despite their relative survivorship across the boundary, therocephalians evidently exhibited low rates of cladogenesis in the Early Triassic (and lower overall turnover rates; Fig. 1.17), and reduced taxonomic richness during the Early and Middle Triassic (Olenekian and Anisian). Ultimately therocephalians were surpassed in all measures of diversity by their cynodont relatives in the Middle and Late Triassic, as the latter group speciated into a wide array of carnivorous and herbivorous forms (Abdala and Ribeiro, 2010).

Conclusions

The systematic relationships of Permian and Triassic therocephalians are reviewed, and their temporal diversity assessed in light of new and re-evaluated specimens and new phylogenetic data. An updated phylogenetic analysis of 56 therapsid taxa (including 49 therocephalians) and 135 morphological characters supports several

Figure 1.17. Time calibrated phylogeny of therocephalians and diversification rates. Estimates of per capita origination (dashed line) and extinction (dotted line) follow raw occurrence data in Figure 1.16. Turnover is highest in the Late Permian and relatively depressed in the Triassic. Dark gray interval indicates approximate position of the earliest Triassic upper Palingkloof Member. PTB = Permian-Triassic boundary.

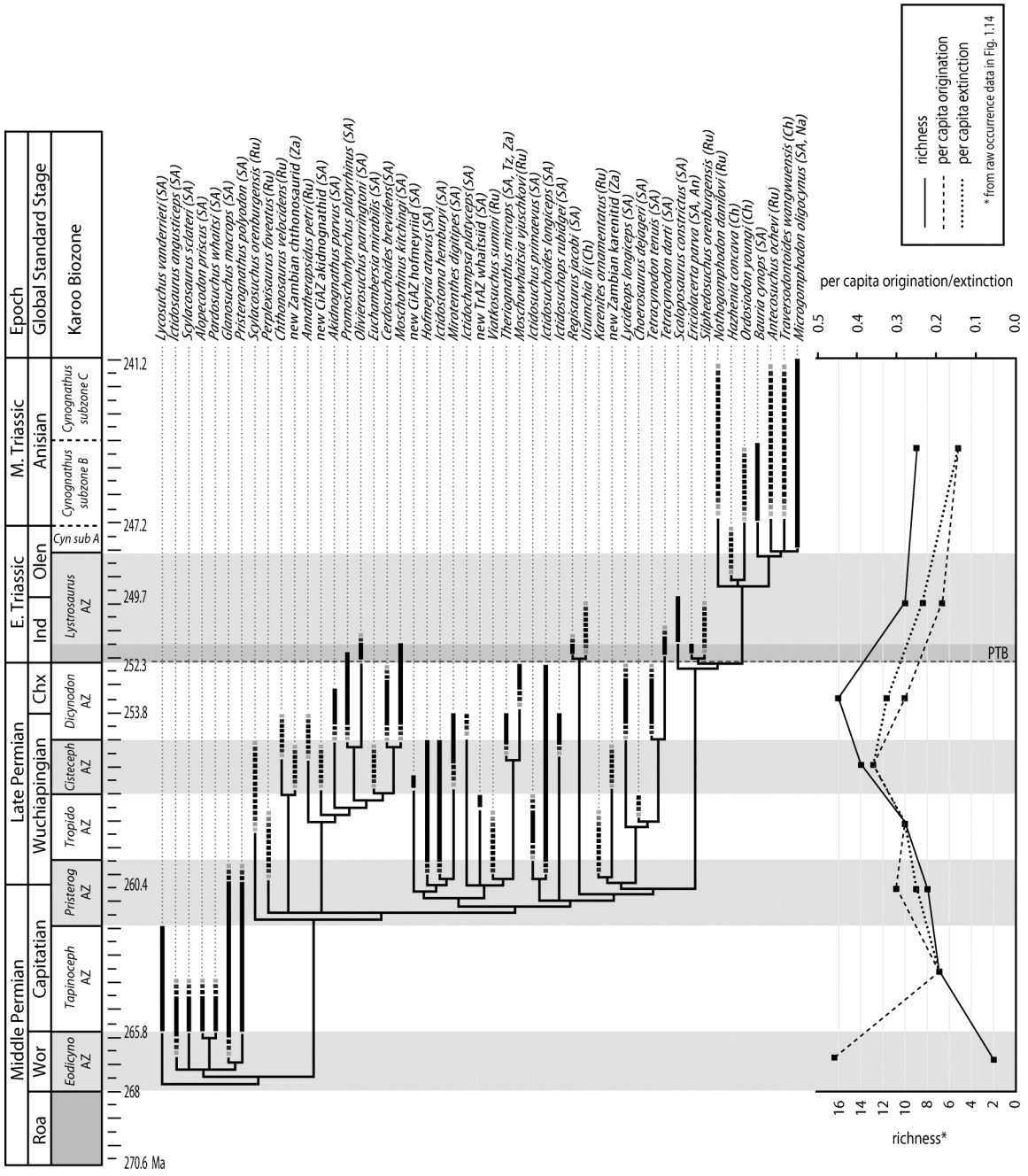
Middle Permian
Late Permian
E. Triassic
M. Triassic
Epoch
Roa
Wor
Capitatian
Wuchiapingian
Chx
Ind
Olen
Anisian
Global Standard Stage
Eodicyno AZ
Tapinoceph AZ
Pristerog AZ
Tropido AZ
Cisteceph AZ
Dicynodon AZ
Lystrosaurus AZ
Cyn sub A
Cynognathus subzone B
Cynognathus subzone C
Karoo Biozone
270.6 Ma
268
265.8
260.4
253.8
252.3
249.7
247.2
241.2
PTB
Lycosuchus vanderrieti (SA)
Ictidosaurus angusticeps (SA)
Scylacosaurus sclateri (SA)
Alopecodon priscus (SA)
Pardosuchus whaitsi (SA)
Glanosuchus macrops (SA)
Pristerognathus polyodon (SA)
Scylacosuchus orenburgensis (Ru)
Perplexisaurus foveatus (Ru)
Chthonosaurus velocidens (Ru)
new Zambian chthonosaurid (Za)
Annatherapsidus petri (Ru)
new CIAZ akidnognathid (SA)
Akidnognathus parvus (SA)
Promoschorhynchus platyrhinus (SA)
Olivierosuchus parringtoni (SA)
Euchambersia mirabilis (SA)
Ceradsuchoides brevidens(SA)
Moschorhinus kitchingi (SA)
new CIAZ hofmeyriid (SA)
Hofmeyria atavus (SA)
Ictidostoma hemburyi (SA)
Miratenthes digitipes (SA)
Ictidochampsa platyceps (SA)
new TrAZ whaitsiid (SA)
Viatkosuchus sumini (Ru)
Theriognathus microps (SA, Tz, Za)
Moschowhaitsia vjuschkovi (Ru)
Ictidosuchus primaevus (SA)
Ictidosuchoides longiceps (SA)
Ictidosuchops rubidge (SA)
Regisaurus jacobi (SA)
Urumchia lii (Ch)
Karenites ornamentatus (Ru)
new Zambian karenitid (Za)
Lycideops longiceps (SA)
Choerosaurus deiger (SA)
Tetracynodon tenuis (SA)
Tetracynodon darti (SA)
Scaloposaurus constrictus (SA)
Ericiolacerta parva (SA, An)
Silpheosuchus orenburgensis (Ru)
Nothogomphodon damiloy (Ru)
Hazhenia concava (Ch)
Ordosiodon youngi (Ch)
Bauria cynops (SA)
Antecosuchus ochevi (Ru)
Traversodontoides wangwuensis (Ch)
Microgomphodon oligocynus (SA, Na)
richness
per capita origination
per capita extinction
* from raw occurrence data in Fig. 1.14
per capita origination/extinction
0.5
0.4
0.3
0.2
0.1
0.0
richness*
16
14
12
10
8
6
4
2
0

traditional groups, including a monophyletic Therocephalia. Additional dental and postcranial characters have helped to improve phylogenetic resolution within Therocephalia, and continued work in these areas will further assess the robustness of cladistic hypotheses to different sources of anatomical data.

Further work is required to resolve the relationships within basal scylacosaurians, particularly within the Scylacosauridae. More detailed anatomical study of basal therocephalian taxa, including assessments of their dental morphology and replacement patterns, will shed light on the diversity and composition of these early therocephalian predators (van den Heever, 1994; Abdala et al., 2008). Likewise, additional work focusing on basal eutherocephalians of Eastern Europe will have the potential to enhance character support and provide more complete character coding in those taxa (given the currently fragmentary nature of many of the specimens and superficial published descriptions). Renewed study of akidnognathids (e.g., Sigurdsen, 2006; Huttenlocker et al., 2011b) is beginning to clarify relationships within and among this group. Akidnognathid systematics would benefit from an analysis of additional genera, including Eastern European representatives (i.e., the basal *Annatherapsidus*). Likewise, the monophyly of non-akidnognathid 'whaitsioids' (hofmeyriids and whaitsiids) should be further tested with a closer analysis of the proposed representatives, such as the hofmeyriids *Hofmeyria* and *Ictidostoma*, and particularly the Eastern European forms *Viatkosuchus* and *Moschowhaitsia*.

Lastly, the present analysis has allowed for the reconstruction of ghost lineages in derived members of Late Permian and Triassic clades, and suggests at least eight lineages of eutheriodonts (six therocephalian and two cynodont lineages) survived the end-Permian extinction. In spite of their survivorship across the Permo-Triassic boundary, rates of cladogenesis in Therocephalia appear to have decreased into the Early Triassic, whereas its sister clade Cynodontia continued to diversify during the Triassic. However, the reasons for this double wedge pattern remain to be elucidated and its dynamics (competitive versus opportunistic replacement) should be further investigated in the context of the Permo-Triassic boundary. Progress toward a working hypothesis of eutheriodont phylogeny and an improved stratigraphic framework will catalyze future studies of evolutionary dynamics before and after the end-Permian extinction (the subject of Chapters 3 and 4).

Chapter 2—Body Size and Growth Patterns in the Therocephalian *Moschorhinus kitchingi* (Therapsida, Eutheriodontia) Before and After the End-Permian Extinction in South Africa

Summary—The continuous fossil record of therocephalian therapsids (Eutheriodontia) across the Permo-Triassic boundary and their differential survivorship of the end-Permian extinction offer an exceptional deep-time perspective on vertebrate life history evolution during episodes of large-scale ecological perturbation. To examine potential impacts of extinction on body size evolution (e.g., 'Lilliput' effects) and growth patterns, I investigated cranial sizes and limb bone histology in the therocephalian *Moschorhinus kitchingi* both before and after the end-Permian extinction, facilitated by analysis of thin-sections of 23 limb bones from an ontogenetic sample of ten individuals across the Permo-Triassic boundary. In general, early subadult *Moschorhinus* displayed propodial cortices with extensive woven- and parallel-fibered bone (PFB) with dense, radial and reticular vascularization and a moderately thickened bone wall with few growth marks. The outer cortex of propodials and epipodials showed a transition to PFB and lamellar bone with longitudinally oriented canals in individuals interpreted as late subadults or adults (>80% largest size). Most elements displayed several (3+) growth marks, though growth marks were more faithfully recorded in the epipodials of Permian

---

Published as: Huttenlocker, A. K., and J. Botha-Brink. 2013. Body size and growth patterns in the therocephalian *Moschorhinus kitchingi* (Therapsida: Eutheriodontia) before and after the end-Permian extinction in South Africa. Paleobiology 39:253–277.

individuals. Pearson product-moment correlation tests were performed to examine the relationship between size and robusticity on growth proxies (% cortical vascularity, mean primary osteon diameter), but variation in histomorphology could not be explained by size alone. Variation in body size may be affected by differences in juvenile growth rate and duration, which are highly variable in environmentally stressed extant reptile species. Geologic stage was a more consistent predictor of cortical vascularity. I suggest that Permian and Triassic *Moschorhinus* exhibited differential rates of early skeletal growth and growth durations, corroborating the hypothesis that increased environmental variability in the earliest Triassic was associated with rapid growth to a minimum body size requirement and, consequently, shortened developmental times.

Introduction

Marking an interval of increased environmental stress and global-scale ecological perturbation in marine and terrestrial realms, the end-Permian biotic crisis (ca. 252.3 million years ago; Shen et al., 2011) resulted in the extinction of 80–95% of animal species and had profound influences on earliest Triassic faunal characteristics and ecosystem dynamics (Erwin, 1998, 2003, 2006; Twitchett et al., 2001; Ward et al., 2005; Smith and Botha, 2005; Botha and Smith, 2006; Roopnarine et al., 2007; Sahney and Benton, 2008). In its aftermath, earliest Triassic terrestrial communities endured intensified seasonal climate variability, and experienced lowland deforestation and, ultimately, reduced overall ecosystem complexity (Smith and Ward, 2001; Huey and

Ward, 2005; Smith and Botha, 2005; Botha and Smith, 2006; Roopnarine et al., 2007; Sahney and Benton, 2008). Trophic network models of earliest Triassic communities in the Karoo Basin of South Africa indicate these communities would have been vulnerable to environmental variability and perturbations to primary productivity, due to decreased herbivore richness and increased predator richness (Roopnarine and Angielczyk, 2012). Recent investigations of Triassic ecosystem recovery have therefore sought adaptive explanations for the success of 'survival' and 'recovery' faunas (Smith and Botha, 2005; Botha and Smith, 2006), noting drought-tolerant food sources, burrowing adaptations, and anecdotal shifts in body size distributions (e.g., Smith, 1995; Sahney and Benton, 2008; Roopnarine and Angielczyk, 2012) as observed in other faunal turnover events that were associated with geologically abrupt changes in the physical environment (e.g., Harries et al., 1996; Clyde and Gingerich, 1998; Secord et al., 2012).

Post-extinction body size reductions, or 'Lilliput' phenomena, have been documented widely in survivor taxa living in perturbed communities in the aftermath of mass extinction events (Urbanek, 1993; Erwin, 1998; Harries and Knorr, 2009), including earliest Triassic marine invertebrate communities (Twitchett, 2007; Luo et al., 2008; Metcalfe et al., 2011; Song et al., 2011). Although nonmarine end-Permian extinctions included the loss of all large-bodied herbivores (>200 kg) and their supposed specialist predators (Sidor and Smith, 2004; Smith and Botha, 2005; Botha and Smith, 2006; Roopnarine et al., 2007; Sahney and Benton, 2008; Roopnarine and Angielczyk, 2012), the extent of body size reductions and their underlying mechanisms are virtually

unknown in terrestrial communities. Some of these mechanisms may include, but are not restricted to, (1) heterochronic shifts within survivor lineages (e.g., paedomorphosis, as originally suggested by Urbanek, 1993 and more recently by Harries et al., 1996), (2) differential extinction of large-bodied lineages, (3) rapid diversifications of new small-bodied lineages (Twitchett, 2007; Harries and Knorr, 2009), or any combination of these processes (Song et al., 2011). Consequently, the variety of processes makes it difficult to discern which 'Lilliput' mechanisms may be at play, especially in the absence of adequate life history data or phylogenetic controls. Investigations of post-extinction body size shifts rarely incorporate these sources of data (Twitchett, 2007; Harries and Knorr, 2009; Metcalfe et al., 2011).

In this study, I evaluate patterns of body size evolution (cranial size and geometry) and vascular growth patterns as inferred by limb bone histomorphology in the Permo-Triassic boundary-crossing therocephalian *Moschorhinus kitchingi*, and investigate its life history tactics in the context of the end-Permian extinction. Therocephalian and cynodont therapsids (Eutheriodontia) have provided important insights into long-term evolutionary trends and the origins of mammalian morphology and physiology (Bennett and Ruben, 1986; Hopson and Barghusen, 1986; Hopson, 1991, 1994; Rubidge and Sidor, 2001; Sidor, 2001, 2003; Kemp, 2006a,b; Ruben et al., 2012), although considerably less is known about their ecology and life history evolution during the end-Permian biotic crisis. The therocephalians were especially diverse and ecologically varied from the early Late Permian until the Middle Triassic (outnumbering

contemporary herbivorous dicynodont therapsids in terms of generic richness in lowermost Triassic rocks) and, remarkably, persisted as important components of terrestrial Triassic survivor communities in the aftermath of the end-Permian extinction (Sidor and Smith, 2004; Smith and Botha, 2005; Botha and Smith, 2006; Huttenlocker et al., 2011b; Botha-Brink and Modesto, 2011). As many as three therocephalian genera have been documented in both the Upper Permian *Dicynodon* (DAZ) and lowermost Triassic *Lystrosaurus* (LAZ) assemblage zones in the Karoo Basin of South Africa; namely *Tetracynodon*, *Promoschorhynchus*, and *Moschorhinus*, the last being the only large-bodied therapsid predator found in both biostratigraphic intervals (Smith and Botha, 2005; Botha and Smith, 2006; Huttenlocker et al., 2011b).

Numerous specimens of the akidnognathid *Moschorhinus* have been found in the Beaufort Group of the Karoo Basin (Fig. 2.1), either as isolated collections or in close association with herbivorous dicynodont remains, including those of *Lystrosaurus* (e.g., SAM-PK-K10015 from Bethal 763; Smith and Botha, 2005; Botha and Smith, 2006; Huttenlocker et al., 2011b). Its cranial anatomy has been described by numerous authors (Broom, 1920; Boonstra, 1934; Brink, 1959; Durand, 1991) making it one of the best known and most recognizable carnivorous therapsids of the Karoo. Although the lowermost extent of the stratigraphic range of *Moschorhinus* is unclear (its first occurrence is either in the uppermost *Cistecephalus* Assemblage Zone (CiAZ) or lower DAZ of Nieu Bethesda), it is widely documented throughout the uppermost Permian

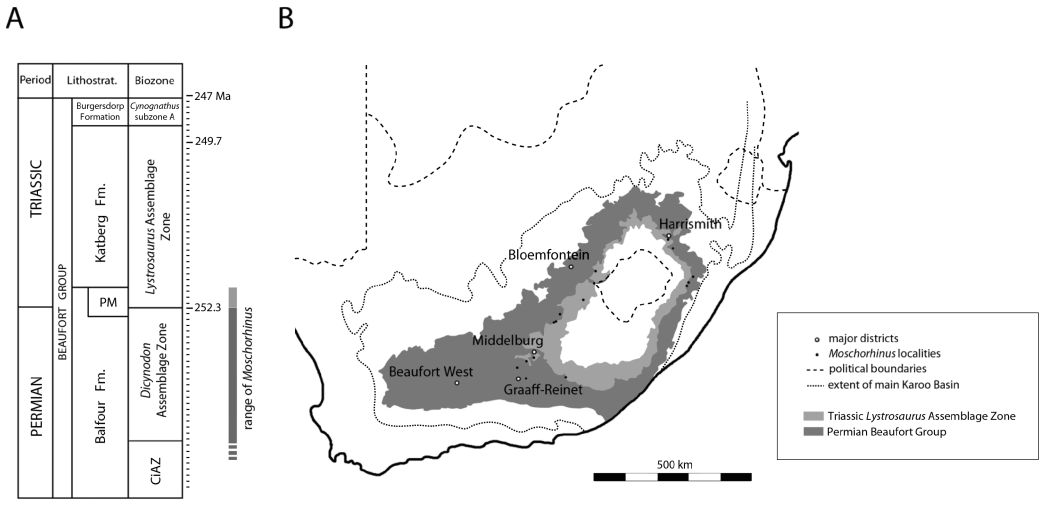

Figure 2.1. Stratigraphy and geographic distributions of principal *Moschorhinus*-bearing localities in the main Karoo Basin, South Africa. **A**, Stratigraphic range of *Moschorhinus* in the Beaufort Group (PM, Palingkloof Member of the Balfour Formation). Approximate dates in millions of years (Ma) adapted from Mundil et al. (2004), Jin et al. (2006); Lehrmann et al. (2006), Botha et al. (2007), Abdala et al. (2008), Abdala and Ribeiro (2010), Smith et al. (2012). **B**, Geologic map illustrating the extent of known *Moschorhinus* localities in the Upper Permian (dark gray) and lowermost Triassic *Lystrosaurus* Assemblage Zone (medium gray).

DAZ (Table 2.1). Recent collections have also confirmed its last occurrence within the Triassic upper Palingkloof Member (Balfour Formation) and equivalent strata (lowermost portion of the LAZ; Fig. 2.1), corroborating in part earlier stratigraphic assignments by Kitching (1977) and Mendrez (1974a). Despite over a decade of intense collecting effort, *Moschorhinus* has yet to be recovered within the overlying Katberg Formation (contra Damiani et al., 2003; see Smith and Botha, 2005 and Botha and Smith, 2006). Thus, the lowermost record is from the upper CiAZ or lowermost DAZ and its last appearance datum occurs in the lower LAZ (where it is rare), bracketing a well-documented record in the Upper Permian DAZ. Along with an extensive stratigraphic range, its relative size disparity, reasonably large sample sizes, and survival of the end-Permian extinction make *Moschorhinus* a worthy case for examining post-extinction body size reductions in a single tetrapod lineage across the Permo-Triassic boundary (PTB).

Present Study

By assessing cranial size and limb bone histovariation in a large sample of Permian and Triassic individuals, I tested the hypothesis that the end-Permian extinction was associated with shifts in life history tactics of the PTB survivor taxon *Moschorhinus*. More specifically, I addressed the questions: (1) Did Triassic *Moschorhinus* exhibit demonstrable size reductions over their Permian predecessors? And, if so, (2) were size reductions associated with observable shifts in subadult growth trajectories as recorded in their limb bone microstructure? In addressing these questions, I present the first statistical investigation of changes in the distributions of cranial size and histomorphometric traits

within a single therapsid genus across a major extinction interval, as well as the first quantitative analysis of both inter- (pooled) and intra-elemental (non-pooled) histovariation in a Permo-Triassic tetrapod. This is also the most complete and intensively sampled investigation of histological variation in a therocephalian therapsid to date. The record of *Moschorhinus* therefore provides a valuable case study into understanding within-lineage life history responses across the PTB, and the role of life history tactics during prolonged periods of environmental stress.

Methods 1: Geometry and Size

Selection of Specimens, Size Proxies, and Comparative Methods

Cranial and postcranial measurements on 40 specimens were recorded and cataloged in a specimen library containing 50 *Moschorhinus* records, mostly documenting skulls and skeletons from South African paleontological collections (Figs. 2.1, 2.2; Table 2.1). Specimens were diagnosed with reference to relatively complete existing material (e.g., NMQR 3351) using an apomorphy-based approach [i.e., broad, fan-shaped vomer with ventral tubercle pair; short, blunt snout with median frontonasal ridge; enlarged incisors with smooth external surface lacking fluting or facets; robust dentary with thickened mentum (but constricted behind the canine); expanded lateral dentary shelf and reduced postcanine count (3-4) (Mendrez, 1974a,b)]. Stratigraphic provenance was validated by reference to sympatric biostratigraphically-informative dicynodonts, as well as field notes and stratigraphic logs when available, including

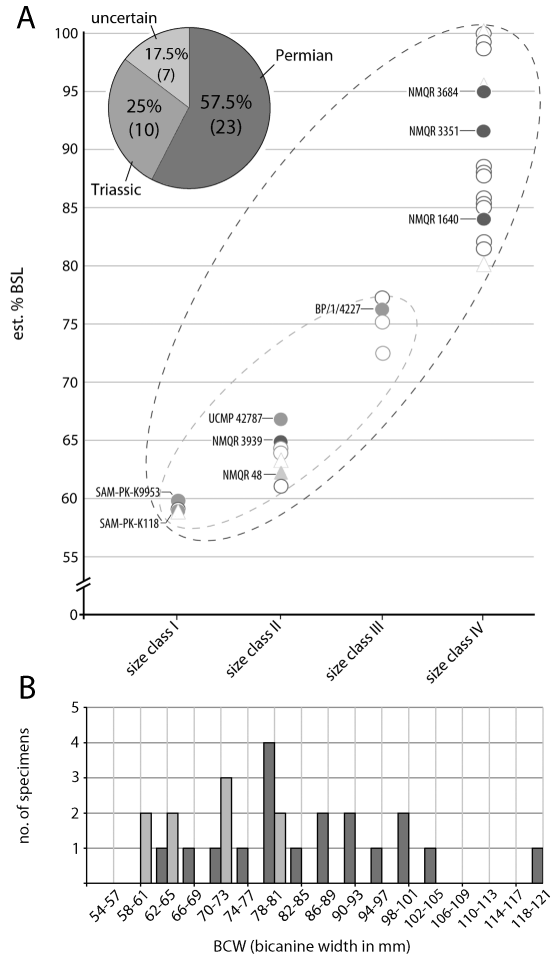

Figure 2.2. Sampling of *Moschorhinus kitchingi* across four size classes. **A**, Distribution of size classes noting specimens that were selected for histology. Open circles represent skulls of known stratigraphic provenance measured in Table 2.1; solid circles represent specimens of known stratigraphic provenance that were histologically sampled (dark gray = Permian subsample; medium gray = Triassic subsample). Light gray triangles represent specimens that were measured (open) or sampled histologically (solid), but lack stratigraphic provenance data. Inset: relative proportions of Permian, Triassic (revised *Lystrosaurus* Assemblage Zone; Botha and Smith 2007), and equivocal records from the 40 sampled specimens. **B**, Histogram of size distributions (bicanine width in mm) of Permian (dark gray) and Triassic (medium gray) *Moschorhinus*.

several recent collections as part of an ongoing project on the Early Triassic recovery (Smith and Ward, 2001; Smith and Botha, 2005; Botha and Smith, 2006). Of the 40 specimens complete enough for measurements, stratigraphic positions for seven could not be determined with confidence. For example, a large skull, BP/1/1713, was discovered by a farmer in the Bergville District at the Boesmansklip locality and assigned to the *Lystrosaurus* Assemblage Zone based on now outdated stratigraphic conventions (Brink, 1959). Although Kitching (1977) subsequently discovered Triassic index taxa at this locality, such as *Lystrosaurus murrayi*, their color, state of preservation, and associated matrix differs markedly from that of BP/1/1713. Moreover, a small non-*Lystrosaurus* dicynodont from this locality that was erroneously identified as a therocephalian (BP/1/4711) represents the presence of a DAZ taxon (AKH, personal observation) as elsewhere throughout the Bergville District where *Daptocephalus* and *L. maccaigi* also co-occur. The stratigraphic provenance of BP/1/1713 is therefore poorly constrained. Continued collecting efforts will allow future refinement to the stratigraphic sampling of *Moschorhinus* and to the hypotheses tested here.

Due to difficulties in reconstructing body mass of fossil taxa, the statistical tests employed here incorporated linear cranial measurements which, in the paucity of completely articulated postcranial material, could be obtained efficiently and with accuracy (recorded with Mitutoyo digital calipers to the nearest millimeter). I chose four standardized cranial size proxies including basal skull length (BSL, measured from the tip of the rostrum to the basioccipital; Fig. 2.3), snout (antorbital) length (SNL),

interorbital breadth (IOB), and bicanine width (BCW) (Abdala and Giannini, 2000, 2002). For a larger sample, and because BSL measurements were not available for incomplete skulls, BSL was supplemented by these additional size proxies. The measured specimens were standardized against the largest observed individual in the sample (BP/1/1713; BSL, 262 mm) and subdivided into four categorical size classes for comparative utility (Chinsamy, 1993; Horner et al., 2000; Ray and Chinsamy, 2004; Ray et al., 2005, 2010): size class I (60% or less greatest size); size class II (61–70%); size class III (71–80%), and size class IV (greater than 80%). For specimens with incomplete BSL data, I estimated size class by regressing available cranial metrics (SNL, IOB, BCW) against 20 complete skulls having known % largest BSL. Permian (CiAZ/DAZ) and Triassic (LAZ) data subsets were compared by performing a series of Welch's *t*-tests on the raw measurements in Table 2.1. Shapiro-Wilk tests for normality were performed on data subsets to confirm the appropriateness of the test statistic and a Kolmogorov-Smirnov (K-S) test was also performed to assess the overall equality of the distributions of Permian and Triassic subsets (useful in cases in which sample sizes were small or the data were not distributed normally, in spite of weaker statistical power).

Table 2.1. Basal skull length (BSL), snout length (SNL), interorbital breadth (IOB), and bicanine width (BCW) in uppermost Permian (CiAZ/DAZ) and lowermost Triassic (LAZ) *Moschorhinus*. Specimens are ordered by stratigraphic interval and size class; specimens with equivocal stratigraphic data or poorly documented provenance were not utilized in the *t*-test, and are listed at the bottom of the table. All measurements are in mm.

Specimen	Description	Locality and age	BSL (% Largest)	SNL	IOB	BCW	Size class
Permian (CiAZ/DAZ**)							
NHMUK R5698 (type)	partial skull	Bethesda Road, Eastern Cape (CiAZ/DAZ)	--	90	59	80	IV
BP/1/3983	partial skull	Nooitgedacht 68, Free State (DAZ)	260 (99%)	91	67	87	IV
NMQR 3835	skull with lower jaw	Elim 623, Free State (DAZ)	254 (97%)	100	74	119	IV
SAM-PK-K10684	partial snout with dentition	Bethal 763, Free State (DAZ)	--	--	--	105(est.)	IV
SAM-PK-K10015b	partial skull, lower jaw	Bethal 763, Free State (DAZ)	--	105	--	--	IV
NMQR 74	partial snout with dentition	Schalkwykskraal, Eastern Cape (DAZ)	--	--	--	100(est.)	IV
NMQR 3351*	skull, lower jaw, nearly complete skeleton	Bokpoort, Wepener, Free State (DAZ)	240 (91%)	106	64	81	IV
RC 32	skull	Compassberg, Eastern Cape (DAZ)	232 (88%)	83	63	98	IV
BP/1/3932	anterior skull	Lootsberg Pass, Eastern Cape (DAZ)	--	--	--	95	IV
SAM-PK-K10015a	skull	Bethal 763, Free State (DAZ)	230(est.) (87%)	96	63	90	IV
NMQR 76	skull	Schalkwykskraal, Eastern Cape (DAZ)	230 (87%)	95	35	88	IV
CGS JFD32/92	skull	Himeville, KwaZulu-Natal, RSA (DAZ)	225 (85%)	92	60	90	IV
NMQR 426	anterior skull	Beskuitfontein, Eastern Cape (DAZ)	--	93	--	--	IV
NMQR 87	anterior skull	Beskuitfontein, Eastern Cape (DAZ)	--	90	59.5	78	IV
RC 99	skull	Brandkraal, Eastern Cape (DAZ)	223 (85%)	75	58	80	IV
NMQR 3921	skull	Nooitgedacht 68, Free State (DAZ)	215 (82%)	78	75	94	IV
BP/1/2788	skull with lower jaw	Stoffelton, KwaZulu-Natal (DAZ)	215 (82%)	--	--	--	IV
NMQR 1640*	skull fragments, postcrania	Nooitgedacht 68, Free State (DAZ)	--	--	--	70	IV
NMQR 3684*	femur	Nooitgedacht 68, Free State (DAZ)	--	--	--	--	IV
CGS GHG299	skull and partial postcranial skeleton	Kommandodrift, Eastern Cape (DAZ)	200 (76%)	90	54	80	III
NMQR 73	disarticulated skull	Beskuitfontein, Eastern Cape (DAZ)	--	--	--	76	III
NMQR 3939*	skull and partial skeleton	Nooitgedacht 68, Free State (DAZ)	170(est.) (65%)	67	48.5	71	II
CGS GHG148	skull and partial postcranial skeleton	Thaba Nchu Commonage, Free State (DAZ)	160 (61%)	62	36	65	II

Triassic (LAZ†)

BP/1/4227*	skull, lower jaw, near complete postcranial skeleton	Admiralty Estates, KwaZulu-Natal (LAZ)	200 (76%)	85	54	70	III
NMQR 3568	skull, vertebrae, pectoral girdle	Skerpioenkraal, Eastern Cape (LAZ)	198 (75%)	83	49	78	III
CGS GHG295	skull and partial postcranial skeleton	Kommandodrift, Eastern Cape (LAZ)	190 (72%)	84	54	80	III
BP/1/5910	partial skull and postcrania	Elim 623, Free State (LAZ)	--	68	40	62	II
SAM-PK-K119	snout and postcranial fragments	Skerpioenkraal, Eastern Cape (LAZ)	--	--	--	63	II
UCMP 42787*	anterior skull, scapula, vertebrae humerus, radius, fibula	Thaba Nchu Commonage, Free State (LAZ)	--	--	--	73	II
SAM-PK-K118*	skull, partial lower jaw, anterior postcrania	Skerpioenkraal, Eastern Cape (LAZ)	157 (59%)	66	35	61	I
SAM-PK-K9953*	skull, lower jaw, semi-articulated postcrania	Lucerne 70, Eastern Cape (LAZ)	155 (59%)	70	45	--	I
SAM-PK-K10698	small lower jaw, ribs, pelvis	Lucerne 70, Eastern Cape (LAZ)	--	--	--	--	I
CGS GHG324	partial skull	Diepfontein, Free State (LAZ)	136 (52%)	53	48	58	I

Interval or provenance uncertain

BP/1/1713	skull	Boesmansklip, KwaZulu-Natal	262 (100%)	89	75	104	IV
BP/1/4636	skull	"Fairydale" (Bethal annex?), Bethulie District, Free State	250 (95%)	109	--	105	IV
NMQR 1393	partial skull	locality unknown	--	95	--	99	IV
CGS JFD9/94	skull and partial postcranial skeleton	Himeville District(?), KwaZulu-Natal	210 (80%)	--	--	80	III
NMQR 48*	skull, lower jaw, partial postcranial skeleton	Zeekoeigat, Eastern Cape	163 (62%)	68	37	69	II
NMQR 1006	partial skull	Thaba NChu Commonage, Free State	--	65	36	63	II
SAM-PK-K120	anterior skull	Groote Valley 133, Eastern Cape	--	--	--	58	I

* Limb bones from specimens in bold and denoted by single asterisk were sampled for histological sectioning
** CiAZ, Permian upper *Cistecephalus* Assemblage Zone; DAZ, Permian *Dicynodon* Assemblage Zone
† LAZ, Triassic *Lystrosaurus* Assemblage Zone

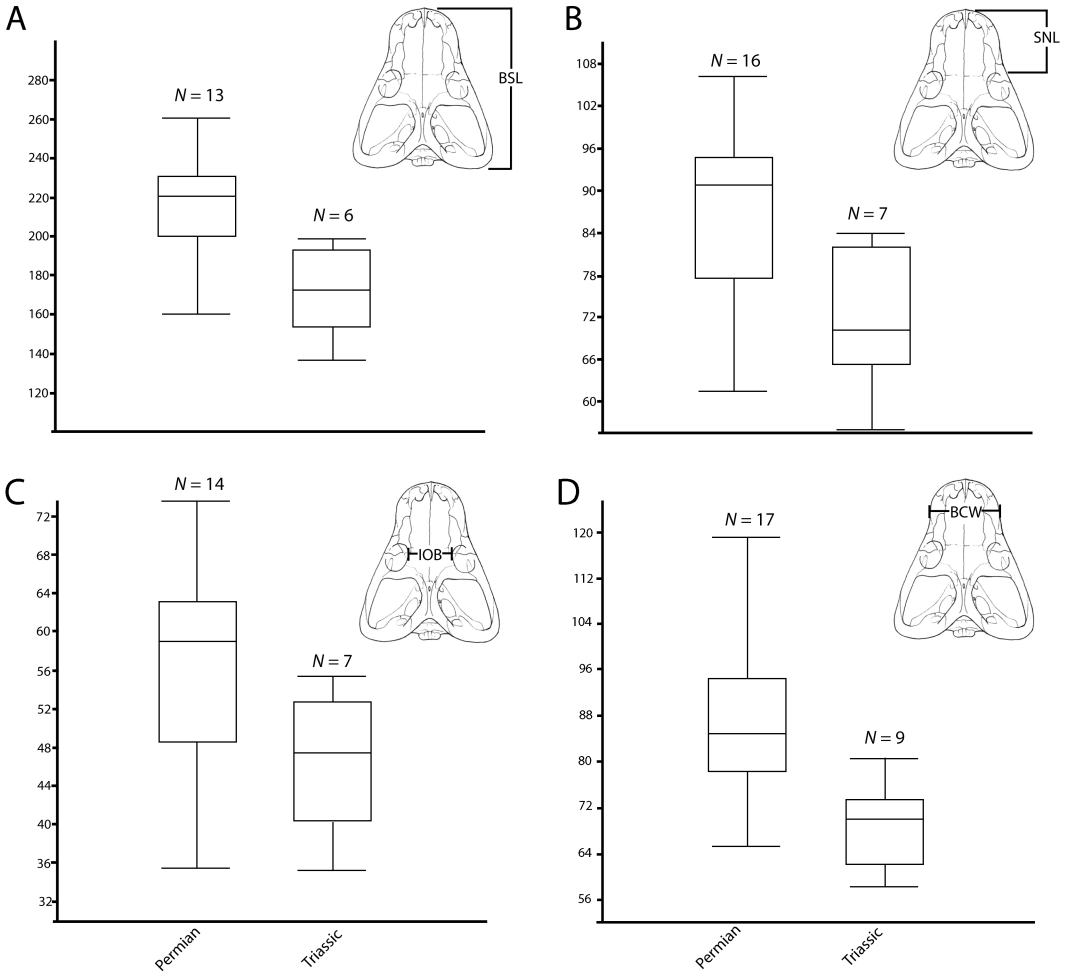

Figure 2.3. Boxplots comparing size distributions in Permian versus Triassic *Moschorhinus*. **A**, Basal skull length (BSL). **B**, Snout length (SNL). **C**, Interorbital breadth (IOB). **D**, Bicanine width (BCW). Vertical units are in mm.

Results 1: Geometry and Size

In a sample of 23 specimens in Table 2.1 preserving complete BSL measurements (19 of which had reliable provenance data), observed BSL ranged from 136 mm to 262 mm. Both Permian and Triassic subsamples showed normal distributions. The Permian distribution demonstrated a mean BSL of 219 mm, as compared to 172 mm in the Triassic subsample. In spite of some overlap within the lower end of the size distributions (due to the possible presence of immature individuals in each), the Permian distribution exhibited a much longer right tail, and sample means were significantly different from equality in a one-tailed test, ($p = 0.002$; see Table 2.2) indicating that the Permian distribution represented a subsample in which the mean skull length was greater than that of the Triassic subsample. Notably, none of the individuals in the Triassic subsample were observed within the largest size class (i.e., more than 80% largest BSL). By contrast, the greatest proportion of specimens within the Permian subsample was observed within size class IV (see Figure 2.2 and Table 2.1).

Other metrics of cranial size were investigated to incorporate a larger sample of individuals in which BSL could not be measured. Due to differences in magnitude of the measurements and potential disparity in scaling, their ability to predict overall skull size with accuracy may vary. For example, interorbital breadth (IOB) does not increase greatly as overall skull size increases, scaling with slight negative allometry. IOB measurements in large specimens may not be substantially greater than in small specimens, such that increased variance from specimen deformation or measurement

error may be more easily introduced. Not surprisingly, when regressed against BSL, IOB had the lowest coefficient of determination ($r^2 = 0.50$) among the supplemental cranial size metrics explored here. Nevertheless, all three of these metrics showed significant differences in their distributions between Permian and Triassic subsamples, with the Triassic distribution lower (and, thus, cranial size smaller) than that of the Permian data set (Fig. 2.3). This was especially evident in comparing bicanine width (BCW) between subsamples, which had the highest available sample sizes and as a likely corollary showed the lowest significance levels for all tests ($p << 0.05$). These comparisons suggest that a significant difference exists in the relative size distributions of Permo-Triassic *Moschorhinus*, with Triassic specimens consistently occupying the far left end of the overall distribution.

Table 2.2. Statistical results of Welch's *t* (one-tailed) and K-S tests on basal skull length (BSL), snout length (SNL), interorbital breadth (IOB), and bicanine width (BCW) compared between Permian and Triassic data subsets.

	BSL		SNL		IOB		BCW	
	Permian	Triassic	Permian	Triassic	Permian	Triassic	Permian	Triassic
Mean*	219[28]	172[26]	88[12]	72[11]	58[11]	46[7]	87[13]	68[7]
Variance	840	708	156	141	141	51	176	61
n	13	6	16	7	14	7	17	9
t	3.480		2.859		2.820		4.551	
p	**0.002**		**0.007**		**0.005**		**<0.001**	
D	0.769		0.687		0.714		0.705	
p (K-S)**	**0.006**		**0.009**		**0.007**		**0.002**	

* Values in brackets represent one standard deviation

** *p*-values in bold are significant at α=0.05

Methods 2: Histomorphology

In addition to cranial size, differences in long bone histomorphology were compared between Permian and Triassic *Moschorhinus*. Histomorphology has proven to be a powerful tool for deducing paleobiological attributes of fossil tetrapods, including aspects of mechanics (locomotion), habitat (aquatic, fossorial), and especially growth dynamics (Chinsamy, 1990, 1993, 2005; Erickson and Tumanova, 2000; Erickson et al., 2001; Horner and Padian, 2004; Cooper et al., 2008; Ricqlès et al., 2008; Chinsamy-Turan, 2011). Only recently have quantitative assessments of growth, based on the principle that periosteal bone typology (including texture and degree of vascularization) is an expression of its rate of apposition (Amprino, 1947), been applied to fossil therapsids (Botha and Chinsamy, 2000, 2004, 2005; Ray and Chinsamy, 2004; Ray et al., 2004, 2005, 2010; Botha-Brink and Angielczyk, 2010). Nonmammalian therapsids frequently exhibit limb bone cortices composed of a fibrolamellar bone complex (or FLB, woven-fibered interstitial extracellular matrix (ECM) with centripetally lamellated primary osteons) and a greater degree of vasculature over basal amniotes and 'anamniotes,' likely reflecting their greater overall growth rates (Ricqlès, 1974a,b, 1976; Bennett and Ruben, 1986; Chinsamy-Turan, 2011). Botha-Brink and Angielczyk (2010) provided a preliminary discussion of histovariation in the Permo-Triassic dicynodont *Lystrosaurus*, but histovariation in temporally successive populations of a single genus has otherwise not been investigated.

Here I compared two vascular growth proxies, % cortical vascularity (sometimes termed ‘porosity’ or ‘vascular density’) and mean primary osteon diameter, in Permian and Triassic midshaft limb bone cortices of *Moschorhinus*. Experimental studies have demonstrated that these proxies (along with bone tissue typology) represent robust indicators of relative bone apposition rates in growing monitor lizards (Buffrénil et al., 2007) and many birds (Castanet et al., 2000; Margerie et al., 2002, 2004). Selection of cortical vascularity as a proxy for relative growth also allows direct comparisons with other therapsids sampled histologically in previous studies where similar measurements were used (e.g. Botha-Brink and Angielczyk, 2010).

Limb bone elements (including both propodials and epipodials) were sampled across a broad range of sizes in an attempt to capture a complete ontogenetic sample for both Permian and Triassic data subsets, and were selected based on availability, preservation, and association with diagnostic cranial material (Fig. 2.2, Table 2.3). Thin-sectioning and microscopy followed standard sectioning procedures modified from Chinsamy and Raath (1992) and Wilson (1994). Prior to sectioning, detailed photographs and gross measurements were taken, and casts were produced when possible to preserve aspects of superficial morphology, size and shape.

The resulting midshaft serial cross-sections were examined on Nikon Eclipse 50i and LV100 POL petrographic microscopes and photographed using a mounted DS-Fi1

Table 2.3. Histomorphometric estimates from uppermost Permian (DAZ) and lowermost Triassic (LAZ) *Moschorhinus*.

	Size Class	%Largest Size*	Element	Growth marks obsv. (measured circ., mm)	Cortical Vascularity (%)	Mean Primary Osteon Diameter (µm)	*K*	*CDI*	*C*
Upper Permian (DAZ)									
NMQR 3939	II	65%	humerus	3-4(-, 43, 47, 51)	20.1[6.9]	134[36]	0.38	0.40	0.65
			radius	3(24, 27, 31)	11.4[2.6]	101[18]	0.31	0.85	0.82
			ulna	3(29,33,38)	10.1[2.1]	120[27]	0.44	0.64	0.81
			femur	3(-, -, 49)	18.4[6.9]	140[32]	0.44	0.58	0.71
			tibia (left)	3-4(-, -, 33, 37)	15.5[1.9]	117[17]	0.30	0.73	0.81
			tibia (right)	3 (-. 33, 37)	15.6[5.8]	119[34]	0.39	0.56	0.74
NMQR 1640a	IV	(84%)	femur	6(-, -, -, -, -, -)	11.1[4.8]	96[12]	0.50	0.47	0.74
NMQR 1640b	IV		tibia	4(-, -, -, -)	09.7[2.5]	106[23]	0.39	0.41	0.70
NMQR 3351	IV	91%	femur	5(-, 65, -, 81, 83)	13.6[5.0]	100[22]	0.55	0.30	0.53
NMQR 3684	IV	(95%)	femur	4(-, -, -, -)	14.2[4.6]	92[17]	0.53	0.67	0.80
Lower Triassic (LAZ)									
SAM-PK-K118	I	59%	humerus	0	25.5[4.9]	100[17]	0.41	0.57	0.77
			radius	0	19.5[3.2]	101[17]	0.54	0.48	0.72
SAM-PK-K9953	I	59%	femur	1(41)	20.9[5.8]	108[15]	0.42	0.51	0.68
UCMP 42787	II	(67%)	humerus	1(56)	19.5[4.0]	107[20]	0.34	0.45	0.76
			radius	1(34)	12.4[3.6]	92[18]	0.27	0.79	0.84
			fibula	1(23)	10.8[1.9]	58[14]	0.28	0.71	0.81
BP/1/4227	III	76%	humerus	2-3(31, 45, -)	12.1[2.9]	100[16]	0.35	0.69	0.86
			radius	3(-, 24, 36)	10.9[2.1]	88[10]	0.36	0.73	0.87
			ulna	2?(-, -)	08.5[2.0]	91[19]	0.48	0.55	0.79
PTB uncertain (DAZ/LAZ)									
NMQR 48†	II	62%	humerus	1(47)	16.6[5.0]	--	0.45	--	--
			radius	4(-, 20, 22, 24)	05.2[2.4]	67[18]	0.40	0.56	0.74
			ulna	4(26, 31, 34, 40)	04.8[1.3]	67[10]	0.43	0.60	0.73
			femur	1(42)	12.8[4.8]	95[13]	0.58	0.35	0.60

values in brackets represent one standard deviation

*Estimates based on relative BSL. Parentheses indicate values estimated by regressing BSL against femoral or humeral diameter for the entire sample (i.e., for specimens in which cranial material was inadequately preserved for a precise BSL measurement).

†Specimen from Waterval part of Zeekoeigat, Venterstad District; collection includes DAZ index taxa such as *Dinanomodon rubidgei* and *L. maccaigi*, but also the LAZ index taxa *L. declivis* and *L. murrayi*; this locality no longer exists and cannot be resolved beyond the PTB Palingkloof Member.

digital image capture system and NIS-Elements imaging software. Relative age and growth patterns in the sampled limb bones were assessed from the rendered cross-sectional images using NIH-ImageJ v. 1.42q software. Bone growth marks (annuli and lines of arrested growth or 'LAGs') were counted where present and the circumferences of complete growth marks were measured in mm around the cortex whenever possible (Table 2.3). Growth marks that were incomplete, poorly preserved, or obscured by resorptive processes were not measured.

Quantitative methods for the estimation of vascular growth proxies are illustrated in Figure 2.4. The protocol for estimating cortical vascularity *(%CV*) is outlined by Lee et al. (2013), in which the area of vascular canals (estimated with NIH-ImageJ by thresholding canals visible in rendered images) is divided by the total area occupied by primary cortical bone and multiplied by 100 (e.g., see Cubo et al., 2005). I performed stratified sampling of 10 standardized subsamples spaced regularly throughout the midcortex of each midshaft cross-section, which is critical in order to assess variance in vascularity around the cross-section, information that is rarely taken advantage of in paleohistological studies. The subsampled regions necessarily excluded areas of erosion cavities and secondary osteonal formation. As with %*CV*, mean primary osteon diameter (*POD*) is a correlative of periosteal bone apposition rates in growing tetrapods (Margerie et al., 2002), and has been shown to vary in different types of bone tissue, although it is generally greatest in highly woven and porous FLB. I estimated *POD* by measuring in

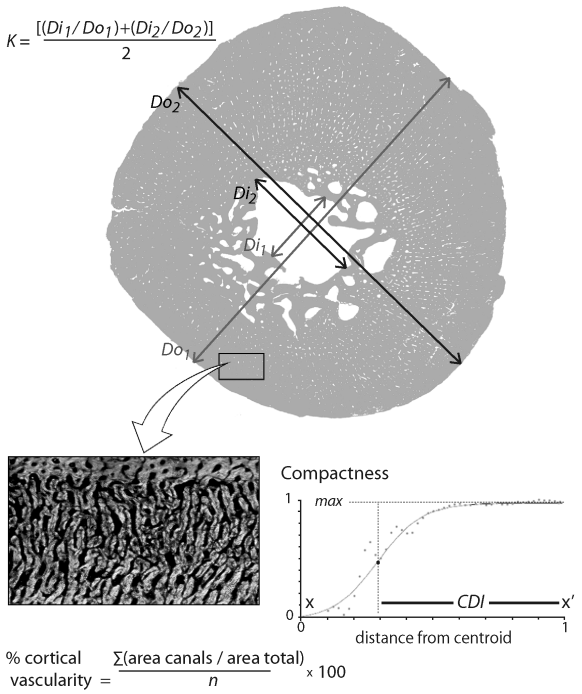

Figure 2.4. Schematic diagram illustrating thresholding and histomorphometric procedures for quantitative assessments of vascularity and robusticity proxies. Compactness (*C*) and cortico-diaphyseal index (*CDI*) were estimated using the bone compactness analysis software Bone Profiler (Girondot and Laurin 2003).

microns (μm) the transverse lengths of primary osteons visible in each sampled region (validated by the 'Maltese cross' pattern they exhibit under polarized light), and averaging them across all subsampled regions within a given bone. Inter-elemental (pooled) and propodial/epipodial-only (non-pooled) comparisons were made between Permian and Triassic subsamples by performing Welch's *t* and K-S tests as described above for the cranial size analysis.

Overall bone compactness (*C*) and two measures of the thickness of the outer bone wall were estimated in order to facilitate inferences of bone robusticity and lifestyle, including (1) *K* value, the ratio of the inner (medullary) to outer diameter of the diaphysis (Currey and Alexander, 1985) and (2) cortico-diaphyseal index (*CDI*), derived using Bone Profiler compactness analysis software (Girondot and Laurin, 2003). *K* and *CDI* measurements are illustrated in Figure 2.4 and values reported in Table 2.3. The *CDI* parameter in Bone Profiler represents the relative distance from the outer surface of the bone to the inflection point (i.e., center of transition zone) between the cancellous medulla and the compact cortex, and is thereby related to the overall "global compactness" of the bone [defined as the relative proportion of mineralized bone area to the total cross-sectional area, including that which consists of cancellous bone (Girondot and Laurin, 2003)]. The influences of these variables on vascularity were compared by additional Pearson product-moment correlation tests in order to identify whether size and robusticity covary with vascularity (discussed below).

Results 2: Histomorphology

Permian (DAZ) Subsample

Size class I (60% or less)—As surveyed Permian specimens rarely fell below 60% of the largest observed size (e.g., BP/1/6978, a single, isolated skull), limb bones from size class I individuals were not available for the Permian histologic sample.

Size class II (61–70%)—In general, the histologic profiles of elements in size class II showed moderate vascularization, but were compact with a thick bone wall (*CDI*, ~0.40–0.85). Great histovariability exists among the different elements sampled, mostly in primary osteon orientation (with combinations of longitudinal and reticular patterns) and tissue-type, including woven-, parallel-fibered, and lamellar bone tissue. The predominant composition, however, consists of large primary osteons (often 100+ μm in diameter) within a woven-fibered interstitial ECM, constituting a fibrolamellar complex. Parallel-fibered bone and localized lamellar bone are more prevalent in the epipodials, which are also less vascularized (%*CV*, ~10–15 %) and show a greater number of more closely spaced growth marks. Propodials tended to show more vascularized FLB and fewer growth zones, even within the same individual, indicating that the epipodials (e.g., radius, ulna, tibia; see Table 2.3) provide a more complete estimate of minimum age.

The humeral midshaft appears relatively compact in histological profile (Fig. 2.5A–C) with a moderately thick bone wall (*CDI*, 0.40) and coarse cancellous bone

Figure 2.5. Bone histology in various size classes of Permian (DAZ) *Moschorhinus.* White arrowheads indicate growth marks. **A**, NMQR 39393 (size class II), humerus midshaft cross-section viewed with crossed nicols. **B**, Same as A viewed under higher magnification showing distinct LAGs (arrowheads) preceded by parallel-fibered bone deposition (expressed as highly birefringent streaks in polarized light). **C**, Same as A and B viewed under higher magnification with normal light, and showing moderate reticular and longitudinal vascularization within a dense woven- and parallel-fibered interstitial matrix punctuated by occasional scalloped LAGs (arrow). **D**, NMQR 3939 (size class II), ulna midshaft cross-section viewed under normal light. **E**, NMQR 1640a (size class IV), femur midshaft cross-section viewed with crossed nicols, showing extensive parallel-fibered and lamellar bone in outer cortex. **F**, NMQR 3684 (size class IV), femur proximal shaft cross-section viewed with crossed nicols showing faint growth marks demarcated by cyclic parallel-fibered bone deposition. Abbreviations: flb, fibrolamellar bone; lb, lamellar bone; nc, nutrient canal; pfb, parallel-fibered bone; po, primary osteons.

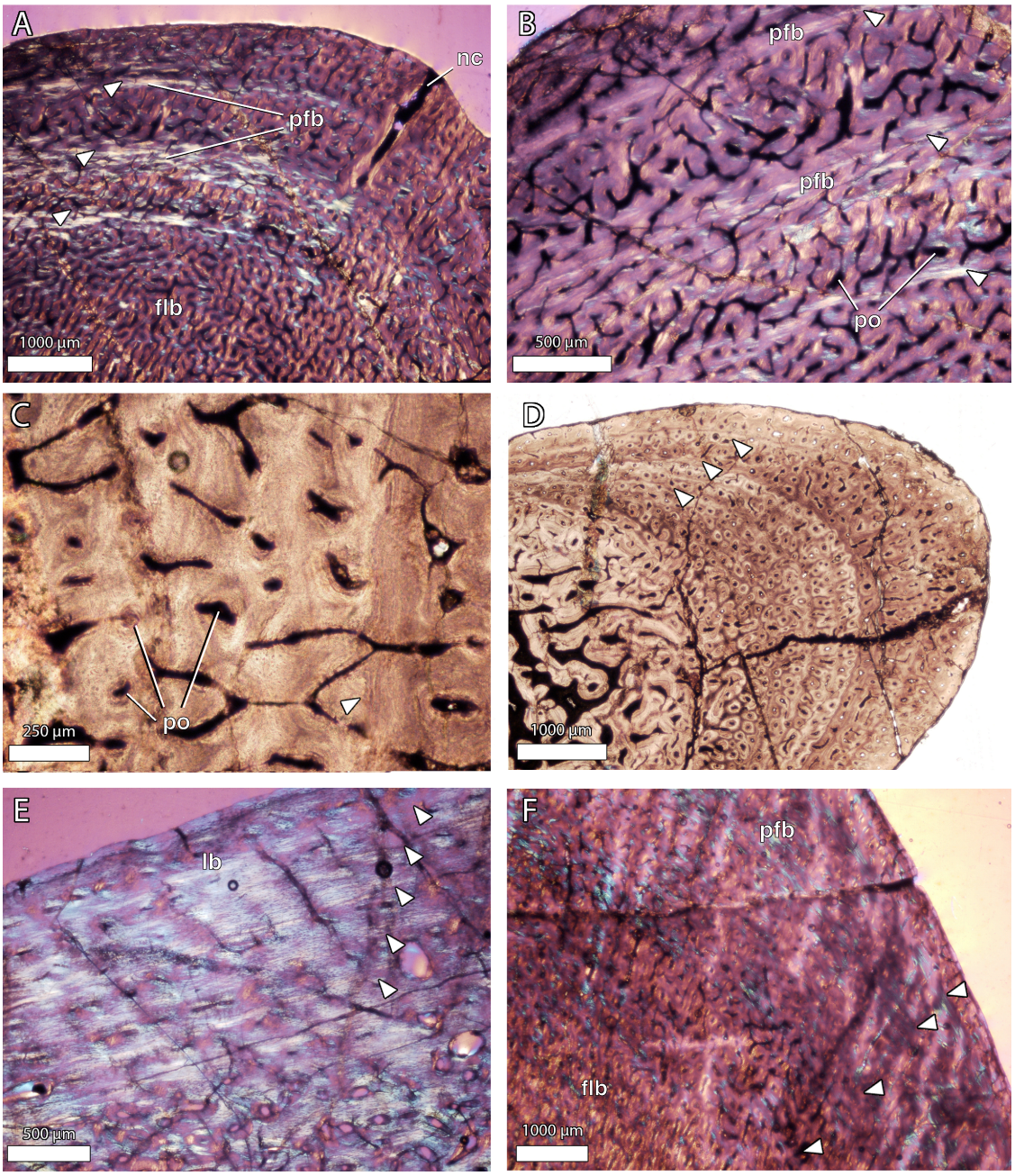
A
nc
pfb
flb
1000 µm
B
pfb
pfb
po
500 µm
C
po
250 µm
D
1000 µm
E
lb
500 µm
F
pfb
flb
1000 µm

occluding the medullary region. Large resorption cavities, however, are present throughout the inner lumen and become fewer as the spongiosa grades gradually into the more compact cortex. In addition to the overall compactness of the bone, the cortex displays a %*CV* of ~20%; higher than most other Permian therapsids (e.g., most early dicynodonts and cynodonts), but approaching that of the PTB survivor taxon *Lystrosaurus* (Ray et al., 2004; Botha and Angielczyk, 2010). The tissue-type is woven-fibered and largely primary, with little evidence of secondary osteonal formation in the outer cortex (i.e., no clear cement lines or overlapping, multigenerational structure). The overall pattern of vascularization is predominately reticular with rare longitudinal canals, but areas adjacent to muscular attachments (e.g., the region of the deltopectoral crest) exhibit canals with a markedly radial orientation and intervening Sharpey's fibers. The disorder of the cortex and internal remodeling obscures a clear record of LAG or annulus formation in some specimens, but at least three and possibly four growth marks are preserved in NMQR 3939 (with a possible, poorly defined annulus in the deep cortex, followed by three distinct LAGs, each preceded by periodic parallel-fibered bone deposition; Fig. 2.5A, B). There is no evidence of cessation of growth and no external fundamental system (EFS, an avascular outer zone of lamellar bone that is an indicator of skeletal maturity in mammals, birds, alligators and nonavian dinosaurs; e.g., Cormack, 1987; Chinsamy, 1990; Reid 1984; Horner et al., 2000; Woodward et al., 2011).

The radius and ulna of NMQR 3939 preserve the record of growth well. As in the humerus, midshaft sections of the radius display a compact cross-sectional profile but

with an even thicker bone wall (*CDI*, 0.85). Coarse cancellous bone constitutes the inner lumen and gives way periosteally to a more compact cortex (Fig. 2.5D). Overall, the cortices of the radius and ulna are much less vascularized than that of the humerus, displaying an increase in the relative proportion of longitudinal primary osteons but with sparse reticular canals present in some areas. The network of longitudinal and reticular primary osteons within a predominantly woven- and parallel-fibered ECM constitutes an overall fibrolamellar complex in both elements (Francillon-Vieillot et al., 1990; Currey, 2002, 2003). This tissue pattern, however, is punctuated by as many as four well-defined growth zones, demarcated by three distinct LAGs (Fig. 2.5D). Localized concentrations of lamellar bone can be found in most growth zones, with the exception of the outermost (subperiosteal) zone. Taken together, this pattern indicates relatively slower and periodically interrupted growth in the radius and ulna compared to the humerus. Like the humerus, however, there is no lamellar bone or EFS present in the outermost cortex, corroborating that the individual was unlikely to be somatically mature. Exceptional preservation of growth zones and LAGs in this individual was possible due to the regular pattern of deposition, thickened (i.e., complete or continuous) bone wall, and limited remodeling within the cortices of the radius and ulna. However, a few sparse secondary osteons (diagnosed by their thick multilamellar structure and demarcated by cement lines) are concentrated near the attachment site of the interosseous membrane, possibly in response to localized strains. Nevertheless, the epipodials (i.e., radius and ulna) appeared to record growth marks more completely than the propodials (Table 2.3).

The hind limb is represented by sections from the femur and both tibiae of NMQR 3939. The femoral midshaft exhibits a compact histological profile, with coarse inner trabeculae giving way gradually to the more compact cortex. The bone wall is comparable in thickness to the humerus (*CDI*, 0.58), being somewhat thinner walled than the epipodial elements described above. The overall histological profile is most similar to the humerus in the irregular and poor definition of the medulla, gradual transition to the compacta, abundance of reticular canals within the cortex (though longitudinal canals are present as in the radius and ulna), and a predominantly woven-fibered ECM in the cortex. Likewise, the erratic organization of the inner cortex, cortical remodeling and associated thinness of the bone wall, preserve a poor record of LAGs compared to the radius and ulna. Three LAGs were identified, but only the outermost could be traced and measured around the cortex (Table 2.3). The histological profiles of the tibiae were similar, showing a moderately thickened bone wall (but with some variation; *CDI*, ~ 0.56–0.73), and slightly better LAG preservation (with as many as three or four growth marks preserved).

Size class III (71–80%)—No limb bones from individuals of size class III were available for sectioning in the Permian subsample.

Size class IV (greater than 80%)—As no individuals from size class III were available in the Permian subsample (Table 2.3), the next size class was represented by individuals estimated to be greater than 80% of the largest size. Several specimens within Size Class IV were available to examine the histomorphology of larger, presumably

somatically mature, individuals. These included three large femora (NMQR 1640a, 3351, 3684) and a tibia (NMQR 1640b). Notably, NMQR 3351, a relatively complete and articulated skeleton in the upper size range of Permian *Moschorhinus*, bears no discernable neurocentral sutures.

In the femur, the histological profile exhibits great variability between the proximal shaft (nearer the metaphysis) and the midshaft. Proximally, the cortex is composed of a thick wall of compact bone, but it is highly porous and gives way to a heavily remodeled endosteal lumen that is occluded by coarse trabecular structures (as exemplified by NMQR 3684). At least four faint growth marks (annuli) are preserved in the proximal diaphysis of NMQR 3684, although none could be precisely measured or completely followed throughout the cortex. The offset position of the lumen, as well as the abundance of radial canals, and enlarged resorption cavities producing compact-to-cancellous conversion record extensive cortical drift at or near the metaphysis. These phenomena further complicate characterization and measurements of LAGs, even in individuals in the lower range of this size class (NMQR 1640a). NMQR 1640a, represented by a moderately large femur from an individual estimated to be 84% of the largest size, was serially sectioned at the proximal shaft (~60 mm distal to the femoral head). The histological profile of the shaft is similar to that described for presumed younger (i.e., size class II) individuals, but exhibits a slightly more abrupt transition between the spongiosa and the compacta, and a dense outer cortex incorporating a greater number of closely spaced growth marks (six in NMQR 1640a, compared to three poorly

preserved growth marks in the same element of NMQR 3939). Canal size and distribution varies throughout the cortex. Primary osteons are abundant in the mid- to outer cortex, but are replaced by densely concentrated resorption cavities closer to the inner endosteal margins. The predominant osteonal orientation is longitudinal and reticular, and the tissue type FLB with a mixed parallel- and woven-fibered ECM, somewhat resembling the primary cortical tissue of the radius and ulna described above for NMQR 3939. However, this pattern was interrupted by areas of highly disorganized, densely woven bone exhibiting high local concentrations of Sharpey's fibers (likely indicating areas of muscular or tendinous entheses). Some local secondary osteonal formation was also evident in areas of the midcortex where the bone wall was thin. This histovariability significantly interrupts the observable flow of growth marks around the cortex, making precise characterization and measurement of growth marks difficult at this late stage of development. Nevertheless, the cortex records the deposition of woven-fibered to parallel-fibered bone, followed by lamellar bone deposited in the subperiosteal region (Fig. 2.5E). The presence of lamellar bone incorporating simple (small, non-osteonal) canals in the subperiosteal region corroborates slowed growth in individuals of this size class.

The femoral midshaft of NMQR 3351 exhibits a relatively thinner bone wall (*CDI*, 0.30) that is demarcated by an abrupt transition with the medullary cavity. Few LAGs or annuli are measurable (three out of five) in this region, although the qualitative pattern of bone deposition is consistent with that described for NMQR 3684: highly

vascularized woven-fibered bone, followed by parallel-fibered bone, followed by a thin layer (~200–250 μm) of poorly vascularized lamellar bone in the subperiosteal region. The predominant pattern of vascularization is longitudinal and reticular (or anastomosing), although radial canals are visible in localized areas of presumed muscle attachment (e.g., the adductor ridge). Secondary osteonal formation is sparse but present, and secondary erosion cavities are generally restricted deep to the midcortex and endosteal margins. The combination of a transition to lamellar bone in the outer cortex, sparse secondary osteonal formation in the inner cortex, and closure of the neurocentral sutures in the vertebrae support that NMQR 3351 was somatically mature.

Triassic (LAZ) Subsample

Size class I (60% or less)—Two forelimb elements from a small Triassic skeleton (SAM-PK-K118) and a femur of a small, semi-articulated skeleton found 12 meters above the PTB (SAM-PK-K9953) were serially sectioned for comparison. Both specimens represent the smallest in the histologic sampling, each with a basal skull length about 59% largest size. The humeral midshaft of SAM-PK-K118 is well vascularized, having the highest %*CV* (25%) of all sampled individuals and elements (Fig. 2.6A, B). The primary osteons are predominantly radial with some reticular anastomoses within a thin, woven-fibered interstitial ECM, creating a cortex of entirely radial FLB. Notably, the radial osteons are so tightly packed that the diameter of each osteon is greater than the interstitial space that separates neighboring osteons (e.g., contrast Fig. 2.5B,C with Fig. 2.6B). The cortex is moderately thickened (*CDI*, 0.57)

Figure 2.6. Bone histology in various size classes of Triassic (LAZ) *Moschorhinus*. White arrows indicate growth marks. **A**, SAM-PK-K118 (size class I), humerus midshaft cross-section viewed with normal light, showing an extensive network of radial and reticular canals. **B**, Same as A viewed under higher magnification with crossed nicols, and showing densely packed radial primary osteons within a thin, woven-fibered interstitial matrix constituting radial FLB (note that the diameter of the osteons is greater than the interstitial space between osteons). **C**, SAM-PK-K9953 (size class I), femur midshaft cross-section viewed with crossed nicols, showing extensive radial FLB interrupted by a single LAG. **D**, UCMP 42787 (size class II), humerus midshaft cross-section viewed with crossed nicols, showing an occluded inner lumen and radial and reticular intracortical FLB, followed by a thin outer layer of parallel-fibered bone, which is punctuated by at least one growth mark. **E**, UCMP 42787 (size class II), radius midshaft cross-section viewed with crossed nicols, showing reticular and longitudinal FLB interrupted by a single growth mark in the outer (subperiosteal) cortex. **F**, BP/1/4227 (size class III), radius midshaft cross-section viewed under normal light, showing densely packed, multi-lamellar primary osteons (note that although the osteons are occluded, the osteonal diameter is greater than the interstitial space between osteons, as seen in B and C). Abbreviations as in Figure 2.5.

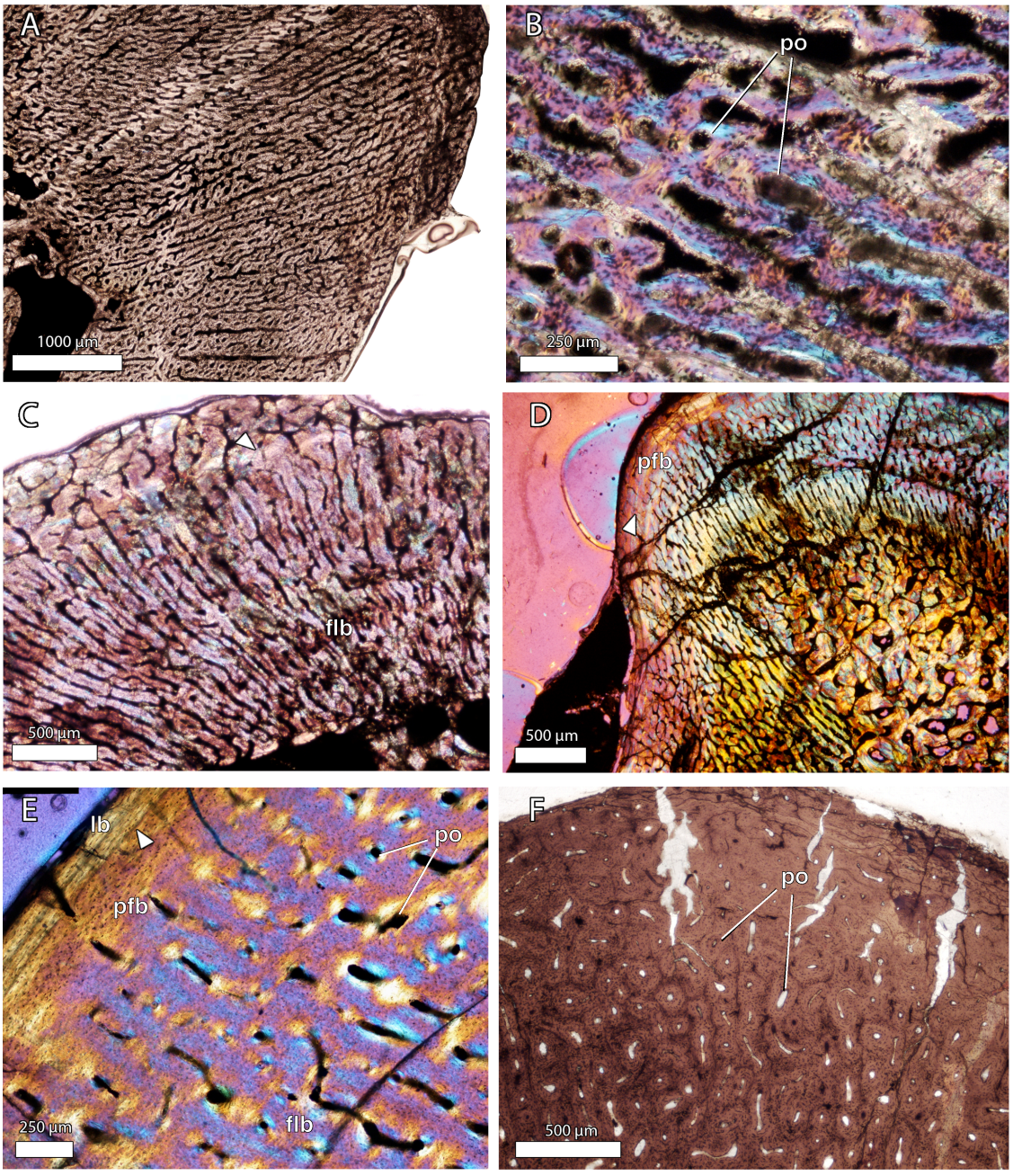
A
1000 µm
B
po
250 µm
C
flb
500 µm
D
pfb
500 µm
E
lb
pfb
po
flb
250 µm
F
po
500 µm

and shows no growth marks. The radius is similarly composed of radial and reticular FLB and also lacks growth marks.

The midshaft of the femur of SAM-PK-K9953 exhibits an abrupt transition between a well-developed medullary cavity and the compacta. The highly vascularized bone wall is moderately thickened as in the humerus (*CDI*, 0.51) and its relatively homogenous matrix composition is formed by a woven-fibered scaffolding with densely intervening radially-oriented primary osteons (Fig. 2.6C). This pattern is interrupted by a single LAG in the midcortex that is traceable around the entire section, but is succeeded by reticular and radially vascularized woven-fibered bone tissue all of the way to the subperiosteal region. The LAG punctuates at least one episodic period of cessation between two relatively rapid annual growth cycles. There is, however, no indication of an overall decrease in growth trajectory and no evidence of cessation of growth in the subperiosteal region during this stage.

Size class II (61–70%)—The midshaft of the humerus of UCMP 42787 is highly compact in histological profile (Fig. 2.6D). The medullary region is occluded by coarse cancellous bone (similar to other humeri in both subsamples) and the cortical bone wall is therefore notably thickened. Surrounding the lumen the inner cortex displays extensive erosion cavities. The mid- to outer cortex is porous (%*CV*, ~ 19%) with densely concentrated primary osteons exhibiting a largely reticular osteonal network, though the canals are more radially oriented nearer the deltopectoral crest. On the medial side of the bone, the vascular network appears more subplexiform where parallel-fibered bone forms

the surrounding matrix. The bone matrix is woven-fibered in deeper layers, but forms a more parallel-fibered matrix approximately 250–300 μm thick in these localized areas of the outermost cortex. Even at this comparatively small body size, a marked transition in the style of bone deposition can be inferred in this outermost region based on the unique localized character of histological structures. High magnification photomicrographs reveal that highly vascularized reticular FLB containing dense concentrations of enlarged, globular osteocyte lacunae in a woven-fibered matrix gave way to more regularly lamellated and poorly vascularized parallel-fibered bone bearing only a few sparse longitudinal canals and less concentrated, uniformly distributed, lenticular osteocyte lacunae.

The radius also consists of well-vascularized FLB (Fig. 2.6E) having a %*CV* of ~12% and a very thick bone wall (*CDI*, 0.79). The majority of the cortex from the medulla to the subperiosteal region is dominated by reticular FLB, exhibiting densely packed reticular and longitudinal primary osteons. However, the concentration of osteons decreases toward the periosteum. The nearly avascular subperiosteal layer is formed of a zone of lamellar bone that is approximately 200–250 μm in thickness, indicating a decelerating trajectory of growth (although this may represent the formation of an annulus at the end of the growing season). A single annulus in this region punctuates the transition from a predominantly FLB to a more lamellar-dominated outer cortex. This pattern differs markedly from that observed in a slightly smaller individual of the same size class from the Permian subsample (NMQR 3939; e.g., Fig. 2.5D), in which the

radius and ulna show multiple growth zones characterized by extensive longitudinally vascularized parallel-fibered and localized lamellar bone interrupted by several LAGs.

The fibula is highly compact with a minute medullary cavity and a very thick bone wall (*CDI*, 0.71). It is largely formed by parallel- and woven-fibered bone, although the woven-fibered matrix is not as prominent as in the humerus. There is also a high occurrence of longitudinal primary osteons with few obliquely oriented canals. In the outermost cortex, a thin zone (~100–150 μm) of parallel-fibered or lamellar bone (variable by location in the section) surrounds this inner growth zone and is demarcated by an abrupt growth mark that is traceable around the entire section (as observed in the radius). There are, thus, at least two observable growth zones; an inner zone of well-vascularized FLB and a thin outer band of less vascularized parallel-fibered and lamellar bone.

Size class III (71–80%)—The midshaft of the humerus of a moderately sized (76% largest size), semi-articulated skeleton, BP/1/4227, was serially sectioned for comparison, and represents the largest in the Triassic subsample (being three-quarters the size of the largest Permian individuals). The midshaft exhibits a very compact histological profile as in individuals of other size classes in both the Permian and Triassic subsamples, having a highly occluded inner lumen. The cortex is composed of well-vascularized FLB exhibiting both radial and longitudinal osteons. The radial osteons were most heavily concentrated in the region of the deltopectoral crest (as in UCMP 42787). The osteons within this largely parallel-fibered scaffolding were subsequently filled in

with centripetally deposited lamellar bone. The numerous multilamellar primary osteons thus formed elaborate ‘protohaversian’ architecture (Enlow and Brown, 1956, 1957; Reid, 1985, 1986). In spite of their thick, multilamellar structure, none of the osteons could be positively diagnosed as secondary Haversian structures, due to a lack of overlap between osteons (i.e., multigenerational osteons) and a lack of clear cement lines cutting through the interstitial ECM (except in the innermost regions of the cortex where erosion cavities formed in the inner lumen).

The radius and ulna of BP/1/4227 exhibit well vascularized FLB as in the humerus, with large multilamellar primary osteons (Fig. 2.6F). The subperiosteal layer is formed of a thin zone of lamellar bone that is approximately 200–250 μm in thickness, indicating a possible decelerating trajectory of growth.

Size class IV (greater than 80%)—None of the histologically sampled or measured specimens in the Triassic subsample exceeded 200 mm in BSL (i.e., 76% largest size) as Triassic *Moschorhinus* were generally smaller in their overall size distribution (Figs. 2.2, 2.3). Thus, size class IV individuals were not represented in the Triassic sampling.

Quantitative Results

In general, qualitative assessments of bone histomorphology show increased vascularity in limb bones from the Triassic subsample in association with thick growth zones of irregularly organized FLB, often having a radial or reticular vascular network, and fewer preserved growth marks in both propodials and epipodials. As Triassic

individuals were generally smaller, this pattern could therefore reflect differences between small juveniles and somatically mature individuals, as juvenile bone is generally more vascularized and porous than that of adults of the same species (Amprino, 1947; Margerie et al., 2002; Currey, 2002, 2003). A tight relationship between size, vascularity, and number of preserved growth marks could therefore provide useful information on inferring relative age in *Moschorhinus*. I performed correlation tests on the quantified bone vasculature for propodial-only and epipodial-only subsets, and pooled (inter-elemental) data to assess the relationships between vascularity and size estimates based on the raw data in Table 2.3. This was supplemented with additional Welch's *t*-tests (as described above for the cranial size comparisons) on a stratified subsample of Permian and Triassic histomorphometric estimates to assess differences in vascularity between Permian and Triassic subsamples.

Effects of size and robusticity—In order to assess the effects of size and robusticity on intracortical vascular patterns, I implemented Pearson product-moment correlation tests. I assessed statistical correlations of %*CV* and *POD* with two metrics of size, including the natural log of BSL and bone midshaft circumference, and three additional measures of robusticity (i.e., *K*, *CDI*, and *C*). The results of these tests are given in Table 2.4. Support for a relationship between size/robusticity and vascularity is generally poor for most measures.

Table 2.4. Pearson product-moment correlation statistics (Pearson's *r* and *p*) for size/robusticity and vascular growth proxies.

	Propodial-only		Epipodial-only		Pooled	
	r	*p**	*r*	*p*	*r*	*p*
Cortical vascularity vs. ln BSL	**−0.663**	**0.026**	−0.210	0.511	−0.303	0.159
Cortical vascularity vs. ln midshaft circumference	**−0.685**	**0.019**	−0.151	0.637	0.169	0.439
Cortical vascularity vs. K	−0.518	0.102	0.035	0.912	0.043	0.843
Cortical vascularity vs. CDI	0.070	0.846	0.032	0.919	−0.224	0.314
Cortical vascularity vs. C	0.058	0.873	0.046	0.885	−0.201	0.368
Primary osteon diameter vs. ln BSL	−0.430	0.214	0.088	0.784	−0.089	0.693
Primary osteon diameter vs. ln midshaft circumference	−0.404	0.246	0.426	0.166	0.349	0.110
Primary osteon diameter vs. K	−0.416	0.231	0.128	0.690	0.056	0.804
Primary osteon diameter vs. CDI	−0.045	0.899	−0.072	0.822	−0.213	0.340
Primary osteon diameter vs. C	−0.152	0.674	0.002	0.993	−0.211	0.343

**r and p*-values in boldface are significant at α = 0.05

For example, BSL and %*CV* were not significantly correlated for the epipodial subset and pooled data. The natural log of BSL and midshaft circumference predict cortical vascularity of the propodials reasonably well, both with a strongly negative correlation. However, none of these measures (including the natural log of BSL and midshaft circumference) predict well *POD* for any of the data subsets. Consequently, these size and robusticity proxies are likely unreliable predictors of vascularity in *Moschorhinus*. These include the additional robusticity proxies (*K*, *CDI*, and *C*), indicating that any observed temporal variation in those quantities is likely due to variation in degree of pachyosteosclerosis of the inner lumen (i.e., thickening of the bone wall and occlusion of the medullary cavity by trabecular structures) rather than variation in vascular density or localized osteosclerosis of the cortical bone.

Geologic interval and bone histomorphology— I performed three sets of *t*-tests on propodial-only, epipodial-only, and pooled data sets to assess whether %*CV*, *POD*, and *K* exhibit significantly different distributions between Permian and Triassic subsamples. Results of the propodial-only and pooled analyses were significant for %*CV*, with vascularity generally being higher in the Triassic (Table 2.5; Fig. 2.7A–C). This finding is weak in the pooled test, and non-significant for the epipodial-only subset, which may be a result of increased variance in the sample introduced by comparing %*CV* estimates from different bones which have different functions and grow with different absolute rates throughout the skeleton (the "long bone effect" of Margerie, 2002; Margerie et al., 2004). Vascular growth proxies differed in their disparity and direction of change between Permian and Triassic populations. In spite of a significant increase in overall cortical vascularity in the Triassic, *POD* decreased in epipodial-only and pooled data sets ($p < 0.001$), although the reduction in size is minute, non-significant in the propodials, and generally remains high with osteons maintaining ~100 μm in diameter (large even for growing mammals and birds). Taken together, this indicates a greater density of canals when the woven-bone scaffolding was laid down in early ontogeny (e.g., Fig. 2.6A–C), and thus greater surface area of the initial vascular network in Triassic individuals. Hence, Triassic decreases in mean size were associated with relatively higher limb bone %*CV* within each element. Moreover, when inter-elemental variation in vascularity is taken into account, geologic interval is a better predictor of

Table 2.5. Propodial/epipodial-only and pooled (inter-elemental) results of Welch's *t* (two-tailed) and K-S tests on cortical vascularity, mean primary osteon diameter, and *K* compared between Permian and Triassic data subsets.

	Propodial-only		Epipodial-only*		Pooled	
Cortical vascularity	Permian	Triassic	Permian	Triassic	Permian	Triassic
Mean	15.5[6.4]	19.5[6.5]	12.1[3.5]	11.7[3.8]	13.6[5]	15.5[6.5]
Variance	41.9	43.1	12.3	15.0	25.0	43.0
n	50	40	49	47	98	90
t	–2.873		0.492		–2.290	
p	**0.005**		0.623		**0.023**	
D	0.31		0.15		0.17	
p (K-S)**	**0.021**		0.589		0.117	
Primary osteon diameter						
Mean	108[25]	104[17]	112[24]	86[21]	110[24]	95[19]
Variance	667	312	587	473	602	394
n	96	80	99	100	194	174
t	--		7.836		6.20	
p	--		**<0.001**		**<0.001**	
D	0.18		0.43		0.279	
p (K-S)**	0.076		**<0.001**		**<0.001**	
K						
Mean	0.48[.06]	0.38[.04]	0.36[.05]	0.38[.12]	0.42[.08]	0.38[.08]
Variance	0.004	0.001	0.003	0.014	0.007	0.007
n	5	4	5	5	10	9
t	2.685		–0.333		0.989	
p	**0.031**		0.750		0.336	
D	0.80		0.400		0.355	
p (K-S)	0.052		0.697		0.489	

* Values in brackets represent one standard deviation
** *p*-values in bold are significant at α=0.05

vascularity than body size alone. Additionally, mean *K* is significantly lower in Triassic propodials (Fig. 2.7G) compared to Permian ones, indicating a reduction in the size of the medullary cavity by the thickening of the cortical bone wall (i.e., increased pachyosteosclerosis) in spite of a more porous (vascularized) intracortical region in the propodials.

Discussion

Size and Earliest Triassic Lilliput Phenomena

Urbanek (1993) originally characterized Lilliput phenomena as temporary body size reductions influenced by heterochronic shifts (i.e., paedomorphosis) within post-extinction survivor lineages, although the definition has been expanded by some authors to incorporate other possible underlying mechanisms (Erwin, 1998; Twitchett, 2007; Harries and Knorr, 2009). Accordingly, Triassic *Moschorhinus* show significant size reductions when compared to their Late Permian predecessors. Notably, the Permian-Triassic transition was characterized by the extinction of large gorgonopsian predators and many large-bodied herbivore lineages (e.g., pareiasaurs and most dicynodonts) as well as replacement of the large-bodied *Lystrosaurus maccaigi* by other much smaller congeners (e.g., *L. declivis*, *L. murrayi*) (Smith, 1995; Sidor and Smith, 2004; Smith and Botha, 2005; Botha and Smith, 2006, 2007). However, as the mechanisms behind many of these body size reductions remain unknown, they could have been achieved by any combination of processes, including differential extinction of large- versus small-bodied

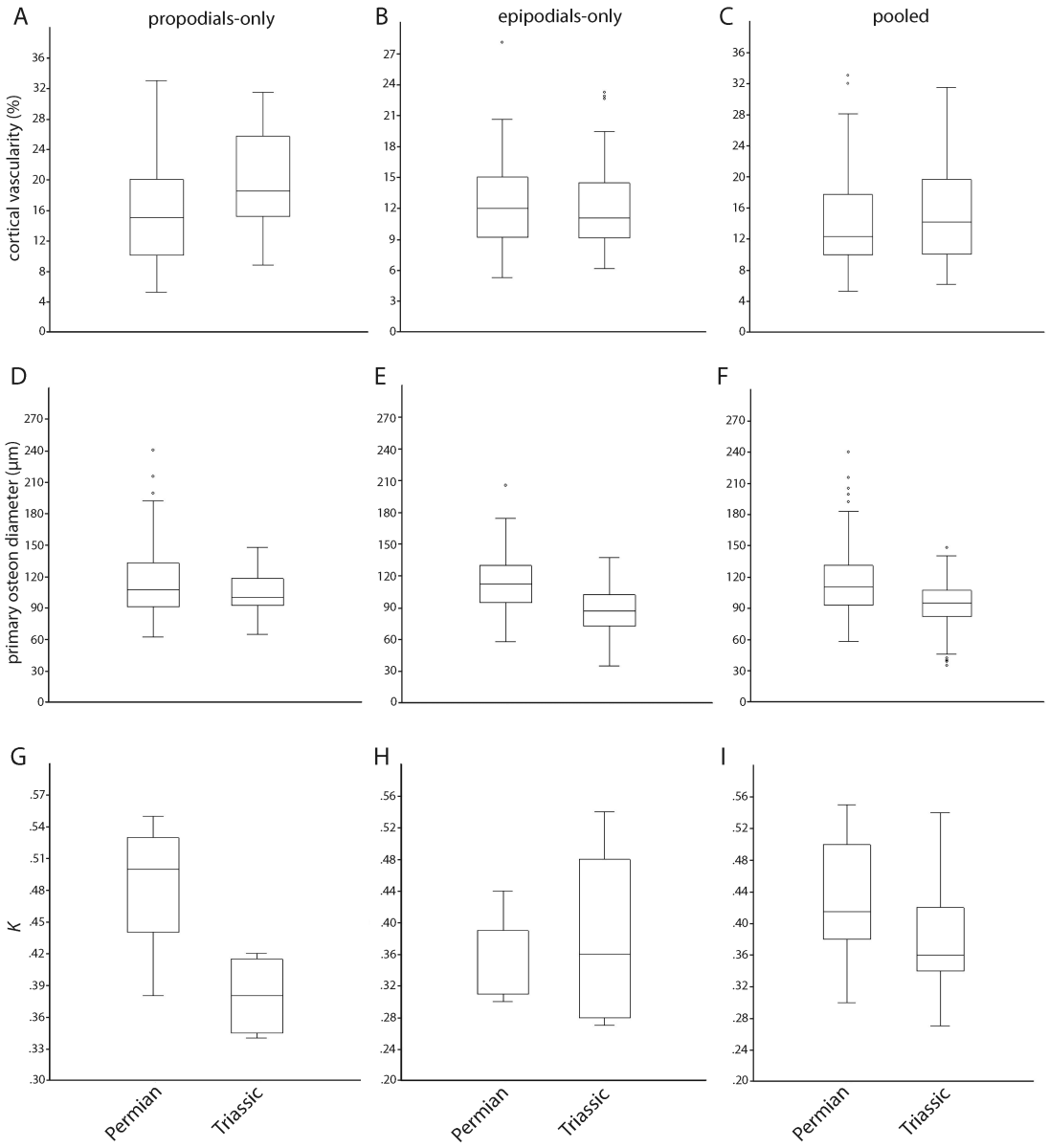

Figure 2.7. Boxplots comparing vascularity and robusticity distributions of Permian versus Triassic *Moschorhinus* for propodial-only (**A, D, G**), epipodial-only (**B, E, H**), and pooled (**C, F, I**) data sets. Resulting statistics are presented in Table 2.5.

clades (e.g., clade-level selection) and within-lineage heterochronic shifts (Harries and Knorr, 2009). Reduction in size and duration of postnatal development achieved by paedomorphosis (i.e., progenesis) is a classic attribute of *r*-strategist populations in perturbed or unstable environments (Gould, 1977; Hanken and Wake, 1993; Harries et al., 1996).

Although my findings are consistent with observations documented in recent literature (e.g., Sahney and Benton, 2008), post-extinction body size reductions have yet to be surveyed broadly across terrestrial Permo-Triassic faunas. Moreover, comparatively little is known about the composition and ecological attributes of latest Permian and earliest Triassic faunas outside the Karoo Basin of South Africa, hindering global assessments of changes in faunal characteristics. The disparity of body sizes, abundance of specimens, and widespread occurrence of the PTB survivor taxon *Lystrosaurus* provide a promising prospect for further assessing body size reductions and life history evolution within a single PTB lineage (Botha-Brink and Angielczyk, 2010; Botha-Brink et al., in press).

Bone Histomorphology and Growth Tactics in Permo-Triassic *Moschorhinus*

A list of qualitative histological comparisons in Permian and Triassic *Moschorhinus* is presented in Table 2.6. The available data suggest that Triassic *Moschorhinus* grew at rates accelerated over those in the Permian, and exhibited an attenuated growth period (possibly accounting for smaller mean and maximum sizes in the earliest Triassic). This inference is based in part on the overall increase in vasculature

Table 2.6. Qualitative comparisons of bone histomorphologies and inferred growth trajectories in Permian and Triassic *Moschorhinus*.

	Permian	Triassic
Primary bone matrix-type(s)	woven- and parallel-fibered bone (lamellar in outer cortex of large individuals)	woven-fibered bone (interrupted by parallel-fibered and lamellar in outermost cortex)
% Cortical vascularity	10-20% in small individuals; 10-15% in larger individuals	~20-25% in small individuals; 10-12% in larger individuals due in part to nonpathologic intracortical osteosclerosis (e.g., BP/1/4227; Fig. 6F)
Primary osteon size and distribution	~100 μm in diameter, decreasing in size in outermost cortex; large individuals show simple canals in outer cortex	≤100 μm in diameter with comparatively less variation in size
Growth marks	abundant in both small and large individuals; propodials and epipodials in small individuals may record 3+ growth marks	sparse, as many as 1-2 restricted to outer cortex of all elements
K	~0.30-0.55 with thin medulla, surrounded by thickened cortex in well-sampled propodials	~0.27-0.54 with medulla nearly occluded in well-sampled propodials
Inferred growth trajectory	prolonged, multi-year (cyclic) growth to large body size	accelerated, sustained growth in early ontogeny

observed in the propodial-only and pooled analyses (Fig. 2.7), and by fewer observed growth marks and growth zones in Triassic individuals regardless of size (e.g., Table 2.3, Fig. 2.6). In sum, size alone is a poor indicator of relative age in *Moschorhinus* unless geologic interval is taken into account. I suggest that variation in size is highly sensitive to variations in juvenile growth rate, and that rapid early growth to a minimum body size requirement (resulting in an overall growth period attenuation) reflects a novel growth tactic suited to Triassic communities. Although a strategy of rapid early development

may at first seem energetically expensive in a resource-limited environment, it is possible that rapid growth to a minimum size requirement may be less costly than prolonged, multi-year growth and maintenance under variable environmental conditions. For example, in insects and other terrestrial invertebrates, accelerated growth rates are often observed in temperate seasonal environments where developmental time horizons are short because the physiological and reproductive costs of rapid larval growth are less than the costs of overwintering (Stearns, 1992; Gotthard, 2001). In the southwestern US, desert tortoises in populations experiencing greater seasonal intensity (i.e., Mojave Desert) tend to grow more rapidly, but mature at smaller body sizes than in populations experiencing less variable conditions (i.e., Sonoran Desert), possibly due to similar trade-offs (Curtin et al., 2009). Likewise, life history tactics in *Moschorhinus* may have optimized body size and developmental times as a means of meeting biologically important time horizons (e.g., hibernation, reproductive schedules) in episodically disturbed environments (Gotthard, 2001). Similarly rapid growth strategies have recently been identified in at least some Triassic archosauromorphs of South Africa (Botha-Brink and Smith, 2011).

Increased representation of juveniles?—Alternatively, as juveniles typically display greater vascularity and higher rates of skeletal growth than somatically mature adults (Amprino, 1947; Margerie et al., 2002), greater mean vascularity accompanied by smaller sizes in the Triassic could be interpreted as overrepresentation of juveniles in the *Lystrosaurus* Assemblage Zone. Similarly, Luo et al. (2008) interpreted size reductions in

earliest Triassic conodonts as evidence of increased juvenile mortality rates, although this was not corroborated by life history data. This hypothesis is rejected in *Moschorhinus* by at least two major findings. Firstly, combined Permian and Triassic data sets subjected to linear regressions indicated that size alone was a poor predictor of vascular growth proxies in *Moschorhinus*. Notably, primary osteon diameter, which is demonstrated to be initially large and to decrease with skeletal maturity in at least some extant tetrapods (Amprino, 1947; Margerie et al., 2002), was actually slightly smaller in the Triassic subsample for some elements despite greater overall density of vascular canals. Both pooled and non-pooled analyses found geologic interval to be a more consistent predictor of vascularity than size in *Moschorhinus*. Secondly, visual comparisons between Permian and Triassic individuals of equivalent size class reveal qualitatively different histological profiles (Table 2.6; Figs. 2.5, 2.6). For example, in spite of their similarity in size (both size class II), the Permian NMQR 3939 exhibits greater multi-zonal intracortical structure incorporating parallel-fibered and lamellar tissue, and punctuated by as many as four growth marks as compared to a single subperiosteal annulus in the Triassic UCMP 42787. It is therefore possible that even small Permian individuals may represent early or late subadults gradually approaching a growth asymptote (but not yet senescent), rather than juveniles; however, this terminology may not apply well to *Moschorhinus* given its diversity in growth style. These caveats highlight the influence of variation in juvenile growth rate on body size at any given point in ontogeny, and caution should therefore be

practiced when attempting to use size alone as an indicator of age in fossil nonmammalian synapsids.

Hypoxia response?—Atmospheric oxygen composition during the PTB has been reconstructed based on mathematical models of burial and oxidative weathering of organic matter (e.g., Berner, 1999, 2003, 2004, 2006), and may have exhibited a long term decrease from 30% during the Early Permian to as low as 15% in the Early Triassic (Huey and Ward, 2005; Berner et al., 2007; Belcher and McElwain, 2008). Recently, it has been suggested that this modeled change from hyperoxic to hypoxic conditions would have had effects on the physiology and morphology of Permo-Triassic tetrapods (Retallack et al., 2003; Angielczyk and Walsh, 2008) or even caused the extinction via altitudinal compression and fragmentation effects (Huey and Ward, 2005).

Experimental data from terrestrial insects and vertebrates indicate that hypoxia negatively influences body size and somatic growth (e.g., Frazier et al., 2001; Woods and Hill, 2004; VandenBrooks, 2007; Owerkowics et al., 2009), which one might consider when interpreting size and histomorphology in Permo-Triassic tetrapods such as *Moschorhinus*. For example, preliminary observations on American alligators raised in hypoxic (12% O_2) conditions reveal acute physiological responses in which limb bone robusticity and mineral content increased compared to normoxic individuals (Owerkowics et al., 2010). However, the underlying processes and possible histomorphologic correlates (e.g., increased pachyosteosclerosis and bone wall thickness, increased intracortical mineral content, decreased intracortical vascular density, etc.) have

not yet been described in detail in extant tetrapods. The increase in limb bone robusticity and increased surface area of the intracortical vascular network in Triassic *Moschorhinus* are intriguing and possibly relevant results, but they may have limited comparative value unless more experimental physiology studies can offer predictive hypotheses that describe the histomorphologic correlates of hypoxia. Moreover, although acute physiological responses are readily interpretable in an experimental setting, hypoxia may select for evolutionary adaptation in physiological transport systems and over time scales not detectable in the geologic record [e.g., hemoglobins and aerobic capacities in high altitude mammals (Snyder, 1981; Hayes and O'Connor, 1999; Russell et al., 2008)].

Finally, investigations of palate and naris morphology and vascular growth patterns in dicynodont therapsids have offered additional challenges, demonstrating strong phylogenetic signal in at least some functional systems, weakening hypoxia-based extinction scenarios, and underscoring pervasive long term phylogenetic trends in Permian therapsids (Angielczyk and Walsh, 2008; Botha-Brink and Angielczyk, 2010). Observed changes in *Moschorhinus* at or near the PTB could similarly reflect long term trends in therocephalian life history evolution, but this has not yet been tested as I have effectively compared only two categorical temporal bins (DAZ and LAZ) and have yet to sample the broader distribution of life history traits in other Permian and Triassic therocephalian clades.

Conclusions

An investigation of size and histovariation in the therocephalian *Moschorhinus* revealed significant variation between Permian and Triassic individuals. Detailed assessments of histovariability and vascular growth proxies suggest that size alone is a poor indicator of skeletal age (e.g., juvenile versus somatically mature adult) unless geologic stage is taken into account. Permian *Moschorhinus* exhibited moderately fast, but periodically interrupted (cyclic) growth over several growing seasons (i.e., prolonged, multi-year growth to large body size), whereas Triassic individuals showed evidence of rapid sustained growth over fewer seasons, and with only peripheral reductions in periosteal apposition rates. In spite of smaller body size, Triassic *Moschorhinus* showed accelerated early skeletal growth, a strategy that together suggests increased selection for shortened growth duration in earliest Triassic animals or, perhaps, a time-correlated phylogenetic trend. Future work will integrate gross anatomical data, hard-tissue histology and phylogenetic comparative methods in order to assess whether body size reductions and attendant changes in vascular growth patterns recorded in the bones of therocephalians and other eutheriodonts were accelerated during the end-Permian extinction or represent longer term trends that were more widespread in nonmammalian therapsid phylogeny.

Chapter 3—Body Size Evolution in Nonmammalian Eutheriodonts (Therapsida) Before and After the End-Permian Extinction

Summary—The extent to which mass extinctions influence body size evolution in major tetrapod clades is inadequately understood. For example, the 'Lilliput effect,' a common feature of mass extinctions, describes a temporary decrease in body sizes of survivor taxa in post-extinction faunas. However, its signature on existing patterns of body size evolution in tetrapods and the persistence of its impacts during post-extinction recoveries are virtually unknown, and rarely compared in both geologic and phylogenetic contexts. Here, I evaluate temporal and phylogenetic distributions of body size in Permo-Triassic therocephalian and cynodont therapsids (eutheriodonts) using a museum collections-based approach and time series model fitting on a regional stratigraphic sequence from the Karoo Basin, South Africa. I further employed rank order correlation tests on global age and clade rank data from an expanded phylogenetic dataset, and performed evolutionary model testing using Brownian (passive diffusion) models. Results support significant size reductions in the immediate aftermath of the end-Permian mass extinction (ca. 252.3 Ma) consistent with some definitions of Lilliput effects. However, this temporal succession reflects a pattern that was underscored largely by Brownian processes and constructive selectivity. Results also support two recent contentions about body size evolution and mass extinctions: 1) active, directional evolution in size traits is rare over macroevolutionary time scales and 2) geologically

brief size reductions may be accomplished by the ecological removal of large-bodied species without rapid originations of new small-bodied clades or shifts from long-term evolutionary patterns.

Introduction

Body size is an important biological trait that affects organismal fitness and imparts a strong influence on ecological, physiological, and life history attributes of species (Peters, 1983; Calder, 1984; Stearns, 1992; Gotthard, 2001). As such, size and size-related traits have received considerable attention from paleobiologists interested in characterizing the tempo and mode of morphological evolution in extinct groups. Famous examples include 'Cope's rule,' an apparent tendency for animal lineages to achieve larger sizes over time (Cope, 1887, 1896; Stanley, 1973), and more recently the 'Lilliput effect,' short-term size reductions in animal taxa following mass extinction events (Urbanek, 1993; Twitchett, 2007; Harries and Knorr, 2009). In the case of Cope's rule, workers historically attributed patterns of body size increase to non-random selection within lineages over geologic time, an intuitive conclusion when surveying some of the best examples of macroevolutionary transitions in the fossil record (Gould, 1997; Laurin, 2004; Kingsolver and Pfennig, 2004; Hone and Benton, 2005). However, several studies suggest that many of these important paleontological transitions (e.g., expansions in dinosaur body sizes) were in fact influenced by Brownian processes of trait evolution, random tendencies for lineages to diffuse through size space with increasing disparity

(Stanley, 1973; McShea, 1994; Carrano, 2006; Sookias et al., 2012a,b). Considerably less attention has been paid to the underlying influences of Lilliput-type patterns and mass extinctions. Background patterns of origination/extinction during the Neogene indicate lower turnover rates (i.e., long species durations) in smaller-bodied mammals, possibly due to their higher reproductive rates, large population sizes, and frequent sleep-or-hide burrowing behavior compared to large mammals (Liow et al., 2008, 2009). Nevertheless, size-related extinction risk remains controversial (McKinney, 1997; Cardillo and Bromham, 2001; Matthews et al., 2011), and the supposed chaotic and indiscriminate nature of mass extinctions, as in the end-Cretaceous and end-Permian mass extinctions, calls into question whether these dynamics are applicable to rapid, global-scale catastrophes (Jablonski, 2005).

Though originally reserved for within-lineage size decreases in survivor taxa (sensu Urbanek, 1993), the term 'Lilliput' has been repurposed as a pattern that may encompass a number of other underlying processes, such as differential extinction of large-bodied taxa and rapid diversifications of new small-bodied clades (Twitchett, 2007; Harries and Knorr, 2009), or a combination of these (Song et al., 2011). These patterns have been well documented in Triassic marine invertebrate communities following the end-Permian extinction (e.g., Payne, 2005; Twitchett, 2007; Luo et al., 2008; Metcalfe et al., 2011; Song et al., 2011) and anecdotally in terrestrial vertebrates of the earliest Triassic *Lystrosaurus* Assemblage Zone, Karoo Basin of South Africa (Smith, 1995; Sahney and Benton, 2008; Retallack, 2013). However, the extent to which the end-

Permian extinction influenced body size reductions and possible departures from background patterns of body size evolution are imprecisely known. This is in part because the temporal and phylogenetic components of body size evolution before and after the extinction have never been compared. Here, I use time series analysis and a reference phylogeny of Permian through Triassic eutheriodont therapsids (therocephalians and cynodonts) to better understand the tempo and mode of body size evolution in the therapsid forerunners of mammals during a mass extinction interval. Notably, therocephalian eutheriodonts originated at relatively large sizes during the Middle Permian (estimated maximum skull length, ~ 40 centimeters; Abdala et al., 2008), while many of their Triassic relatives, including some cynodonts and baurioid therocephalians, achieved comparatively diminutive sizes (estimated skull length ~ 2.5-3.0 centimeters in brasilodontids and early Mammaliaformes). Therocephalians and cynodonts provided a rare opportunity to study post-extinction body size shifts in terrestrial vertebrates due to their range of sizes, relative generic richness in earliest Triassic faunas, and differential survivorship of the end-Permian extinction (Botha and Smith, 2006; Huttenlocker et al., 2011b). I identify short-term reductions in maximum and mean body sizes during the earliest Triassic, and suggest that geologic patterns of size reductions in lowermost Triassic rocks do not reflect rapid diversifications of new small-bodied clades or changes in evolutionary patterns following the extinction. Rather, observed short-term body size reductions arose from interplay between a backdrop of

increasing size disparity and a temporary culling of large-bodied therapsid predators during the end-Permian extinction.

Approach

Stratigraphic (Non-phylogenetic) Patterns

Non-random extinction patterns may be discernible with regard to some organismal traits, especially when studied in the context of existing patterns of trait evolution during background intervals. Non-phylogenetic investigations of selectivity in Cretaceous-Paleogene marine invertebrates have suggested that mass extinction may bring about changes in selectivity patterns that reset the stage for biotic recoveries. This departure from normal (background) selectivity patterns has been termed "non-constructive selectivity" (Jablonski, 2005). Patterns of ecomorphological change have been well-studied in stratigraphic series, particularly in Permo-Triassic and Cretaceous-Paleogene marine faunas (Erwin, 1998; Erwin et al., 2003; Jablonski, 2005), but similar approaches have only been recently applied to body size in terrestrial vertebrates. For example, Wilson (2013) identified significant post-extinction body size reductions in a succession of Cretaceous-Paleogene mammals from northeastern Montana, and suggested constructive selectivity against large, dietary specialists possibly due to depressed primary productivity during that time. Similar patterns have been suggested in earliest Triassic terrestrial disaster faunas, including selection for small-bodied generalists with drought-tolerant food sources and fossorial or semi-aquatic habits (Smith, 1995; Smith

and Botha, 2005; Botha and Smith, 2006; Sahney and Benton, 2008). I propose that investigations of selectivity during the end-Permian mass extinction should address firstly whether non-random patterns are discernible and, if so, whether they deviate from pre-existing patterns of trait evolution. First, I test whether maximum and mean body sizes decreased significantly in the earliest Triassic *Lystrosaurus* Assemblage Zone (herein 'AZ') using non-phylogenetic time series and statistical comparisons of size distributions between temporally disjunct eutheriodont assemblages. Second, I chose to implement time series modeling and rank correlation tests to evaluate whether reductions, if present, signified transient shifts or longer-term directional size shifts both across the extinction and during pre-extinction intervals. A transient shift following mass extinction (an expectation of Lilliput-type patterns) would be indicated by short-term shifts in stratigraphic series without a significant mean step change across the entire sampled interval (or during pre-extinction intervals).

Geologic controls and sampling—Sampling of non-isotaphonomic intervals and unevenness of sampling may bias the quality and size controls of the present sample. These can include but are not restricted to available outcrop area, collection intensity, and sediment coarseness and sorting, which should be considered given the comparatively small sizes observed in the Triassic *Lystrosaurus* AZ. Recent assessments of geologic controls on paleodiversities have found potential associations between outcrop area and taxonomic richness of pre-extinction assemblages, but the outlying *Lystrosaurus* AZ exhibits unexpectedly modest richness that is unexplainable by outcrop area alone (Irmis

et al., 2012; Fröbisch, 2013), in spite of intense collecting effort and large numbers of specimens from this interval. A comparison of the diversities of therocephalians and cynodonts from these assemblages yields comparable results (Appendices 6, 7). Also, differences in grain sizes may produce differential size-sorting in fossil assemblages, where coarse sediments deposited in high-energy environments may preferentially preserve larger, more robust skeletal remains. However, the fine-grained floodplain deposits and paleosols of the Permian Balfour Formation give way to rhythmically-bedded sheet sandstone bodies and thick channel sands and conglomerates of the Triassic Katberg Formation, producing a general coarsening upward in the Permo-Triassic boundary sequence of the Karoo. It is therefore unlikely that this coarsening upward has produced a bias in small-bodied eutheriodonts in the *Lystrosaurus* AZ. While taphonomic and collecting biases are important considerations, I suggest that they have had limited impacts on diversity and body size shifts observed in the *Lystrosaurus* AZ.

Phylogenetic Patterns

Size shifts in post-extinction faunas, if present, may have been underpinned to some extent by stochastic processes of trait evolution. Long-term negative shifts observed throughout the sampled interval may indicate background patterns of trait evolution (e.g., tendencies toward body size reductions). Size shifts may alternatively represent rapid diversifications of new clades whose success was associated with the trait in question (in this case, small body size). Rapid diversification of small-bodied taxa following extinction is one explanation for Lilliput-type patterns, although few examples have been

demonstrated (Song et al., 2011; Rego et al., 2012). Nevertheless, an inadequate understanding of phenotypic evolution during background intervals hinders comparisons of post-extinction dynamics. It is therefore informative to compare stratigraphic patterns of trait evolution to those patterns inferred by cladogenetic branching events. This approach allows investigators to identify directionality, characterize the timing and location of important cladogenetic events, and distinguish those features from more general (long-term) features of phenotypic evolution during background intervals. I chose to implement ancestor-descendant tests in order to (1) evaluate the relative frequency at which smaller descendants evolved from larger ancestors in a reconstructed lineage of ancestor-descendant pairs, and to (2) identify the branches (internodes) in which those negative shifts occurred. Diversification rate shifts were also assessed to determine whether post-extinction radiations of small, Triassic taxa during biotic recovery could have contributed to observed shifts in size distributions of eutheriodont faunas. Finally, I evaluated the fit of phylogenetic models to determine whether trait evolution was best approximated by directional, 'stabilized,' or initially rapid but decelerating ('early burst') models, or a Brownian motion model. These approaches establish a baseline of pre-extinction evolutionary dynamics, and help to determine whether selectivity during the extinction was constructive (i.e., whether it mirrored background patterns) or non-constructive in nature. I argue here that extinctions were largely size selective, but were constructive, dependent upon existing patterns of trait evolution, and did not result in shifts from long-term phylogenetic patterns in the study group.

Methods 1: Stratigraphic Patterns

Database Assembly

Specimen sampling—I assembled a database of specimen measurements and stratigraphic occurrences for 72 species of Permian and Triassic therocephalians and cynodonts. The majority of measurements were taken directly from museum specimens, but data for some non-African taxa that were inaccessible during the study period were taken from the literature. By incorporating data from museum specimens, I was able to assess variation within species, including maximum sizes, rather than representative samples from the literature. A rigorous, collections-based survey therefore allows previous literature-based assessments of body size evolution in Permo-Triassic therapsids to be improved upon (i.e., Sookias et al., 2012a,b). Taxa were assigned to one or more stratigraphic bins, which mainly follow the biozonation of the Karoo Basin, the best-sampled and most complete terrestrial Permo-Triassic boundary succession in the world (Rubidge, 1995, 2005). The Karoo biozonation includes distinct assemblage zones identified by their fossil tetrapod associations: *Eodicynodon*, *Tapinocephalus*, *Pristerognathus*, *Tropidostoma*, *Cistecephalus*, *Dicynodon*, *Lystrosaurus*, and *Cynognathus* AZs. Additional global data, collected to distinguish non-regional geologic and phylogenetic trends in all sampled Permian and Triassic taxa, covered a wider stratigraphic interval so that late-Middle Triassic (Ladinian) and Late Triassic (Carnian, Norian, Rhaetian) global standard stages were also included as distinct bins. The sample was limited to Permian and Triassic genera only, and to specimens having well-preserved

skulls for complete skull length measurements. Several Early Jurassic nonmammaliaform cynodonts from the Karoo (e.g., *Diarthrognathus, Pachygenelus, Tritylodon*) and those lacking complete skulls were therefore excluded from the dataset. The resulting database included 347 complete cranial specimens and 72 species of Permian through Triassic therocephalians and cynodonts from the Karoo Basin and contemporaneous basins. Sources for occurrence data, including voucher specimens and absolute dates, are provided in Appendices 8 and 10. Stratigraphic nomenclature and dates for Middle-to-Late Triassic basins follow Abdala et al. (2006), Abdala and Ribeiro (2010), Irmis et al. (2010) and references cited therein.

Measurements—From the complete database, 57 measurements were retained for time series analysis of the Karoo assemblages, and 72 measurements were retained for rank order analyses of the global dataset representing the maximum basal skull lengths of the 72 sampled taxa from the stratigraphic interval of their first appearance (therocephalians: N = 37; cynodonts: N = 35). Basal skull length (BSL), measured from the tip of the snout to the occiput in millimeters (mm), was chosen as a proxy for body size because many of the fossil taxa examined here are best represented by cranial material and because skull length correlates well with other linear skeletal measurements in therapsids (e.g., femur length; Sookias et al., 2012a,b). Measurements were recorded to the nearest mm using digital Mitutoyo calipers. For each taxon, the 'max lnBSL' represents the natural log of BSL for the largest measurable individual observed within a given interval. By assessing only the maximum lnBSL of each taxon (rather than taxon

averages), these measures permitted both a conservative estimate of size reductions from one interval to the next while also reducing the effects of differences in relative abundance.

Evaluation of Time Series Models

Time series data represent a sequence of observations repeated over elapsed time, and can be conceptualized in a paleontological context as ancestor-descendant relationships (in as much as they assume that traits in daughter populations are a product of evolutionary change from the preceding parent lineage or clade) (Hunt, 2007; Hunt and Carrano, 2010). I performed time series analysis to evaluate regional patterns of body size evolution in a stratigraphic succession of therocephalians and cynodonts from the Permian-Triassic Beaufort Group, Karoo Basin, South Africa. First, I evaluated the probability that the body size samples from the Late Permian (*Cistecephalus* and *Dicynodon* AZs) and earliest Triassic (*Lystrosaurus* AZ) were drawn from equivalent distributions using a Kolmogorov-Smirnov (K-S) test. Then, I evaluated the likelihood that observed negative shifts in size distributions (if present) represent a random evolutionary walk (rather than a long-term directional trend) by assessing the record of body size evolution over eight stratigraphic bins of the Karoo succession. Mean lnBSL was estimated for each of eight stratigraphic bins by taking the average of the maximum known lnBSL for each taxon within a given bin, therefore representing a per taxon average (rather than an average of all specimens, which could otherwise be skewed by taxa with unusually high abundances). In contrast to the rank order correlation tests,

which examined only size at first appearance (discussed below), taxa whose ranges spanned multiple assemblage zones were included in each bin in which they occurred in order to capture more fully the variance within each bin. Mean sizes were estimated in each bin for all eutheriodonts, as well as separately for therocephalians and cynodonts in order to evaluate the pervasiveness of potential trends among the therapsid subclades.

Mean lnBSL and disparity (as measured by variance) were estimated from the database for each Karoo biozone (average bin duration ≈ 3 Myr) and imported into the 'R' version 2.15.1 statistical environment using the 'paleoTS' package (Hunt, 2007). The 'paleoTS' package permited evaluation of temporal patterns of body size evolution across the Karoo succession, using several models that fall into two general categories: non-directional and directional. Non-directional models implemented by the 'paleoTS' package include unbiased random walk (or 'URW') and stasis. URW models evolution as a volatile Brownian process with observable step variance but no mean step change, whereas stasis models evolution with modest deviations that are uncorrelated and normally distributed around the trait mean (Hunt and Carrano, 2010). Directional evolution is modeled as a generalized random walk ('GRW') having a positive or negative mean step change. The relative fit of non-directional and directional evolutionary models was evaluated using likelihood methods and goodness-of-fit tests. My expectation is that, if short-term (Lilliput-type) size reductions are a unique signature of the Triassic *Lystrosaurus* AZ, then longer-term size reductions should not be manifested in the Karoo time series, with non-directional models best fitting the data (i.e.,

URW and stasis). If, on the other hand, body size evolution was driven by longer-term trends beginning in the Permian, then a directional model with a negative mean step change should best fit the data.

The relative fit of the three models (URW, stasis, and GRW) was assessed using Akaike's information criterion corrected for small sample sizes (AICc). AICc is an information loss metric that is used to compare models both through their goodness-of-fit and model complexity (i.e., the number of adaptable model parameters). AICc diminishes the problem of overfitting complex models, and is widely used for small paleontological and neontological datasets. Akaike weights ('AW') are estimated by converting the individual AICc scores for each candidate model into a proportional value representing the model's relative support (with the sum of the values adding to 1.0 across all models); the model with the highest weight represents that with the least information loss (and, thus, the most desirable model). A more complete description of AICc and its application to time series and phylogenetic model fitting can be found in Hunt and Carrano (2010).

Rank Order Correlations

Rank order statistics provide additional tests for identifying directional trends in ranked paleontological data (in this case age ranks, clade ranks and patristic distances) (Norell and Novacek, 1992; Carrano, 2000, 2006; Sidor, 2001, 2003). 'Age rank' represents an ordered numerical representation of the stratigraphic bin in which a taxon first appeared. Rank order correlations were performed to assess the relationship between size and age rank, as well as the relationships between size, clade rank and patristic

distance (discussed below). Stratigraphic bins were divided into 13 ranks (average duration ≈ 5 Ma), increased from eight in the Karoo-only time series to accommodate late-Middle and Late Triassic taxa. Each taxon in the global dataset was assigned an age rank, according to the ranked stratigraphic bin in which it first appeared, and an associated maximum lnBSL within that bin. Correlations between size and age rank were assessed using Spearmans' rho (ρ) and Kendall's tau (τ) rank order tests. These tests allowed potentially positive or negative trends in the global dataset to be evaluated as a monotonic function (the Spearman's rank correlation describing the strength of a monotonic association, and Kendall's tau assessing the probability of observing concordant and discordant pairs among ranked variables). Importantly, unlike Pearson's product moment correlation, the tests are robust even when the association is not linear. Three separate data subsets were analyzed to evaluate directional size trends in eutheriodonts ($N = 72$) and therocephalian ($N = 37$) and cynodont ($N = 35$) subclades from the Middle Permian through Late Triassic. For Eutheriodontia and its subclades, I evaluated ρ and τ coefficients for negative trends in two ways, assessing 1) data subsets that included taxa only having first appearances in the Permian and 2) the total Permian-Triassic dataset. By examining Permian-only and excluding Triassic originations, I was able to assess the extent to which general trends in the total Permian-Triassic dataset were influenced by new size distributions of post-extinction taxa (versus pre-existing or 'background' patterns of trait evolution). Trends were considered only weakly significant if both coefficients were negative but non-significant for one of the tests (Table 3.2).

Results 1: Stratigraphic Patterns

Time Series Model Fitting

My evaluation of stratigraphic (i.e., non-phylogenetic) patterns failed to identify long-term negative trends in eutheriodont body size evolution, instead showing a short-term reduction in mean sizes in the Triassic *Lystrosaurus* Assemblage Zone. Visual inspection of the Karoo time series data suggests a transient decrease in mean size from the Late Permian *Dicynodon* AZ to the *Lystrosaurus* AZ, which rebounded subsequently in the *Cynognathus* AZ (Fig. 3.1). Kolmogorov-Smirnov tests on size distributions from the *Lystrosaurus* AZ suggest significant decreases when compared against the Late Permian *Cistecephalus* and *Dicynodon* AZs (therocephalians: $D = 0.61$, $p < 0.001$; cynodonts: $D = 0.38$, $p = 0.021$). A binomial test on the Karoo dataset using the *binom.test* function of paleoTS (Hunt and Carrano, 2010) found no systematic tendency for decreases in mean size of eutheriodonts over the Karoo succession, suggesting that this geologically abrupt shift was not part of an observable long-term trend. This may, however, reflect the poor ability of the statistical test to reject the null hypothesis of a random walk, given the small number of stratigraphic bins available. I therefore used the small sample size version of Akaike's Information Criterion (AICc) to evaluate the relative fit of directional (generalized random walk or 'GRW') and non-directional (unbiased random walk or 'URW' and evolutionary stasis) candidate models, but non-directional models found the best support as size differences accrued with noticeable trait variance but with a step mean of zero (Table 3.1). Observed size decreases in the

Figure 3.1. Karoo time series and age rank results for observed geologic distributions of maximum basal skull length (lnBSL) for each taxon. **A**, Regional patterns of trait evolution in Karoo eutheriodonts (black) (therocephalian subclade = blue; cynodont subclade = gold) fit a non-directional model throughout the Karoo succession (see Table 3.1). Squares represent clade averages (with 95% confidence intervals), circles represent maximum known sizes for each species recorded in a given stratigraphic interval (Ma, millions of years ago). **B**, Spearman's rank correlation tests on global age rank data (used for the phylogenetic sampling) reveal a weakly negative trend in species maximum sizes (ρ = -0.259; p = 0.028) with a short-term bottleneck in size maxima in the Early Triassic *Lystrosaurus* AZ (arrow). Permian-Triassic boundary (PTB) represented by dashed line.

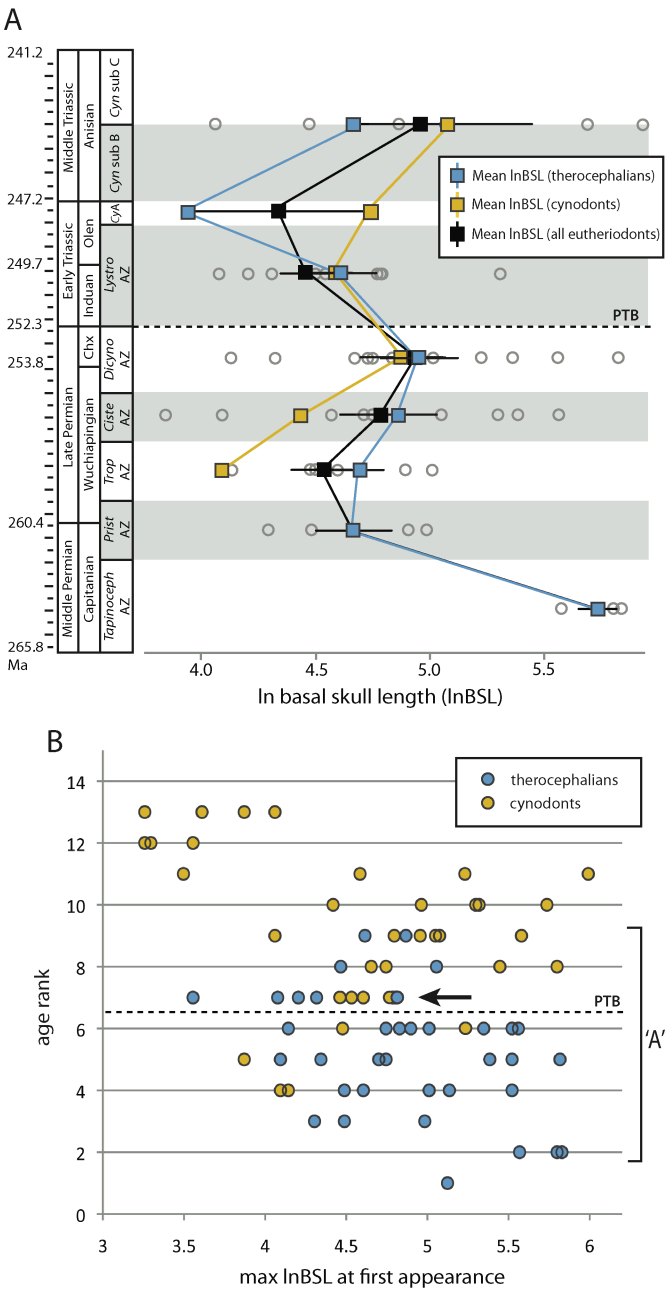
A
241.2
247.2
249.7
252.3
253.8
260.4
265.8
Ma
Middle Triassic
Early Triassic
Late Permian
Middle Permian
Anisian
Olen
Induan
Chx
Wuchiapingian
Capitanian
Cyn sub C
Cyn sub B
CyA
Lystro AZ
Dicyno AZ
Ciste AZ
Trop AZ
Prist AZ
Tapinoceph AZ
PTB
Mean lnBSL (therocephalians)
Mean lnBSL (cynodonts)
Mean lnBSL (all eutheriodonts)
4.0
4.5
5.0
5.5
ln basal skull length (lnBSL)
B
therocephalians
cynodonts
age rank
0
2
4
6
8
10
12
14
PTB
'A'
3
3.5
4
4.5
5
5.5
6
max lnBSL at first appearance

Table 3.1. Time series model fitting of body size evolution in Karoo therocephalians and cynodonts.

	GRW			URW			Stasis		
	AICc	AW	μ, σ^2	AICc	AW	σ^2	AICc	AW	θ, ω
Eutheriodontia$_{Karoo}$	19.848	0.025	-0.029, 0.042	14.601	0.349	0.045	**13.435**	**0.625**	**4.794, 0.077**
Therocephalia$_{Karoo}$	16.669	0.159	-0.038, 0.000	**14.540**	**0.462**	**0.031**	14.942	0.378	4.818, 0.079
Cynodontia$_{Karoo}$	16.937	0.033	0.052, 0.000	**11.495**	**0.503**	**0.008**	11.658	0.464	4.702, 0.023

GRW, generalized random walk (directional); URW, unbiased random walk
AICc, Akaike's Information Criterion corrected for small sample size; AW, Akaike weight
μ, step mean; σ^2, step variance; θ, trait mean; ω, trait variance

Lystrosaurus AZ therefore cannot be attributed to a long-term directional trend when evaluated as a time series.

Age Ranks and Rank Order Correlations

Rank order correlations between age rank and size at first appearance, on the other hand, may indicate a weak negative trend for some groups such as therocephalians, which originated at their largest sizes in the Permian (Fig. 3.1B, Table 3.2). This correlation, however, is likely influenced both by a lack of originations of new large Triassic therocephalians (pulling higher age ranks into the lower end of size space) and the ranking and evaluation of data as a monotonic function. When Triassic taxa are removed from the analysis, correlation coefficients are only weakly negative and non-significant, indicating an inability of the tests to identify long-term negative trends from Permian size distributions. Permian cynodonts, however, were difficult to evaluate due to their low taxonomic richness during the Permian and, consequently, small sample sizes. In summary, Early Triassic eutheriodont faunas were on average smaller-bodied than in preceding Permian assemblages. However, Permian stratigraphic trends alone provide little evidence of long-term declines in mean body sizes.

Table 3.2. Results of rank correlations, Spearman's rho (ρ) and Kendall's tau (τ), for global age ranks.

Age rank *v.* lnBSL		*N* taxa	ρ	*p*(ρ)	τ	*p*(τ)
Eutheriodontia	(Permian taxa only)	32	-0.089	0.621	-0.054	0.693
Therocephalia	(Permian taxa only)	27	-0.153	0.443	-0.089	0.559
Cynodontia	(Permian taxa only)	5	--	--	--	--
Eutheriodontia	(Permian + Triassic)	72	**-0.261**	**0.025**	**-0.173**	**0.037**
Therocephalia	(Permian + Triassic)	37	**-0.370**	**0.023**	**-0.254**	**0.035**
Cynodontia	(Permian + Triassic)	35	-0.265	0.115	-0.113	0.362

Methods 2: Phylogenetic Patterns

Reference Cladogram, Clade Ranks and Patristic Distances

Cladistic data were also ranked to permit the evaluation of directional trends in size data with respect to relative branching events in a reference cladogram (Fig. 3.2). I constructed a reference cladogram primarily from the literature, although some new taxa and specimens are included here in an expanded analysis of therocephalian therapsid relationships (updated from Huttenlocker, 2009; Huttenlocker et al., 2011b; Sigurdsen et al., 2012). Inclusion of these additional taxa facilitated the most comprehensive phylogenetic sample of therocephalian therapsids to date (Chapter 1). I follow several sources for cynodont phylogeny, which has received greater attention in the literature (Hopson and Kitching, 2001; Abdala et al., 2006; Sidor and Hancox, 2006; Oliveira et al., 2010; Liu and Olsen, 2010; Ranivoharimanana et al., 2011). 'Clade ranks' (CR) were assigned based on the number of nodes passed along the backbone of the tree (e.g., Cynodontia to Mammaliaformes) without incorporating branching events of clades off the primary axis (Norell and Novacek, 1992; Sidor and Hopson, 1998).

Figure 3.2. Complete reference cladogram with nodes numbered for estimation of patristic distances. Sources include: therocephalians, Huttenlocker (2009), Huttenlocker et al. (2011b), Sigurdsen et al. (2012); cynodonts, Abdala et al. (2006), Sidor and Hancox (2006), Oliveira et al. (2010), Liu and Olsen (2010), Ranivoharimanana et al. (2011).

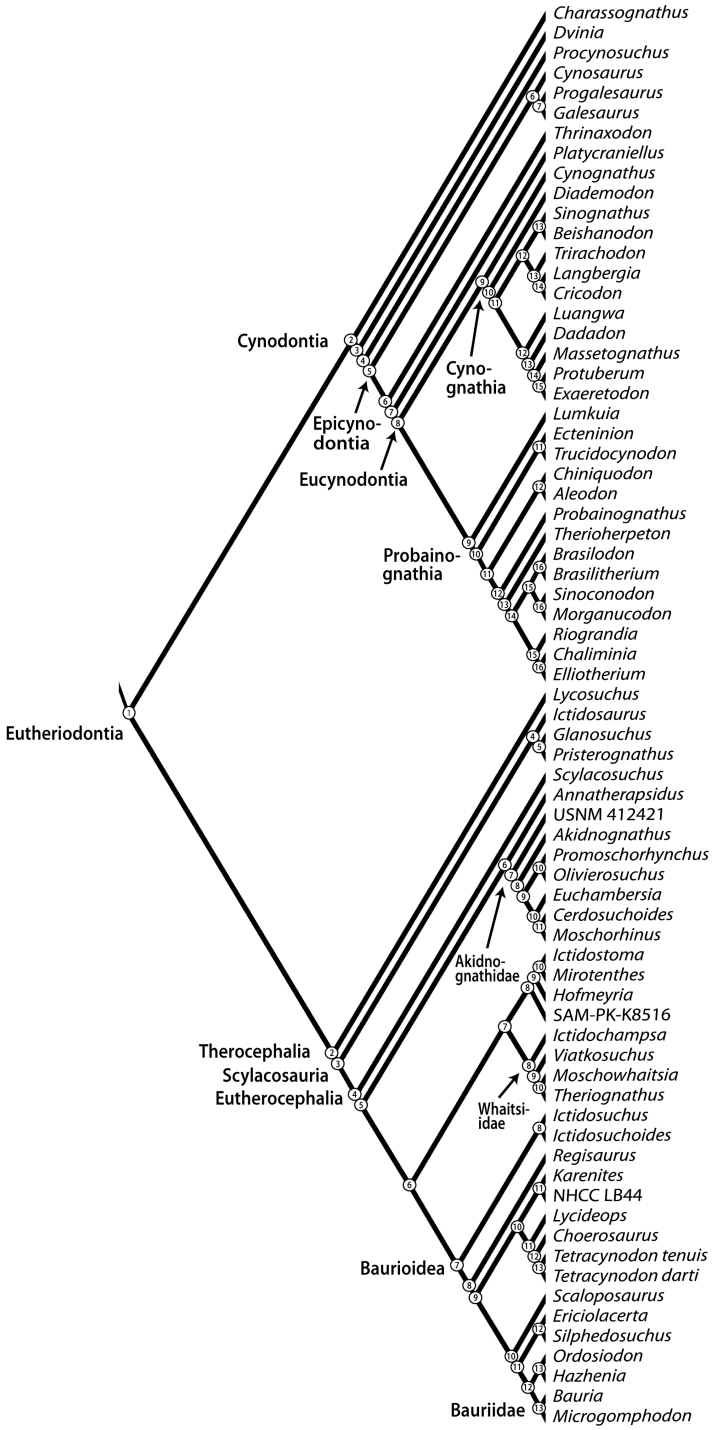
Charassognathus
Dvinia
Procynosuchus
Cynosaurus
Progalesaurus
Galesaurus
Thrinaxodon
Platycraniellus
Cynognathus
Diademodon
Sinognathus
Beishanodon
Trirachodon
Langbergia
Cricodon
Luangwa
Dadadon
Massetognathus
Protuberum
Exaeretodon
Lumkuia
Ecteninion
Trucidocynodon
Chiniquodon
Aleodon
Probainognathus
Therioherpeton
Brasilodon
Brasilitherium
Sinoconodon
Morganucodon
Riograndia
Chaliminia
Elliotherium
Lycosuchus
Ictidosaurus
Glanosuchus
Pristerognathus
Scylacosuchus
Annatherapsidus
USNM 412421
Akidnognathus
Promoschorhynchus
Olivierosuchus
Euchambersia
Cerdosuchoides
Moschorhinus
Ictidostoma
Mirotenthes
Hofmeyria
SAM-PK-K8516
Ictidochampsa
Viatkosuchus
Moschowhaitsia
Theriognathus
Ictidosuchus
Ictidosuchoides
Regisaurus
Karenites
NHCC LB44
Lycideops
Choerosaurus
Tetracynodon tenuis
Tetracynodon darti
Scaloposaurus
Ericiolacerta
Silphedosuchus
Ordosiodon
Hazhenia
Bauria
Microgomphodon
Cynodontia
Cyno-
gnathia
Epicyno-
dontia
Eucynodontia
Probaino-
gnathia
Eutheriodontia
Therocephalia
Scylacosauria
Eutherocephalia
Akidno-
gnathidae
Whaitsi-
idae
Baurioidea
Bauriidae

'Patristic distances' (PD) represented the number of nodes passed through from the hypothetical ancestor at the base of the tree to each of the tips (Sidor, 2001). Therocephalians and cynodonts were analyzed separately for correlations with CR because these two main subclades replicate CR values (Fig. 3.3). PD values bear no such constraint and were estimated directly from the complete reference phylogeny in Figure 3.2. Rank order correlation coefficients were estimated from Permian-only and combined Permian-Triassic datasets as in the aforementioned age rank analysis. Statistical results are presented in Table 3.3.

Ancestor-Descendant Tests

Ancestor-descendant tests were performed as an extension of the CR analyses in order to assess tendencies toward negative versus positive size changes in the phylogenetic tree between reconstructed ancestor and descendant nodes (McShea, 1994; Carrano, 2006). Whereas CR analyses allowed interpretations only from observed tip data, this analysis relies on squared-change parsimony to reconstruct the hypothetical traits of ancestors (which cannot be observed, only estimated). Ancestral states were estimated using squared-change parsimony in Mesquite version 2.0 (Maddison and Maddison, 2007). For each nested clade, I then manually estimated the mean step change, the number of positive and negative changes between internodes (internodes having zero change were not counted), and the skewness, providing measures of tendency that could contribute to directional evolution in the tree. Results are presented in Table 3.4.

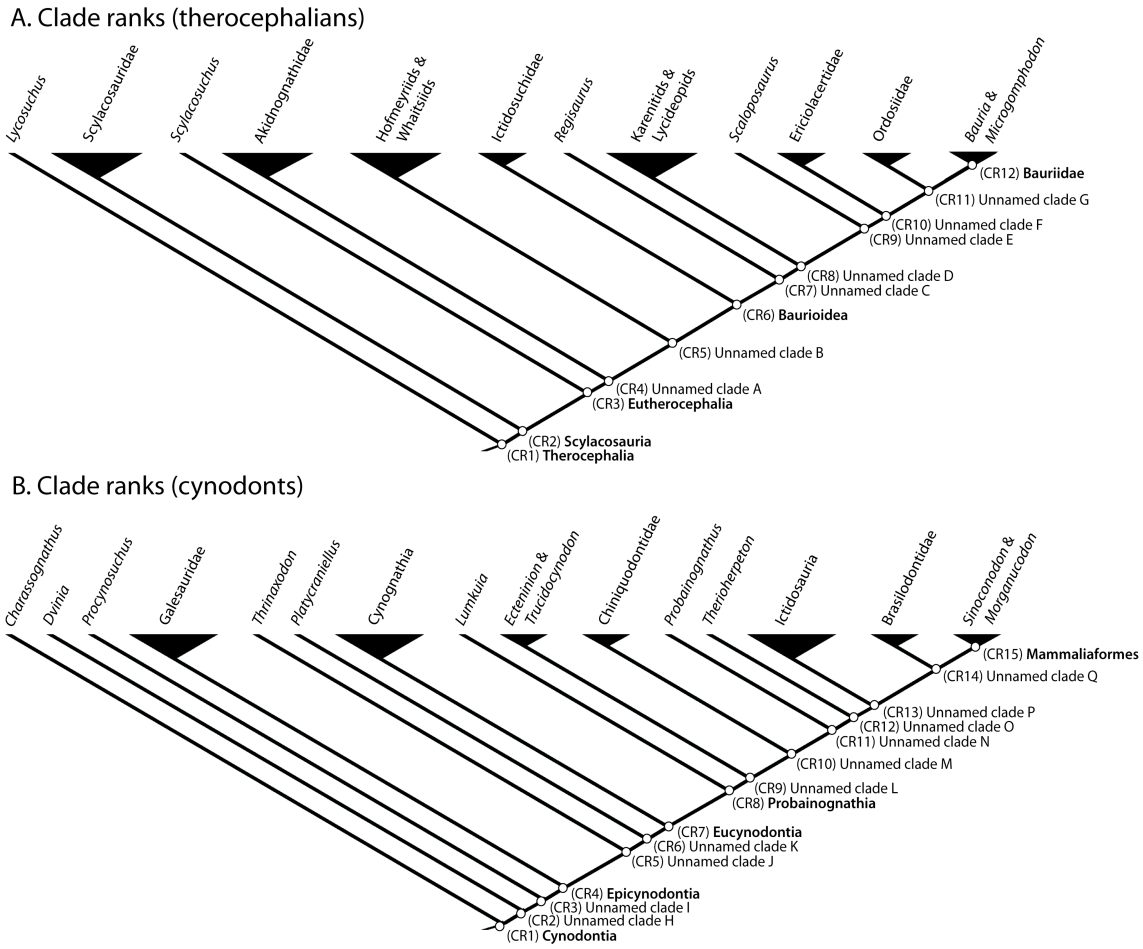

Figure 3.3. Ranking of side-branches within the two major subgroups: Therocephalia (**A**) and Cynodontia (**B**) (from the reference cladogram in Fig. 3.2).

Diversification Rate Shifts

To assess the hypothesis that shifts in mean body size represented post-extinction radiations of small-bodied eutheriodont clades, a phylogeny was constructed using all studied taxa in Figure 3.2 and tested for variations in diversification rates using the topology-based method of Chan and Moore (2004). The software SYMMETREE version 1.1 was used to evaluate the topological distribution of taxic diversity across branches in the reference phylogeny (i.e., its symmetry) and to identify regions of the tree that contribute to significant imbalance in diversity. This operation was performed by calculating the Δ_1 and Δ_2 statistics (Chan and Moore, 2004), functions of two likelihood ratios that represent the probability of observing a shift in diversification rate along the internal branch of a three-taxon tree (composed of a local outgroup and two basalmost subclades of the ingroup). For each node, the ratios compared the likelihood of yielding the observed distribution of diversity under an equal-rates Markov branching model to that under a two-rate model. Importantly, the inclusion of non-contemporaneous clades sampled from disjunct stratigraphic bins may violate an assumption of the equal-rates Markov model by heterogeneously sampling diversity through time (Ruta et al., 2007; Botha-Brink and Angielczyk, 2010). Therefore, five trees were subsampled from the reference phylogeny, representing a cross-section of diversity for each of the five best sampled assemblage zones spanning the Permian-Triassic transition: *Tropidostoma*, *Cistecephalus*, *Dicynodon*, *Lystrosaurus*, and *Cynognathus* AZs. Following Botha-Brink and Angielczyk (2010), trees were pruned such that they only included taxa and ghost

lineages present within the given stratigraphic bin. The trees were then evaluated in SYMMETREE to identify diversification rate shifts in post-extinction clades (e.g., bauriids; cynognathians or other eucynodonts) or in clades that diversified before the extinction (e.g., eutherocephalians; basal cynodonts).

Evaluation of Phylogenetic Models

Finally, stochastic models of Brownian evolution were fitted to observed patterns of body size evolution in a comprehensive global phylogeny of eutheriodonts, permitting a marriage of temporal and topology-based methods. Phylogenetic model fitting was performed in R using 'ape' and 'geiger' packages (Hunt and Carrano, 2010). The global reference phylogeny was exported into Newick notation and zero length branches that constrained ghost lineages of their sister clades were augmented using the smoothing distribution of the *date.phylo()* function (http://www.graemetlloyd.com/methdpf.html). Skull length data were imported and joined to individual taxon labels (corresponding to 71 tip taxa present on the tree), then assigned to the body size vector. Using 'geiger,' I evaluated the relative fit of four phylogenetic models in order to approximate the mode of body size evolution observed on the tree: Brownian motion (BM), Brownian motion with trend (BM_T), Ornstein-Uhlenbeck (OU), and early burst Brownian motion (EB). BM models evolution as a process of passive diffusion (equivalent to an unbiased random walk); BM_T, models evolution as a generalized random walk having a positive or negative mean step change (equivalent to a 'directional trend'); OU models trait evolution as a constrained process approaching some optimal value (sometimes equated

Figure 3.4. Spearman's rank correlation tests on clade rank (**A**, **B**) and patristic distance (**C**) versus maximum basal skull length for the global dataset of Middle Permian through Late Triassic eutheriodonts. Solid circles represent Permian taxa (therocephalian subclade = blue; cynodont subclade = gold), open diamonds represent Early Triassic *Lystrosaurus* Assemblage Zone (LAZ) taxa, and open circles represent Triassic post-LAZ taxa.

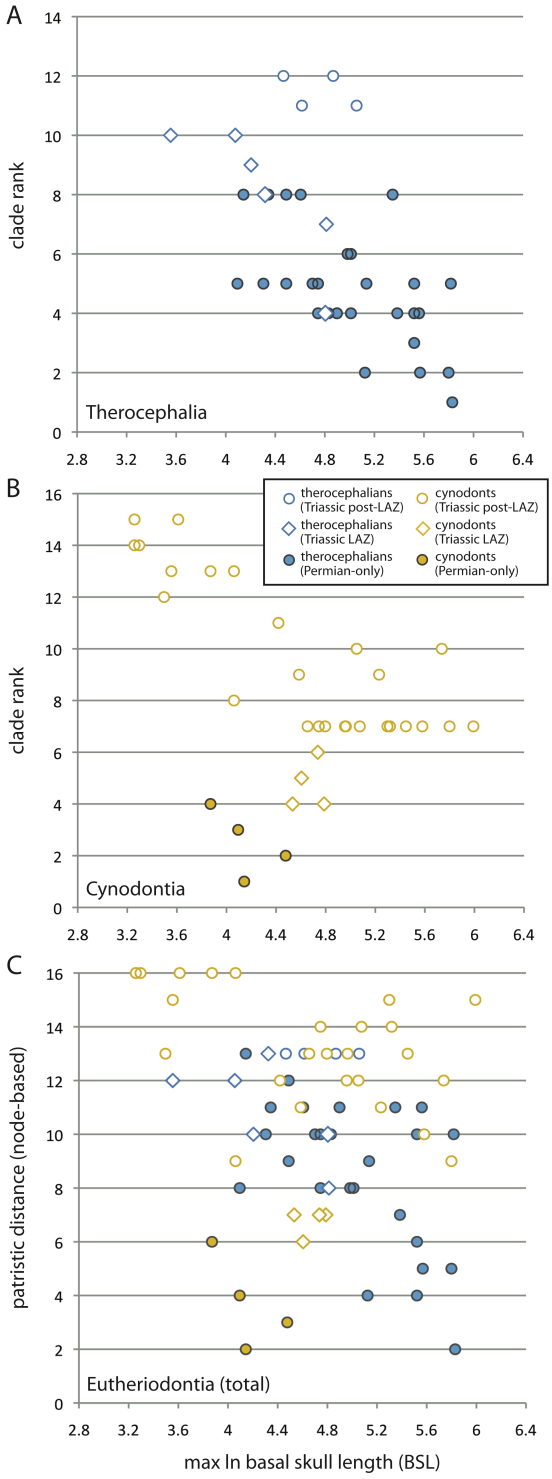
A
clade rank
Therocephalia
B
clade rank
Cynodontia
therocephalians (Triassic post-LAZ)
cynodonts (Triassic post-LAZ)
therocephalians (Triassic LAZ)
cynodonts (Triassic LAZ)
therocephalians (Permian-only)
cynodonts (Permian-only)
C
patristic distance (node-based)
Eutheriodontia (total)
max ln basal skull length (BSL)

to ‘stabilizing selection’); and EB approximates a Brownian process in which the rate of trait evolution exponentially decreases (‘decays’) over time. Models were fitted to the data using ‘geiger,’ and likelihood ratio tests were performed to determine whether multiparameter models should be selected over the null BM model. Goodness-of-fit tests implementing AICc were also used to evaluate the candidate models as in the time series analysis. Results are presented in Table 3.5.

Results 2: Phylogenetic Patterns

Cladogenetic Branching

Cladistically-informed analyses were better able to detect long-term body size trends than stratigraphic data alone (Fig. 3.4; Table 3.3), with some groups expanding into smaller sizes relatively early on in their phylogenetic histories and continuing in

Table 3.3. Results of rank correlations, Spearman’s rho (ρ) and Kendall’s tau (τ), for clade ranks and patristic distances.

Clade rank *v.* lnBSL		***N* taxa**	**ρ**	***p*(ρ)**	**τ**	***p*(τ)**
Therocephalia	(Permian taxa only)	27	**-0.608**	**0.001**	**-0.488**	**<0.001**
Cynodontia	(Permian taxa only)	4	--	--	--	--
Therocephalia	(Permian + Triassic)	37	**-0.622**	**<0.001**	**-0.484**	**<0.001**
Cynodontia	(Permian + Triassic)	34	**-0.371**	**0.032**	-0.234	0.064
Patristic distance *v.* lnBSL						
Eutheriodontia	(Permian taxa only)	31	-0.135	0.467	-0.136	0.306
Therocephalia	(Permian taxa only)	27	**-0.508**	**0.007**	**-0.407**	**0.005**
Cynodontia	(Permian taxa only)	4	--	--	--	--
Eutheriodontia	(Permian + Triassic)	71	**-0.281**	**0.019**	**-0.189**	**0.022**
Therocephalia	(Permian + Triassic)	37	**-0.546**	**<0.001**	**-0.417**	**<0.001**
Cynodontia	(Permian + Triassic)	34	-0.192	0.279	-0.093	0.439

Table 3.4. Summary of ancestor-descendant step changes in the therocephalian and cynodont trees (ancestral states reconstructed using squared-change parsimony).

Eutheriodontia	BSL_{anc}	$lnBSL_{anc}$	Mean Δ	+	−	Skewness
Therocephalia	170	5.135	-0.006	9	25	1.213
Scylacosauria	170	5.135	-0.006	9	25	1.199
Eutherocephalia	162	5.087	-0.023	8	23	1.314
Unnamed clade A	151	5.017	-0.022	8	22	1.282
Unnamed clade B	140	4.941	-0.032	6	16	1.273
Baurioidea	135	4.905	-0.081	3	11	1.431
Unnamed clade C	128	4.852	-0.095	2	10	1.493
Unnamed clade D	120	4.787	-0.098	2	9	1.474
Unnamed clade E	56	4.025	0.077	2	3	1.379
Unnamed clade F	53	3.970	0.110	2	2	1.180
Unnamed clade G	153	5.030	-0.270	1	1	--
Cynodontia	61	4.110	0.016	15	15	0.173
Unnamed clade H	61	4.110	0.016	15	15	0.165
Unnamed clade I	60	4.094	0.018	15	14	0.153
Epicynodontia	48	3.871	0.026	15	13	0.093
Unnamed clade J	92	4.521	-0.026	13	13	-0.124
Unnamed clade K	88	4.477	-0.025	13	12	-0.129
Eucynodontia	219	5.389	-0.064	12	12	-1.370
Probainognathia	112	4.718	-0.045	7	5	-1.531
Unnamed clade L	123	4.812	-0.058	6	5	-1.402
Unnamed clade M	134	4.897	-0.096	4	5	-1.091
Unnamed clade N	82	4.406	-0.065	3	4	-1.464
Unnamed clade O	33	3.496	0.075	3	3	1.609
Unnamed clade P	30	3.401	0.109	3	2	1.509
Unnamed clade Q (incl. Mammaliaformes)	28	3.332	0.032	1	1	--

Ancestral basal skull length estimates (BSL_{anc}) are in mm; mean change refers to log change between ancestor-descendant pairs;
+, number of internodes having a positive step change; −, number of internodes having a negative step change.

more deeply nested clades. Size exhibits a strong negative correlation with clade rank in therocephalians (ρ = -0.622, $p < 0.001$; τ = -0.484, $p < 0.001$) and a weakly negative correlation in cynodonts (ρ = -0.371, $p = 0.032$; τ = -0.234, $p = 0.064$). The same result is true for therocephalians whether analyzed with or without Triassic taxa, indicating that

Figure. 3.5. Cladograms subsampled from five stratigraphic bins for analysis of diversification rate shifts. **A**, *Tropidostoma* Assemblage Zone. **B**, *Cistecephalus* Assemblage Zone. **C**, *Dicynodon* Assemblage Zone. **D**, *Lystrosaurus* Assemblage Zone. **E**, *Cynognathus* Assemblage Zone. Gray branches represent ghost lineages for terminal taxa or clades that appear in a succeeding stratigraphic interval. Numbers at nodes represent *p*-values near or below 0.05 for the Δ_1 (top) and Δ_2 (bottom) statistics. Significant shifts are observed along the branch between the node of Eutherocephalia and non-*Scylacosuchus* eutherocephalians for the *Tropidostoma* AZ subsample (A), and a marginally significant shift is observed along the branch between Eutheriodontia and Eutherocephalia for the *Cistecephalus* AZ (B).

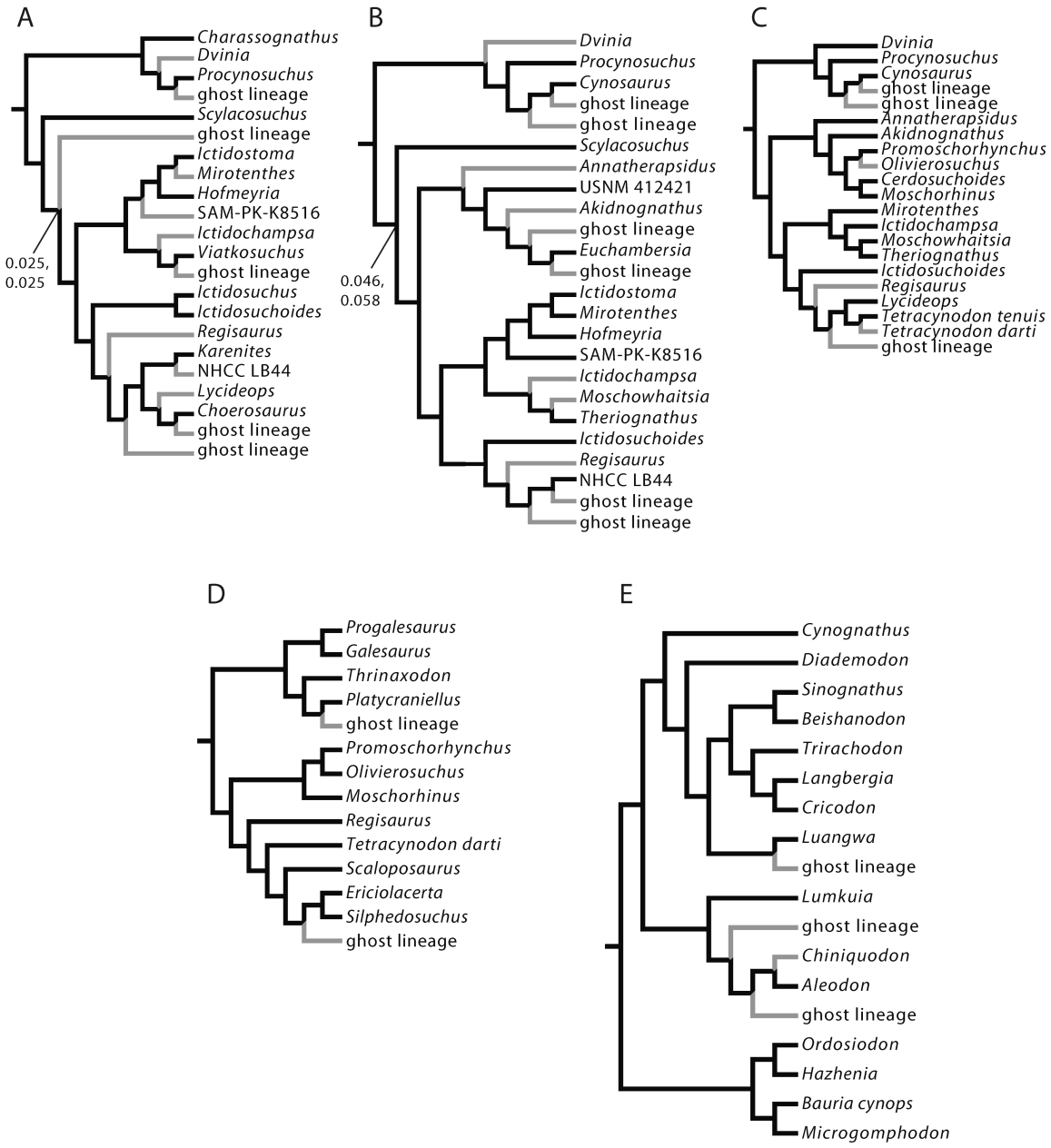
A
Charassognathus
Dvinia
Procynosuchus
ghost lineage
Scylacosuchus
ghost lineage
Ictidostoma
Mirotenthes
Hofmeyria
SAM-PK-K8516
Ictidochampsa
Viatkosuchus
ghost lineage
Ictidosuchus
Ictidosuchoides
Regisaurus
Karenites
NHCC LB44
Lycideops
Choerosaurus
ghost lineage
ghost lineage
0.025,
0.025
B
Dvinia
Procynosuchus
Cynosaurus
ghost lineage
ghost lineage
Scylacosuchus
Annatherapsidus
USNM 412421
Akidnognathus
ghost lineage
Euchambersia
ghost lineage
Ictidostoma
Mirotenthes
Hofmeyria
SAM-PK-K8516
Ictidochampsa
Moschowhaitsia
Theriognathus
Ictidosuchoides
Regisaurus
NHCC LB44
ghost lineage
ghost lineage
0.046,
0.058
C
Dvinia
Procynosuchus
Cynosaurus
ghost lineage
ghost lineage
Annatherapsidus
Akidnognathus
Promoschorhynchus
Olivierosuchus
Cerdosuchoides
Moschorhinus
Mirotenthes
Ictidochampsa
Moschowhaitsia
Theriognathus
Ictidosuchoides
Regisaurus
Lycideops
Tetracynodon tenuis
Tetracynodon darti
ghost lineage
D
Progalesaurus
Galesaurus
Thrinaxodon
Platycraniellus
ghost lineage
Promoschorhynchus
Olivierosuchus
Moschorhinus
Regisaurus
Tetracynodon darti
Scaloposaurus
Ericiolacerta
Silphedosuchus
ghost lineage
E
Cynognathus
Diademodon
Sinognathus
Beishanodon
Trirachodon
Langbergia
Cricodon
Luangwa
ghost lineage
Lumkuia
ghost lineage
Chiniquodon
Aleodon
ghost lineage
Ordosiodon
Hazhenia
Bauria cynops
Microgomphodon

size reductions began in relatively shallowly-nested nodes in the tree (i.e., early-diverging groups which include Permian taxa) and continued into the Triassic. Correlations with patristic distance have lower statistical support, but are still significant for Permian-only and Permian-Triassic therocephalians indicating the influence of therocephalians on the overall pattern. I carried out ancestor-descendant tests following the method of Carrano (2006) to supplement the rank correlation tests and to assess the tendency and relative frequency of negative size changes between reconstructed ancestor-descendant nodes. The results in Table 3.4 also indicate a strong tendency toward size reductions in therocephalians, with the number of ancestor-descendant decreases outnumbering increases by as much as three to five times. Cynodonts, which originated at relatively small sizes, showed no such tendency with the number of size decreases approximately equaling the number of increases.

Diversification Rate Shifts

Results of rank order correlation and ancestor-descendant tests indicate that body sizes decreased on average in progressively deeper nested therocephalian subclades, presenting a prior expectation that body size shifts were not necessarily influenced by post-extinction diversity shifts (although they may have been associated with earlier diversifications). No significant rate shifts were detected in tree topologies constructed from Triassic *Lystrosaurus* or *Cynognathus* AZ diversity partitions, suggesting that either sampling is too poor to detect a shift or that the impact of the extinction on diversification rates in eutheriodonts was limited. The only significant diversification rate shift occurred

Table 3.5. Phylogenetic model fitting results.

	BM			BM_T			OU			EB		
	AICc	AW	β	AICc	AW	β,μ,θ	AICc	AW	β,α	AICc	AW	β,r
$Eutheriodontia_{total}$	113.72	0.276	0.05	115.61	0.107	0.05,0.01,5.15	113.41	0.270	0.06,0.02	**112.79**	**0.346**	**0.09,-0.03**
$Therocephalia_{total}$	**51.49**	**0.439**	**0.05**	53.48	0.162	0.05,0.01,5.28	52.51	0.263	0.06,0.04	53.85	0.134	0.05,-0.006
$Cynodontia_{total}$	58.32	0.118	0.05	60.48	0.049	0.05,0.01,4.11	59.00	0.068	0.06,0.03	**54.99**	**0.764**	**0.17,-0.08**

Model selection based on comparison of corrected AICs and Akaike weights (AW) for Brownian motion (BM), Brownian motion with trend (BM_T), Ornstein-Uhlenbeck (OU), and early burst (EB) models;
AICc, Akaike's Information Criterion corrected for small sample size; AW, Akaike weight;
β, BM rate parameter; μ, step mean; θ, trait mean; α, constraint parameter; r, decay rate

at the early-Late Permian divergence of Eutherocephalia (Fig. 3.5A,B), a result that is consistent with the relatively high rates of per capita origination and extinction in Late Permian eutherocephalians (see Chapter 1). This early diversification rate shift also mirrors previous findings in stratigraphically contemporaneous bidentalian dicynodonts (Botha-Brink and Angielczyk, 2010). Alternatively, the high diversity of therapsids in the Late Permian *Tropidostoma* and *Cistecephalus* AZs could be a sampling artifact (Fröbisch, 2013). Nevertheless, no shift is detected in the well-sampled *Lystrosaurus* AZ following the extinction.

Phylogenetic Model Fitting and Body Size Evolution

Goodness-of-fit tests found that active 'directional' (BM_T) and 'stabilizing' (OU) models fit poorly when compared to other candidate models of passive, Brownian motion evolution (BM and EB). Likelihood ratio tests and comparisons of Akaike weights indicate that EB best approximates the mode of body size evolution across the global dataset of eutheriodonts (Figure 3.6; Table 3.5). Body size evolution was better approximated by the null BM model when therocephalians were analyzed separately, indicating that derived cynodont subclades strongly influenced the decay rate parameter

for the EB model. In particular, late-Middle and Late Triassic cynodont clades (e.g., stem-mammaliaforms and other probainognathians) that include members from outside of the Karoo succession became more constrained in size space with decreasing variance over time, but not other lineages that lived in the immediate aftermath of the end-Permian extinction in the Karoo. In short, reductions in sizes of *Lystrosaurus* AZ eutheriodonts were likely to have been underpinned by passive processes, rather than long-term directional trends or constraints on evolutionary modes during the end-Permian extinction.

Discussion

Body size evolution before and immediately after the end-Permian extinction cannot demonstrably be classified as active (or "driven" sensu McShea, 1994), because size increases were generally associated with as many or more decreases and with expanding size disparity. Moreover, short-term reductions in mean and maximum sizes in the earliest Triassic *Lystrosaurus* AZ were not associated with changes in these background patterns of Brownian evolution, but were instead a product of the temporary ecological removal of medium to large-bodied predators (in addition to anagenetic size reduction in at least one predator lineage; see Chapter 2). In spite of its devastating ecological impacts, short-term shifts during the end-Permian extinction had negligible long-lasting effects on subsequent patterns of body size evolution in eutheriodont therapsids. Summary diagrams of eutheriodont body size evolution are provided in Figures 3.7 and 3.8, showing frequent size reductions beginning in the Permian with

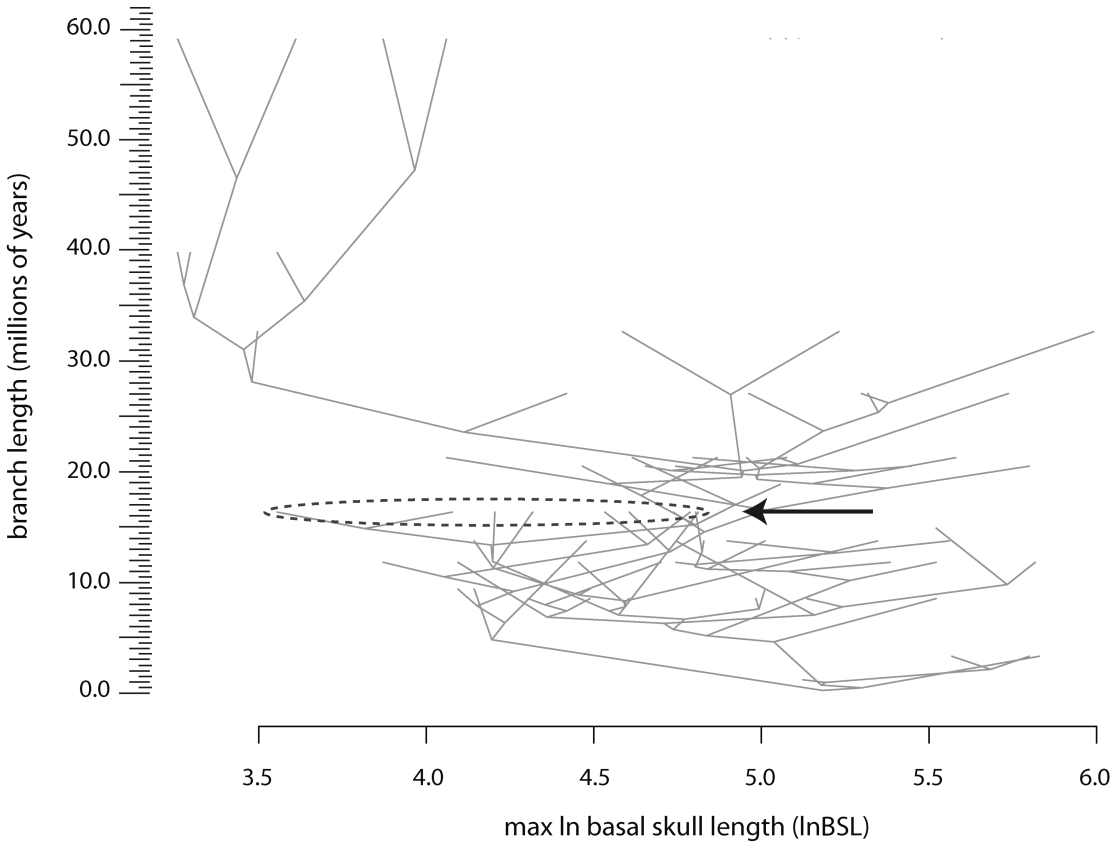

Figure 3.6. Traitgram of body size evolution in a global sample of Permian through Triassic eutheriodonts (spanning ~60 Myr) approximates an 'early burst' Brownian process (EB) of trait evolution. Arrow denotes location of *Lystrosaurus* Assemblage Zone taxa along the time-axis. Graphic produced using the *traitgram()* function in 'picante.'

occasional increases in some lineages (contributing to increased disparity), and an overall drop in body size distributions in the Triassic *Lystrosaurus* AZ. Though in conflict with traditional views of the fossil record, this finding corroborates more recent suggestions that large-scale patterns of trait evolution rarely yield active, directional trends (Hunt, 2007; Sookias, 2012a,b). Negative shifts were likely passive and, in the case of therocephalians, may underscore a fundamental asymmetry in size evolution: that size decreases can often occur with higher frequency than increases due to physiological and/or environmental constraints (Evans et al., 2012). The success of small-bodied lineages may therefore represent a more general feature of size evolution operating during background intervals, thereby representing a case of constructive selectivity as recently noted in Mesozoic mammals during the end-Cretaceous extinction (Wilson, 2012, 2013). Early cynodonts apparently do not mirror the therocephalian pattern given the present sampling. However, it is noteworthy that they exhibited unusually small sizes relatively early in their evolutionary history, remained small for much of the Late Permian and earliest Triassic, and radiated into a wide range of sizes that included large-bodied forms only after the extinction of other large theriodont predators (e.g., *Theriognathus*, *Moschorhinus,* and gorgonopsians which were excluded in the present analysis). An unexpected result is the protracted and increasingly constrained evolutionary rates in late-Middle to Late Triassic cynodonts. The factors influencing their constrained phenotypic evolution are beyond the scope of the present analysis, but may include intrinsic factors (developmental canalization) or extrinsic selective pressures

(competition with larger-bodied archosaurs or other emerging clades) that merit future study.

The sudden and short-lived nature of Early Triassic size reductions is compatible with some ecological explanations for Lilliput effects. Suggested mechanisms driving Lilliput patterns have included 1) within-taxon size reductions in relict lineages, 2) extinction of large taxa, and/or 3) post-extinction radiations of small taxa (Twitchett, 2007; Harries and Knorr, 2009). The phylogenetic models evaluated here do not support a post-extinction radiation of small taxa. In fact, several small-bodied *Lystrosaurus* AZ taxa and clades have Permian ghost lineages (Figs. 3.7, 3.8), implying preferential survivorship of these small-bodied lineages. Unfortunately, this latter scenario is difficult to assess because the small sample size of surviving genera in the Karoo (only four observed records) is not amenable to the desired statistical tests (e.g., logistic regression of size-specific survivorship). At least one large-bodied eutheriodont, *Moschorhinus*, exhibited within-lineage reductions in body size across the extinction boundary, implying that the extinction also had the potential to act upon microevolutionary processes in a constructive manner (Huttenlocker and Botha-Brink, 2013). Similar body size reduction characterizes the Permian and Triassic species of the dicynodont *Lystrosaurus* (Botha and Smith, 2004; Botha-Brink and Angielczyk, 2010).

This interplay of Lilliput mechanisms parallels that of some Permian-Triassic marine invertebrate clades in some respects, but differs in others. Global surveys of marine gastropods suggest strong within-lineage size decreases as well as size-selective

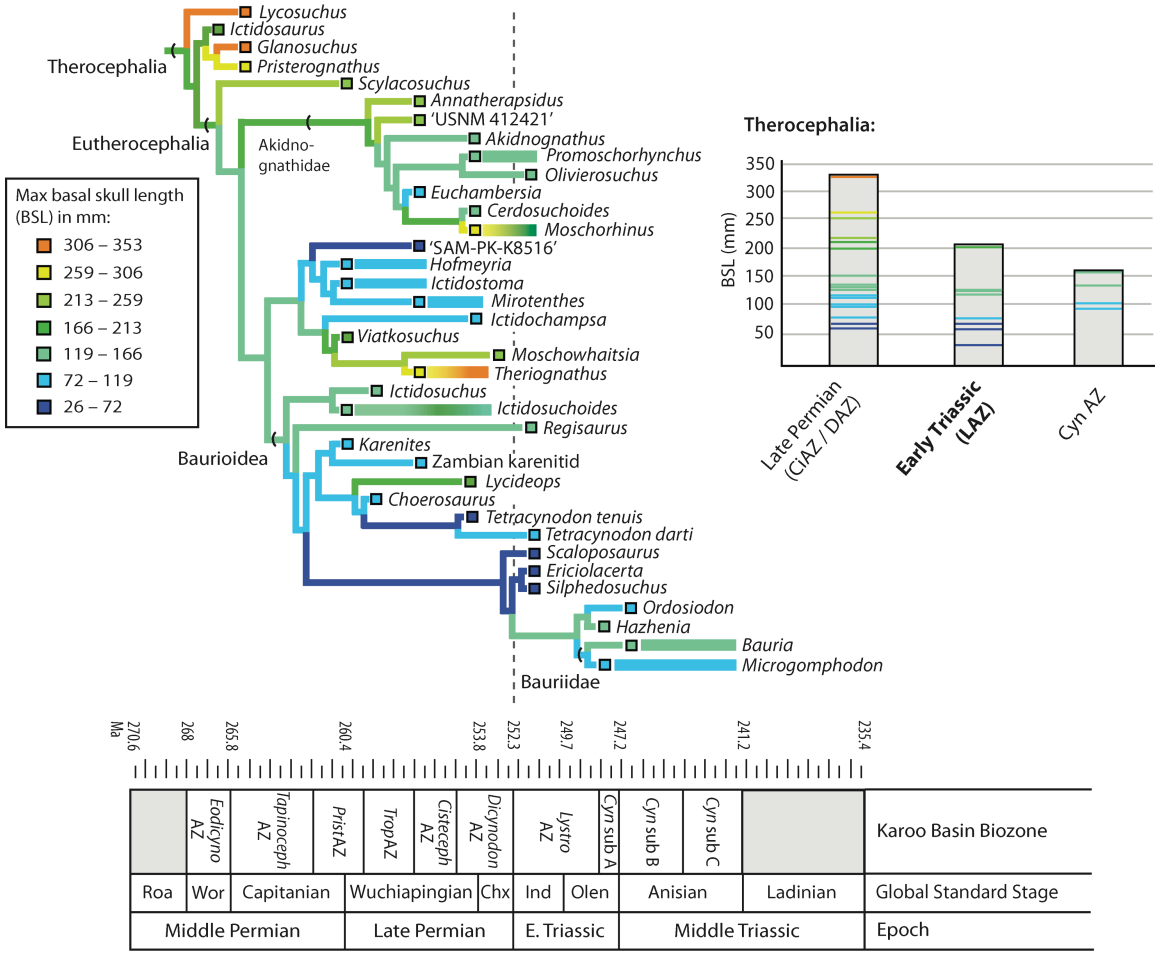

Figure 3.7. Ancestral state reconstructions for basal skull length in Permian and Triassic therocephalians. Colored horizontal bars indicate ranges of taxa spanning more than one stratigraphic bin. Note that significant decreases in mean sizes of major subgroups across the Permian-Triassic boundary (dashed line) were associated with the loss of large-bodied taxa and the survival of pre-existing small-bodied taxa or clades. Abbreviations: CiAZ, *Cistecephalus* Assemblage Zone; CynAZ, *Cynognathus* Assemblage Zone; DAZ, *Dicynodon* Assemblage Zone; LAZ, *Lystrosaurus* Assemblage Zone.

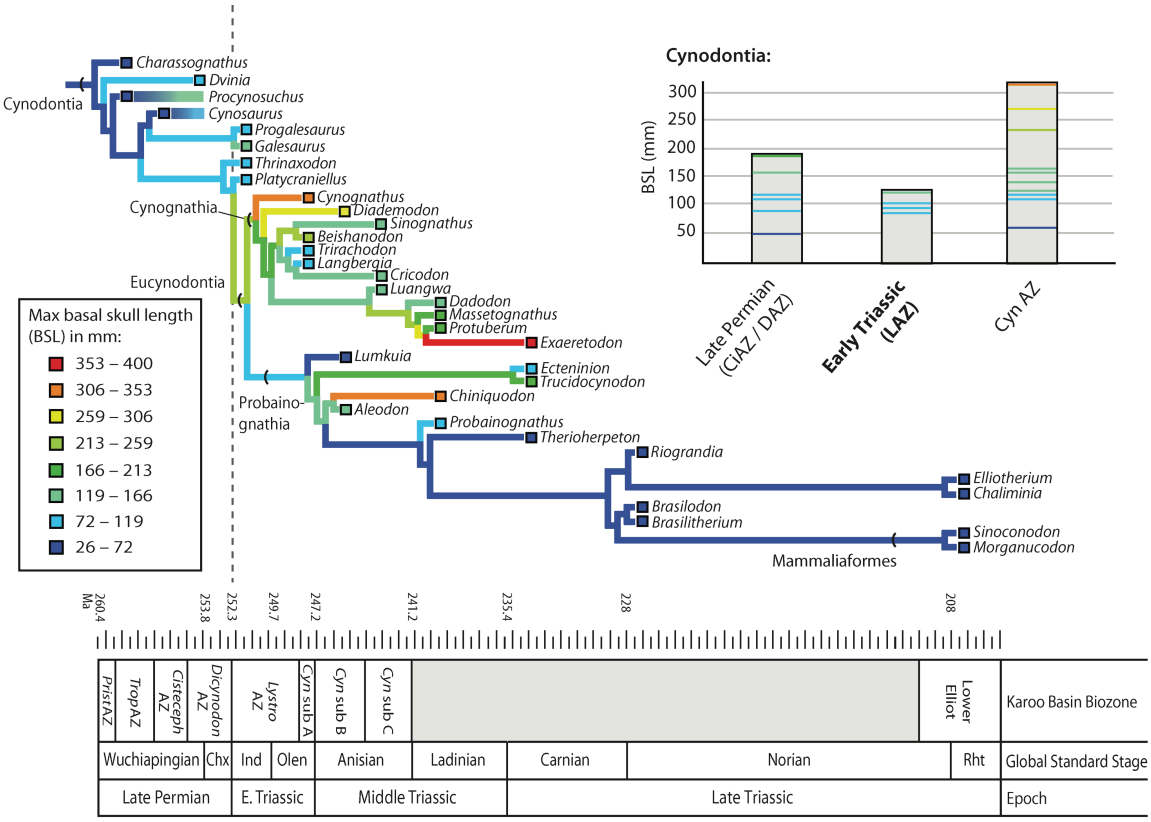

Figure 3.8. Ancestral state reconstructions for basal skull length in Permian and Triassic cynodonts. Colored horizontal bars indicate ranges of taxa spanning more than one stratigraphic bin (*Procynosuchus*, *Cynosaurus*). Abbreviations: CiAZ, *Cistecephalus* Assemblage Zone; CynAZ, *Cynognathus* Assemblage Zone; DAZ, *Dicynodon* Assemblage Zone; LAZ, *Lystrosaurus* Assemblage Zone.

extinction (Payne, 2005). Earliest Triassic foraminifera from South China provide evidence of all three underlying processes (Song et al., 2011), although within-lineage effects drive global size distributions of foraminifera most strongly (Rego et al., 2012). Notably, within-lineage decreases in lingulid brachiopods underscore hitherto unexplored ecophysiological effects, as they were associated with more frequent interruptions to growth and slower overall growth rates (perhaps in response to ocean acidification and hypercapnia) (Metcalfe et al., 2011). Within-lineage size decreases are observed in some nonmarine tetrapods (e.g., *Moschorhinus* and *Lystrosaurus*), but more general shifts toward smaller terrestrial vertebrate taxa were likely accentuated by the ecological removal of large-bodied Permian species (although small size did not necessarily ensure survival). Recent surveys of bone histology in these Permian-Triassic survivor taxa provide little evidence that Triassic therapsids grew more slowly than their Permian predecessors, and in some cases they may have grown more quickly or over shorter durations (Botha-Brink and Angielczyk, 2010; Huttenlocker and Botha-Brink, 2013). More data on the life histories of earliest Triassic terrestrial vertebrates will shed further light on the physiological and ecological underpinnings of these large-scale patterns and selectivity during the end-Permian biotic crisis.

Chapter 4—Growth Patterns and the Evolution of Bone Microstructure in Permo-Triassic Therocephalians (Therapsida, Eutheriodontia) of South Africa

Summary—A phylogenetic survey of growth patterns and histomorphology in limb bones of therocephalian therapsids from the Karoo Basin of South Africa is presented. The diversity of therocephalians and their differential survival of the end-Permian extinction offer the potential to investigate the evolution of growth patterns across the clade and their underlying influences on post-extinction body size reductions, or 'Lilliput effects.' Histologic sections were prepared from 80 limb bones from 11 genera of Permian and Triassic therocephalians. Histological indicators of growth, including cortical vascularity (%*CV*) and primary osteon diameters (*POD*), were evaluated in a phylogenetic comparative framework and assessed for correlations with other biologically significant variables (e.g., limb bone size and robusticity). Both %*CV* and *POD* correlated strongly with evolutionary changes in body size (e.g., smaller-bodied descendants tended to have lower %*CV* than their larger-bodied ancestors across the tree). Cortical bone wall thickness tended to be very high in early therocephalians and much lower in the gracile-limbed baurioids, but bone wall thickness showed no general correlation with cross-sectional area or degree of vascularity (and, thus, growth). Clade-level patterns deviated from previously studied within-lineage patterns. For example, *Moschorhinus*, one of few therapsid genera to have survived the extinction boundary, demonstrated higher %*CV* in the Triassic than in the Permian in spite of its smaller size.

Results support a synergistic model of size reductions for Triassic therocephalians, influenced both by within-lineage heterochronic shifts in survivor taxa (as in *Moschorhinus* and the dicynodont *Lystrosaurus*) and cladistically inferred survival of small-bodied taxa with short growth durations (e.g., baurioids). These findings mirror the multi-causal Lilliput patterns described in marine faunas, but contrast with skeletochronologic studies that suggest slow, prolonged shell secretion in marine benthos. Subjecting new histologic data to phylogenetic comparative methods will improve our understanding of the generality of growth and size shifts in Triassic Lilliput faunas and interplay between macroevolution and extinction during this time.

Introduction

Mass extinctions are frequently followed by short-term reductions in body sizes of survivor lineages, a pattern known as the 'Lilliput effect' (Urbanek, 1993; Harries et al., 1996). However, in the absence of adequate phylogenetic and life history data, the mechanisms of size reductions can be unclear and may differ across environments, taxonomic groups, and extinction events (Twitchett, 2007; Harries and Knorr, 2009). Lilliput patterns have been documented widely in marine invertebrate groups following the end-Permian extinction (Payne, 2005; Twitchett, 2007; Luo et al., 2008; Mutter and Neuman, 2009; Metcalfe et al., 2011; Song et al., 2011; Rego et al., 2012), and anecdotally in tetrapods of the Triassic *Lystrosaurus* Assemblage Zone in the Karoo Basin of South Africa (ca. 252.3 Ma), but growth dynamics underlying these patterns are

not fully understood. Therocephalians, for example, were a diverse clade of nonmammalian therapsids that thrived from the Middle Permian to Middle Triassic, and survived the end-Permian extinction as important components of Triassic survivor and recovery faunas in the Karoo Basin (Botha and Smith, 2006). In addition to the dicynodont *Lystrosaurus*, at least three genera of therocephalians in two major groups have observed stratigraphic occurrences that span the extinction boundary in the Karoo: the baurioid *Tetracynodon*, and the akidnognathids *Promoschorhynchus* and *Moschorhinus* (Smith and Botha, 2005; Botha and Smith, 2006; Huttenlocker et al., 2011b). Other Triassic taxa (e.g., *Olivierosuchus*, *Regisaurus*) have long ghost lineages extending into the Permian, indicating that they too survived the extinction but lack a Permian record within the depositional basin (Huttenlocker, 2009; Huttenlocker et al., 2011b). Although therocephalians are generally exceeded in abundance by dicynodont therapsids in the Karoo Basin, their diversity, extensive stratigraphic range, and success during the end-Permian extinction make them an ideal group to study evolutionary patterns during the Permian-Triassic transition.

Previous morphological studies of therocephalians have emphasized their functional anatomy, including streptostylic jaw structure and locomotory specializations (e.g., Kemp, 1972, 1978, 1986; Fourie and Rubidge, 2007, 2009). Recent collaborative work on therocephalians has emphasized integration of their fine structure and internal anatomy to resolve paleobiological questions, including tooth replacement patterns, braincase structure, and growth and histomorphologic structure (Abdala et al., 2008;

Sigurdsen et al., 2012; Huttenlocker and Botha-Brink, 2013). Detailed investigations of histmorphology are particularly useful, permitting assessments of growth patterns and variation within or among closely related therapsid species (e.g., Botha and Angielczyk, 2007; Huttenlocker and Botha-Brink, 2013). Moreover, as growth patterns are directly associated with organismal fitness, recent investigations into bone microstructure have inquired into whether certain growth strategies conferred an advantage on some groups during the end-Permian extinction (e.g., rapid growth in the dicynodont *Lystrosaurus*; Botha-Brink and Angielczyk, 2010).

Bone Microstructure in Therapsids

Bone histology has offered insights into the lifestyles and growth patterns of many of the major subclades of nonmammalian therapsids. Recent examples include investigations of feeding and locomotory mechanics, habitat use, and especially growth dynamics (e.g., Ray et al., 2005; Jasinoski et al., 2010; Chinsamy-Turan, 2012). Earlier surveys of bone histology emphasized differences between basal (pelycosaurian-grade) synapsid and therapsid tissue composition, matrix organization, and degree of vasculature of the limb bones (Enlow and Brown, 1957; Enlow, 1969; Ricqlès, 1969, 1974a, 1974b, 1976). Particularly, fibrolamellar tissue complexes were found to be near ubiquitous among limb elements of sampled therapsids, suggesting to workers that this tissue complex appeared early during therapsid evolution (Ray et al., 2004; Chinsamy and Hurum, 2006; Ray et al., 2009). Indeed, fibrolamellar bone has been reported in basal therapsids (e.g., *Biarmosuchus*: Ricqlès, 1974b), as well as in some immature

pelycosaurian-grade synapsids (e.g., *Sphenacodon* juveniles) and in fast-growing portions of the skeleton of other basal synapsids (e.g., the elongated neural spines of *Dimetrodon* and crossbars on the neural spines of *Edaphosaurus*) (Huttenlocker et al., 2010, 2011a; Huttenlocker and Rega, 2012). However, there is great histovariability in the organization of fibrolamellar bone even within major subclades of therapsids. Fibrolamellar bone may be formed by varying degrees of woven- and parallel-fibered interstitial matrix and incorporates a variety of vascular motifs, and may be zonal (punctuated by cyclic growth marks) or azonal. Ray et al. (2004) reported the presence of zonal fibrolamellar bone in many Permian and Middle Triassic taxa, but suggested that sustained (non-cyclic) growth patterns might have arisen occasionally in a number of phylogenetically disparate taxa (gorgonopsian *Aelurognathus*; eucynodont *Cynognathus*; and some bidentalian dicynodonts). The abundance of dicynodont fossils in Permian and Triassic rocks and recent advances in their systematic relationships have permitted comparative surveys of growth patterns in this diverse subclade (Chinsamy and Rubidge, 1993; Botha, 2003; Ray and Chinsamy, 2004; Ray et al., 2005; Botha and Angielczyk, 2007; Ray et al., 2009; Botha-Brink and Angielczyk, 2010; Green et al., 2010; Nasterlack et al., 2012; Ray et al., 2012). Phylogenetic comparative surveys have revealed patterns of increasing tissue vascularity during the evolutionary history of bidentalian dicynodonts (especially in Triassic forms like *Lystrosaurus*), and determinate growth patterns with peripheral rest lines and systematic cortical remodeling in large kannemeyeriiforms (Botha-Brink and Angielczyk, 2010; Green et al., 2010; Ray et al., 2012).

The diversity of growth patterns in other nonmammalian therapsid groups, as well as their phylogenetic and temporal distributions, is incompletely known. A body of literature on nonmammalian cynodont histology has accrued in recent years (e.g., Ricqlès, 1969; Botha and Chinsamy, 2000, 2004, 2005; Chinsamy and Abdala, 2008; Ray et al., 2004; Botha-Brink et al., 2012), but sampling has been more limited in gorgonopsians and therocephalians (Ray et al., 2004; Chinsamy-Turan and Ray, 2012). Ricqlès (1969) suggested differential rates of growth between a basal therocephalian from the Middle Permian of South Africa and the Late Permian whaitsiid '*Notosollasia'* (=*Theriognathus*). Given the comparatively more vascularized cortical bone in the radius of the whaitsiid (1969: plate IV), Ricqlès suggested that therocephalians might have exhibited accelerated growth rates later in their evolutionary history, paralleling the aforementioned temporal pattern of increasing growth rates in some dicynodonts. More recently, Ray et al. (2004) and Chinsamy-Turan and Ray (2012) analyzed additional material from an indeterminate scylacosaurid (erroneously identified as '*Pristerognathus'*) and argued for similar 'flexible' growth patterns in gorgonopsians, basal therocephalians, and most early cynodonts. The authors suggested that more rigorous taxonomic sampling would better substantiate parallel trends toward a loss in developmental plasticity and acceleration of growth rates as in dicynodonts. Inadequate sampling of Late Permian and Triassic eutherocephalians limits our understanding of evolutionary patterns in therapsid histomorphology and skeletal growth during this important geologic transition.

Present Study

Although eutherocephalians have not been sampled histologically for such comparisons, recent revisions to Permo-Triassic boundary-crossing taxa have necessitated cursory descriptions of eutherocephalian histology for its ontogenetic and paleobiological implications (*Tetracynodon*: Sigurdsen et al., 2012; *Moschorhinus*: Huttenlocker and Botha-Brink, 2013 and Chapter 2 of this dissertation). During the course of this work, I developed a database of histological data and images with the goal of addressing features of life history evolution in Permian and Triassic eutheriodonts (therocephalians and cynodonts), particularly in the context of the end-Permian extinction. Here, I present a reappraisal of limb bone microstructure in Permian and Triassic therocephalians based on new histologic sampling, and offer a hypothesis of the evolution of their growth patterns. I contend that therocephalians provide a robust study system for investigating the evolution of growth strategies during the Permian-Triassic transition, and a useful point of comparison to other groups that lived during this time (e.g., dicynodonts, cynodonts).

Materials and Methods

Specimen Selection and Histological Processing

Specimens were selected based on completeness and availability for histological processing, but a broad sample of the major representatives of South African therocephalians was desired in order to recognize long-term patterns (if present) or clade

specific histomorphology. Specimens that were semi-articulated and included diagnostic cranial material were preferred for accuracy of taxonomic identifications. Some specimens were not diagnosable to genus, but were resolved to their respective higher taxon as in the case of five indeterminate scylacosaurids described here. Scylacosaurids are generally difficult to identify unless a complete and accurate antecanine tooth count can be made, and some authors have suggested that the diversity of scylacosaurids is over-split because variations in tooth count may be ontogenetically variable (e.g., Abdala et al., 2008). The sample therefore included 80 limb elements from 33 individuals in 11 genera: *Lycosuchus*, *Glanosuchus*, *Moschorhinus*, *Olivierosuchus*, *Hofmeyria*, *Mirotenthes*, *Theriognathus*, *Ictidosuchoides*, *Tetracynodon*, *Scaloposaurus*, and *Microgomphodon* (Fig. 4.1), plus additional scylacosaurid material not diagnosed to genus. Histological sections were prepared using standard histological techniques modified from Chinsamy and Raath (1992) and Wilson (1994). Limb bone midshafts were sampled cross-sectionally and imaged using Nikon Eclipse 50i and LV100 POL petrographic microscopes with a digital image capture system. Histomorphometric variables (discussed below) were measured using NIS-Elements and NIH ImageJ v. 1.42q software. *Moschorhinus* histomorphology was excluded from present description as it has been discussed elsewhere (Huttenlocker and Botha-Brink, 2013; see Chapter 2 of this dissertation), but data from *Moschorhinus* were included in the quantitative analyses (Table 4.1).

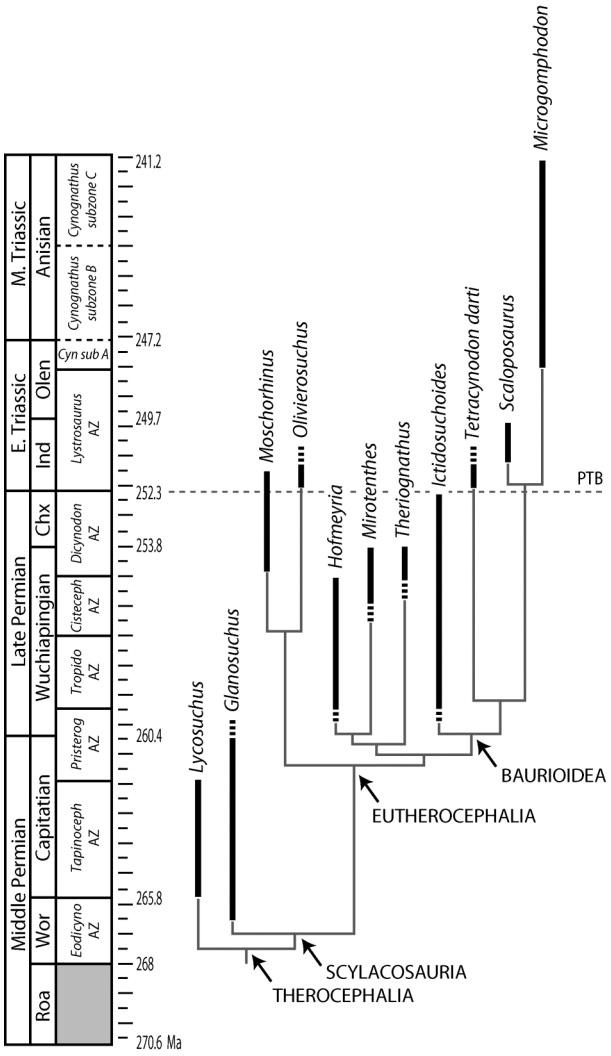

Figure 4.1. Stratigraphic ranges of therocephalians sampled histologically in the present study. Dashed line indicates position of Permian-Triassic Boundary (PTB). Abbreviations: Chx, Changxingian; *Cisteceph* AZ, *Cistecephalus* Assemblage Zone; *Cyn* sub A, *Cynognathus* subzone A; *Eodicyno* AZ, *Eodicynodon* Assemblage Zone; Ind, Induan; Olen, Olenekian; *Pristerog* AZ, *Pristerognathus* Assemblage Zone; Roa, Roadian; *Tapinoceph* AZ, *Tapinocephalus* Assemblage Zone; *Tropido* AZ, *Tropidostoma* Assemblage Zone; Wor, Wordian.

Bone Tissue Typology: Definitions and Selection of Growth Proxies

Bone tissue texture exhibited marked variation in therocephalians and other therapsids, varying from highly organized and lamellar to disorganized and woven. Only a few recent studies have integrated qualitative and quantitative assessments of tissue texture and vascular proxies of growth in Permo-Triassic therapsids (Botha and Chinsamy 2000, 2004, 2005; Ray and Chinsamy 2004; Ray et al., 2004, 2005, 2010; Botha-Brink and Angielczyk 2010; Huttenlocker and Botha-Brink, 2013). Generally, cellular bone forms as osteoblasts become incorporated into the extracelluar (or interstitial) matrix (ECM) forming quiescent osteocytes. The overall bone apposition rate affects the texture of the mineralized ECM, with collagen fibers and crystallites bearing a more lamellar organization under slower growth and a nonlamellar (woven-fibered) texture under faster growth. Parallel-fibered bone (as with lamellar bone) can be identified by its 'streaky' appearance under polarized light, with the predominant fiber orientation being parallel to the surface of the bone and forming a woven-basket texture in most cases. In cases in which birefringent properties have been disrupted by diagenetic processes, it is possible to approximate the relative organization of mineralized fibers with reference to the organization of the lacunocanalicular network within the ECM (Stein and Prondvai, 2013). In contrast to parallel-fibered bone, woven-fibered bone includes large, globular osteocyte lacunae that are usually densely packed within the mineralized ECM. Nonlamellar tissues (parallel- and woven-fibered) may frequently incorporate large vascular canals that later become infilled with one or two concentric

lamellae forming primary osteons (diagnosed by their ‘Maltese cross’ pattern of birefringence under polarized light). These tunnels form passageways for blood vessels and nerves while also contributing to the structural integrity of the bone by providing added bone mass and helping to blunt microcracks. The result is a fibrolamellar bone complex (herein ‘FLB’), in which a disorganized, fibrous or nonlamellar interstitial matrix incorporates an anastomosing network of centripetally lamellated primary osteons. Currey (1987, 2002) defined FLB broadly as a tissue complex formed by parallel- (or woven-) fibered bone with primary osteons (2002: p.18). By contrast, Ricqlès (1974a) originally restricted the term ‘fibrolamellar’ to tissues formed largely by woven-fibered bone with primary osteons, excluding parallel-fibered bone from this category. Here, I follow the traditional usage, but temper this strict definition by noting that parallel- and woven-fibered bone form a continuum that is often ill-defined, and in many therapsid bony tissues may be present simultaneously. Bone cortices formed primarily by lamellar tissue, which forms at relatively slower apposition rates (~1 μm/day or less), do not typically incorporate primary osteons, instead bearing simple vascular canals or being avascular (Appendix 9). In lamellar bone, the lacunocanalicular network is ordered, the osteocyte lacunae being small and more lenticular in appearance with the long axis oriented parallel to the surface of the bone. Both tissue complexes can be zonal (periodically interrupted by growth marks) or azonal. Growth marks in zonal bone may be present in the form of lines of arrested growth or ‘LAGs’ (denoted by an opaque cement line, traceable around the entire cortex, and indicative of a temporary cessation of

growth) or annuli (thin bands of dense, annular tissue, usually parallel-fibered or lamellar, deposited during periods of slowed growth).

For quantitative histomorphometric analysis, two vascular proxies of skeletal growth were selected: cortical vascularity and mean primary osteon diameter. These proxies were selected in order to evaluate the extent to which histological correlatives of growth varied across phylogeny, and whether their evolution was tied to body size or other biological factors. Vascular proxies have offered useful indicators of skeletal growth in extant and extinct tetrapods (Castanet et al., 2000; Margerie et al., 2002, 2004; Buffrénil et al., 2007; Cubo et al., 2012), and their utility here allows comparisons with other histological studies of therapsids in which similar measures were used (e.g., Botha-Brink and Angielczyk 2010; Huttenlocker and Botha-Brink, 2013). Notably, ontogenetic variation in growth may introduce a lesser degree of cortical vascularity in adult bones that exhibited decreasing apposition rates prior to death and burial, or may introduce variation in a single cross-section. Nonmammalian therapsids, however, are well suited to relative growth rate estimation based on tissue texture and vascularity, due to their generally thick bone walls (preserving the early record of primary growth) and limited secondary remodeling (Botha-Brink and Angielczyk, 2010). Measurement of cortical vascularity (%*CV*, the relative area of the cortex that is occupied by porous, vascular spaces) follows Lee et al. (2013) and Chapter 2 of this dissertation. Measurements were restricted to the inner two-thirds to three-quarters of the cortex where the bone formed at high, sustained growth rates (Cubo et al., 2012), and were averaged from ten quadrants

sampled circularly around each midshaft cross-section. The subsampled quadrants excluded areas of secondary reconstruction and outer regions of simple canals. I also estimated mean primary osteon diameter (*POD*) by measuring in microns the transverse (or minimum) widths of 15 primary osteons visible in the subsampled regions and averaging them across all regions within a given midshaft cross-section.

To examine potential effects of size and robusticity on measured histomorphometric variables, I also estimated two proxies of overall bone robusticity: *K* and relative bone wall thickness (*RBT*). These variables play a frequent role in histological studies of fossil tetrapod bone, as bone robusticity may correspond to habitat preferences or mechanical loading (Wall, 1983; Currey and Alexander, 1985; Currey, 2002; Laurin et al., 2004; Germain and Laurin, 2005; Kriloff et al., 2008). However, their relationships to size, growth, and vascularity have been underexplored in a comparative framework. Whereas *K* represents the proportional diameter of the medullary region relative to the total diameter of the cross-section (Currey and Alexander, 1985), *RBT* represents a percentage of the average cross-sectional thickness of the bone wall relative to the total diameter of the cross-section (Chinsamy, 1993). These measurements, as well as cross-sectional area at midshaft, were attained using NIH ImageJ, and were tested for correlations with vascular growth proxies using Pearson's product-moment correlation tests. Histomorphometric data are recorded in Table. 4.1.

Correlation Tests

Pearson's product-moment correlation tests—I performed a series of correlation tests in order to evaluate the extent to which variations in vascular growth proxies were dependent upon size and robusticity, which bear a strong influence on many aspects of organismal biology (Peters, 1983; Calder, 1984; Stearns, 1992). For instance, small-bodied therocephalians might have achieved their increasingly diminutive sizes by having a slower growing, less vascularized skeleton compared to their larger-bodied predecessors. In this scenario, one would expect a correlation between smaller size and slower growth, and between larger size and faster growth across clades. In extant vertebrates, small-bodied species generally exhibit slower growth rates than other larger-bodied groups (Case, 1978), a general feature that has also been identified from histologic data in fossil non-avian dinosaurs (Erickson et al., 2004; Lee, 2007). On the other hand, smaller sizes may have been achieved by shortening the duration of the growth period, in which case no generalized correlations between size and vascular proxies of skeletal growth are necessary. To address these hypotheses, histomorphometric data (%*CV*, *POD*, *RBT*) and midshaft cross-sectional area were recorded for each sectioned limb bone. The data were organized into propodial, epipodial, and pooled subsets to control for the effects of increased variance from pooling limb bones of different types (although the effects appeared to be minimal as all tests ultimately yielded similar results). For each data partition, Pearson's product-moment correlation tests were performed between histomorphometric variables (%*CV*, *POD*, *RBT*) and the natural log

Table 4.1. Specimens, elements, and histomorphometric measurements in studied therocephalians.

	% Largest*	Element	Midshaft cross-sectional area (mm^2)	*RBT* (%)	*K*	Cortical vascularity (%)	Mean POD (µm)
Lycosuchus							
SAM-PK-9084	100%	radius	296.76	16	0.42	10.7[5.5]	101[11]
		ulna	325.40	25	0.38	15.7[2.0]	109[26]
SAM-PK-K9012	--	femur	1276.60	15	0.67	16.9[6.2]	168[17]
Glanosuchus							
BP/1/6228	47%	ulna	57.62	20	0.42	04.9[0.9]	51[13]
Scylacosauridae indet.							
BP/1/5576	--	radius	30.99	19	0.47	10.3[2.2]	68[10]
		ulna	36.63	24	0.53	09.7[4.3]	71[08]
BP/1/5587	--	humerus	169.42	33	0.29	13.3[3.2]	75[08]
		radius	88.26	23	0.46	03.5[0.7]	71[15]
		ulna	120.25	24	0.44	06.0[0.8]	85[07]
CGS R300	--	humerus	308.56	31	0.32	15.9[6.5]	112[13]
SAM-PK-5018	--	humerus	--	--	--	--	--
		radius	--	17	--	--	--
		femur	--	15	--	--	--
		tibia	83.86	24	0.60	10.3[1.5]	55[10]
		fibula	--	--	--	--	--
SAM-PK-11557	--	fibula	49.10	25	0.47	07.0[2.8]	44[07]
Moschorhinus							
NMQR 48	62%	humerus	205.85	30	0.45	16.6[5.0]	--
		radius	48.10	26	0.40	05.2[2.4]	67[18]
		ulna	102.67	27	0.43	04.8[1.3]	67[10]
		femur	263.13	22	0.58	12.8[4.8]	95[13]
NMQR 3939	65%	humerus	212.25	35	0.38	20.1[6.9]	134[36]
		radius	92.77	34	0.31	11.4[2.6]	101[18]
		ulna	101.86	29	0.44	10.1[2.1]	120[27]
		femur	206.82	28	0.44	18.4[6.9]	140[32]
		tibia (l)	103.85	37	0.30	15.5[1.9]	117[17]
		tibia (r)	114.28	31	0.39	15.6[5.8]	119[34]
NMQR 1640a	(84%)	femur	325.70	25	0.50	11.1[4.8]	96[12]
NMQR 1640b	--	tibia	427.87	35	0.39	09.7[2.5]	106[23]
NMQR 3351	91%	femur	488.65	21	0.55	13.6[5.0]	100[22]
NMQR 3684	(95%)	femur	378.12	27	0.53	14.2[4.6]	92[17]
SAM-PK-K118	59%	humerus	161.60	28	0.41	25.5[4.9]	100[17]
		radius	62.80	23	0.54	19.5[3.2]	101[17]
SAM-PK-K9953	59%	femur	155.13	25	0.42	20.9[5.8]	108[15]
UCMP 42787	(67%)	humerus	209.64	35	0.34	19.5[4.0]	107[20]
		radius	83.64	35	0.27	12.4[3.6]	92[18]
		fibula	42.53	32	0.28	10.8[1.9]	58[14]
BP/1/4227	76%	humerus	312.00	33	0.35	12.1[2.9]	100[16]
		radius	103.60	30	0.36	10.9[2.1]	88[10]
		ulna	96.00	26	0.48	08.5[2.0]	91[19]

Table 4.1. (Continued)

Olivierosuchus							
NMQR 3605	100%	humerus	47.54	36	0.38	09.9[1.8]	99[10]
SAM-PK-K10617	(65%)	femur	23.72	19	0.65	03.4[1.1]	75[10]
Hofmeyria							
BP/1/4404	69%	humerus	12.56	31	0.32	07.5[1.4]	72[11]
		radius (l)	4.80	35	0.26	03.4[1.0]	46[05]
		radius (r)	4.04	40	0.15	04.8[1.9]	47[05]
		ulna (l)	3.63	39	0.22	03.0[0.6]	39[05]
		ulna (r)	4.30	39	0.20	04.7[1.1]	43[08]
Mirotenthes							
SAM-PK-K6511	78%	humerus	17.12	32	0.31	05.4[1.5]	54[07]
		radius	6.28	34	0.33	03.5[1.5]	38[07]
		ulna	5.24	32	0.42	02.0[0.5]	41[07]
		femur	19.40	25	0.42	03.6[0.6]	58[07]
		tibia	11.28	31	0.31	03.1[0.8]	38[06]
		fibula	3.64	32	0.39	03.9[1.1]	32[04]
Theriognathus							
NMQR 3375	38%	femur	43.45	24	0.51	06.2[2.0]	65[10]
BP/1/719	(62%)	femur	140.21	20	0.59	06.8[1.4]	87[11]
Ictidosuchoides							
SAM-PK-K8659	50%	humerus	23.92	22	0.56	07.3[2.0]	45[05]
		radius	10.08	24	0.52	04.2[1.1]	38[05]
		femur	45.64	--	--	--	38[05]
		tibia	28.32	16	0.63	02.8[1.0]	43[08]
		fibula	10.44	22	0.59	03.8[1.5]	40[07]
SAM-PK-K10423	(50%)	femur	34.80	14	0.71	04.7[1.8]	65[08]
		tibia	9.52	23	0.49	04.3[1.5]	39[05]
		fibula	19.60	19	0.47	04.7[1.6]	40[08]
BP/1/75	--	humerus	44.27	19	0.64	11.1[1.4]	52[06]
BP/1/4092	100%	humerus	60.19	22	0.56	10.2[2.1]	60[07]
		radius	39.52	21	0.58	11.1[3.1]	62[08]
		ulna	74.67	26	0.54	08.3[2.1]	52[08]
Tetracynodon							
NMQR 3745	85%	humerus	11.44	22	0.56	8.1[3.2]	36[10]
UCMP 78395	(94%)	humerus	16.48	24	0.49	4.9[1.7]	42[05]
		radius	8.40	27	0.43	1.9[0.5]	42[10]
		ulna	6.12	31	0.33	2.8[1.0]	38[06]
		femur	18.28	17	0.66	5.0[2.5]	39[06]
		tibia	12.48	25	0.48	3.9[0.7]	42[06]
UCMP 78396	(94%)	humerus	16.96	21	0.54	4.7[1.9]	42[12]
		femur	18.16	17	0.62	4.3[1.1]	42[07]
		fibula	5.19	25	0.53	2.3[0.5]	35[06]
Scaloposaurus							
SAM-PK-K4638	67%	humerus	15.34	--	--	06.6[1.6]	62[08]

Table 4.1. (Continued)

Microgomphodon							
NMQR 3189	(82%)	humerus	11.04	21	0.61	08.8[2.1]	43[08]
		femur	16.52	18	0.61	06.1[1.6]	44[08]
		tibia	7.86	24	0.51	08.0[3.2]	41[09]
		fibula	3.33	29	0.39	04.2[0.9]	32[04]

*Based on relative basal skull length (BSL). Parentheses indicate estimates for incomplete skulls.

of midshaft cross-sectional area. Vascular growth proxies were also tested for correlations with bone robusticity independent of size, and with each other to assess whether %*CV* and *POD* provided comparable estimates of vascularization.

Phylogeny-independent contrasts—Independent contrast methods were carried out to control for the effects of phylogenetic non-independence of putative correlations (Felsenstein, 1985; Garland et al., 2005). For example, one might find low tissue vascularity in Triassic baurioids due to their generally small sizes, or due to their close relatedness (and, by extension, their inherited phenotypic similarities). I carried out additional correlation tests on an augmented data set using the PDAP:PDTREE module (Midford et al., 2011) in Mesquite version 2.0 (Maddison and Maddison, 2007). This required a tree and branch lengths (adapted from Chapters 1 and 3) pruned to the 11 histologically sampled taxa. First, tip data for each of the 11 taxa were recorded in a NEXUS file, including average %CV, POD, RBT and the natural log of midshaft area of the propodials and epipodials respectively (limb bones were not pooled for independent contrasts). Second, ancestral character states (estimated using squared-change parsimony) were checked for the assumption of Brownian motion evolution that governs independent

contrasts (Felsenstein, 1985; Díaz-Uriarte and Garland, 1996). This was performed by running assumption-testing operations in PDAP that evaluate the relationship between the absolute values of independent contrasts and their corresponding standard deviations. Non-significant relationships were determined for each of the data partitions, indicating that a Brownian motion model adequately fit the tip data. Finally, the same sets of regressions were performed on independent contrasts as in the untransformed data for the raw Pearson's correlation tests (size, robusticity, and vascular growth proxies).

Description

THEROCEPHALIA

Lycosuchidae

Lycosuchus vanderrieti

(Fig. 4.2)

General—SAM-PK-9084 (radius, ulna), from Reitkuil, Beaufort West (Middle Permian, *Tapinocephalus* AZ); SAM-PK-K9012 (femur), from Klein Koedoes Kop, Beaufort West (Middle Permian, *Tapinocephalus* AZ). The histological profiles of long bone shafts reveal well-vascularized cortical bone with multiple growth zones incorporating nonlamellar interstitial ECM (including woven- and parallel-fibered tissue)

with reticular to subplexiform primary osteons, interrupted by cyclic growth marks (annuli or LAGs). Secondary osteons are apparently absent in all elements.

Radius—The radius (Fig. 4.2A, B) is a robust element with a circular cross-section at mid-diaphysis, revealing a compact cortex that grades into a porous spongiosa (the medullary region largely being occluded by cancellous bone). The bone wall thickness at the midshaft is moderate (*RBT*, 16%; *K*, 0.42) and composed of FLB with many large primary osteons. The osteons are arranged into both longitudinal and reticular orientations. The interstitial ECM is woven-fibered, but with some parallel-fibered tissue deposited periodically near growth marks. Intervening osteocyte lacunae are highly concentrated and disorganized between adjacent primary osteons and are generally globular in shape (resembling the 'static osteogenic-derived woven bone' of Stein and Prondvai, 2013). The densely packed longitudinal and reticular primary osteons are distributed in an ordered fashion within circularly organized growth zones. The canals become smaller and more sparsely distributed in the outermost cortex where they are also predominantly longitudinal in orientation. The average mid-cortical vascularity (%*CV*) is 10.7 and the mean primary osteon diameter (*POD*) is 101 μm. Tissue structures, including growth marks, are well visible and there are at least three growth marks (LAGs) preserved in the cortex. The spacing of successive growth marks decreases toward the periosteal surface, and there is a strongly defined LAG in the outer region where the vasculature becomes more sparse and oriented longitudinally. Although

Figure 4.2. Bone histology in *Lycosuchus vanderrieti* from the Middle Permian *Tapinocephalus* Assemblage Zone. **A**, SAM-PK-9084, radius midshaft, cortical fibrolamellar bone viewed at high magnification (crossed-nicols with wave plate). **B**, Same as 'A,' viewed under normal polarized light without wave plate. **C**, SAM-PK-9084, ulna midshaft, cortex showing growth marks and well-vascularized fibrolamellar bone viewed at low magnification (non-polarized light). Note the thick bone wall and inner coarse cancellous structure. **D**, SAM-PK-K9012, femur midshaft, dorsal cortex showing subplexiform fibrolamellar bone viewed under non-polarized light. **E**, SAM-PK-K9012, femur midshaft, posterior region of cortex showing three bands of parallel-fibered bone (blue bands denoted by arrows) representing possible growth marks, viewed at low magnification (crossed-nicols with wave plate). Arrows denote growth marks. Abbreviations: po, primary osteon.

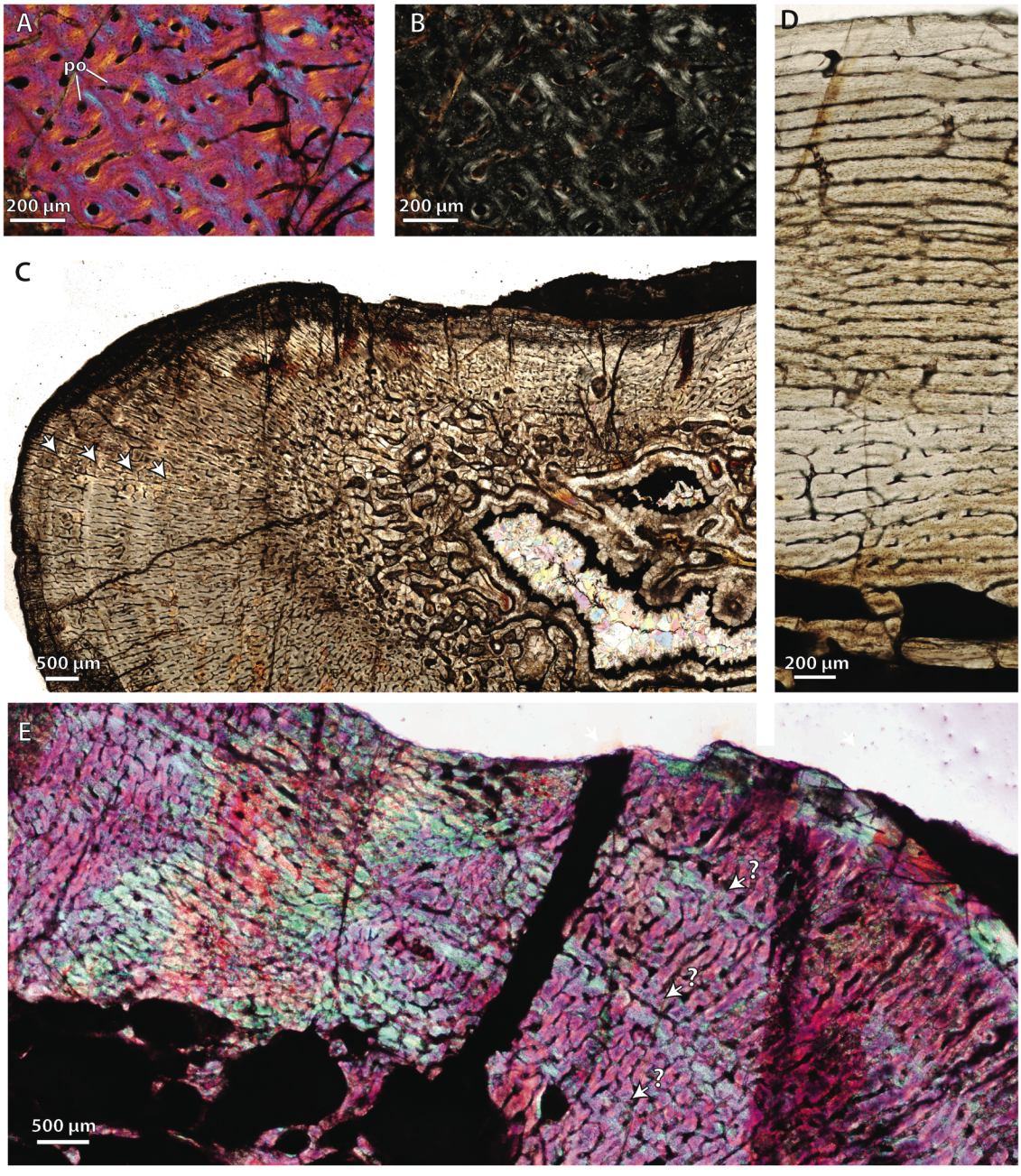
A
po
200 µm
B
200 µm
D
200 µm
C
500 µm
E
?
?
?
500 µm

apposition rate likely decreased toward the outer perimeter, there is no external fundamental system (EFS).

Ulna— The ulna (Fig. 4.2C) bears a broad, flat midshaft such that the cross-sectional profile is roughly ellipsoid to figure-8. As in the radius, the moderately porous cortex grades into a more cancellous medullary region that is largely occluded by fine cancellous bone and a few trabecular structures. The cortex is somewhat thicker than in the radius (*RBT*, 25%; *K*, 0.38). A small marrow cavity is present. The cortex consists of fibrolamellar structure, composed of primary osteons within a woven-fibered interstitial ECM but with some parallel-fibered tissue. The dense and disorganized lacunocanalicular network between primary osteons resembles that of the radius. The primary osteon orientation is predominantly reticular and radial. The %*CV* is 15.7 and the mean *POD* is 109 µm. The vascular canals (which are of moderate size) become finer and more sparsely distributed in the outermost cortex, indicative of growth attenuation. The vasculature is ordered within growth zones as in the radius, several of which can be discerned by well-defined LAGs. There are as many as four preserved LAGs in total. The LAGs become more closely spaced near the periosteal surface as in the radius. Although the outer region of the bone becomes more parallel-fibered, there is no EFS in the subperiosteal region.

Femur—The femur (Fig. 4.2D, E) is a short, robust bone with a compressed shaft that is oval in cross-section (unlike the rounded cross-section of later eutherocephalians). In section, the midshaft is of moderate thickness, but thinner than the forelimb elements

(*RBT*, 15%; *K*, 0.67). It is composed of FLB with large primary osteons of varying orientations. The vascular motifs are somewhat complex, the predominant orientation being subplexiform, but with some reticular and radial osteons at muscular attachment sites, such as the adductor ridge. The degree of vascularization of the femur is generally greater than in the radius and ulna (%*CV*, 16.9; mean *POD*, 168 µm). Growth marks are difficult to distinguish due to the circular arrangement of primary osteons within the subplexiform network, although three faint bands (annuli?) of parallel-fibered bone can be observed in the posteroventral quadrant where the osteons form a more reticular arrangement. Faint bundles of Sharpey's fibers are also evident near the adductor ridge in the outer cortex, indicating attachment of the adductor musculature. The matrix composing the outermost cortex is highly birefringent, indicative of its strong parallel-fibered and lamellar structure. The lacunocanalicular network also includes more lenticular osteocyte lacunae that are sparsely distributed. Although the bone being laid down in this region was no longer fibrolamellar and the vascular canals became sparser, the tissue lacks the avascular and multi-lamellar structure characteristic of a true EFS.

SCYLACOSAURIA

Scylacosauridae

Glanosuchus macrops

(Fig. 4.3A)

Figure 4.3. Bone histology in Scylacosauridae from the Middle Permian *Tapinocephalus* Assemblage Zone. **A**, *Glanosuchus macrops*, BP/1/6228, ulna midshaft, cortical fibrolamellar bone viewed at low magnification (crossed-nicols with wave plate). **B**, Scylacosauridae indet., SAM-PK-5018, fibula midshaft close-up of secondary osteon in deep cortex (crossed-nicols with wave plate). **C**, Scylacosauridae indet., CGS R300, humerus midshaft cortex viewed at low magnification showing growth marks (crossed-nicols with wave plate). **D**, Scylacosauridae indet., BP/1/5576, ulna midshaft cortex viewed at low magnification showing growth marks (crossed-nicols with wave plate). **E**, Scylacosauridae indet., BP/1/5587, ulna midshaft cortex viewed at low magnification showing growth marks (crossed-nicols with wave plate). Arrows denote growth marks. Abbreviations: cl, cement line; Hc, Haversian canal; po, primary osteon.

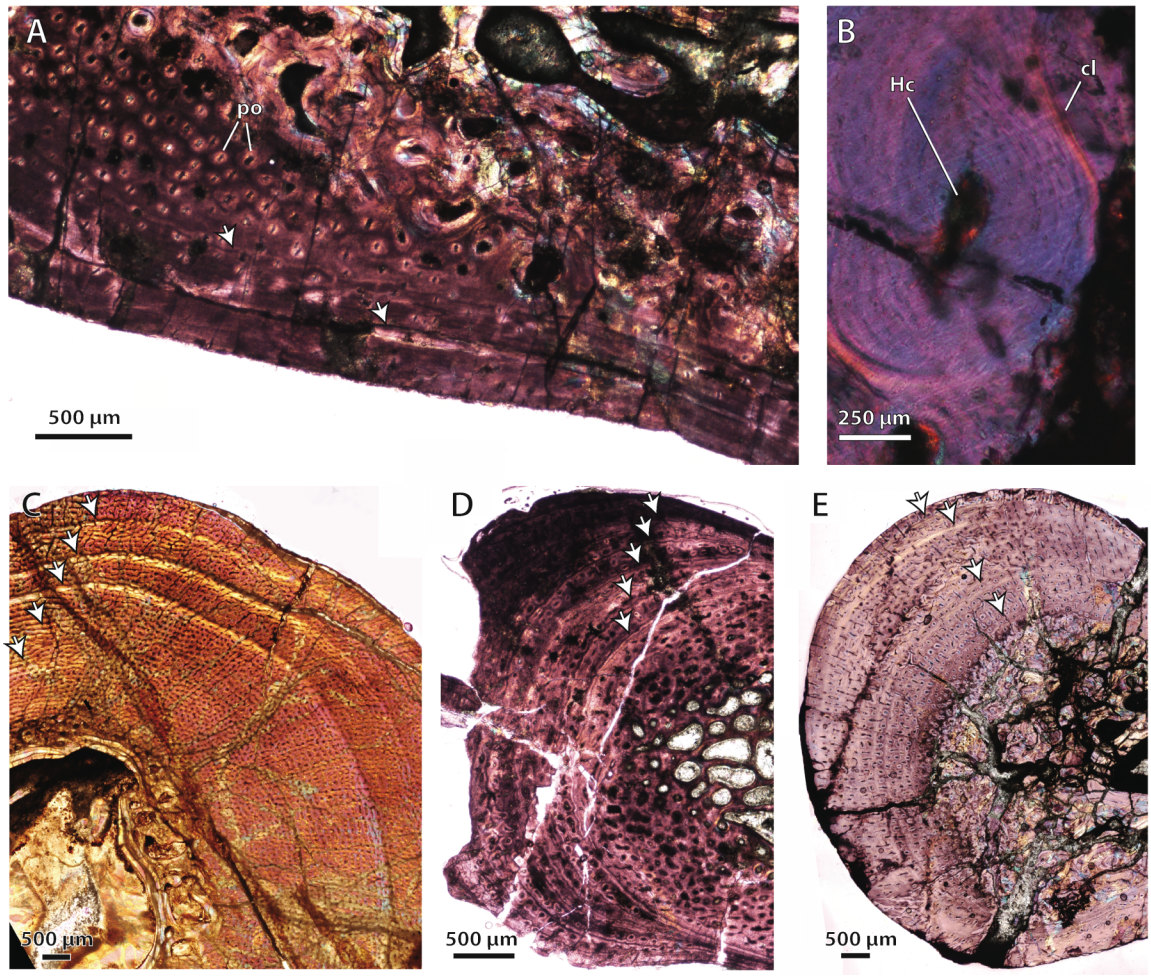
A
po
500 µm
B
Hc
cl
250 µm
C
500 µm
D
500 µm
E
500 µm

General—BP/1/6228 (ulna), from the Grant, Albany (Middle Permian, *Tapinocephalus* AZ).

Ulna—The ulna (BP/1/6228) is a relatively flat element with an ellipsoid to figure-8 cross-section along the midshaft. The bone is relatively dense with a highly cancellous internal structure deep to the cortex with poor development of the marrow cavity. The cortex is moderately thick (*RBT*, 20%; *K*, 0.42) and composed of fibrolamellar and parallel-fibered bone with primary osteons, periodically interrupted by growth marks. Localized areas contain lenticular osteocyte lacunae, particularly in the outer cortex, although the majority of osteocyte lacunae are globular and haphazardly organized. Secondary structure is limited; secondary osteons are apparently absent, but resorption cavities formed in the deep cortex near the compact-cancellous transition. The vascular network is predominantly made up of longitudinal primary osteons, which are distributed most densely in the anterior (preaxial) and posterior (postaxial) sides of the bone where the growth zones are thickest. The longitudinal primary osteons are generally largest deeper in the cortex, and become smaller and more sparsely distributed in the outer cortex, closest to the subperiosteal region. However, in the outer cortex along the anterior and posterior margins, the primary osteons generally maintain their size and form a slightly more reticular motif. The %*CV* is 4.9 and the average primary osteon diameter is 51 μm, therefore having a comparatively lesser degree of vascularization than in *Lycosuchus*. Growth zones delimited by opaque growth marks are easily distinguishable in the specimen. There are at least three annuli traceable around the bone. Their spacing

does not decrease toward the periphery, and the outermost growth zones maintain moderate vascularity with reticular FLB in some areas. Primary osteons were still forming in the subperiosteal region and no EFS was laid down by the time of death.

Scylacosauridae indet.

(Fig. 4.3B-E)

General—BP/1/5576 (radius, ulna), from Combrinckskraal, Prince Albert District (Middle Permian, *Tapinocephalus* AZ); BP/1/5587 (humerus, radius, ulna), from Wolwekuil, Victoria West (Middle Permian, *Tapinocephalus* AZ); CGS R300 (humerus), locality unknown; SAM-PK-5018 (humerus, radius, femur, tibia, fibula), from Abrahamskraal, Prince Albert District (Middle Permian, *Tapinocephalus* AZ); SAM-PK-11557 (fibula), from De Cypher, Beaufort West (Middle Permian, *Tapinocephalus* AZ). Long bone microstructure has been described in scylacosaurids (Ricqlès, 1969; Ray et al., 2004; Chinsamy-Turan, 2012), but previous genus-level identifications of these specimens are dubious due to inadequate diagnostic skull material. As two of the studied specimens have been described elsewhere (SAM-PK-5018, 11557) the present analysis serves to supplement these earlier descriptions with additional material.

Humerus—The humerus is a robust bone with a thick cortex at midshaft (*RBT*, ~30%; *K*, ~0.30) and an open marrow cavity with a few coarse trabeculae and lined by endosteal lamellae. The cortex is composed predominantly of FLB with densely packed

primary osteons having a variety of orientations in localized regions. Ray et al. (2004) reported a laminar to subplexiform arrangement of osteons with occasional subreticular osteons in localized regions, corroborated here by study of additional specimens (BP/1/5587, CGS R300). Independent observations suggest that a subplexiform pattern of vascularization in the humerus midshaft was characteristic of scylacosaurids, but with strongly oblique or reticular patterns localized near sites of muscle insertion that are also associated with Sharpey's fibers (i.e., deltopectoral crest). No secondary osteons are present in the humerus. The %*CV* is ~13-15% and the average primary osteon diameter bears a wide range of ~75-112 μm, which is generally high for therapsids. The interstitial ECM is more parallel-fibered than woven and the primary osteons are lined by thick circumferential lamellae, so that there is strong birefringence under crossed-polarized light. Osteocyte lacunae are well concentrated, globular and disorganized, but are more lenticular where they are associated with streaks of parallel-fibered bone preceding growth marks. Parallel-fibered bone is common in growth increments immediately preceding growth marks (LAGs), indicating decelerating growth before periodic cessation. The number of preserved growth marks varies among individuals, but ranges from three to five LAGs.

Radius—The radius midshaft is subtriangular in cross-section and bears a moderately thick bone wall (*RBT*, ~17-23%; *K*, ~0.46-0.47) with an open marrow cavity lined by sparse trabecular structures, but generally with a sharp delineation of the cortex. Primary osteons are scattered throughout the cortex in a predominantly longitudinal

orientation, though canals are more obliquely radial in localized areas such as the attachment site of the interosseous membrane. The interstitial ECM is more parallel-fibered than woven and punctuated by occasional growth marks. Areas of parallel-fibered bone bear more sparsely distributed and ordered lenticular osteocyte lacunae, especially in the outer cortex and near growth marks. In BP/1/5587, the exact number of growth marks is difficult to discern and the outer layers of bone appear to have been actively deposited during the time of death (with primary osteons forming around the subperiosteal region). By contrast, BP/1/5576 exhibits four or more growth marks that appear in the outer half of the cortex and become progressively closer spaced toward the subperiosteal margin, indicating that growth had slowed prior to death in spite of its smaller size compared to BP/1/5587. However, there was no EFS as in the other studied elements.

Ulna—The histological profile of the ulna is near identical to the radius, although the oblate nature of the bone with wider growth zones allows the number of growth marks to be more reliably estimated. BP/1/5587 exhibits at least three thick growth zones with sparse longitudinal and reticular osteons and weakly radial osteons along the expanded anterior and posterior sides of the bone. These osteons were still being formed at the time of death, corroborating the observations from the radius of the same individual. BP/1/5576 differs in that as few as five (and as many as six) growth marks accompanied by incremental lamellae (annuli) are apparent in the outer cortex, becoming closer spaced toward the subperiosteal margin as in the radius. The primary osteons are

longitudinally oriented with occasional subreticular orientations in some areas. Among-individual histovariation suggests the existence of variation in subadult growth rates within these two scylacosaurids.

Femur—The femur of SAM-PK-5018 was described by Ray et al. (2004). It bears a relatively thin bone wall compared to the forelimbs that is composed of moderately vascularized FLB. The primary osteons are predominantly longitudinal to subreticular in orientation. The perimedullary region bears extensive resorption cavities and a few secondary osteons as reported by Ray et al. (2004). There were apparently no growth marks preserved in the specimen.

Tibia—The tibia (SAM-PK-5018) is a thick bone, though with an open marrow cavity and moderately thick bone wall as in the forelimb epipodial elements (*RBT*, 24%; *K*, 0.60), but thinner than the humerus. The cortex is predominantly composed of FLB with subreticular primary osteons as described by Ray et al. (2004). Additionally, there are at least three growth marks visible (a faint inner annulus and two sharply defined LAGs in the outer cortex) demarcating growth zones of variable thicknesses. Toward the periphery the primary osteons become more obliquely oriented, taking on a strong radial orientation in the outer two growth zones and communicating with the periosteal surface (indicating active bone growth at the time of death). The lacunocanalicular network is too poorly preserved to be described and osteocyte lacunae are not discernible. Secondary osteons are absent.

Fibula—The fibula is extremely poorly preserved in SAM-PK-5018, primarily due to obliteration of the outer cortical surface, thereby making growth interpretations difficult. Deep portions of the cortex in this specimen reveal large erosion cavities and secondary osteons. Discussion of primary growth in the fibula is herein limited to SAM-PK-11557, which preserves a thick cortical wall with coarse trabeculae surrounding a marrow cavity. Resorption cavities are extensive throughout the perimedullary region and are lined endosteally by lamellar bone. The fibrolamellar cortex is densely compacted with large, infilled primary osteons tightly packed and predominantly longitudinal in orientation (though with sparse reticular osteons and anastomoses). The lacunocanalicular network between osteons is formed by haphazardly arranged globular osteocyte lacunae. The exact number of growth marks is difficult to discern, but a relatively thick growth zone with abundant primary osteons gives way to a series of closely spaced annuli near the periphery. The vasculature in this outer region also became sparse, suggesting an overall decrease in growth prior to death. Osteocyte lacunae in this region were more sparse and lenticular in shape. Secondary osteons are occasionally present in the deep cortex, diagnosed clearly by their scalloped cement lines (Fig. 4.3B).

EUTHEROCEPHALIA

Akidnognathidae

Olivierosuchus parringtoni

(Fig. 4.4A-C, E, F)

Figure 4.4. Bone histology in the akidnognathid *Olivierosuchus parringtoni* from the Triassic *Lystrosaurus* Assemblage Zone. **A**, NMQR 3605, cross-sectional profile of humerus midshaft viewed at low magnification (crossed-nicols with wave plate). Note the occluded medullary region and relatively thick cortical bone wall. **B**, NMQR 3605, humerus midshaft, cortical fibrolamellar bone showing large primary osteons preceding a thin zone of parallel-fibered bone near a LAG (crossed-nicols with wave plate). **C**, NMQR 3605, humerus midshaft, cortex showing thick zone of reticular fibrolamellar bone followed by parallel-fibered bone and a LAG (crossed-nicols with wave plate). **D**, Triassic *Moschorhinus* (SAM-PK-K118) humerus midshaft shown at same scale as 'C' for comparison (crossed-nicols with wave plate). Note the densely packed reticular and radial primary osteons and globular osteocyte lacunae. **E**, SAM-PK-K10617, femur midshaft, cortical fibrolamellar bone viewed at low magnification (crossed-nicols with wave plate). **F**, SAM-PK-K10617, femur midshaft, close-up of primary osteons and interstitial bone matrix (normal polarized light at maximum extinction). Arrows denote growth marks. Abbreviations: pfb, parallel-fibered bone; po, primary osteon.

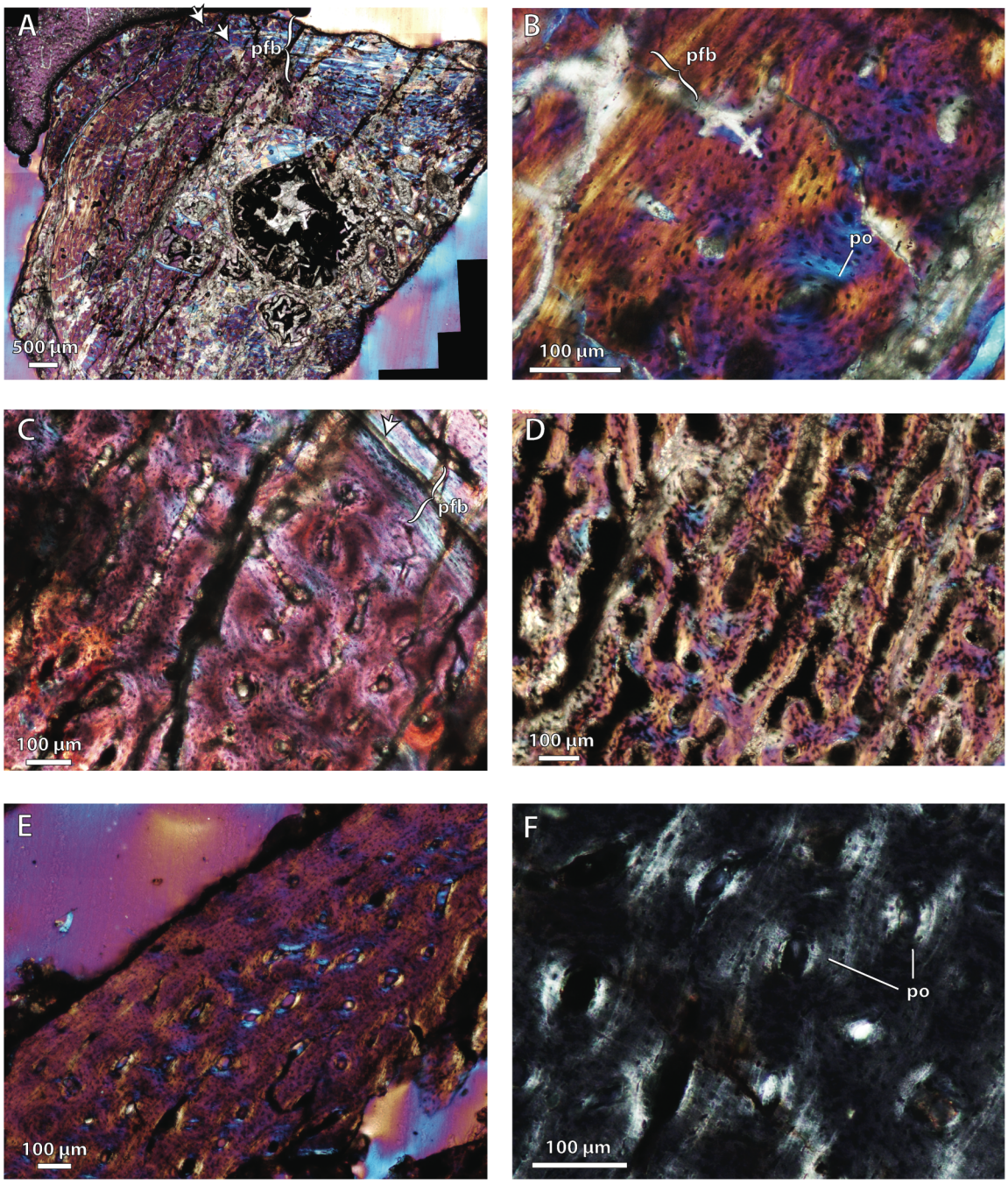
A
pfb
500 µm
B
pfb
po
100 µm
C
pfb
100 µm
D
100 µm
E
100 µm
F
po
100 µm

General—NMQR 3605 (humerus), from Barendskraal, Middleburg (Lower Triassic, *Lystrosaurus* AZ); SAM-PK-K10617 (femur), from Wapadsberg Pass, Zeekoegat, Graaff-Reinet District (Lower Triassic, *Lystrosaurus* AZ). The cross-sectional profiles of limb bone shafts in *Olivierosuchus* reflect general tendencies in other therocephalians, in that the forelimb was robust and thick-walled whereas the hindlimb was relatively gracile and thinner-walled (the humeral cortex being extremely thickened and marrow cavity occluded; the femur having a relatively open marrow cavity with few trabeculae). The cortex predominantly incorporates a nonlamellar interstitial ECM with dense, reticular vascularization as in *Moschorhinus* (see Chapter 2). Growth marks are few and confined to the outer cortex and secondary reconstruction is limited. There are no secondary osteons.

Humerus—The humerus (NMQR 3605) (Fig. 4.4A-C) bears a prominent deltopectoral crest that traverses most of the length of the shaft, producing a subtriangular or tear-shaped cross-section as in *Moschorhinus* and other medium-to-large therocephalians. Notably, the bone is extremely compacted in section and most of the medullary region is occluded by coarse trabeculae such that the marrow cavity is extremely reduced (approximate radius of cavity ~ 2 mm). As a result, the cortex is extremely thick (*RBT*, 36%; *K*, 0.38). The cortical bone consists of both longitudinal and reticular primary osteons in a woven-fibered interstitial ECM, although the matrix becomes more parallel-fibered in the outer half of the cortex. The large, intervening osteocyte lacunae between osteons are numerous between primary osteons, highly

concentrated and almost exclusively globular in shape. The cortical bone is moderately well-vascularized and the primary osteons are large (%*CV*, 9.9; mean *POD*, 99 μm). Several of these features resemble *Moschorhinus*, including the occluded lumen, disorganized woven-fibered matrix, abundant reticular canals, and large primary osteons. Kitching (1977) suggested that *Olivierosuchus* might represent a juvenile of *Moschorhinus*. However, the specimen NMQR 3605 is interpreted here as near somatic maturity as suggested by Botha-Brink and Modesto (2011). It is the largest known specimen of its kind (BSL = 122 mm), exhibits fused neurocentral sutures, and records the transition to outer parallel-fibered bone in the humeral cortex with two distinct LAGs. This contrasts with the condition in a slightly larger *Moschorhinus* specimen from coeval Triassic rocks, which shows heavily vascularized FLB with no growth marks (Fig. 4.4 C, D).

Femur—The femur (SAM-PK-K10617) (Fig. 4.E, F) is more elliptical in cross-section, although some dorsoventral compression has distorted the shaft slightly, flattening and cracking it. The cortical bone is relatively well preserved, revealing a somewhat thinner diaphyseal bone wall than in the humerus. Some coarse cancellous bone is present around the perimedullary region. The cortex is composed of FLB with longitudinal primary osteons. Osteocyte lacunae are large, highly concentrated and haphazardly distributed. There is a moderate to weak degree of vascularization, although the osteons are relatively large (%*CV*, 3.4; mean *POD*, 75 μm). The interstitial ECM is

predominantly woven-fibered but with some patches of parallel-fibered bone in the outer cortex. There are no growth marks visible in the specimen and no secondary osteons.

Hofmeyriidae

Hofmeyria atavus

(Fig. 4.5)

General—BP/1/4404 (humerus, radius, ulna), from Matjiesfontein (Highlands), Victoria West (Upper Permian, *Cistecephalus* AZ). The bones are remarkably robust and thick-walled relative to the size of the individual (BSL = 67 mm). The cross-sectional profile of the mid-diaphysis in all bones includes a distinct central cavity with a smooth, circular rim of endosteal lamellar bone (rather than irregularly organized cancellous bone tissue). The tissue composition of the cortex is generally more parallel-fibered than woven and the outer cortex of the epipodials preserves numerous annular growth marks. Primary osteons are primarily longitudinally oriented (though with many reticular connections in the humerus) and mostly reside in the inner half to two-thirds of the cortex. There are no secondary osteons in any of the studied elements.

Humerus—The humeral diaphysis (Fig. 4.5A) bears a relatively compact cross-sectional profile as in most of the other elements, given its thick cortex (*RBT*, 31%; *K*, 0.32) and sharp boundary between the cortical bone wall and the diminutive central cavity. There are a few coarse trabeculae around the marrow cavity, rather than the

extensive cancellous tissue observed in earlier therocephalians. The interstitial ECM of the cortical bone appears to incorporate some woven-fibered structure, but is primarily parallel-fibered, especially nearing the subperiosteal margin. Osteocyte lacunae are primarily large, globular, and well-concentrated. The primary osteons are fairly densely-packed throughout much of the cortex and form a reticular network with occasional longitudinal canals. The cortex is moderately vascularized, although the primary osteons are relatively small (%*CV*, 7.5; mean *POD*, 72 μm). Growth marks are not easily distinguishable in the humerus. However, when viewed under polarized light, three bundles or 'waves' of highly birefringent parallel-fibered bone are visible in the outer half of the cortex, possibly indicating cyclic alternations in rate of bone accretion. Parallel-fibered bone predominates in the outer cortex, but still incorporates abundant primary osteons.

Radius—The radius (Fig. 4.5B-D) generally resembles the humerus in its overall cross-sectional profile, but with a thicker bone wall and more diminutive marrow cavity (*RBT*, 35-40%; *K*, 0.15-0.26) as is typical of the epipodial elements. The small central cavity is lined by a thick, multi-lamellar layer of endosteal bone. The total diameter of the cavity varies between 0.25-0.50 mm. The cortical bone is composed of a predominantly parallel-fibered bone matrix with sparse primary osteons. The lacunocanalicular network was also somewhat sparse and osteocytes became increasingly lenticular in shape toward the outer margin of the bone. The primary osteons are mainly oriented longitudinally, but with a few reticular connections. They are concentrated in the inner half to two-thirds of

Figure 4.5. Bone histology in the hofmeyriid *Hofmeyria atavus*. **A**, BP/1/4404, cortex of humerus midshaft viewed at low magnification (crossed-nicols with wave plate). **B**, BP/1/4404, cross-sectional profile of radius midshaft viewed at low magnification (crossed-nicols with wave plate). **C**, Same as 'B,' close-up of cortex showing growth marks and lamellar bone in outer cortex (crossed-nicols with wave plate). **D**, Same as 'B,' close-up of cortex showing longitudinal primary osteons and outer lamellar bone (crossed-nicols with wave plate). **E**, BP/1/4404, ulna midshaft cross-section viewed at low magnification (crossed-nicols with wave plate). **F**, BP/1/4404, ulna midshaft cortex viewed at high magnification, showing sharp transition to lamellar bone in outer cortex (crossed-nicols with wave plate). Brackets denote outer zone of lamellar bone with simple canals, indicating marked decrease in bone apposition. Abbreviations: pfb, parallel-fibered bone; po, primary osteon.

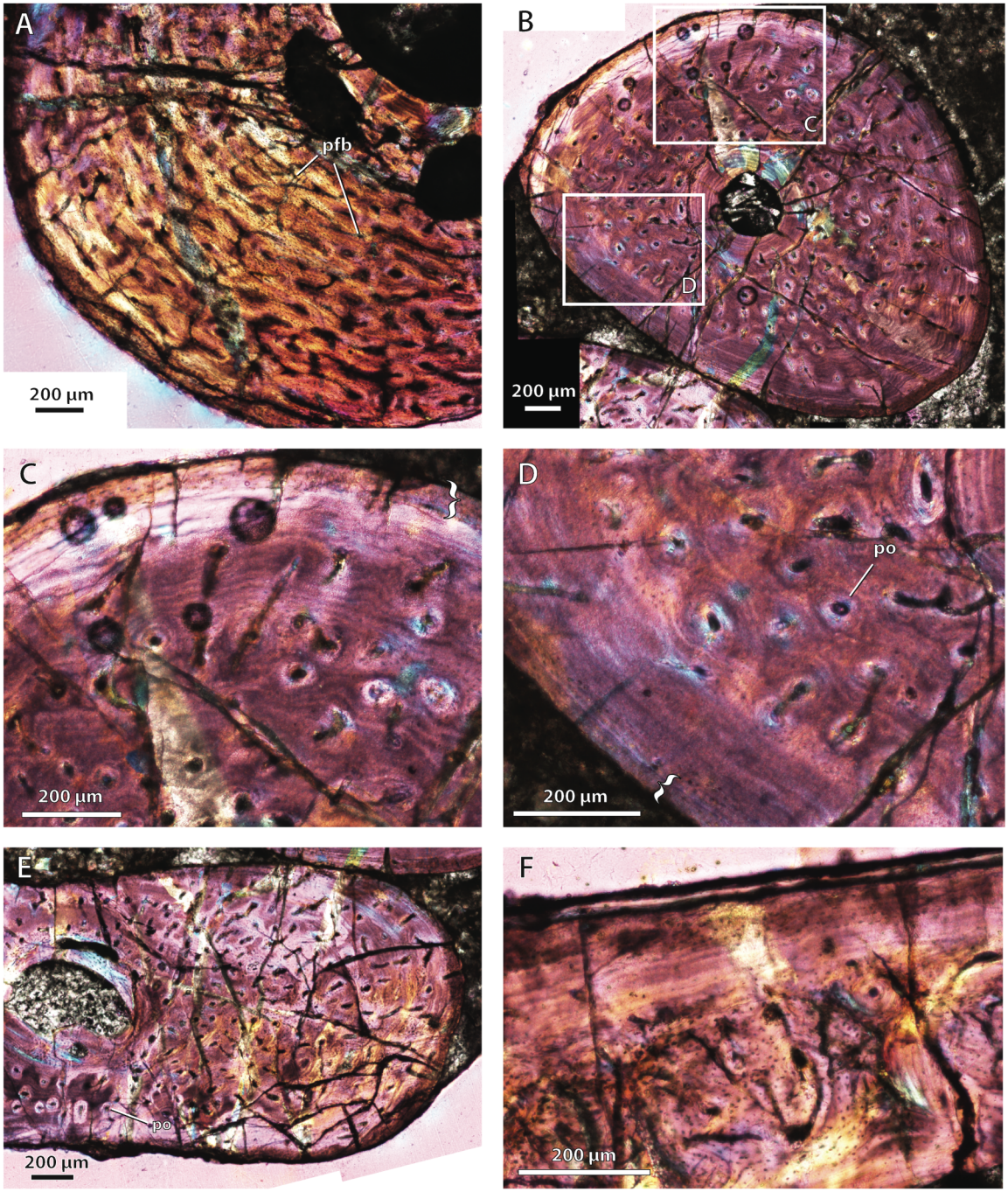
A
pfb
200 µm
B
C
D
200 µm
C
200 µm
D
po
200 µm
E
po
200 µm
F
200 µm

the cortex and become very sparse in the outer cortex, where the vasculature mainly consists of a few simple canals. The overall degree of vascularization is quite low (%*CV*, 3.4-4.8; mean *POD*, 46-47 μm). Growth marks are better recorded in the epipodials than in the humerus of BP/1/4404. At least three (and possibly four) growth marks are preserved throughout the cortex, although their precise number is difficult to count due to their association with fine incremental lines. Association of incremental lamellar bone and a lack of sharply defined cement lines indicate that these waves of growth marks represent annuli (as opposed to LAGs) marking periodic decelerations in growth rather than cessations. The growth marks become more closely spaced in the subperiosteal region, but do not form an avascular EFS (as suggested by the presence of simple canals).

Ulna—Apart from its more flattened cross-sectional shape, the ulna (Fig. 4.5E, F) is near identical to the radius in its histological profile and tissue structures. The cortical bone wall is similarly thick (*RBT*, 39%; *K*, 0.20-0.22) and dominated by parallel-fibered bone with longitudinal primary osteons and cyclic growth marks (annuli). Osteocyte lacunae are sparse and strongly lenticular in shape in the outer cortex as in the radius. The cortex is also only modestly vascularized (%*CV*, 3.0-4.7; mean *POD*, 39-43 μm). Some osteons in regions where the bone wall is relatively thinner have the gross appearance of secondary osteons (Fig. 4.5E). However, this is mainly due to their large size and multi-lamellar infilling. Close inspection reveals that there is no cement line surrounding these osteons, and that the surrounding fabric of the interstitial ECM also conforms to their shape. Secondary osteons are therefore absent.

Mirotenthes digitipes

(Fig. 4.6)

General—SAM-PK-K6511 (humerus, radius, ulna, femur, tibia, fibula) from Steenkampshoek (Upper Permian, *Cistecephalus* AZ). As in *Hofmeyria* (BP/1/4404), limb bone shafts are thick-walled for their small size, and the cortex is composed of moderately vascularized FLB with primary osteons (and simple canals) and a predominantly parallel-fibered interstitial ECM. Cyclic growth marks are present throughout the cortex, especially toward the outer periphery. The subperiosteal region of some elements preserves more parallel-fibered or lamaller bone with sparse vascular canals. Secondary osteons are absent in all elements.

Humerus—The humerus shaft (Fig. 4.6A) exhibits a compact cross-sectional profile with a thick bone wall (*RBT*, 32; *K*, 0.31) and a small central cavity with a slightly irregular endosteal margin and some trabecular structures occupying the cavity. The cortex incorporates numerous primary osteons within a predominantly parallel-fibered interstitial ECM. Osteocyte lacunae were well-concentrated and became increasingly lenticular toward the periphery of the bone. The vasculature is very simple in its organization, mainly consisting of many sparsely distributed longitudinal primary osteons and occasional simple canals (%*CV*, 5.4; mean *POD*, 54 μm). The primary osteons occasionally (though infrequently) bear radial and circular anastomoses, especially deeper in the cortex. Closer to the periphery, primary osteons become fewer and give way

Figure 4.6. Bone histology in the hofmeyriid *Mirotenthes digitipes*. **A**, SAM-PK-K6511, humerus midshaft cross-section viewed at low magnification (crossed-nicols with wave plate). **B**, SAM-PK-K6511, radius midshaft cortex (crossed-nicols with wave plate). **C**, SAM-PK-K6511, ulna midshaft cortex (crossed-nicols with wave plate). **D**, SAM-PK-K6511, femur midshaft cortex showing extensive parallel-fibered and lamellar bone (normal polarized light at maximum extinction). **E**, SAM-PK-K6511, tibia midshaft cross-section viewed at low magnification (non-polarized light). **F**, SAM-PK-K6511, fibula midshaft cross-section viewed at low magnification (non-polarized light). Bracket indicates avascular outer zone. Abbreviations: pfb, parallel-fibered bone; po, primary osteon.

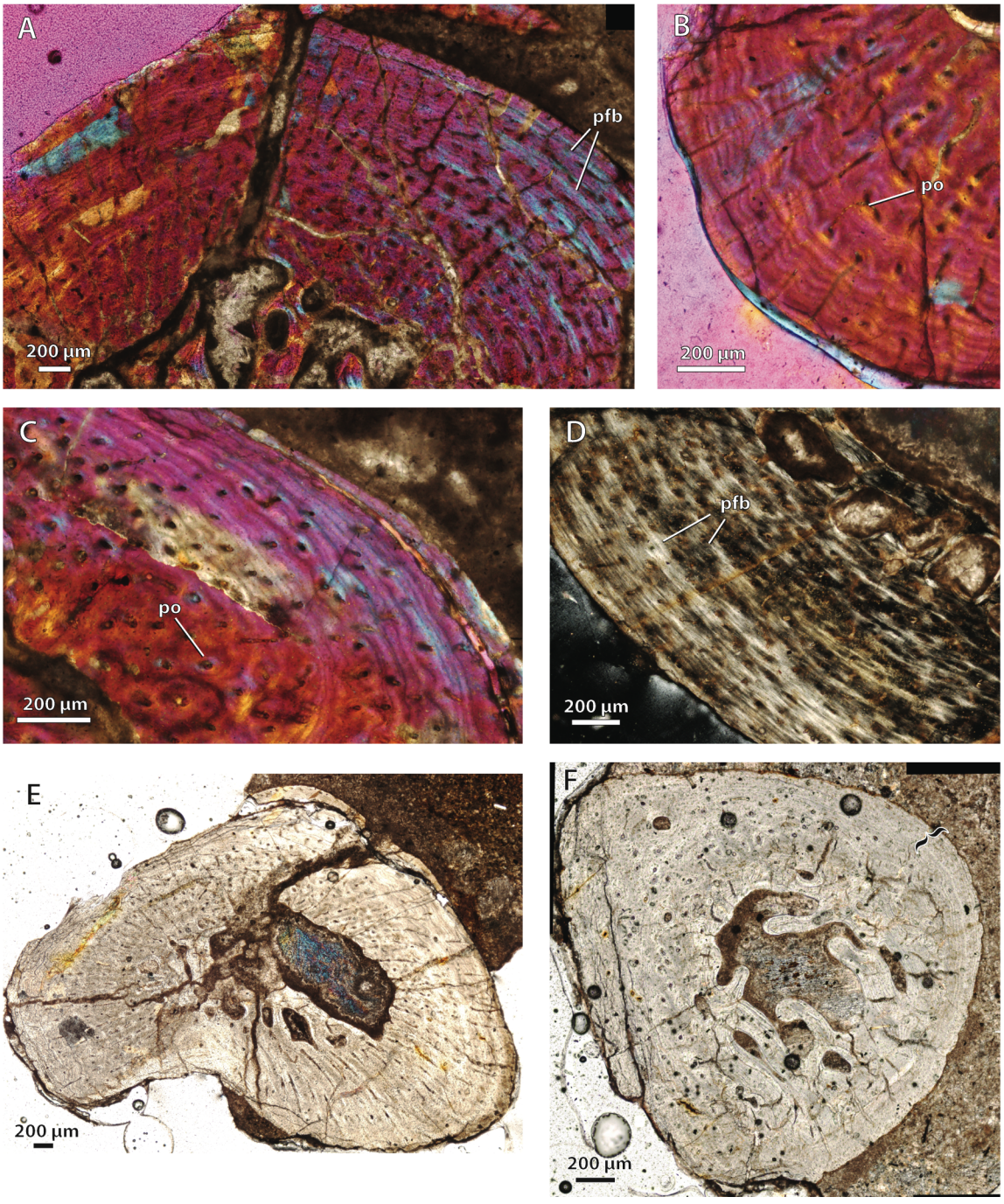
A
pfb
200 µm
B
po
200 µm
C
po
200 µm
D
pfb
200 µm
E
200 µm
F
200 µm

to simple canals of varying orientations. Growth marks are more clearly delineated in this humerus than in that of BP/1/4404, and are best visualized in normal (non-polarized) light. Three evenly spaced growth marks are present in the mid-cortex, and a fourth in the subperiosteal region. As in BP/1/4404, growth marks are preserved in the form of annuli, and are associated with faint incremental lines and waves of birefringent parallel-fibered bone when viewed under polarized light. There is no EFS.

Radius—The radius (Fig. 4.6B) has a similarly thickened bone wall at midshaft (*RBT*, 34; *K*, 0.33) with a small but relatively open central cavity. The cavity is unobstructed by trabecular or cancellous structures, instead lined by a smooth layer of endosteal lamellar bone, and is approximately 0.80 mm in diameter. The cortex is formed primarily by parallel-fibered bone that is modestly vascularized by sparse primary osteons and simple canals (%*CV*, 3.5; mean *POD*, 38 μm). The lacunocanalicular network is poorly preserved in this element, but osteocyte lacunae apparently became more sparse in the outer cortex. Most of the vascular network is localized within the inner half of the cortex (but with a few simple canals present in the outer half). At least five annuli are present, more distinct than in the humerus, and are very closely spaced in the outer cortex forming an EFS-like structure that is nearly avascular, but not acellular.

Ulna—The histological profile of the ulna (Fig. 4.6C) is near identical to that of the radius, except for its more flattened, ellipsoidal shape in section. The bone wall is thick (*RBT*, 32; *K*, 0.42), the cortex is composed of parallel-fibered bone with many small primary osteons (%*CV*, 2.0; mean *POD*, 41 μm), and at least four or five growth marks

(annuli) are present throughout the cortex. Osteocyte lacunae became increasingly sparsely distributed in the outer cortex.

Femur—The femur midshaft (Fig. 4.6D) resembles the humerus in its overall cross-sectional profile and distribution of histological features, although it is slightly thinner-walled than any of the forelimb elements (*RBT*, 25; *K*, 0.42). There is a wide, open marrow cavity with some trabeculae and erosion cavities forming within the surrounding deep cortex. A thin layer of lamellar bone lines the endosteal margin of the cortex. The deep cortex is formed by moderately vascularized FLB, consisting of a parallel- and woven-fibered matrix with longitudinally oriented primary osteons. The lacunocanalicular network is sparse and osteocytes became more lenticular in shape in the outmost cortex. The primary osteons are more consistently longitudinal than in the humerus, with fewer anastomoses, but the overall degree of vascularization is comparable (%*CV*, 3.6; mean *POD*, 58 μm). Primary osteons become fewer in the outer cortex, but are still present with few simple canals. Growth marks are present throughout the cortex, but are best seen in the outer regions where primary osteons are less densely concentrated and parallel-fibered bone dominates. There are at least four growth marks, which become progressively closer spaced toward the periphery as in the humerus. There is no EFS in this element.

Tibia—The tibia (Fig. 4.6E) exhibits an irregular, slightly figure-8 cross-sectional shape and a relatively thick bone wall (*RBT*, 31; *K*, 0.31) as in the other epipodial elements. The marrow cavity, however, is also irregular in shape with coarse trabeculae

and occasional small resorption cavities forming along the endosteal margins. The cortex is formed by parallel-fibered bone with small, longitudinally and radially oriented primary osteons that are most concentrated in the deep cortex. The lacunocanalicular network is too poorly preserved for adequate description. The overall degree of vascularization is fairly modest (%*CV*, 3.1; mean *POD*, 38 μm). Numerous growth marks are preserved in the outer cortex, especially near the subperiosteal region where they form a nearly avascular EFS-like structure as in the radius.

Fibula—The fibula (Fig. 4.6F), apart from being more triangular in cross-section, resembles the tibia in its overall histological profile. It has a thick bone wall at midshaft (*RBT*, 32; *K*, 0.39) with some trabecular architecture in the marrow cavity. The cortex is formed by parallel-fibered bone with few longitudinally oriented primary osteons, and is poorly vascularized (%*CV*, 3.9; mean *POD*, 32 μm). Osteocyte lacunae are poorly preserved as in the tibia. Growth marks are faint, but an avascular EFS-like structure forms a distinctive collar around the bone.

Whaitsiidae

Theriognathus microps

(Fig. 4.7)

General—BP/1/719 (femur) from Swaelkrans, Murraysburg District (Upper Permian, *Dicynodon* AZ); NMQR 3375 (femur) from Tafelkop 712, Bloemfontein

District (Upper Permian, *Dicynodon* AZ). The histological structure of the radius in *Theriognathus* has previously been described by Ricqlès (1969) (as '*Notosollasia'*). The specimen was recovered from the Doornplaats locality (*Dicynodon* AZ) where this taxon occurs abundantly. Based on the author's detailed descriptions and photographic plates, the structure of the radius midshaft resembles that of the hofmeyriids described above in having an extremely thick bone wall and reduced central cavity without cancellous structure (Ricqlès, 1969). The vascular motif was primarily longitudinal and radial. Secondary osteons are absent in all studied specimens.

Femur—Two femora are described here to supplement the description by Ricqlès (1969). It is worth noting that the femur of *Theriognathus* is unique in its strongly golf club-shaped head that fits into a deep acetabulum, and a bowed shaft that orients the distal condyles directly ventrally, placing the lower leg under the hip in a semi-erect stance. The midshaft is rounded in cross-section and bears a relatively thick wall (*RBT*, ~20-24%; *K*, ~0.51-0.59) compared to the hind limbs of other therocephalians, possibly related to impact loading imposed by this orientation. The thick cortical bone wall is composed of cyclically deposited FLB with numerous primary osteons in a parallel- and woven-fibered matrix. Osteocyte lacunae are generally numerous, haphazardly distributed, and globular in shape within growth zones, but more lenticular and ordered near growth marks. In the small subadult specimen sampled here (NMQR 3375), primary osteons are abundant and take on a predominantly radial orientation, but with a few longitudinal osteons arranged in radial rows or bearing radial and reticular

Figure 4.7. Bone histology in the whaitsiid *Theriognathus microps*. **A**, NMQR 3375, femur midshaft cross-section viewed at low magnification (non-polarized light). **B**, NMQR 3375, femur midshaft cortical bone viewed at medium magnification showing growth marks (arrows) (non-polarized light). **C**, same as 'B,' viewed at high magnification with wave plate, showing close-up of outer zone of well-vascularized fibrolamellar bone (bracket). **D**, BP/1/719, femur midshaft cortex (crossed-nicols with wave plate). Arrows denote growth marks. Abbreviations: flb, fibrolamellar bone; rc, radial canals.

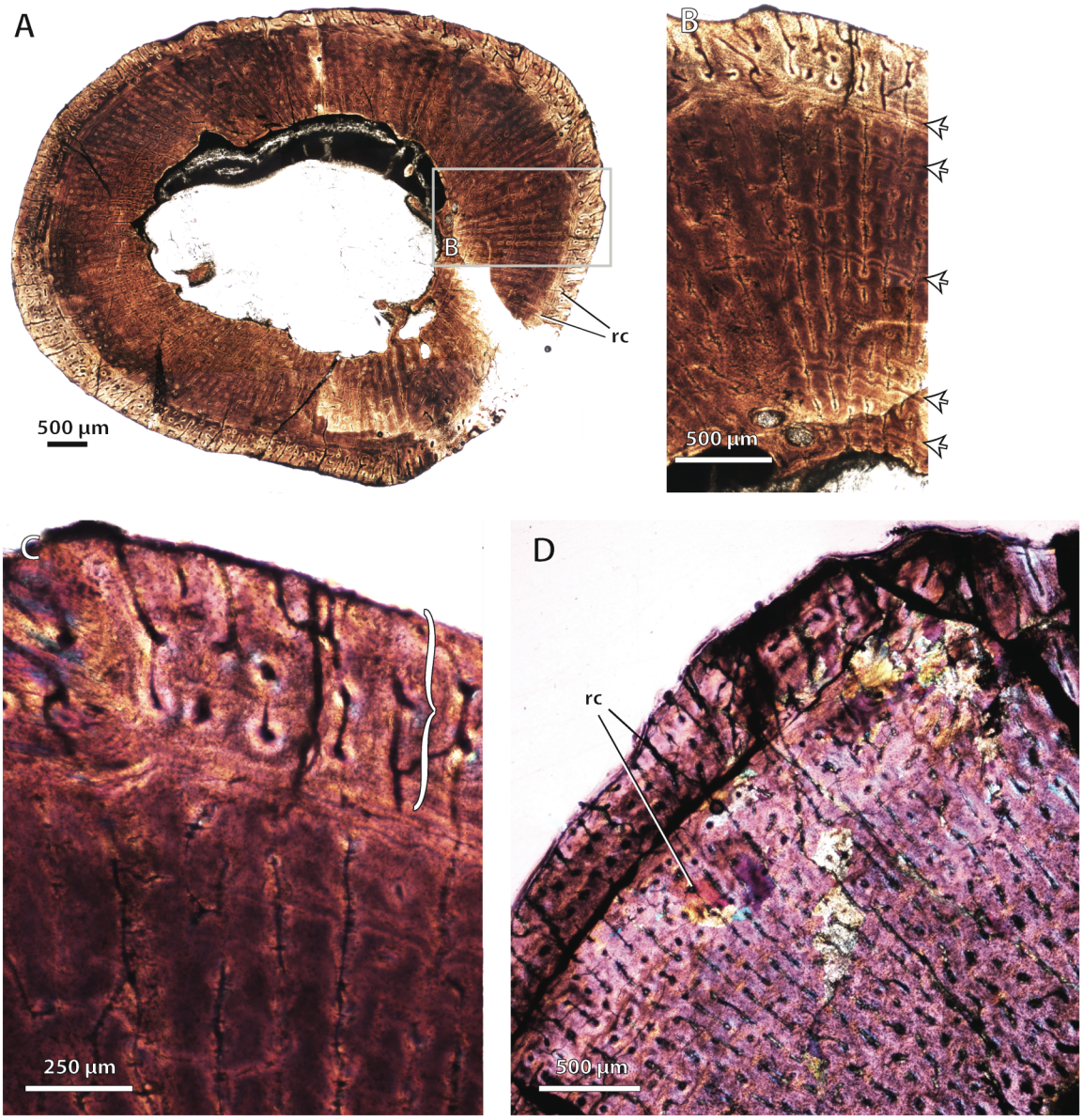
A
B
rc
500 µm
B
500 µm
C
250 µm
D
rc
500 µm

ramifications. Numerous growth marks (LAGs) record a cyclic growth pattern, with five irregularly spaced growth marks punctuating the cortex in NMQR 3375, followed by a thick, well vascularized growth zone in the outermost cortex indicating a brief 'spurt' prior to death. In the larger femur (BP/1/719) there is a lesser degree of radial vasculature, the primary osteons being almost exclusively longitudinal (although with some reticular anastomoses in the outer cortex). In general, the cortex bears a moderate degree of vascularization (%*CV*, 6.2-6.8; mean *POD*, 65-87 μm). BP/1/719 preserves at least four growth marks, although its early growth record has been lost by formation of resorption cavities in the perimedullary region. The number and spacing of growth marks suggests some degree of plasticity in the growth style of *Theriognathus*.

BAURIOIDEA

Ictidosuchidae

Ictidosuchoides longiceps

(Fig. 4.8)

General—BP/1/75 (humerus), from Sondasgriviershoek, Cambedoo, Graaff-Reinet District (Upper Permian, *Cistecephalus* AZ); BP/1/4092 (humerus, radius, ulna) from Matjiesfontein, Victoria West (Upper Permian, *Cistecephalus* AZ); SAM-PK-K8659 (humerus, radius, femur, tibia, fibula) from Wilgerboskloof, Prince Albert District (Upper Permian, *Tropidostoma* AZ); SAM-PK-K10423 (femur, tibia, fibula) from

Doornplaats, Graaff-Reinet District (Upper Permian, *Dicynodon* AZ). The specimens present a variety of sizes and ages, ranging from the small skeleton SAM-PK-K8659 (BSL = 101 mm), which bears neurocentral sutures, to the largest known specimen BP/1/4092 (BSL = 200 mm). Mid-diaphyseal sections reveal somewhat thinner bone walls in *Ictidosuchoides* (and perhaps baurioids in general) than in other therocephalians with *RBT*s generally ranging from 14-26% (rather than 25-40% in akidnognathids and hofmeyriids). The cortices are formed by moderately vascularized parallel-fibered bone with reticular and longitudinal primary osteons, and punctuated by cyclic growth marks. There are no secondary osteons.

Humerus—The humerus (Fig. 4.8A, G, H) is a slender bone with a well-defined shaft having a subcircular cross-sectional profile. The overall compactness of the bone is low with a fairly thin bone wall (*RBT*, ~19-22%; *K*, ~0.56-0.64). The marrow cavity is large and relatively hollow with little cancellous structure (a few trabeculae are present in proximal shaft of BP/1/75). The endosteal perimedullary margin is smooth at the midshaft. Resorption cavities are near absent in the perimedullary region. The remaining cortex generally consists of reticular FLB in a parallel- and woven-fibered matrix. Osteocyte lacunae are generally numerous and disorganized with a globular shape in growth zones, but more lenticular and ordered near growth marks as in the femur of *Theriognathus*. The reticular primary osteons occasionally bear circular anastomoses that give a subplexiform appearance in localized regions of the cortex. The osteons are quite small, but the bone is moderately well vascularized overall (%*CV*, ~7.3-11.1; mean *POD*,

Figure 4.8. Bone histology in the baurioid *Ictidosuchoides longiceps*. **A**, SAM-PK-K8659, humerus midshaft cross-section viewed at low magnification (normal polarized light). **B**, SAM-PK-K8659, radius midshaft cortex and inner cancellous bony scaffold (crossed-nicols with wave plate). **C**, SAM-PK-K8659, tibia midshaft cortex and inner cancellous bony scaffold (crossed-nicols with wave plate). **D**, SAM-PK-K8659, femur midshaft showing inner cancellous bone and outer bone compacta with a woven-fibered matrix (crossed-nicols with wave plate). **E**, SAM-PK-K10423, femur distal shaft cortex (crossed-nicols with wave plate). **F**, SAM-PK-K10423, fibula proximal shaft cortex (crossed-nicols with wave plate). **G**, BP/1/75, humerus midshaft cortex (crossed-nicols with wave plate). **H**, BP/1/4092, midshaft cross-section of large humerus viewed at low magnification (crossed-nicols with wave plate). **I**, BP/1/4092, radius close-up showing growth mark (annulus) in outer cortex (non-polarized light). Arrows denote growth marks. Abbreviations: nc, nutrient canal; pfb, parallel-fibered bone; spc, subplexiform canals; wb, woven-fibered bone.

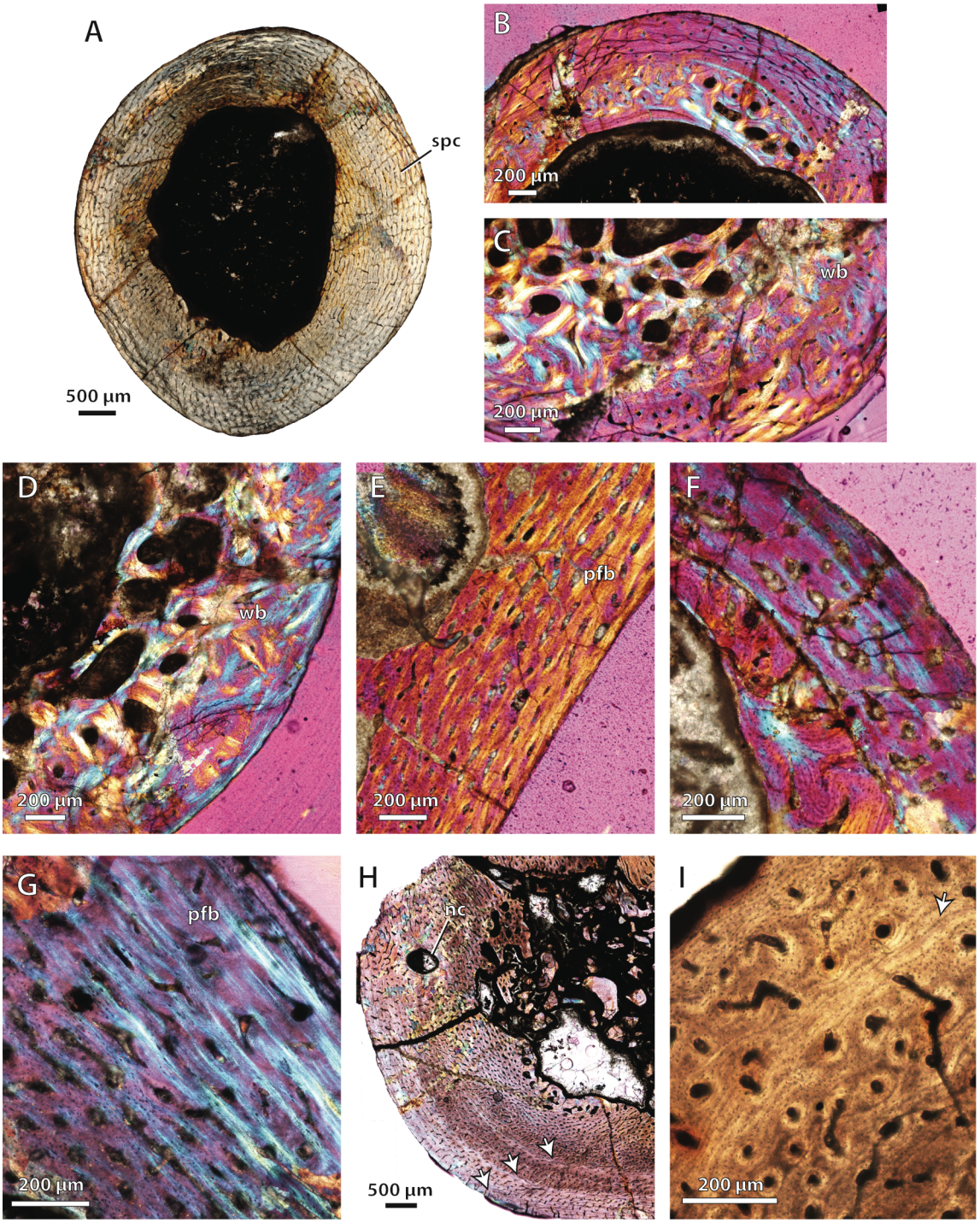
A
spc
500 µm
B
200 µm
C
wb
200 µm
D
wb
200 µm
E
pfb
200 µm
F
200 µm
G
pfb
200 µm
H
nc
500 µm
I
200 µm

~45-60 μm) with most of the osteons being concentrated within the deep cortex. Cyclic growth marks are faint but present, usually in the form of annuli with associated waves of 'streaky' parallel-fibered bone as in the hofmeyriids. The number of growth marks varies, with a single subperiosteal annulus in the small SAM-PK-K8659, two faint annuli preserved in the medium BP/1/75, and three annuli in the largest BP/1/4092. Growth apparently did not fully cease in the largest individual, but more parallel-fibered and lamellar bone formation occurred in the outer half of the cortex, with more lamellar fibers and flattened osteocyte lacunae appearing after the third (outermost) annulus.

Radius—The radius (Fig. 4.8B, I), like the humerus, bears a slender shaft having a bone wall of moderate thickness (*RBT*, ~21-24%; *K*, ~0.52-0.58), contrasting with the forelimb epipodials of other non-baurioid therocephalians. The endosteal perimedullary margin is relatively smooth at the midshaft and there are few trabeculae within the marrow cavity. The cortical bone wall is composed of FLB with small, longitudinal primary osteons and the interstitial ECM apparently became increasingly parallel-fibered toward the outer periphery. Osteocyte lacunae are generally numerous and disorganized, and globular in shape, but became sparser and more lenticular near growth marks and in the outer cortex of large individuals. Osteons are very small and mostly longitudinal, but exhibit occasional reticular motifs. The transition to parallel-fibered bone occurred early during the bone's growth, as it is evident in the smallest specimen (SAM-PK-K8659) where bundles of parallel-fibered bone were deposited just prior to formation of a subperiosteal annulus (as in the humerus). The larger BP/1/4092, retains a similar pattern,

with alternating waves of deposition of parallel-fibered bone concentrated near three faint annuli moving toward the outer periphery. The size and concentration of primary osteons also decreases toward the periphery and overall vascularity is moderate to low (%*CV*, ~4.2-11.1; mean *POD*, ~38-62 μm). No more than three growth marks are observed throughout the cortex in the largest specimens and there is no EFS.

Ulna—The ulna (BP/1/4092) forms a flattened diaphysis with an oval cross-section and a bone wall that is of moderate thickness (*RBT*, 26%; *K*, 0.54). The marrow cavity is large with an irregular endosteal margin and several trabeculae present within the cavity. The structure of the cortex closely resembles the radius, being composed of FLB with small, longitudinal and reticular primary osteons and occasional streaks of parallel-fibered bone when viewed under polarized light. As in the radius, osteocyte lacunae are disorganized and globular, but became sparser and more lenticular near growth marks and in the outer cortex. Frequent reticular canals are present throughout the preaxial region of the cortex, forming primary osteons of moderate size in a woven- and parallel-fibered matrix incorporating dense clusters of globular osteocyte lacunae. The overall %*CV* is 8.3 and the mean *POD* is 52 μm. Growth marks, though present, are difficult to distinguish due to poor preservation, and a complete count cannot be performed. At least one distinct annulus can be observed in the outer two-thirds of the cortex, but there were likely more given those recorded in the radius and humerus of the same individual.

Femur—The femur (Fig. 4.8D, E) bears a long, straight shaft that is thinner walled than in any of the forelimb elements (*RBT*, 14%; *K*, 0.71). The marrow cavity is very large with an irregular boundary of coarse, trabecular bone between it and the more compact cortex. In the small SAM-PK-K8659, prominent trabecular structures are present along the perimedullary margins and large cavities (~60-100 μm in diameter) not interpreted as erosion cavities are surrounded by highly woven bone before giving way to a very thin layer of woven- and parallel-fibered bone with primary osteons in the outmost region of the mid- and distal shaft. The highly woven texture preserved in the perimedullary region resembles the endochondral scaffold of perinatal bone in mammals and some archosaurs (Horner et al., 2001). In general, the primary osteons are fairly small and have both longitudinal and radial orientations (%*CV*, 4.7; mean *POD*, ~38-65 μm). Parallel-fibered bone became more prominent in the outermost regions of the midshaft in SAM-PK-K10423. The lacunocanalicular network is poorly preserved in both femur specimens. A possible subperiosteal annulus was formed in SAM-PK-K10423, but no growth marks were otherwise detected in either specimen. Some obliquely oriented Sharpey's fibers are preserved on the ventral surface of the distal shaft. No EFS was observed in the femur.

Tibia—The tibia (Fig. 4.8C) exhibits a structure similar to the radius and ulna. It bears a flattened cross-section with a modest bone wall (*RBT*, ~16-23%; *K*, ~0.49-0.63). The small SAM-PK-K8659 records the same transition between the porous, woven perimedullary bone and parallel-fibered cortical bone as in the radius and femur. The

cortex is composed of parallel-fibered bone with small longitudinal and reticular primary osteons and some intervening Sharpey's fibers preserved in the anterior region in SAM-PK-K8659. The cortex is poorly vascularized (%*CV*, 2.8-4.3; mean *POD*, 39-43 μm). Two annuli are preserved in the cortex of SAM-PK-K10423. There is no EFS.

Fibula—The fibula (Fig. 4.F) exhibits a subcircular cross-section, and resembles the tibia in its histological profile. The bone wall is moderately thin at the midshaft (*RBT*, ~19-22%; *K*, ~0.47-0.59) and retains some of the porous, woven architecture in the perimedullary region as observed in the radius, femur, and tibia of SAM-PK-K8659. The transition to the compact cortex is marked by a sharp cement line, followed by deposition of sparsely vascularized parallel-fibered bone as in the tibia. The overall vascularization is fairly modest (%*CV*, ~3.8-4.7; mean *POD*, 40 μm). The primary osteons are longitudinally oriented and there are a few simple canals. Growth marks are not distinguishable in the fibula and there is no EFS.

Lycideopidae

Tetracynodon darti

(Fig. 4.9)

General—NMQR 3745 (humerus), from Bethal, Bethulie District (Lower Triassic, *Lystrosaurus* AZ); UCMP 78395 (humerus, radius, ulna, femur), from Wonderkrantz, Harrismith District (Lower Triassic, *Lystrosaurus* AZ); UCMP 78396

(humerus, femur, fibula), from Wonderkrantz, Harrismith District (Lower Triassic, *Lystrosaurus* AZ). Sigurdsen et al. (2012) briefly described bone histology in the humerus and femur of *Tetracynodon* with the purpose of determining age. The bone walls are generally thin (as in other baurioids), especially in the femur. In all elements, the mid-diaphyseal cortex consists of moderately vascularized woven- and parallel-fibered bone, usually with longitudinal primary osteons. The cortices are, in general, less vascularized than in its Permian counterpart *Ictidosuchoides*. Growth marks are often absent indicating a relatively short growth period in sampled specimens, although there may be one or two preserved in the mid- to outer cortex in some specimens. Secondary reconstruction was limited and there are no secondary osteons.

Humerus—The humerus (Fig. 4.9A-C) exhibits an intermediate bone wall thickness (*RBT*, ~21-24%; *K*, ~0.49-0.56) and preserves well the general pattern of growth. The large, open marrow cavity is bordered by smooth endosteal lamellar bone, demarcating the transition to the cortex. There are occasional trabecular structures localized in the proximal shaft near the deltopectoral crest. The crest is more restricted along the shaft than in earlier (non-baurioid) therocephalians, such that the cross-section is more subcircular than tear-shaped. The cortex consists of moderately vascularized woven- and parallel-fibered bone incorporating longitudinal primary osteons with occasional reticular anastomoses (%*CV*, ~4.7-8.1; mean *POD*, ~36-42 μm). The deep cortex maintains a clear fibrolamellar structure with densely-packed primary osteons within a woven-fibered interstitial ECM. The lacunocanalicular network of the deep

cortex is generally disorganized with large, globular osteocyte lacunae, but quickly transitioned to more ordered, lenticular osteocytes in the outer half of the cortex. The cortical bone of *Tetracynodon* bears the highest proportion of ordered, lenticular osteocytes than any studied therocephalian. In NMQR 3745, this pattern gave way to more parallel-fibered bone with lenticular osteocytes in the outer half of the cortex. This transition is demarcated by a single LAG, although a second faint annulus associated with bundles of parallel-fibered bone is present in the outer cortex. Other specimens (e.g., UCMP 78395, 78396) show more consistent parallel-fibered bone deposition. The outer cortex incorporates lamellar tissue with fewer vascular canals and is punctuated by a single LAG near the subperiosteal region. The LAG is succeeded by a thin band of parallel-fibered and lamellar bone (varying from ~50 to 100 μm) with few simple canals located near the periosteal margin, indicating that although growth had attenuated it had not fully ceased. No EFS is present in any of the specimens.

Radius—The radius (UCMP 78395) (Fig. 4.9D) has a subcircular cross-section at midshaft and bears a slightly thicker bone wall than in the humerus (*RBT*, 27%; *K*, 0.43). The perimedullary region bears a relatively smooth ring of endosteal lamellar bone marking the border with the marrow cavity. A few resorption cavities are present in the perimedullary region, especially near the postaxial region of the bone. This region also preserves abundant Sharpey's fibers throughout much of the cortex. The cortex is predominately formed by poorly vascularized parallel-fibered bone with primary osteons and simple canals (%*CV*, 1.9; mean *POD*, 42 μm). Osteocyte lacunae are globular in

Figure 4.9. Bone histology in the baurioid *Tetracynodon darti*. **A**, NMQR 3745, humerus midshaft cross-sectional profile viewed at low magnification (non-polarized light). **B**, UCMP 78396, humerus midshaft cortex (normal polarized light at maximum extinction). Bracket denotes outer zone of parallel-fibered and lamellar bone. **C**, UCMP 78396, humerus midshaft cortex showing outer line of arrested growth (demarcated by cement line at arrow) (non-polarized light). **D**, UCMP 78395, radius midshaft cortex and perimedullary region viewed at low magnification (crossed-nicols with wave plate). **E**, UCMP 78396, femur midshaft cortex and perimedullary region showing woven- and parallel-fibered bone (crossed-nicols with wave plate). **F**, UCMP 78396, femur midshaft cortex close-up (normal polarized light at maximum extinction). **G**, UCMP 78396, fibula midshaft cortical bone packed with longitudinal primary osteons (non-polarized light). Arrows denote growth marks. Abbreviations: elb, endosteal lamellar bone; pfb, parallel-fibered bone; po, primary osteon; Sf, Sharpey's fibers; wb, woven-fibered bone.

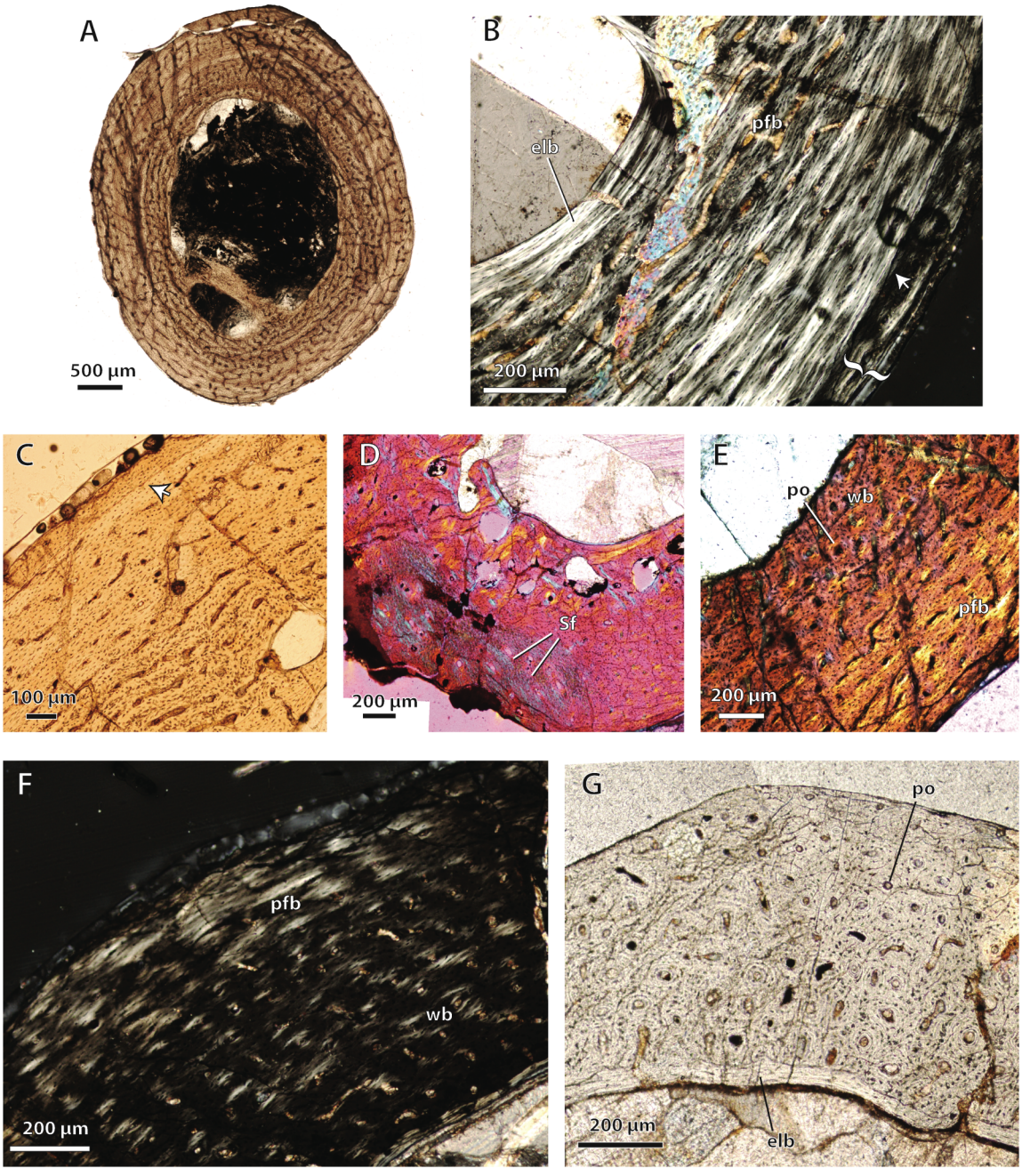
A
500 µm
B
elb
pfb
200 µm
C
100 µm
D
Sf
200 µm
E
po
wb
pfb
200 µm
F
pfb
wb
200 µm
G
po
200 µm
elb

shape and haphazardly arranged, but are sparsely distributed and became more lenticular in some areas of the outer cortex. The sparse vascular canals bear an exclusively longitudinal orientation. Growth marks appear to be absent in the studied specimen.

Ulna—The ulna (UCMP 78395) is similar to the radius in its histological profile, although it is more flattened and bears more trabecular architecture in the marrow cavity. The bone wall is somewhat thicker (*RBT*, 31%; *K*, 0.33) and the transition between the marrow cavity and the cortex is irregular and less abrupt. Large resorption cavities are present in the perimedullary region and the inner half of the cortex exhibits abundant woven-fibered tissue. The lacunocanalicular network is sparse as in the radius, with osteocytes becoming fewer and more lenticular in the outer cortex. The vasculature becomes extremely sparse in the outer cortex (%*CV*, 2.8; mean *POD*, 38 μm) where there is also more parallel-fibered bone. Vascular canals are almost exclusively longitudinal as in the radius, although there are a few reticular canals. Growth marks are apparently absent in the ulna and there is no EFS.

Femur—The femur (Fig. 4.9E, F) has a slender shaft that is subcircular in section, exposing a thin bone wall and a large, open marrow cavity (*RBT*, 17%; *K*, 0.66). The transition between the marrow cavity and the cortex is abrupt, demarcated by a smooth layer of endosteally deposited lamellar bone. The composition of the cortex is similar to that of the humerus, although there is more woven-fibered tissue. As in the humerus, the osteocyte lacunae are frequently lenticular in shape, but are somewhat less ordered. The cortex is dominated by FLB having woven- and parallel-fibered interstitial

ECM and numerous small primary osteons (%*CV*, ~4.3-5.0; mean *POD*, ~39-42 μm). The primary osteons are both longitudinal and reticular. In UCMP 78396, there is a transition to parallel-fibered and lamellar bone in the outermost cortex that is associated with a possible annulus. This transition is also associated with a decrease in the size and concentration of vascular canals toward the subperiosteal surface. Growth marks are otherwise absent from the cortex and there is no true EFS. In addition to cross-sectional sampling, longitudinal sections were possible across the head of the femur in UCMP 78396, allowing brief discussion of longitudinal growth. Most of the subarticular bone formed columns of longitunally oriented trabeculae that are preserved throughout much of the epiphyseal region. The well developed articular surface of the femoral head bears a remarkably thin (~50 microns) layer of calcified cartilage, further supporting that longitudinal growth was nearing completion but had probably not fully ceased. There is no evidence of a secondary ossification center.

Fibula—The fibula (Fig. 4.9G) is a long, thin bone that is subcirular in section at midshaft and has a bone wall of moderate thickness (*RBT*, 25%; *K*, 0.53). The marrow cavity is lined by smooth endosteal lamellar bone and there are few resorption cavities formed in the perimedullary region. The cortex is composed of modestly vascularized FLB having a woven- and parallel-fibered interstitial ECM and numerous small primary osteons (%*CV*, 2.3; mean *POD*, 35 μm). The osteons are almost exclusively longitudinal but with very few reticular anastomoses. The bone maintains a relatively disorganized appearance all the way to the subperiosteal region, with abundant woven-fibered texture

and globular osteocyte lacunae. There are no growth marks apparent in the cortex and no EFS.

Scaloposauridae

Scaloposaurus constrictus

(Fig. 4.10)

General—SAM-PK-K4638 (humerus), from Vegtlager 801, Wagendriftdam (Lower Triassic, *Lystrosaurus* AZ).

Humerus—A single humerus was available for sectioning. However, poor preservation and slight crushing have distorted aspects of the specimen's cross-sectional shape. The shaft is short but slender, and bears a subcircular cross-section as in other baurioids. The bone wall appears to have been relatively thin, with a large marrow cavity having a few trabeculae as in other baurioids. The trabeculae were formed around the perimedullary region but tended to be localized toward the deltopectoral crest. There appears to have been some endosteal erosion and none of the internal endochondral bone (as reported above in small *Ictidosuchoides*) is retained despite the small size of the individual. The cortex was formed intramembranously by subperiosteally deposited primary bone. The overall tissue texture is fibrolamellar, having a woven-fibered interstitial ECM that incorporated primary osteons. The osteons are relatively small and longitudinally oriented with a few reticular canals. The overall degree of vascularization

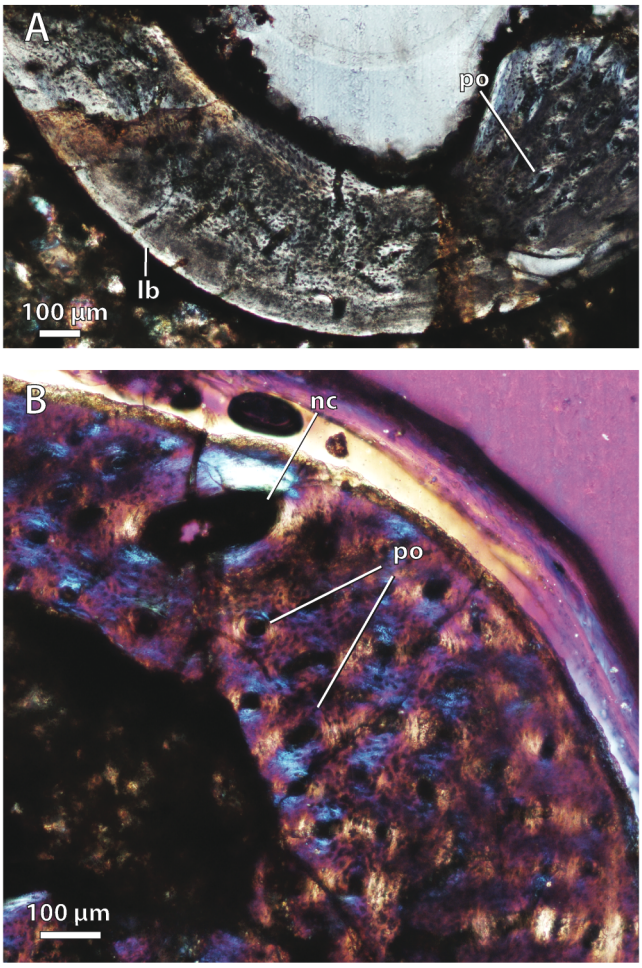

Figure 4.10. Bone histology in the baurioid *Scaloposaurus constrictus*. **A**, Humerus midshaft cross-section showing fibrolamellar bone deposition followed by a thin collar of lamellar bone in the subperiosteal region (normal polarized light at maximum extinction). **B**, Humerus midshaft cortex close-up showing longitudinal primary osteons and a large nutrient canal within a woven-fibered bone matrix (crossed-nicols with wave plate). Abbreviations: lb, lamellar bone; nc, nutrient canal; po, primary osteon.

is somewhat moderate (%*CV*, 6.6; mean *POD*, 62 µm). Growth marks are absent from the inner cortex, although the texture of the interstitial ECM became more parallel-fibered to lamellar in the outermost cortex with a subperiosteal collar of lamellar bone (~30-40 µm in thickness). Although osteocyte lacunae are generally large, globular and highly concentrated through much of the cortex, they take on an abrupt lenticular appearance and more ordered arrangement within the outer collar of lamellar bone. Although the subperiosteal structure indicates deceleration of growth prior to death, it does not exhibit characteristics of an EFS. Moreover, the full extent of this zone around the periphery of the bone is uncertain due to imperfect preservation and loss of some subperiosteal bone during preparation. Secondary osteons were absent.

Bauriidae

Microgomphodon oligocynus

(Fig. 4.11)

General—NMQR 3189 (humerus, femur, tibia, fibula), from Eerstegeluk 131, Bethlehem (Middle Triassic, *Cynognathus* AZ). King (1996) described the morphology of the studied specimen. It consists of a small, disarticulated skeleton preserved within a burrow. In general the limb bones are relatively slender with thin bone walls, bearing large, open marrow cavities as in other baurioids. The cortex consists of FLB with longitudinal, radial, and circular (laminar) primary osteons. Absence of cyclic growth

rings indicates fast, sustained growth in the individual. There are no secondary osteons in any of the studied elements.

Humerus—The humerus (Fig. 4.11A) has a long, slender shaft with a subcircular cross-section. The bone wall is fairly thin as in other baurioids (*RBT*, 21%; *K*, 0.61) and borders a wide, open marrow cavity that is unobstructed by trabecular structures. A few trabeculae are present in the perimedullary region of the proximal shaft near the deltopectoral crest. The cortex is formed by FLB with a woven- and parallel-fibered matrix and longitudinal and reticular primary osteons (with localized circular canals and abundant parallel-fibered bone along the ventral cortical wall). Osteocyte lacunae are abundant, globular in shape and haphazardly arranged throughout the entire cortex. The cortex is moderately well-vascularized (%*CV*, 8.8; mean *POD*, 43 μm). Growth marks were apparently absent and there is no EFS.

Femur—The histological profile of the femur midshaft (Fig. 4.11B, C) somewhat resembles that of the humerus, bearing a similarly thin wall (*RBT*, 18%; *K*, 0.61). The marrow cavity is wide, circular and unobstructed by trabeculae, with an abrupt transition to the cortex. There are few resorption cavities along the perimedullary margins. Unlike the humerus, the entire cortex is composed of reticular FLB. The interstitial ECM is predominantly woven-fibered, being disorganized with high concentrations of globular osteocyte lacunae as in the humerus. The reticular primary osteons are densely distributed all the way to the subperiosteal region. Overall, the cortex exhibits moderate

vascularization (%*CV*, 6.1; mean *POD*, 44 μm). No growth marks are preserved and there is no EFS.

Tibia—The tibia (Fig. 4.11D) is somewhat mediolaterally compressed in section and records an irregular transition between the marrow cavity and the cortex at the midshaft. The bone wall is of moderate thickness (*RBT*, 24%; *K*, 0.51), thicker than that of the propodial elements. There are some coarse trabecular structures and a few large resorption cavities along the perimedullary margins. Like the femur, the cortex is largely formed by FLB, although the primary osteons bear a predominantly longitudinal orientation (with occasional reticular anastomoses). The globular osteocytes were densely-packed around the primary osteons, which were in turn well-concentrated throughout the cortex (%*CV*, 8.0; mean *POD*, 41 μm). No growth marks are preserved and there is no EFS.

Fibula—The fibula (Fig. 4.11E) is a long, slender bone with an oval midshaft cross-section. The bone wall is somewhat thicker than in the other studied elements (*RBT*, 29%; *K*, 0.39), and the transition to the cortex is relatively abrupt. There were no resorption cavities along the perimedullary regions. Much of the inner cortex bears large, densely packed osteocyte lacunae within a woven-fibered bone matrix. The overall tissue composition is fibrolamellar with longitudinal and occasional radial primary osteons (the latter being most obvious along the posterior region of the bone). The anterior region of the bone bears obliquely-oriented Sharpey's fibers. The overall vascularization is fairly

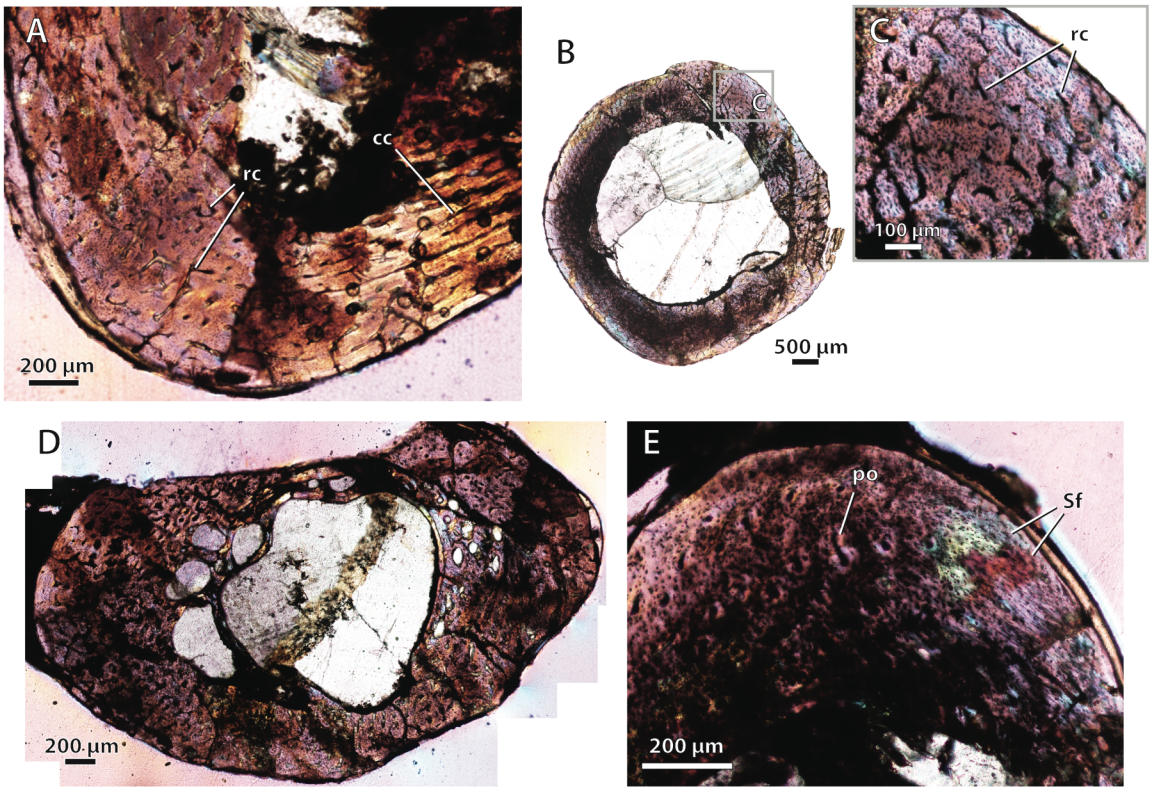

Figure 4.11. Bone histology in the baurioid *Microgomphodon oligocynus*. **A**, NMQR 3605, humerus midshaft cross-section viewed at low magnification (crossed-nicols with wave plate). Note local histovariation in the arrangements of vascular canals. **B**, NMQR 3605, femur midshaft cross-sectional profile viewed at low magnification (crossed-nicols with wave plate). **C**, Close-up of 'B' showing abundant reticular canals in cortex and lack of growth marks. **D**, NMQR 3605, tibia midshaft cross-sectional profile viewed at low magnification (crossed-nicols with wave plate). **E**, NMQR 3605, fibula midshaft cortex (crossed-nicols with wave plate). Abbreviations: cc, circular canal; rc, reticular canal; po, primary osteon; Sf, Sharpey's fibers.

modest (%*CV*, 4.2; mean *POD*, 32 μm). Growth marks are not observed and there is no EFS.

Quantitative Results

Pearson's Product-Moment Correlation and Independent Contrasts

Results of raw and phylogeny-corrected correlation tests are presented in Table 4.2. Correlation tests on raw data found that vascular growth proxies were strongly positively correlated with the natural log of midshaft cross-sectional area, underscoring greater overall tissue vascularity in large bones from larger taxa (e.g., *Lycosuchus*, scylacosaurids, *Moschorhinus*) (Fig. 4.12; Table 4.2). Both %*CV* and *POD* also exhibited a strong positive correlation with each other, indicating that %*CV* and *POD* represent equivalent proxies for understanding relationships between bone tissue vascularization and growth across the therocephalian clade. Whereas these growth proxies shared a consistent positive relationship with size for all data partitions, putative associations between robusticity and size were less clear. Correlation tests on raw size data and *RBT* were non-significant. Likewise, correlation tests on raw vascular growth proxies and *RBT* either yielded non-significant *p*-values or, in the case of the propodial-only data partition, had low correlation coefficients with only a weakly positive association. This result is likely due to the fact that even some small-bodied taxa exhibited unexpectedly thick bone walls, as in the case of the hofmeyriids *Hofmeyria* and *Mirotenthes*. Bone wall thickness correlates poorly with size and growth proxies, suggesting that size and rate of growth

Table. 4.2. Pearson's product-moment correlation statistics (Pearson's *r* and *p*) for size, robusticity, and vascular growth proxies in therocephalians.

	Propodial-only		Epipodial-only		Pooled	
	r	*p**	*r*	*p*	*r*	*p*
All therocephalians, raw data						
ln midshaft area vs. RBT	0.309	0.109	–0.186	0.267	–0.126	0.301
ln midshaft area vs. %CV	**0.744**	**<0.001**	**0.714**	**<0.001**	**0.746**	**<0.001**
ln midshaft area vs. POD	**0.853**	**<0.001**	**0.847**	**<0.001**	**0.850**	**<0.001**
RBT vs. %CV	**0.452**	**0.012**	0.034	0.839	0.149	0.217
RBT vs. POD	**0.360**	**0.050**	0.111	0.512	0.143	0.237
%CV vs. POD	**0.760**	**<0.001**	**0.802**	**<0.001**	**0.796**	**<0.001**
All therocephalians, independent contrasts						
ln midshaft area vs. RBT	–0.466	0.174	–0.476	0.232	--	--
ln midshaft area vs. %CV	**0.765**	**0.006**	**0.807**	**0.015**	--	--
ln midshaft area vs. POD	**0.656**	**0.028**	**0.859**	**0.006**	--	--
RBT vs. %CV	–0.077	0.831	–0.224	0.592	--	--
RBT vs. POD	–0.472	0.168	–0.010	0.979	--	--
%CV vs. POD	**0.639**	**0.034**	**0.877**	**0.004**	--	--

**r and p*-values in boldface are significant at α = 0.05

may have had limited influence over bone robusticity as compared to other aspects of organismal biology such as mechanical regime (e.g., locomotor behavior, stance or gait; Currey and Alexander, 1985) and ecology or habitat preference (e.g., burrowing, semi-aquatic/aquatic; Wall, 1983; Laurin et al., 2004; Germain and Laurin, 2005).

Phylogeny-independent contrasts—Results of phylogeny-corrected correlations further indicated a strong relationship between size and histomorphology (but not with limb bone robusticity) (Table 4.2). Evolutionary decreases in cross-sectional area of limb bones were generally associated with decreases in average %*CV* and *POD*. Eutherocephalians and particularly baurioids demonstrated a noteworthy pattern in which reconstructed ancestor-descendant size reductions of Late Permian and Triassic lineages

Figure 4.12. Linear regression of vascular growth proxies against size (midshaft cross-sectional area) from limb bone elements. **A**, Mean cortical vascularity (%*CV*) against midshaft cross-sectional area. **B**, Mean primary osteon diameter (*POD*) against midshaft cross-sectional area. **C**, mean %*CV* against mean *POD*. All correlations between vascular growth proxies and size are strongly positively correlated for both propodials (solid regression line) and epipodials (dashed regression line). Blue circles = propodials. Red circles = epipodials.

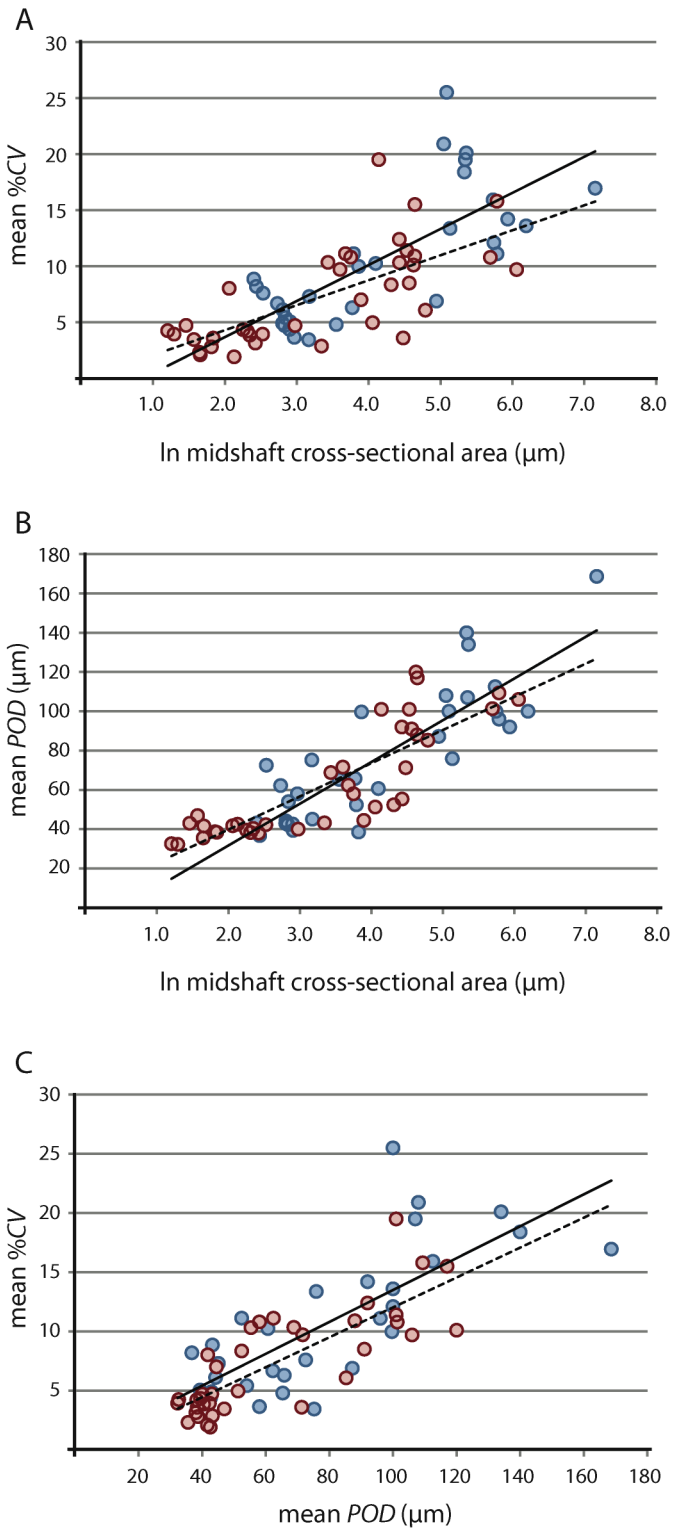
A
mean %CV
ln midshaft cross-sectional area (µm)
B
mean POD (µm)
ln midshaft cross-sectional area (µm)
C
mean %CV
mean POD (µm)

were associated with decreases in the average level of tissue vascularization. Patterns in limb bone robusticity were less clear. As in the analyses of the raw data, phylogeny-corrected correlations between *RBT* and size or growth proxies were non-significant.

Discussion

General Histological Patterns

Limb bone cortices in studied therocephalians were generally formed by FLB with varying degrees of vascularization. In Permian therocephalians, multiple growth zones were frequently present, demarcated by cyclic growth marks indicative of periodic cessations of growth as in other Permian therapsids (Ray et al., 2004, 2012; Botha-Brink and Angielczyk, 2010; Botha-Brink et al., 2012). Some small-bodied taxa tended to incorporate more parallel-fibered bone or showed evidence of increased parallel-fibered and lamellar bone deposition toward the outer cortex, indicative of growth attenuation and attainment of somatic maturity (Margerie et al., 2002). Fewer taxa demonstrated an EFS-like structure in the outer cortex (*Mirotenthes* being a notable exception). Systematic cortical remodeling by Haversian bone formation was rare and only a few sparse secondary osteons were identified in some scylacosaurian taxa (e.g., an indeterminate scylacosaurid and *Moschorhinus*) contrary to exaggerated reports of skeletal remodeling suggested by Chinsamy-Turan and Ray (2012: p. 203). Most basal therocephalians and eutherocephalians also exhibited remarkably thick bone walls (~20-35% *RBT* in forelimb elements; ~40% in forelimbs of hofmeyriids) as in other therapsids in which histology is

well known (e.g., dicynodonts). This condition, however, was lost in baurioids, which were instead characterized by a much thinner cortical bone wall (< 25% in the forelimb and propodials) and more gracile limb bones.

Size, robusticity, and vascular growth proxies—Biologically meaningful associations are detectable in therocephalian histology, as in some other therapsid groups. For example, vascular growth proxies were strongly positively correlated with size as larger-bodied species typically exhibited greater overall tissue vascularity (e.g., *Lycosuchus*, scylacosaurids, *Moschorhinus*). Previous tests incorporating a large histologic sample of dicynodonts and other therapsids found similar correlations between raw vascular growth proxies and size (estimated from skull lengths), although tests on a subset of dicynodonts were only marginally significant and non-significant when independent contrasts were evaluated (Botha-Brink and Angielczyk, 2010). The new data agree with these earlier results by large measure. However, the present analysis found a strongly positive correlation between size and both vascular growth proxies (%*CV* and *POD*) even when corrected for phylogeny. Prior analyses implementing phylogeny-independent contrasts on dicynodonts were unable to identify similar patterns, despite a significant correlation between the raw data (Botha-Brink and Angielczyk, 2010). Improved statistical results in this study are a likely consequence of sampling bones of particular types separately (rather than averaging vascularity across all bones) and using cross-sectional measurements from sampled bones as a size proxy (rather than skull lengths from specimens that were not sampled histologically). Tests on raw cortical

thickness (*RBT*) in dicynodonts also showed no clear association with size or degree of vascularization as in the present study, even though a positive association with size was discovered when corrected for phylogeny. No correlation was observed between bone robusticity (*RBT*) and size or degree of vascularization in therocephalians (raw or phylogeny-corrected), suggesting that bone robusticity is not necessarily tied directly to growth (perhaps being constrained by ecology, habitat, or mechanical regimen in different groups of therocephalians). Similarly, initial data on the genus *Moschorhinus* indicated that overall bone compactness was related to the thickness of the bone wall, but was independent of growth and degree of vascularity (Huttenlocker and Botha-Brink, 2013; see Chapter 2 of this dissertation).

Phylogenetic Patterns

Previous interpretations of growth patterns in early therocephalians were based on limited information from poorly preserved specimens (Ricqlès, 1969; Ray et al., 2004; Chinsamy-Turan and Ray, 2012). Additional specimens described here suggest that at least some large-bodied predators from the Middle Permian, including *Lycosuchus* and some scylacosaurids (e.g., CGS R300), exhibited subplexiform FLB in propodial elements. Some of the larger-bodied predators in the sample also showed the highest degree of cortical vascularization. A simple regression between thicknesses of individual growth zones and their average primary osteon diameters shows that the sizes of the reticular and subplexiform primary osteons formed by these large predators correlated with the amount of tissue deposited over a year (Fig. 4.13). This is remarkable, as

subplexiform FLB is one of the most rapidly deposited tissue-types in archosaurian and mammalian limb bones, and similarly vascularized bone in birds and mammals forms periosteally at a rate often greater than 15 μm/day (Castanet et al., 2000; Margerie et al., 2002; Cubo et al., 2012; see Appendix 9). It is noteworthy that the subplexiform tissue complex, present in *Lycosuchus* and scylacosaurids, represents the prototype upon which earlier workers first described FLB (see Stein and Prondvai, 2013 for a review). This subplexiform condition is conspicuously lacking in the whaitsiid *Theriognathus* (Fig. 4.14) and some later eutherocephalians. Consequently, the evolutionary implications suggested by Ricqlès (1969), critically re-examined by Chinsamy-Turan and Ray (2012), are incorrect: basal therocephalians exhibited highly vascularized FLB and likely grew at accelerated rates compared to some later eutherocephalians (with the exception of the akidnognathid *Moschorhinus,* which maintained relatively fast growth).

Moreover, elevated vascularity and rapid growth may be a characteristic of larger bodied taxa, an interpretation that is supported by observations in other large predatory theriodonts such as the cynodont *Cynognathus* and some large gorgonopsians (Botha-Brink et al., 2012; Chinsamy-Turan and Ray, 2012). Importantly, evolutionary decreases in body size during the Permian were associated with decreases in overall degree of skeletal vascularization. Both hofmeyriids and *Theriognathus* (in spite of its substantial

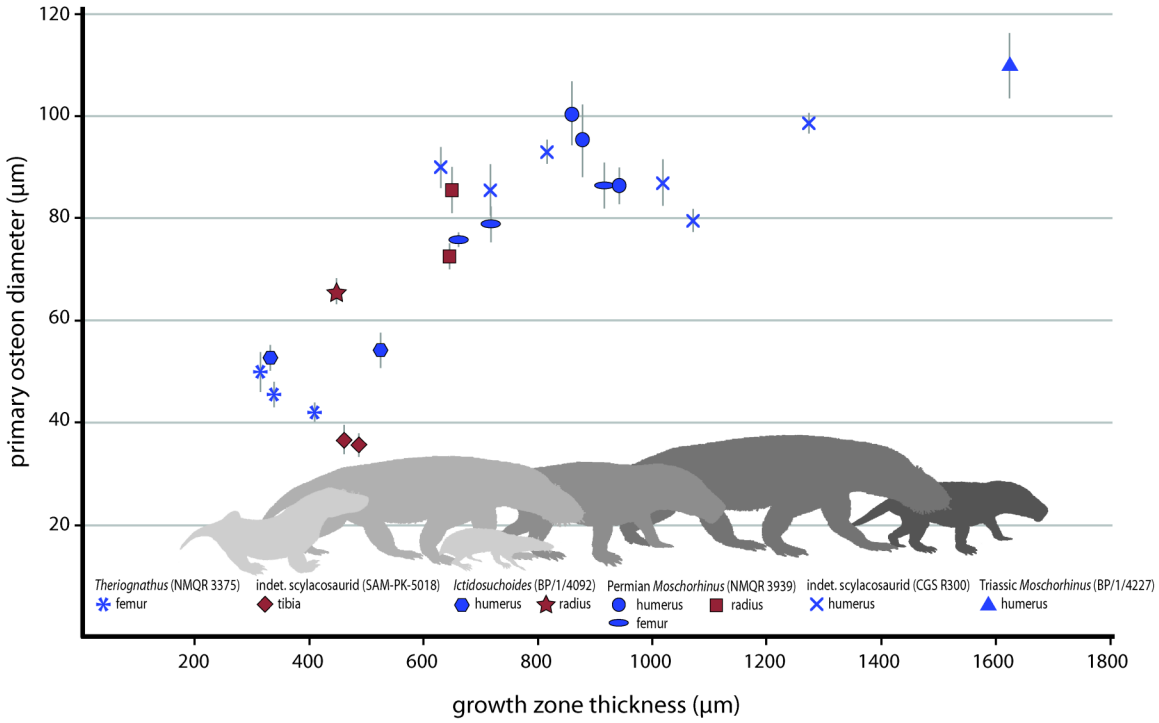

Figure 4.13. Primary osteon diameter (*POD*) versus growth zone thickness from selected limb bone elements (blue = propodials; red = epipodials). Osteons were measured within individual growth zones to more directly assess relationships between bone apposition and degree of vascularization within and among individual bony elements (supplementing measurements of average midcortical vascularization in bony elements). Growth zones bounded by more widely spaced growth marks tended to be more richly vascularized (e.g., *Moschorhinus*) compared to those having more closely spaced growth marks (e.g., whaitsiids and baurioids). Vertical bars represent 95% confidence intervals.

size) showed modest cortical vascularity and smaller primary osteons than in basal lycosuchids, scylacosaurids or akidnognathids, but the baurioids (which are deeply nested in the tree and generally smaller-bodied) had the least vascularized bone tissue (Fig. 4.15). These clade-level patterns suggest that reductions in body size of some Late Permian eutherocephalians were coupled with decreased rates of skeletal growth leading up to the end-Permian extinction.

Growth and the End-Permian Extinction

The end-Permian extinction was associated with evidence of temporary body size reductions, restricted primarily to faunas of the earliest Triassic (Induan). Such geologically abrupt size shifts have been documented previously based on invertebrate burrows, foraminifera, brachiopods, gastropods, bivalves, conodonts, and fish (Twitchett and Barras, 2004; Payne, 2005; Twitchett, 2007; Luo et al., 2008; Mutter and Neuman, 2009; Metcalfe et al., 2011; Song et al., 2011; Rego et al., 2012). Whereas a variety of patterns of size evolution have been identified in these groups, questions remain regarding the evolution of growth patterns and their underlying influence on size shifts (Twitchett, 2007; Harries and Knorr, 2009; Metcalfe et al., 2011). For example, organisms may have experienced slower overall growth rates in response to more limited resources or poor environmental conditions. Growth mark analyses on marine brachiopod shells (i.e., '*Lingula'*) have indicated slow growth rates with frequent interuptions to growth in earliest Triassic shells (Metcalfe et al., 2011). The authors attributed their results to suboptimal environmental conditions, including episodes of benthic hypoxia,

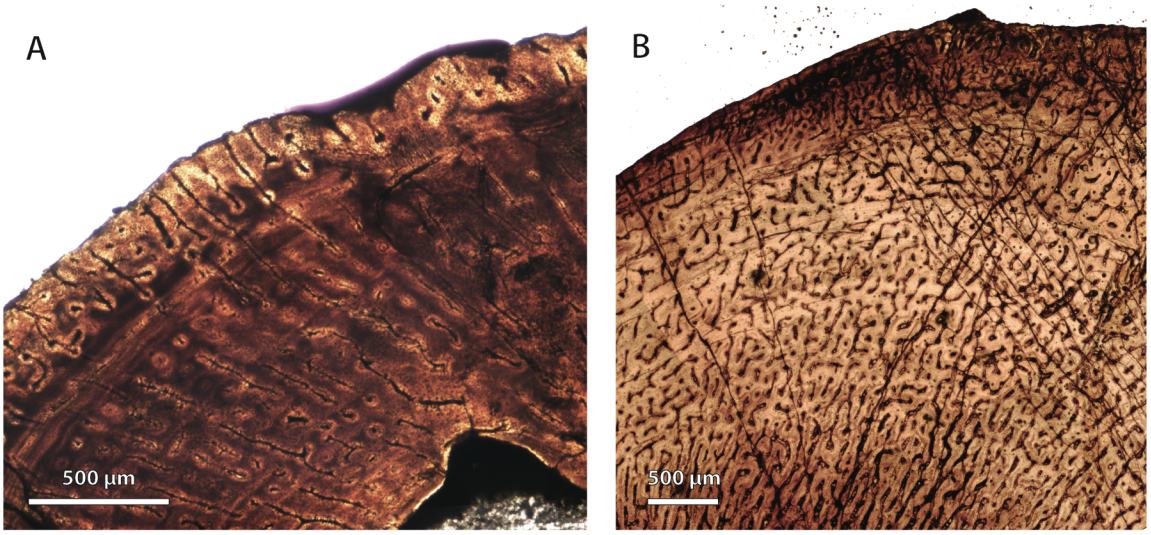

Figure 4.14. Comparison of bone histology and microvasculature in Permian *Theriognathus* and *Moschorhinus*. **A**, *Theriognathus* (NMQR 3375) femur midshaft cortex (non-polarized light). **B**, *Moschorhinus* (NMQR 3939) humerus midshaft cortex (non-polarized light). Note the greater overall degree of vascularity in 'B.'

hypercapnea, ocean acidification, and/or disruptions to primary productivity. Such environmental factors would place strong physiological limits on shell formation. However, identifications of lingulid specimens were tenuous given conservatism in external morphology of the group, and growth marks were only studied in shells from Triassic survival and recovery faunas without being compared to Permian specimens. Alternatively, surviving lineages could have exhibited heterochronic shifts shortening time to maturity (e.g., progenesis) and thus rapid, sustained growth over a brief growth period. Progenesis is a classic example of an *r*-selection strategy in perturbed or unstable environments (Gould, 1977) and has been identified as a potential mechanism of some Lilliput patterns (Harries et al., 1996). Finally, if shifts in body size distributions were influenced primarily by differential extinction of large- versus small-bodied forms (Chapter 3), then there may have been no resulting changes in growth patterns at all (that is to say, changes in growth dynamics are not necessary to explain post-extinction body size distributions).

Growth patterns in Permo-Triassic therapsids compared—New data on growth patterns in nonmammalian therapsids (as well as other Permo-Triassic tetrapods) offer the potential to further evaluate patterns of selectivity during mass extinctions (Botha-Brink and Angielczyk, 2010; Botha-Brink and Smith, 2011). Bone histology has been studied in numerous genera of Permian and Triassic dicynodont therapsids (Chinsamy and Rubidge, 1993; Ray et al., 2004, 2009, 2012) and recent progress in

Figure 4.15. Mirror phylogenies of Permo-Triassic therocephalians sampled for bone histology (scaled to geologic time). Phylogenetic character mapping of histological traits estimated from propodials (left) and epidpodials (right) reveals comparable ancestor-descendant changes for each pool of skeletal elements. **A**, average cortical vascularity (%*CV*). **B**, average primary osteon diameter (*POD*). **C**, relative bone wall thickness (*RBT*). Ancestral states were reconstructed using squared-change parsimony in Mesquite version 2.0 (Maddison and Maddison, 2007). Trees modified from Chapters 1 and 3.

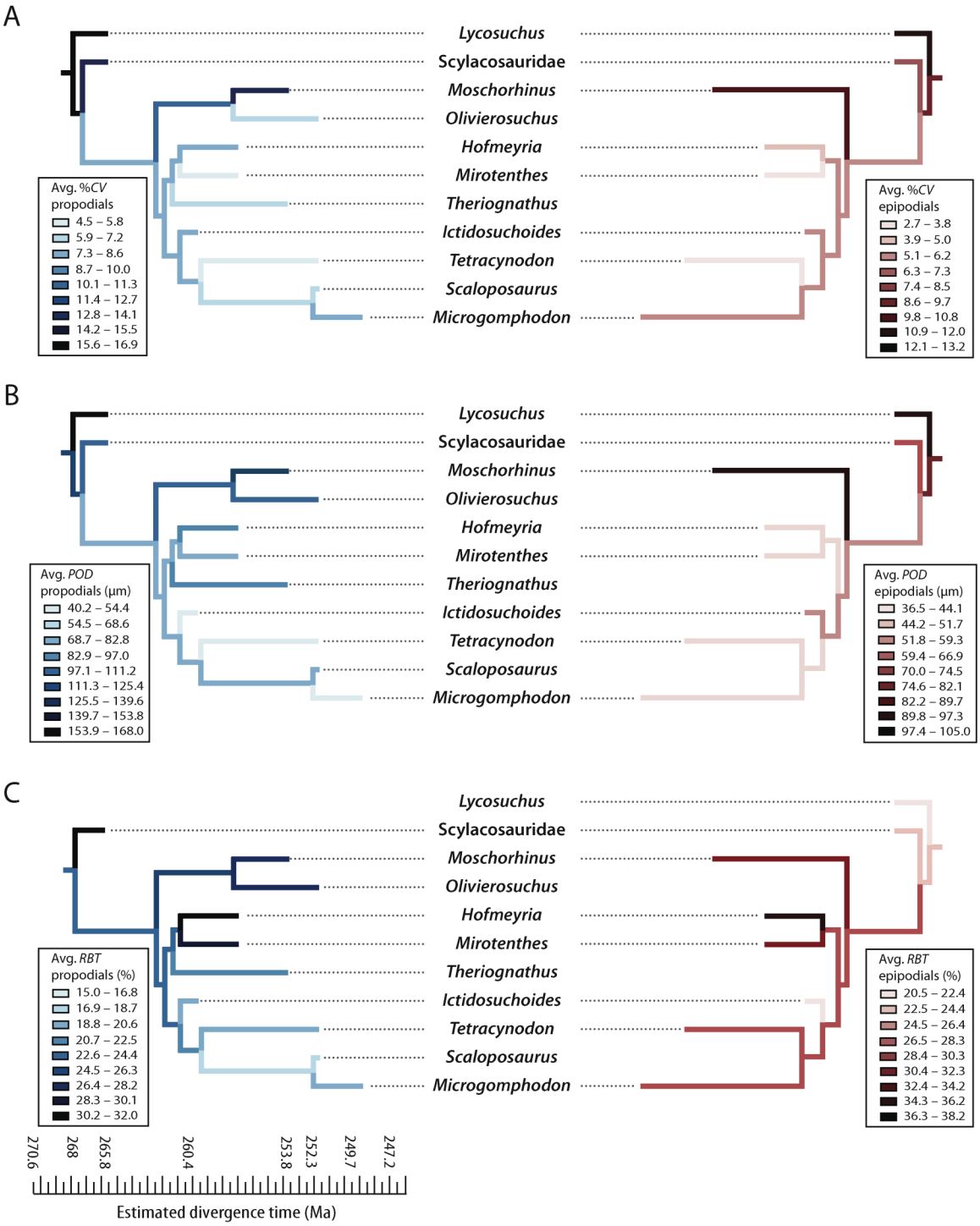
A
Lycosuchus
Scylacosauridae
Moschorhinus
Olivierosuchus
Hofmeyria
Mirotenthes
Theriognathus
Ictidosuchoides
Tetracynodon
Scaloposaurus
Microgomphodon
Avg. %CV propodials
4.5 – 5.8
5.9 – 7.2
7.3 – 8.6
8.7 – 10.0
10.1 – 11.3
11.4 – 12.7
12.8 – 14.1
14.2 – 15.5
15.6 – 16.9
Avg. %CV epipodials
2.7 – 3.8
3.9 – 5.0
5.1 – 6.2
6.3 – 7.3
7.4 – 8.5
8.6 – 9.7
9.8 – 10.8
10.9 – 12.0
12.1 – 13.2
B
Avg. POD propodials (µm)
40.2 – 54.4
54.5 – 68.6
68.7 – 82.8
82.9 – 97.0
97.1 – 111.2
111.3 – 125.4
125.5 – 139.6
139.7 – 153.8
153.9 – 168.0
Avg. POD epipodials (µm)
36.5 – 44.1
44.2 – 51.7
51.8 – 59.3
59.4 – 66.9
70.0 – 74.5
74.6 – 82.1
82.2 – 89.7
89.8 – 97.3
97.4 – 105.0
C
Avg. RBT propodials (%)
15.0 – 16.8
16.9 – 18.7
18.8 – 20.6
20.7 – 22.5
22.6 – 24.4
24.5 – 26.3
26.4 – 28.2
28.3 – 30.1
30.2 – 32.0
Avg. RBT epipodials (%)
20.5 – 22.4
22.5 – 24.4
24.5 – 26.4
26.5 – 28.3
28.4 – 30.3
30.4 – 32.3
32.4 – 34.2
34.3 – 36.2
36.3 – 38.2
270.6
268
265.8
260.4
253.8
252.3
249.7
247.2
Estimated divergence time (Ma)

dicynodont paleobiology has permitted evolutionary investigations of their growth patterns (Botha-Brink and Angielczyk, 2010). Increased rates of skeletal growth originated relatively early, either within or prior to the divergence of bidentalian dicynodonts (e.g., *Dicynodon*, *Lystrosaurus*) by the early-Late Permian. Late Permian dicynodonts continued to show patterns of increased cortical vascularity, especially within the Permo-Triassic boundary-crossing genus *Lystrosaurus*, which demonstrated some of the highest levels of tissue vascularity (~20%). Triassic specimens of *Lystrosaurus* showed relatively higher vascularity and fewer growth marks. In the therocephalian *Moschorhinus*, the only large therapsid predator to cross the Permian-Triassic boundary, within-lineage size reductions were associated with rapid but attenuating growth over a short period. This pattern suggests that *Moschorhinus* was under selection for reaching its adult size relatively more quickly than in the Permian (Chapter 2). Notably, *Moschorhinus* exhibited comparably high levels of tissue vascularity as *Lystrosaurus* during the Triassic (~20-25%).

Whereas anecdotal evidence in *Lystrosaurus* and *Moschorhinus* is highly suggestive of within-lineage heterochronic shifts, at least between predator-prey associations, clade-level patterns introduce a more complex explanation for observed body size reductions in therocephalians. In particular, body size reductions occurred early during the evolution of eutherocephalians and were associated with a lesser degree of cortical vascularity in medium-to-small-bodied Permian forms (e.g., hofmeyriids and especially baurioids). The two major subclades of therocephalians that persisted into the

earliest Triassic, Akidnognathidae and Baurioidea, revealed distinctly different growth patterns from each other as interpreted through their tissue texture and degree of vascularity. Their histology suggests a bimodality of life history strategies in earliest Triassic therocephalians: small-to-medium akidnognathids with well-vascularized (fast-growing) bone and smaller-bodied baurioids with less vascularized (slower-growing) bone. However, both groups shared a reduced number of growth marks compared to their Permian relatives in addition to their generally smaller sizes. This nuance is not evident from the quantitative analysis based on vascular proxies of growth rate alone, but is evident from growth mark counts in surveyed specimens. Permian theriodonts that have been sampled histologically, including some gorgonopsians, the cynodont *Procynosuchus*, basal therocephalians, Permian (but not Triassic) specimens of *Moschorhinus*, hofmeyriids, and *Theriognathus*, typically showed evidence of prolonged, multi-year growth often to larger body sizes, a pattern that is not represented in earliest Triassic therapsids sampled to date (Botha-Brink and Angielczyk, 2010; Botha-Brink et al., 2012).

Microstructural and macrostructural evolution during the Permian-Triassic transition—The present discussion of associations between micro- and macrostructure provides a more functional and wholistic context for the evolution of histological features in Permian and Triassic therocephalians. However, it is important to note that the patterns discussed here have not been evaluated quantitatively and therefore merit future investigation.

Figure 4.16. Summary of evolution of size and bone microstructural traits. Black bars represent stratigraphic ranges of taxa that were sampled histologically. Numbers in parentheses to right of black bars denote maximum size of taxon in interval of first appearance. In graph at top of figure, circles represent average %CV and squares average POD of propodials (blue) and epipodials (red). Abbreviations: Chx, Changxingian; *Cisteceph* AZ, *Cistecephalus* Assemblage Zone; *Cyn* sub A, *Cynognathus* subzone A; *Eodicyno* AZ, *Eodicynodon* Assemblage Zone; Ind, Induan; Olen, Olenekian; *Pristerog* AZ, *Pristerognathus* Assemblage Zone; Roa, Roadian; *Tapinoceph* AZ, *Tapinocephalus* Assemblage Zone; *Tropido* AZ, *Tropidostoma* Assemblage Zone; Wor, Wordian.

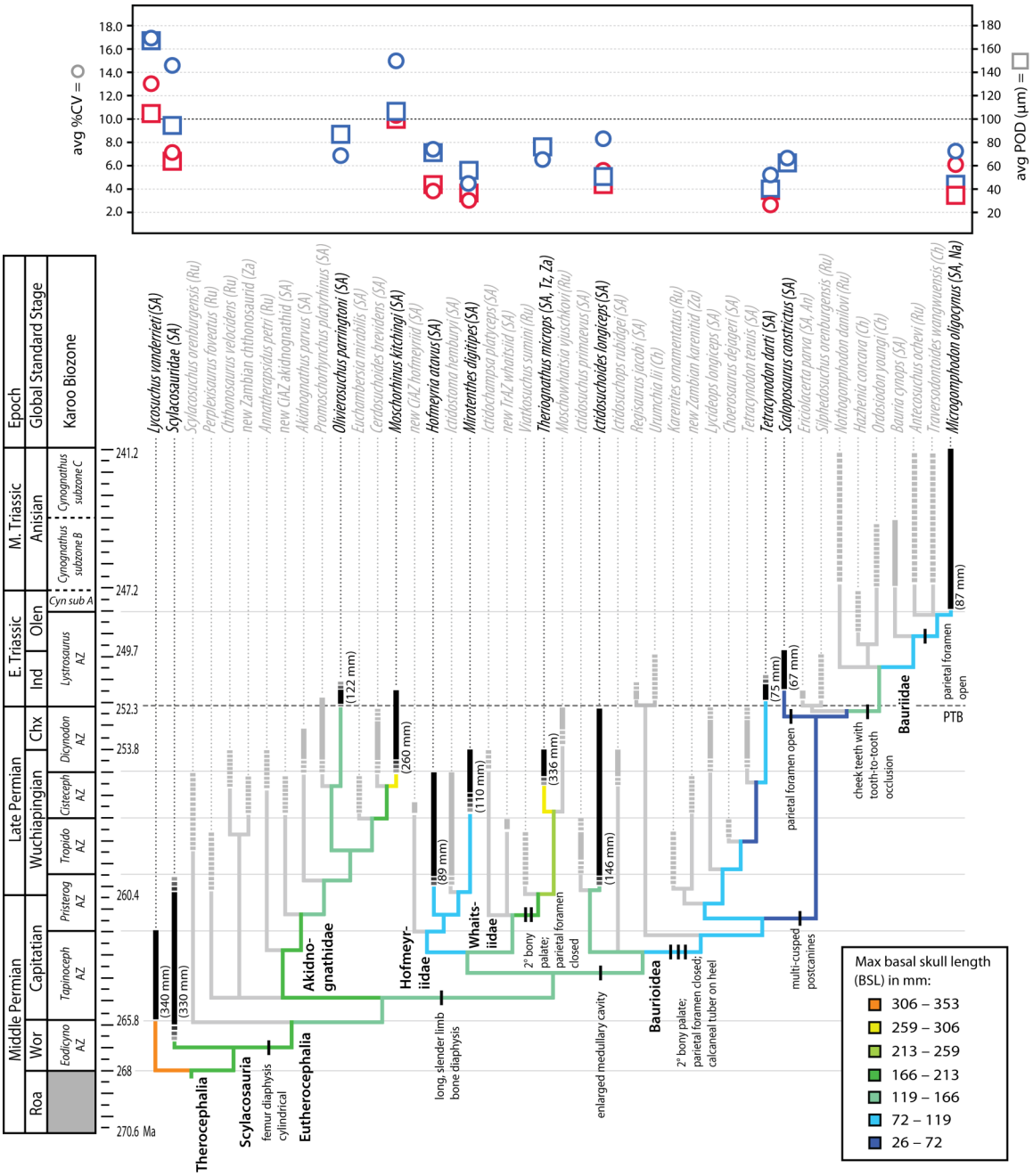
avg %CV = ○
avg POD (μm) = □
Middle Permian
Late Permian
E. Triassic
M. Triassic
Epoch
Roa
Wor
Capitatian
Wuchiapingian
Chx
Ind
Olen
Anisian
Global Standard Stage
Karoo Biozone
Eodicyno AZ
Tapinoceph AZ
Pristerog AZ
Tropido AZ
Cisteceph AZ
Dicynodon AZ
Lystrosaurus AZ
Cyn sub A
Cynognathus subzone B
Cynognathus subzone C
241.2
247.2
249.7
252.3
253.8
260.4
265.8
268
270.6 Ma
Lycosuchus vanderrieti (SA)
Scylacosauridae (SA)
Scylacosuchus orenburgensis (Ru)
Perplexisaurus foveatus (Ru)
Chthonosaurus velocidens (Ru)
new Zambian chthonosaurid (Za)
Annatherapsidus petri (Ru)
new CIAZ akidnognathid (SA)
Akidnognathus parvus (SA)
Promoschorhynchus platyrhinus (SA)
Olivierosuchus parringtoni (SA)
Euchambersia mirabilis (SA)
Cerdosuchoides brevidens (SA)
Moschorhinus kitchingi (SA)
new CIAZ hofmeyriid (SA)
Hofmeyria atavus (SA)
Ictidostoma hemburyi (SA)
Mirotenthes digitipes (SA)
Ictidochampsa platyceps (SA)
new TrAZ whaitsiid (SA)
Vatkosuchus summi (Ru)
Theriognathus microps (SA, Tz, Za)
Moschowhaitsia vjuschkovi (Ru)
Ictidosuchus primaevus (SA)
Ictidosuchoides longiceps (SA)
Ictidosuchops rubriger (SA)
Regisaurus jacobi (SA)
Urumchia lii (Ch)
Karenites ornamentatus (Ru)
new Zambian karenitid (Za)
Lydadeops longiceps (SA)
Choerosaurus dejageri (SA)
Tetracynodon tenuis (SA)
Tetracynodon darti (SA)
Scaloposaurus constrictus (SA)
Ericiolacerta parva (SA, An)
Silphedosuchus orenburgensis (Ru)
Nothogomphodon daniilovi (Ru)
Huzhenia concava (Ch)
Ordosiodon youngi (Ch)
Bauria cynops (SA)
Antecosuchus ochevi (Ru)
Traversodontoides wangwuensis (Ch)
Microgomphodon oligocynus (SA, Na)
(340 mm)
(330 mm)
(122 mm)
(260 mm)
(89 mm)
(110 mm)
(336 mm)
(146 mm)
(75 mm)
(67 mm)
(87 mm)
Therocephalia
Scylacosauria
femur diaphysis cylindrical
Eutherocephalia
Akidno-gnathidae
Hofmeyr-iidae
long, slender limb bone diaphysis
Whaits-iidae
2° bony palate; parietal foramen closed
enlarged medullary cavity
Baurioidea
2° bony palate; parietal foramen closed; calcaneal tuber on heel
parietal foramen open
multi-cusped postcanines
cheek teeth with tooth-to-tooth occlusion
Bauriidae
parietal foramen open
PTB
Max basal skull length (BSL) in mm:
306 – 353
259 – 306
213 – 259
166 – 213
119 – 166
72 – 119
26 – 72

Recent large-scale phylogenetic studies in other therapsids have addressed how life history and functional morphology might have contributed to the success of some groups during the Late Permian and Triassic (e.g., bidentalian dicynodonts) (Angielczyk and Walsh, 2008; Botha-Brink and Angielczyk, 2010). For example, the degree of development of the secondary palate has been linked anecdotally to new environmental conditions with the onset of the Early Triassic, particularly a rapid decline in atmospheric PO_2 from the Late Permian and continuing into the Middle Triassic (Retallack et al., 2003). However, a rigorous collections-based study found no difference between secondary palate length in Permian and Triassic dicynodonts when corrected for size and phylogeny (Angielczyk and Walsh, 2008). Similarly, a bony secondary palate can be found in a number of therocephalian subgroups, both in the Permian and Triassic, and Triassic therocephalian faunas consisted of species both with (e.g., baurioids) and without (e.g., akidnognathids) a secondary palate (Fig. 4.16). No clear association with global hypoxia and respiratory efficiency can be made based on this character, and, as a result, other factors may have been more important in maintaining and shaping the evolution of the secondary palate (e.g., feeding mechanics; Thomason and Russell, 1986).

Similar studies addressing the possible effects of hypoxia on cortical tissue vascularity have found few differences between Permian and Triassic therapsids, instead demonstrating that highly vascularized tissues with enlarged canals evolved early in bidentalian dicynodonts (Botha-Brink and Angielczyk, 2010). In therocephalians, variation in the degree of vascularization of limb cortices is best explained by size

variation observed across clades (Fig. 4.16). Most smaller-bodied groups exhibited less vascularized limb bone cortices, a character that evolved relatively early in the evolutionary history of eutherocephalians and held over in some small Triassic taxa. The smallest Triassic forms, derived bauroids, typically had lighter, more gracile skeletons with an open medullary cavity, thinner bone walls, and few to no growth marks. In addition to longer, more slender limb bones, they also had an elongate hind foot with a calcaneal tuber on the heel, maxillary bridge forming a bony secondary palate (discussed above), increasingly specialized multi-cusped teeth, and often lacked a parietal foramen (or diminished the pineal body altogether as in *Tetracynodon*; e.g., Sigurdsen et al., 2012). The selective value of maintaining a parietal eye for temperature regulation and modulating melatonin production may have been diminished in some small, nocturnal or crepuscular baurioid therocephalians, or in short-lived animals less dependent on seasonal cues in photoperiodicity (Roth et al., 1986). The latter scenario is consistent with the lack of cyclic bone deposition and paucity of growth marks in small Triassic baurioids (although *Scaloposaurus* notably differed from other small baurioids in retaining a parietal foramen).

Conclusion

A survey of histological patterns in therocephalians found that limb bone cortices composed of thick deposits of FLB with cyclic growth marks were widespread in early therocephalians, but evolutionary decreases in adult body sizes of some clades were

associated with reductions in cortical vascularity and skeletal growth leading up to the end-Permian mass extinction. In Permo-Triassic therocephalians, a pattern of multi-year growth to large body size that was common in the Permian was selected against in the earliest Triassic. This conclusion is supported by (1) ecological removal of large-bodied taxa having prolonged, multi-year growth patterns; (2) cladistically inferred survival of small-bodied taxa with short growth durations (i.e., baurioids); and (3) within-lineage shifts in growth patterns observed in boundary-crossing genera in the Karoo (i.e., *Lystrosaurus* and *Moschorhinus*). A synergistic combination of local within-lineage effects and differential extinction patterns influenced Triassic Lilliput faunas, weakening the role of rapid originations of new small-bodied taxa. Similar within-lineage size decreases and size selective extinctions contributed strongly to Lilliput patterns in marine gastropods, foraminifera, and brachiopods, although all three mechanisms have been invoked to explain Early Triassic foraminifera size distributions (Payne, 2005; Metcalfe et al., 2011; Song et al., 2011; Rego et al., 2012). Contrary to the present results, growth mark analyses on lingulid brachiopods are suggestive of different physical factors influencing skeletal growth in marine benthos (due to slowed, but prolonged shell secretion) (Metcalfe, et al., 2011). More skeletochronologic and phylogenetic data are needed, however, to understand the generality of these patterns among Permo-Triassic Lilliput taxa in marine and terrestrial realms.

Although some effects on size and growth are observable in Triassic therocephalians (and perhaps therapsids more generally), it is important to note that much

of the diversity observed in the earliest Triassic *Lystrosaurus* Assemblage Zone of the Karoo originated during the Late Permian, and that variation in body sizes and growth patterns during the Late Permian was supplanted by increased bimodality in the Early Triassic *Lystrosaurus* AZ: small-to-medium, fast-growing akidnognathids and the still smaller, slower-growing baurioids. Small size and short growth duration were dominant life history strategies of Early Triassic therocephalians in the Karoo, and reductions in size were typically associated with lesser tissue vascularity and growth rates across but not within taxa. Furthermore, although these strategies were apparently common in the post-extinction environment, their success was temporary. Low rates of origination in therocephalians during this time, coupled with small sizes and reduced niche occupation may have afforded the opportunity for more marginalized groups to diversify (e.g., cynodonts and archosauromorphs). Future applications of phylogenetic comparative methods to studies of body size and growth during the Permo-Triassic will enhance our understanding of interplay between macroevolution and extinctions, and will identify areas of phylogeny that correspond to shifts in trait evolution that conferred success on lineages.

List of References

1. Abdala, F. 2007. Redescription of *Platycraniellus elegans* (Therapsida, Cynodontia) from the Lower Triassic of South Africa, and the cladistic relationships of eutheriodonts. Palaeontology 50:591–618.

2. Abdala, F. In press. New material of *Microgomphodon oligocynus* (Eutherapsida, Therocephalia) and the taxonomy of southern African Bauriidae. In C. F. Kammerer, K. D. Angielczyk, and J. Fröbisch (eds.) Early Evolutionary History of the Synapsida. Springer.

3. Abdala, F., and N. P. Giannini. 2000. Gomphodont cynodonts of the Chañares Formation: the analysis of an ontogenetic sequence. Journal of Vertebrate Paleontology 20:501–506.

4. Abdala, F., and N. P. Giannini. 2002. Chiniquodontid cynodonts: systematic and morphometric considerations. Palaeontology 45:1151–1170.

5. Abdala, F., and A. M. Ribeiro. 2010. Distribution and diversity patterns of Triassic cynodonts (Therapsida, Cynodontia) in Gondwana. Palaeogeography, Palaeoclimatology, Palaeoecology 286:202–217.

6. Abdala, F., J. Neveling, and J. Welman. 2006. A new trirachodontid cynodont from the lower levels of the Burgersdorp Formation (Lower Triassic) of the Beaufort Group, South Africa and the cladistic relationships of Gondwanan gomphodonts. Zoological Journal of the Linnean Society 147:383–413.

7. Abdala, F., B. S. Rubidge, and J. van den Heever. 2008. The oldest therocephalians (Therapsida, Eutheriodontia) and the early diversification of Therapsida. Palaeontology 51:1011–1024.

8. Amalitzky, V. P. 1922. Diagnoses of the new forms of vertebrates and plants from the Upper Permian of North Dvina, Izv. Ross. Akad. Nauk 25:1–12.

9. Amprino, R. 1947. La structure du tissu osseux envisagée comme expression de différences dans la vitesse de l'accroissement. Archives de Biologie 58:315–330. [in French]

10. Angielczyk, K. D. 2004. Phylogenetic evidence for and implications of a dual origin of propaliny in anomodont therapsids (Synapsida). Paleobiology 30: 268–296.

11. Angielczyk, K. D. 2009. Dimetrodon is not a dinosaur: using tree thinking to understand the ancient relatives of mammals and their evolution. Evolution: Education and Outreach 2:257–271.

12. Angielczyk, K. D., and M. L. Walsh. 2008. Patterns in the evolution of nares size and secondary palate length in anomodont therapsids (Synapsida): implications for hypoxia as a cause of end-Permian tetrapod extinctions. Journal of Paleontology 82:528-542.

13. Attridge, J. 1956. The morphology and relationships of a complete therocephalian skeleton from the *Cistecephalus* Zone of South Africa. Proceedings of the Royal Society of Edinburgh. Section B. Biology 66:59–93.

14. Battail, B. and M. V. Surkov. 2000. Mammal-like reptiles from Russia: Pp. 86–119 *in* M. J. Benton, M. A. Shishkin, D. M. Unwin, and E. N. Kurochkin (eds.), The Age of Dinosaurs in Russia and Mongolia. Cambridge University Press, Cambridge.

15. Belcher, C. M., and J. C. McElwain. 2008. Limits for combustion in low O_2 redefine paleoatmospheric predictions for the Mesozoic. Science 321:1197–1200.

16. Bennett, A. F., and J. A. Ruben. 1986. The metabolic and thermoregulatory status of therapsids: Pp. 207–218 *in* N. Hotton, P. D. MacLean, J. J. Roth, and E. C. Roth (eds.), The Ecology and Biology of Mammal-like Reptiles. Smithsonian Institution Press, Washington, D.C.

17. Benton, M. J., V. P. Tverdokhlebov, and M. V. Surkov. 2004. Ecosystem remodeling among vertebrates at the Permian-Triassic boundary in Russia. Nature 432:97–100.

18. Berner, R. A. 1999. Atmospheric oxygen over Phanerozoic time. Proceedings of the National Academy of Sciences USA 96:10955–10957.

19. Berner, R. A. 2003. The rise of trees and their effects on Paleozoic atmospheric CO_2 and O_2. Comptes Rendus Geoscience 335:1173–1177.

20. Berner, R. A. 2004. The Phanerozoic Carbon Cycle: CO_2 and O_2. Oxford University Press, New York.

21. Berner, R. A. 2006. GEOCARBSULF: a combined model for Phanerozoic atmospheric O_2 and CO_2. Geochimica et Cosmochimica Acta 70:5653–5664.

22. Berner, R. A., J. M. VandenBrooks, and P. D. Ward. 2007. Oxygen and evolution. Science 316:557–558.

23. Blomberg, S. P., T. Garland Jr., and A. R. Ives. 2003. Testing for phylogenetic signal in comparative data: behavioral traits are more labile. Evolution 57:717–745.

24. Boonstra, L. D. 1934. A contribution to the morphology of the mammal-like reptiles of the suborder Therocephalia. Annals of the South African Museum 31:215–267.

25. Boonstra, L. D. 1935. On some South African reptiles of the suborder Therocephalia preserved in the American Museum of Natural History. American Museum Novitates no. 771:1–12.

26. Boonstra, L. D. 1938. On a South African mammal-like reptile, *Bauria cynops*. Palaeobiologica 6:164–183.

27. Boonstra, L. D. 1953. A new Scaloposaurian genus. The Annals and Magazine of Natural History 6:601–605.

28. Boonstra, L. D. 1954a. The pristerognathid therocephalians from the *Tapinocephalus* zone in the South African Museum. Annals of the South African Museum 42:65–107.

29. Boonstra, L. D. 1954b. A scaloposaurid from the *Tapinocephalus* zone. Annals and Magazine of Natural History 7:153–157.

30. Boonstra, L. D. 1969. The fauna of the *Tapinocephalus* zone (Beaufort Beds of the Karoo). Annals of the South African Museum 56:1–73.

31. Botha, J. 2003. Biological aspects of the Permian dicynodont *Oudenodon* (Therapsida:Dicynodontia) deduced from bone histology and cross-sectional geometry. Palaeontologia Africana 39:37–44.

32. Botha, J., and K. Angielczyk. 2007. An integrative approach to distinguishing the Late Permian dicynodont species *Oudenodon baini* and *Tropidostoma microtrema* (Therapsida: Anomodontia). Palaeontology 50:1175–1209.

33. Botha, J., and A. Chinsamy. 2000. Growth patterns deduced from the histology of the cynodonts *Diademodon* and *Cynognathus*. Journal of Vertebrate Paleontology 20:705–711.

34. Botha, J., and A. Chinsamy. 2004. Growth and lifestyle adaptations of the Triassic non-mammalian cynodont *Trirachodon*. Acta Palaeontologica Polonica 49:619–627.

35. Botha, J., and A. Chinsamy. 2005. Growth patterns of *Thrinaxodon*, a non-mammalian cynodont from the Early Triassic of South Africa. Palaeontology 48:385–394.

36. Botha, J., and R. M. H. Smith. 2006. Rapid vertebrate recuperation in the Karoo Basin of South Africa following the end-Permian extinction. Journal of African Earth Sciences 45:502–514.

37. Botha, J., and R. M. H. Smith. 2007. *Lystrosaurus* species composition across the Permian-Triassic boundary in the Karoo Basin of South Africa. Lethaia 40:125–137.

38. Botha, J., F. Abdala, and R. Smith. 2007. The oldest cynodont: new clues on the origin and early diversification of Cynodontia. Zoological Journal of the Linnean Society 149:477–492.

39. Botha-Brink, J., and K. Angielczyk. 2010. Do extraordinarily high growth rates in Permo-Triassic dicynodonts (Therapsida, Anomodontia) explain their success before and after the end-Permian extinction? Zoological Journal of the Linnean Society 160:341–365.

40. Botha-Brink, J., and S. P. Modesto. 2011. A new skeleton of the therocephalian synapsid *Olivierosuchus parringtoni* from the Lower Triassic South African Karoo Basin. Palaeontology 54:591–606.

41. Botha-Brink, J., and R. M. H. Smith. 2011. Osteohistology of the Triassic archosauromorphs *Prolacerta*, *Proterosuchus*, *Euparkeria*, and *Erythrosuchus* from the Karoo Basin of South Africa. Journal of Vertebrate Paleontology 31:1238–1254.

42. Botha-Brink, J., F. Abdala, and A. Chinsamy-Turan. 2012. The radiation and osteohistology of nonmammaliaform cynodonts. Pp. 223–246 *in* A. Chinsamy-Turan, ed., Forerunners of Mammals: Radiation, Histology, Biology, Indiana University Press, Bloomington.

43. Botha-Brink, J., A. K. Huttenlocker, and S. P. Modesto. In press. Vertebrate paleontology of Nooitgedacht 68: A *Lystrosaurus maccaigi*-rich Permo-Triassic boundary locality in South Africa: *In* C. Kammerer, K. Angielczyk, and J.

Fröbisch (eds.), Early Evolutionary History of the Synapsida. Springer, Dordrecht.

44. Brink, A. S. 1954. On the Whaitsiidae, a family of therocephalian mammal-like reptiles. Transactions of the Royal Society of South Africa 34:43–59.

45. Brink, A. S. 1956. On *Aneugomphius ictidoceps* Broom and Robinson. Palaeontologia Africana 4:97–115.

46. Brink, A. S. 1957. On the skeleton of *Aneugomphius ictidoceps* Broom and Robinson. Palaeontologia Africana 5:29–37.

47. Brink, A. S. 1958. Notes on some whaitsiids and moschorhinids. Palaeontologia Africana 6:23–49.

48. Brink, A. S. 1960. On some small therocephalians. Palaeontologia Africana 7:155–182.

49. Brink, A. S. 1963. On *Bauria cynops* Broom. Palaeontologia Africana 8:39–56.

50. Brink, A. S. 1965. A new ictidosuchid (Scaloposauria) from the *Lystrosaurus*-Zone. Palaeontologia Africana 9:129–138.

51. Brink, A. S. 1980. On the genus *Theriognathus* Owen (including *Whaitsia*, *Notosollasia*, *Alopecopsis*, *Notaelurops*, *Moschorhynchus* and *Aneugomphius*). Annals of the Geological Survey of South Africa 14:1–37.

52. Brink, A. S. 1986. Illustrated bibliographic catalogue of the Synapsida I. Republic of South Africa Department of Energy and Mineral Affairs, Pretoria, South Africa.

53. Brink, A. S. 1988. Illustrated bibliographic catalogue of Synapsida II. Republic of South Africa Department of Energy and Mineral Affairs, Pretoria, South Africa.

54. Brinkman, D. 1981. The structure and relationships of the dromasaurs (Reptilia: Therapsida). Breviora 465:1–34.

55. Broom, R. 1900. On a new theriodont reptile (*Ictidosuchus primaevus*) from the Karroo beds, South Africa. Annals and Magazine of Natural History 6:314–316.

56. Broom, R. 1903. On the classification of the theriodonts and their allies. Report of the South African Association for the Advancement of Science 1:286–294.

57. Broom, R. 1904. On two new Therocephalian reptiles (*Glanosuchus macrops* and *Pristerognathus baini*). Transactions of the South African Philosophical Society 15:85–88.

58. Broom, R. 1905. On the use of the term Anomodontia. Records of the Albany Museum 1:266–269.

59. Broom, R. 1908. On the interrelationships of the known therocephalian genera. Annals of the South African Museum 4:369–372.

60. Broom, R. 1909. Notice of some new South African fossil amphibians and reptiles. Annals of the South African Museum 7:270–278.

61. Broom, R. 1911. On some new South African Permian reptiles. Proceedings of the Zoological Society of London 81:1073–1082.

62. Broom, R. 1914. Croonian lecture: on the origin of mammals. Philosophical Transactions of the Royal Society of London. Series B, Containing Papers of a Biological Character 206:1–48.

63. Broom, R. 1920. On some new therocephalian reptiles from the Karroo beds of South Africa. Proceedings of the Zoological Society 3:343–353.

64. Broom, R. 1925. On some carnivorous therapsids. Records of the Albany Museum 25:309–326.

65. Broom, R. 1931. Notices of some new genera and species of Karroo fossil reptiles. Records of the Albany Museum 4:161–166.

66. Broom, R. 1932. The Mammal-like Reptiles of South Africa and the Origin of Mammals. H. F. & G. Witherby.

67. Broom, R. 1935. On some new genera and species of Karroo fossil reptiles. Annals of the Transvaal Museum 18:55–72.

68. Broom, R. 1936a. On the structure of the skull in the mammal-like reptiles of the suborder Therocephalia. Philosophical Transactions of the Royal Society of London. Series B, Biological Sciences 226:1–42.

69. Broom, R. 1936b. On some new genera and species of Karroo fossil reptiles, with notes on some others. Annals of the Transvaal Museum 18:349–386.

70. Broom, R. 1937. A few more new fossil reptiles from the Karroo. Annals of the Transvaal Museum 19:141–146.

71. Broom, R. 1938. On a new type of primitive fossil reptile from the Upper Permian of South Africa. Proceedings of the Zoological Society of London 108:535–542.

72. Broom, R. 1940. Some new Karroo reptiles from the Graaff-Reinet district. Annals of the Transvaal Museum 20:71–87.

73. Broom, R. 1948. A contribution to our knowledge of the vertebrates of the Karroo beds of South Africa. Transactions of the Royal Society of Edinburgh 61:577–629.

74. Broom, R., and J. T. Robinson. 1948. Some new fossil reptiles from the Karoo Beds of South Africa. Proceedings of the Zoological Society of London 118: 392–407.

75. Buffrénil, V. de, A. Houssaye, and W. Böhme. 2007. Bone vascular supply in monitor lizards (Squamata: Varanidae): implications of size, growth, and phylogeny. Journal of Morphology 269:533–543.

76. Calder, W. A. III. 1984. Size, Function, and Life History. Harvard University Press, Cambridge: 431 pp.

77. Cardillo, M., and L. Bromham. 2001. Body size and extinction risk in Australian mammals. Conservation Biology 15:1435–1440.

78. Carrano, M. T. 2000. Homoplasy and the evolution of dinosaur locomotion. Paleobiology 26:489–512.

79. Carrano, M. T. 2006. Body-size evolution in the Dinosauria: Pp. 225–268 *in* M. T. Carrano, R. W. Blob, T. J. Gaudin, and J. R. Wible (eds.) Amniote

Paleobiology: Perspectives on the Evolution of Mammals, Birds, and Reptiles. University of Chicago Press.

80. Case, T. J. 1978. On the evolution and adaptive significance of postnatal growth rates in the terrestrial vertebrates. The Quarterly Review of Biology 53:243–282.

81. Castanet, J., K. Curry Rogers, J. Cubo, J.-J. Boisard. 2000. Periosteal bone growth rates in extant ratites (ostrich and emu): implications for assessing growth in dinosaurs. Comptes Rendus de l'Académie des Sciences de Paris**,** Science de la Vie 323:543–550.

82. Catuneanu, O., H. Wopfner, P. G. Eriksson, B. Cairncross, B. S. Rubidge, R. M. H. Smith, and P. J. Hancox. 2005. The Karoo basins of south-central Africa. Journal of African Earth Sciences 43:211–253.

83. Chan, K. M. A., and B. R. Moore. 2004. SYMMETREE: whole-tree analysis of differential diversification rates. Bioinformatics 21:1709–1710.

84. Chen, Z.-q., and M. J. Benton. 2012. The timing and pattern of biotic recovery following the end-Permian mass extinction. Nature Geoscience 5:375–383.

85. Chinsamy, A. 1990. Physiological implications of the bone histology of *Syntarsus rhodesiensis* (Saurischia: Theropoda). Palaeontologia Africana. 27:77–82.

86. Chinsamy, A. 1993. Bone histology and growth trajectory of the prosauropod dinosaur *Massospondylus carinatus* Owen. Modern Geology 18:319–329.

87. Chinsamy, A. 2005. The microstructure of dinosaur bone: deciphering biology with fine-scale techniques. Johns Hopkins University Press, Baltimore.

88. Chinsamy, A., and F. Abdala. 2008. Paleobiological implications of the bone microstructure of South American traversodontids (Therapsida: Cynodontia). South African Journal of Science 104:225–230.

89. Chinsamy, A., and J. Hurum. 2006. Bone microstructure and growth patterns of early mammals. Acta Palaeontologica Polonica 51:325–338.

90. Chinsamy, A., and M. Raath. 1992. Preparation of fossil bone for histological examination. Palaeontologia Africana 29:39–44.

91. Chinsamy, A. and B. S. Rubidge. 1993. Dicynodont (Therapsida) bone histology: Phylogenetic and physiological implications. Palaeontologia Africana 30:97–102.

92. Chinsamy-Turan, A. 2012. Forerunners of Mammals: Radiation, Histology, Biology. Indiana University Press, Bloomington.

93. Chinsamy-Turan, A., and S. Ray. 2012. Bone histology of some therocephalians and gorgonopsians, and evidence of bone degradation by fungi: Pp. 199–221 *in* A. Chinsamy-Turan (ed.), Forerunners of Mammals: Radiation, Histology, Biology. Indiana University Press, Bloomington.

94. Clyde, W. C., and P. D. Gingerich. 1998. Mammalian community response to the latest Paleocene thermal maximum: an isotaphonomic study in the northern Bighorn Basin, Wyoming. Geology 26:1011–1014.

95. Colbert, E. H., and J. W. Kitching. 1981. Scaloposaurian reptiles from the Triassic of Antarctica. American Museum Novitates 2709:1–22.

96. Coney, L., W. U. Reimold, P. J. Hancox, D. Mader, C. Koeberl, I. McDonald, U. Struck, V. Vajda, and S. L. Kamo. 2007. Geochemical and mineralogical investigation of the Permian-Triassic boundary in the continental realm of the southern Karoo Basin, South Africa. Palaeoworld 16:67–104.

97. Cooper, L. N., A. H. Lee, M. L. Taper, and J. R. Horner. 2008. Relative growth rates of predator and prey dinosaurs reflect effects of predation. Proceedings of the Royal Society of London B 275:2609–2615.

98. Cope, E. D. 1870. Synopsis of the extinct Batrachia and Reptilia of North America. Transactions of the American Philosophical Society 14:1–235.

99. Cope, E. D. 1877. Descriptions of Extinct Vertebrata from the Permian and Triassic Formamations of the United States. Proceedings of the American Philosophical Society 17:182–193.

100. Cope, E. D. 1878. Descriptions of extinct Batrachia and Reptilia from the Permian formation of Texas. Proceedings of the American Philosophical Society 17:505–530.

101. Cope, E. D. 1887. The Origin of the Fittest. Appleton and Company, New York.

102. Cope, E. D. 1896. The Primary Factors of Organic Evolution. Open Court Publishing Company.

103. Cormack, D. 1987. Ham's histology. Lippincott, New York.

104. Crompton, A. W. 1955. A revision of the Scaloposauridae with special reference to kinetism in this family. Navorsinge van die Nasionale Museum 1:149–183.

105. Cubo, J., F. Ponton, M. Laurin, E. de Margerie, and J. Castanet. 2005. Phylogenetic signal in bone microstructure of sauropsids. Systematic Biology 54:562–574.

106. Cubo, J., N. Le Roy, C. Martinez-Maza, and L. Montes. 2012. Paleohistological estimation of bone growth rate in extinct archosaurs. Paleobiology 38:335–349.

107. Currey, J. D. 1987. The evolution of the mechanical properties of amniote bone. Journal of Biomechanics 20:1035–1044.

108. Currey, J. D. 2002. Bones: Structure and Mechanics, 2nd ed. Princeton University Press, Princeton, N.J.

109. Currey, J. D. 2003. The many adaptations of bone. Journal of Biomechanics 36:1487–1495.

110. Currey, J. D., and R. McN. Alexander. 1985. The thickness of the walls of tubular bones. Journal of Zoology 206:453–468.

111. Curtin, A. J., G. R. Zug, and J. R. Spotila. 2009. Longevity and growth strategies of the desert tortoise (*Gopherus agassizii*) in two American deserts. Journal of Arid Environments 73:463–471.

112. Cys, J. M. 1971. The palate and affinities of *Mirotenthes* (Reptilia: Theriodontia). Journal of Paleontology 45:122–125.

113. Damiani, R., J. Neveling, S. Modesto, and A. Yates. 2003. Barendskraal, a diverse amniote locality from the *Lystrosaurus* Assemblage Zone, Early Triassic of South Africa. Palaeontologia Africana 39:53–62.

114. Díaz-Uriarte, R., and T. Garland. 1996. Testing hypotheses of correlated evolution using phylogenetically independent contrasts: sensitivity to deviations from Brownian motion. Systematic Biology 45:27–47.

115. Durand, J. F. 1991. A revised description of the skull of *Moschorhinus* (Therapsida, Therocephalia). Annals of the South African Museum 99:381–413.

116. Elliot, D. H., E. H. Colbert, W. J. Breed, J. A. Jensen, and J. S. Powell. 1970. Triassic tetrapods from Antarctica: evidence for continental drift. Science 169:1197–1201.

117. Enlow, D. H. 1969. The bone of reptiles: Pp. 45-77 *in* C. Gans, A. Bellairs, and T. Parsons (eds.) Biology of the Reptilia, Volume 1: Morphology A. Academic Press, London.

118. Enlow, D. H., and S. O. Brown. 1956. A comparative histological study of fossil and Recent bone tissues, Part I. Texas Journal of Science 8:405–443.

119. Enlow, D. H., and S. O. Brown. 1957. A comparative histological study of fossil and Recent bone tissues, Part II. Texas Journal of Science 9:186–214.

120. Erickson, G. M., and T. A. Tumanova. 2000. Growth curve of *Psittacosaurus mongoliensis* Osborn (Ceratopsia: Psittacosauridae) inferred from long bone histology. Zoological Journal of the Linnean Society 130:551–566.

121. Erickson, G. M., K. Curry Rogers, and S. A. Yerby. 2001. Dinosaurian growth patterns and rapid avian growth rates. Nature 412:429–433.

122. Erickson, G. M., P. J. Makovicky, P. J. Currie, M. A. Norell, S. A. Yerby, and C. A. Brochu. 2004. Gigantism and comparative life-history parameters of tyrannosaurid dinosaurs. Nature 430:772–775.

123. Erwin, D. H. 1998. The end and the beginning: recoveries from mass extinctions. Trends in Ecology and Systematics 13:344–349.

124. Erwin, D. H. 2006. Extinction: how life on earth nearly ended 250 million years ago. Princeton University Press, Princeton, N.J.

125. Erwin, D. H., S. A. Bowring, and J. Yugan. 2003. End-Permian mass extinctions: a review: Pp. 363–383 *in* C. Koeberl and K. G. MacLeod (eds.) Catastrophic Events and Mass Extinctions: Impacts and Beyond. Geological Society of America Special Paper 356.

126. Evans, A. R., D. Jones, A. G. Boyer, J. H. Brown, D. P. Costa, S. K. M. Ernest, E. M. G. Fitzgerald, M. Fortelius, J. L. Gittleman, M. J. Hamilton, L. E. Harding, K. Lintulaasko, S. K. Lyons, J. G. Okie, J. J. Saarinen, R. M. Sibly, F. A. Smith, P. R. Stephens, J. M. Theodor, and M. D. Uhen. 2012. The maximum rate of mammal evolution. Proceedings of the National Academy of Sciences 109:4187–4190.

127. Felsenstein, J. 1985. Phylogenies and the comparative method. American Naturalist 125:1–15.

128. Findlay, G. H. 1968. On the scaloposaurid skull of Olivieria parringtoni, Brink, with a note on the origin of hair. Palaeontologia Africana 11:47–52.

129. Fourie, H., and B. S. Rubidge. 2007. The postcranial skeletal anatomy of the therocephalian *Regisaurus* (Therapsida: Regisauridae) and its utilization for biostratigraphic correlation. Palaeontologia Africana 42:1–16.

130. Fourie, H., and B. S. Rubidge. 2009. The postcranial skeleton of the basal therocephalian *Glanosuchus macrops* (Scylacosauridae) and comparison of morphological and phylogenetic trends amongst the Theriodontia. Palaeontologia Africana 44:27–39.

131. Francillon-Vieillot, H., V. de Buffrénil, J. Castanet, J. Géraudie, F. J. Meunier, J. Y. Sire, L. Zylberberg, and A. de Ricqlès. 1990. Microstructure and mineralization of vertebrate skeletal tissue: Pp. 471–530 *in* J. G. Carter (ed.) Skeletal Biomineralization: Patterns, Processes and Evolutionary Trends, Vol. I. Van Nostrand Reinhold, New York.

132. Frazier, M. R., H. A. Woods, and J. F. Harrison. 2001. Interactive effects of rearing temperature and oxygen on the development of *Drosophila melanogaster*. Physiological and Biochemical Zoology 74:641–650.

133. Fröbisch, J. 2008 Global taxonomic diversity of anomodonts (Tetrapoda, Therapsida) and the terrestrial rock record across the Permian-Triassic Boundary. PLoS ONE 3(11): e3733. doi:10.1371/journal.pone.0003733.

134. Fröbisch, J. 2013. Vertebrate diversity across the end-Permian mass extinction – separating biological and geological signals. Palaeogeography, Palaeoclimatology, Palaeoecology 372:50–61.

135. Garland, T., A. F. Bennett, and E. L. Rezende. 2005. Phylogenetic approaches in comparative physiology. Journal of Experimental Biology 208:3015–3035.

136. Germain, D., and M. Laurin. 2005. Microanatomy of the radius and lifestyle in amniotes (Vertebrata, Tetrapoda). Zoologica Scripta 34:335–350.

137. Girondot, M., and M. Laurin. 2003. Bone Profiler: a tool to quantify, model, and statistically compare bone-section compactness profiles. Journal of Vertebrate Paleontology 23:458–461.

138. Gotthard K. 2001. Growth strategies of ectothermic animals in temperate environments: Pp. 287–303 *in* D. Atkinson and M. Thorndyke (eds.) Environment and Animal Development: Genes, Life Histories, and Plasticity. BIOS Scientific Publishers, Oxford.

139. Gould, S. J. 1977. Ontogeny and Phylogeny. Belknap Press of Harvard University Press, Cambridge.

140. Gould, S. J. 1997. Cope's rule as psychological artefact. Nature 385:199–200.

141. Gradstein, F. M., and J. G. Ogg. 2004. Geologic Time Scale 2004 – why, how, and where next! Lethaia 37:175–181.

142. Gradstein, F. M., J. G. Ogg, and A. G. Smith. 2004. A Geologic Time Scale. Cambridge University Press: 610 pp.

143. Green, J. L., M. H. Schweitzer, and E.-T. Lamm. 2010. Limb bone histology and growth in *Placerias hesternus* (Therapsida: Anomodontia) from the Upper Triassic of North America. Palaeontology 53:347–364.

144. Hancox, P. J., and B. S. Rubidge. 2001. Breakthroughs in the biodiversity, biogeography, biostratigraphy, and basin analysis of the Beaufort group. Journal of African Earth Sciences 33:563–577.

145. Hancox, P. J., M. A. Shishkin, B. S. Rubidge, and J. W. Kitching. 1995. A threefold subdivision of the *Cynognathus* Assemblage Zone (Beaufort Group, South Africa) and its palaeogeographical implications. South African Journal of Earth Science 91:143–144.

146. Hanken, J., and D. B. Wake. 1993. Miniaturization of body size: organismal consequences and evolutionary significance. Annual Review of Ecology, Evolution, and Systematics 24:501–519.

147. Harries, P. J., and P. O. Knorr. 2009. What does the 'Lilliput Effect' mean? Palaeogeography, Palaeoclimatology, and Palaeoecology 284:4–10.

148. Harries, P. J., E. G. Kauffman, and T. A. Hansen. 1996. Models of biotic survival following mass extinction: Pp. 41–60 *in* M. B. Hart (ed.) Biotic Recovery from Mass Extinction Events. Geological Society of London Special Publication 102.

149. Haughton, S. H. 1918. Some new carnivorous Therapsida, with notes upon the braincase in certain species. Annals of the South African Museum 12:175–216.

150. Haughton, S. H. 1924. A bibliographical list of pre-Stormberg Karroo Reptilia, with a table of horizons. Transactions of the Royal Society of South Africa 12:51–104.

151. Haughton, S. H. 1929. On some new therapsid genera. Annals of the South African Museum 28:55–78.

152. Hayes, J. P., and C. S. O'Connor. 1999. Natural selection on thermogenic capacity of high-altitude deer mice. Evolution 53:1280–1287.

153. Heever, J. A. van den. 1980. On the validity of the therocephalian family Lycosuchidae (Reptilia, Therapsida). Annals of the South African Museum 81:111–125.

154. Heever, J. A. van den. 1987. The comparative and functional cranial morphology of the early Therocephalia (Amniota: Therapsida). Unpublished PhD dissertation. University of Stellenbosch:576 pp.

155. Heever, J. van den. 1994. The cranial anatomy of the early Therocephalia (Amniota: Therapsida). Annals of the University of Stellenbosch 1:1–59.

156. Hillenius, W. J. 2000. Septomaxilla of nonmammalian synapsids: Soft-tissue correlates and a new functional interpretation. Journal of Morphology 245:29–50.

157. Hone, D. W. E., and M. J. Benton. 2005. The evolution of large size: how does Cope's Rule work? TRENDS in Ecology and Evolution 20:4–6.

158. Hopson, J. A. 1991. Systematics of nonmammalian Synapsida and implications for patterns of evolution in Synapsida: Pp. 635–693 *in* H.-P. Schultze and L. Trueb (eds.) Origins of the Higher Groups of Tetrapods: Controversy and Consensus. Cornell University Press, Ithaca.

159. Hopson, J. A. 1994. Synapsid evolution and the radiation of non-eutherian mammals: Pp. 190-219 *in* D. B. Prothero and R. M. Schoch (eds.) Major Features of Vertebrate Evolution. Paleontological Society Short Courses in Paleontology 7. Paleontological Society, Knoxville.

160. Hopson, J. A., and H. Barghusen. 1986. An analysis of therapsid relationships: Pp. 83–106 *in* N. Hotton, P. D. MacLean, J. J. Roth, and E. C. Roth (eds.) The Ecology and Biology of Mammal-like Reptiles. Smithsonian Institution Press, Washington, D.C.

161. Hopson, J. A., and J. W. Kitching. 1972. A revised classification of cynodonts (Reptilia; Therapsida). Palaeontologia Africana 14:71-85.

162. Hopson, J. A., and J. W. Kitching. 2001. A probainognathian cynodont from South Africa and the phylogeny of nonmammalian cynodonts. Bulletin of the Museum of Comparative Zoology 156:5–35.

163. Horner, J. R., A. de Ricqlès, and K. Padian. 2000. Long bone histology of the hadrosaurid dinosaur *Maiasaura peeblesorum*: growth dynamics and physiology based on an ontogenetic series of skeletal elements. Journal of Vertebrate Paleontology 20:115–129.

164. Horner, J. R., K. Padian, and A. de Ricqlès. 2001. Comparative osteohistology of some embryonic and perinatal archosaurs: developmental and behavioral implications for dinosaurs. Paleobiology 27:39–58.

165. Hou, L. 1979. On a new theriodont from Inner Mongolia. Vertebrata Palasiatica 17:121-130.

166. Huene, F. von. 1950. Die Theriodontier des ostafrikanischen Ruhuhu-Gebietes in der Tübinger Sammlung. Neues Jahrbuch für Geologie und Paläontologie Beilage-Band 92:47–136. [in German]

167. Huey, R. B., and P. D. Ward. 2005. Hypoxia, global warming, and terrestrial Late Permian extinctions. Science 308:398-401.

168. Hunt, G. 2007. The relative importance of directional change, random walks, and stasis in the evolution of fossil lineages. Proceedings of the National Academy of Sciences 104:18404–18408.

169. Hunt, G., and M. T. Carrano. 2010. Models and methods for analyzing phenotypic evolution in lineages and clades: Pp. 245–269 *in* J. Alroy and G. Hunt (eds.) Quantitative Methods in Paleobiology: Paleontological Society Papers 16. The Paleontological Society.

170. Huttenlocker, A. K. 2009. An investigation into the cladistic relationships and monophyly of therocephalian therapsids (Amniota: Synapsida). Zoological Journal of the Linnean Society 157:865–891.

171. Huttenlocker, A. K., and J. Botha-Brink. 2013. Body size and growth patterns in the therocephalian *Moschorhinus kitchingi* (Therapsida: Eutheriodontia) before and after the end-Permian extinction in South Africa. Paleobiology 39:253–277.

172. Huttenlocker, A. K., D. Mazierski, and R. Reisz. 2011a. Comparative osteohistology of hyperelongate neural spines in the Edaphosauridae (Amniota: Synapsida). Palaeontology 54:573–590.

173. Huttenlocker, A. K., and E. Rega. 2012. The paleobiology and bone microstructure of pelycosaurian-grade synapsids: Pp. 90–119 *in* A. Chinsamy-Turan (ed.) Forerunners of Mammals: Radiation, Histology, Biology. Indiana University Press, Bloomington.

174. Huttenlocker, A. K., E. Rega, and S. S. Sumida. 2010. Comparative anatomy and osteohistology of hyperelongate neural spines in the sphenacodontids *Sphenacodon* and *Dimetrodon* (Amniota: Synapsida). Journal of Morphology 271:1407–1421.

175. Huttenlocker, A. K., and C. A. Sidor. 2012. Taxonomic revision of therocephalians (Therapsida: Theriodontia) from the Lower Triassic of Antarctica. American Museum Novitates 3738:1–19.

176. Huttenlocker, A. K., C. A. Sidor, and R. M. H. Smith. 2011b. A new specimen of *Promoschorhynchus* (Therapsida: Therocephalia: Akidnognathidae) from the Lower Triassic of South Africa and its implications for theriodont survivorship across the Permo-Triassic boundary. Journal of Vertebrate Paleontology 31:405–421.

177. Huxley, T. H. 1859. On some amphibian and reptilian remains from South Africa and Australia. Quarterly Journal of the Geological Society 15:642–658.

178. Irmis, R. B., J. W. Martz, W. G. Parker, and S. J. Nesbitt. 2010. Re-evaluating the correlation between Late Triassic terrestrial vertebrate biostratigraphy and the GSSP-defined marine stages. Albertiana 38:40–52.

179. Irmis, R. B., J. H. Whiteside, and C. F. Kammerer. 2013. Non-biotic controls of observed diversity in the paleontologic record: An example from the Permo-Triassic Karoo Basin of South Africa. Palaeogeography, Palaeoclimatology, Palaeoecology 372:50–61.

180. Ivakhnenko, M. F. 2011. Permian and Triassic Therocephals (Eutherapsida) of Eastern Europe. Paleontological Journal 45:981–1144.

181. Jablonski, D. 2005. Mass extinctions and macroevolution: Pp. 192–210 *in* E. S. Vrba and N. Eldredge (eds.) Macroevolution: Diversity, Disparity, Contingency. Paleobiology 31(supplement to 2).

182. Jasinoski, S. C., E. J. Rayfield, and A. Chinsamy. 2010. Functional implications of dicynodont cranial suture morphology. Journal of Morphology 271:705–728.

183. Jin, Y., Y. Wang, C. Henderson, B. R. Wardlaw, S. Shen, and C. Cao. 2006. The global boundary stratotype section and point (GSSP) for the base of Changhsingian stage (Upper Permian). Episodes 29:175–182.

184. Kammerer, C., and C. A. Sidor. 2002. Replacement names for the therapsid genera *Criocephalus* Broom 1928 and *Olivieria* Brink 1965. Palaeontologia Africana 38:71–72.

185. Kemp, T. S. 1969. On the functional morphology of the gorgonopsid skull. Philosophical Transactions of the Royal Society of London: Series B 256:1–83.

186. Kemp, T. S. 1972a. Whaitsiid Therocephalia and the origin of cynodonts. Philosophical Transactions of the Royal Society of London: Series B 264:1-54.

187. Kemp, T.S. 1972b. The jaw articulation and musculature of the whaitsiid Therocephalia; pp. 213-230 in K.A. Joysey and T.S. Kemp (eds.), *Studies in Vertebrate Evolution.* Winchester Press, New York, U.S.

188. Kemp, T. S. 1978. Stance and gait in the hindlimb of a therocephalian mammal-like reptile. Journal of Zoology 186:143–161.

189. Kemp, T. S. 1979. The primitive cynodont *Procynosuchus*: functional anatomy of the skull and relationships. Philosophical Transactions of the Royal Society of London: Series B. 288:73–122.

190. Kemp, T. S. 1982. Mammal-like Reptiles and the Origin of Mammals. Academic Press, London: 363 pp.

191. Kemp, T. S. 1986. The skeleton of a baurioid therocephalian therapsid from the Lower Triassic (*Lystrosaurus* Zone) of South Africa. Journal of Vertebrate Paleontology 6:215–232.

192. Kemp, T. S. 2005. The Origin and Evolution of Mammals. Oxford University Press, Oxford: 331 pp.

193. Kemp, T. S. 2006a. The origin and early radiation of the therapsid mammal-like reptiles: a paleobiological hypothesis. Journal of Evolutionary Biology 19:1231–1247.

194. Kemp, T. S. 2006b. The origin of mammalian endothermy: a paradigm for the evolution of complex biological structure. Zoological Journal of the Linnean Society 147:473–488.

195. Keyser, A. W., and A. S. Brink. 1979. A new bauriamorph (*Herpetogale marsupialis*) from the Omingonde Formation (Middle Triassic) of South West Africa. Annals of the Geological Survey of the Republic of South Africa 12:91–105.

196. King, G. M. 1988. Anomodontia. Encyclopedia of Paleoherpetology 17C. Gustav Fischer Verlag, Stuttgart: 174 pp.

197. King, G. M. 1991. Terrestrial tetrapods and the end Permian event: a comparison of analyses. Historical Biology 5:239–255.

198. King, G. M. 1996. A description of the skeleton of a bauriid therocephalian from the Early Triassic of South Africa. Annals of the South African Museum 104:379–393.

199. Kingsolver, J. G., and D. W. Pfennig. 2004. Individual-level selection as a cause of Cope's Rule of phyletic size increase. Evolution 58:1608–1612.

200. Kitching, J. W. 1970. A short review of the Beaufort zoning in South Africa: Pp. 309–312 *in* S. H. Haughton (ed.) IUGS, 2nd Symposium on Gondwana Stratigraphy and Paleontology.

201. Kitching, J. W. 1977. The Distribution of the Karroo Vertebrate Fauna. Bernard Price Institute for Palaeontological Research Memoir 1. The Natal Witness Ltd.: 131 pp.

202. Kriloff, A., D. Germain, A. Canoville, P. Vincent, M. Sache, and M. Laurin. 2008. Evolution of bone microanatomy of the tetrapod tibia and its use in paleobiological inference. Journal of Evolutionary Biology 21:807–826.

203. Laurin, M. 1998. New data on the cranial anatomy of Lycaenops (Synapsida, Gorgonopsidae), and reflections on the possible presence of streptostyly in gorgonopsians. Journal of Vertebrate Paleontology 18:765-776.

204. Laurin, M. 2004. The evolution of body size, Cope's rule and the origin of amniotes. Systematic Biology 53:594–622.

205. Laurin, M., M. Girondot, and M. Loth. 2004. The evolution of long bone microstructure and lifestyle in lissamphibians. Paleobiology 30:589–613.

206. Lee, A. H. 2007. Interplay Between Growth and Mechanics in the Evolution of Bone Microstructure in Dinosaurs. Unpublished Ph.D. dissertation. University of California, Berkeley: 210 pp.

207. Lee, A. H., A. K. Huttenlocker, K. Padian, and H. N. Woodward. 2013. Chapter 8: Analysis of growth rates: Pp. 209–243 *in* K. Padian and E.-T. Lamm (eds.)

Bone Histology of Fossil Tetrapods: Advancing Methods, Analysis, and Interpretation. University of California Press, Berkeley.

208. Lehrmann, D. J., J. Ramezani, S. A. Bowring, M. W. Martin, P. Montgomery, P. Enos, J. L. Payne, M. J. Orchard, W. Hongmei, and W. Jiayong. 2006. Timing and recovery from the end-Permian extinction: geochronologic and biostratigraphic constraints from south China. Geology 34:1053–1056.

209. Lewis, P. O. 2001. A likelihood approach to estimating phylogeny from discrete morphological character data. Systematic Biology 50:913–925.

210. Li, Y. 1984. On a new scaloposaurid from Inner Mongolia. Vertebrata Palasiatica 22:21–28.

211. Liow, L. H., M. Fortelius, E. Bingham, K. Lintulaakso, H. Mannila, L. Flynn, and N. C. Stenseth. 2008. Higher origination and extinction rates in larger mammals. Proceedings of the National Academy of Sciences 105:6097–6102.

212. Liow, L. H., M. Fortelius, K. Lintulaakso, H. Mannila, and N. C. Stenseth. 2009. Lower extinction risk in sleep-or-hide mammals. The American Naturalist 173:264–272.

213. Liu, J., and P. Olsen. 2010. The phylogenetic relationships of Eucynodontia (Amniota: Synapsida). Journal of Mammalian Evolution 17:151–176.

214. Liu, J., B. Rubidge, and J. Li. 2010. A new specimen of *Biseridens qilianicus* indicates its phylogenetic position as the most basal anomodont. Proceedings of the Royal Society B: Biological Sciences 277:285–292.

215. Lucas, S. G. 1998. Global Triassic tetrapod biostratigraphy and biochronology. Palaeogeography, Palaeoclimatology, Palaeoecology 143:347–384.

216. Lucas, S. G. 2001. Chinese Fossil Vertebrates. Columbia University Press: 375 pp.

217. Lucas, S. G. 2005. Permian tetrapod faunachrons. New Mexico Museum of Natural History and Science Bulletin 30:197–201.

218. Lucas, S. G. 2009. Timing and magnitude of tetrapod extinctions across the Permo-Triassic boundary. Journal of Asian Earth Sciences 36:491–502.

219. Luo, G., X. Lai, G. R. Shi, H. Jiang, H. Yin, S. Xie, J. Tong, K. Zhang, W. He, and P. B. Wignall. 2008. Size variation of conodont elements of the *Hindeodus-Isarcicella* clade during the Permian-Triassic transition in South China and its implications for mass extinction. Palaeogeography, Palaeoclimatology, Palaeoecology 264:176–187.

220. MacLeod, K. G., R. M. H. Smith, P. L. Koch, and P. D. Ward. 2000. Timing of mammal-like reptile extinctions across the Permian-Triassic boundary in South Africa. Geology 28:227–230.

221. Maddison, W. P., and D. R. Maddison. 2007. Mesquite: a modular system for evolutionary analysis. Version 2.0. http://mesquiteproject.org

222. Maier, W. 1999. On the evolutionary biology of early mammals with methodological remarks on the interaction between ontogenetic adaptation and phylogenetic transformation. Zoologischer Anzeiger 238:55–74.

223. Maier, W., J. van den Heever, and F. Durand. 1996. New therapsid specimens and the origin of the secondary hard and soft palate of mammals. Journal of Zoological Systematics and Evolutionary Research 34:9–19.

224. Margerie, E. de. 2002. Laminar bone as an adaptation to torsional loads in flapping flight. Journal of Anatomy 201:521–526.

225. Margerie, E. de, J. Cubo, and J. Castanet. 2002. Bone typology and growth rate: testing and quantifying 'Amprino's rule' in the mallard (*Anas platyrhynchos*). Comptes Rendus Biologies 325:221–30.

226. Margerie, E. de, J.-P. Robin, D. Verrier, J. Cubo, R. Groscolas, and J. Castanet. 2004. Assessing a relationship between bone microstructure and growth rate: a fluorescent labeling study in the king penguin chick (*Aptenodytes patagonicus*). Journal of Experimental Biology 207:869–879.

227. Matthews, L. J., C. Arnold, Z. Machanda, and C. L. Nunn. 2011. Primate extinction risk and historical patterns of speciation and extinction in relation to body mass. Proceedings of the Royal Society B 278:1256–1263.

228. McKinney, M. L. 1997. Extinction vulnerability and selectivity: combining ecological and paleontological views. Annual Review of Ecology and Systematics 28:495–516.

229. McShea, D. W. 1994. Mechanisms of large-scale evolutionary trends. Evolution 48(6):1747–1763.

230. Mendrez, C. H. 1972. On the skull of *Regisaurus jacobi*, a new genus and species of Bauriamorpha Watson and Romer 1956 (= Scaloposauria Boonstra 1953), from the *Lystrosaurus*-zone of South Africa: Pp. 191-212 *in* K. A. Josey and T. S. Kemp (eds.) Studies in Vertebrate Evolution. Oliver and Boyd, Edinburgh.

231. Mendrez, C. H. 1974a. Etude du crane d'un jeune specimen de *Moschorhinus kitchingi* Broom, 1920 (?*Tigrisuchus simus* Owen, 1876), Therocephalia, Pristerosauria, Moschorhinidae d'Afrique Australe (Remarques sur les Moschorhinidae et les Whaitsiidae). Annals of the South African Museum 64:71–115. [In French.]

232. Mendrez, C. H. 1974b. A new specimen of *Promoschorhynchus platyrhinus* Brink 1954 (Moschorhinidae) from the *Daptocephalus*-zone (Upper Permian) of South Africa. Palaeontologia Africana 17:69–85.

233. Mendrez, C. H. 1975. Principales variations du palais chez les thérocéphales Sud-Africains (Pristerosauria et Scaloposauria) au cours du Permien Supérieur et du Trias Inférieur. Colloque International C.N.R.S. Problèmes Actuels de Paléontologie-Évolution des Vertébrés 218: 379–408. [in French]

234. Mendrez-Carroll, C. H. 1979. Nouvelle etude du crane du type de *Scaloposaurus constrictus* Owen, 1876, specimen jeune, Therocephalia, Scaloposauria, Scaloposauridae, de la zone a *Cistecephalus* (Permien superieur) d'Afrique australe. Bulletin du Museum National d'Histoire Naturelle C 1:155–201. [in French]

235. Metcalfe, B., R. J. Twitchett, and N. Price-Lloyd. 2011. Size and growth rate of 'Lilliput' animals in the earliest Triassic. Palaeogeography, Palaeoclimatology, Palaeoecology 308:171–180.

236. Midford, P. E., T. Garland, and W. P. Maddison. 2011. PDAP:PDTREE module for Mesquite (version 1.16). http://mesquiteproject.org/pdap_mesquite/index.html.

237. Modesto, S., B. Rubidge, and J. Welman. 1999. The most basal anomodont therapsid and the primacy of Gondwana in the evolution of the anomodonts. Proceedings of the Royal Society of London. Series B: Biological Sciences 266:331–337.

238. Mundil, R., P. Brack, M. Meier, H. Rieber, and F. Oberli. 1996. High resolution U/Pb dating of Middle Triassic volcaniclastics: time-scale calibration and verification of tuning parameters for carbonate sedimentation. Earth and Planetary Science Letters 141:137–151.

239. Mundil, R., I. Metcalfe, K. R. Ludwig, P. R. Renne, F. Oberli, and R. S. Nicoll. 2001. Timing of the Permian-Triassic biotic crisis: implications from new zircon U/Pb age data (and their limitations). Earth and Planetary Science Letters 187:131–145.

240. Mundil, R., K. R. Ludwig, I. Metcalfe, and P. R. Renne. 2004. Age and timing of the Permian mass extinctions: U/Pb dating of closed-system zircons. Science 305:1760–1763.

241. Mutter, R. J., and A. G. Neuman. 2009. Recovery from the end-Permian extinction event: evidence from "Lilliput *Listracanthus*." Palaeogeography, Palaeoclimatology, Palaeoecology 284:22–28.

242. Muttoni, G., A. Nicora, P. Brack, and D. V. Kent. 2004. Integrated Anisian-Ladinian boundary chronology. Palaeogeography, Palaeoclimatology, Palaeoecology 208:85–102.

243. Nasterlack, T., A. Canoville, A. Chinsamy-Turan. 2012. New insights into the biology of the Permian genus *Cistecephalus* (Therapsida, Dicynodontia). Journal of Vertebrate Paleontology 32:1396–1410.

244. Neveling, J. 2004. Stratigraphic and Sedimentological Investigation of the Contact Between the *Lystrosaurus* and the *Cynognathus* Assemblage Zones (Beaufort Group: Karoo Supergroup). Council for Geoscience South Africa Bulletin 137: 165 pp.

245. Nicolas, M., and B. S. Rubidge. 2010. Changes in Permo-Triassic terrestrial tetrapod ecological representation in the Beaufort Group (Karoo Supergroup) of South Africa. Lethaia 43:45–59.

246. Nopsca, F. von. 1923. Die Familien der Reptilien. Fortschritte der Geologie und Palaeontologie, Berlin 2:1–210.

247. Nopsca, F. von. 1928. The genera of reptiles. Palaeobiologica 1:163–188.

248. Norell, M. A., and M. J. Novacek. 1992. The fossil record and evolution: comparing cladistic and paleontologic evidence for vertebrate history. Science 255:1690–1693.

249. Oliveira, T. V., M. B. Soares, C. L. Schultz. 2010. *Trucidocynodon riograndensis* gen. nov. et sp. nov. (Eucynodontia), a new cynodont from the Brazilian Upper Triassic (Santa Maria Formation). Zootaxa 2382:1–71.

250. Osborn, H. F. 1903. On the primary division of the Reptilia into two sub-classes, Synapsida and Diapsida. Science 17:275–276.

251. Owen, R. 1845a. Report on the Reptilian Fossils of South Africa: Part I—Description of certain fossil crania, discovered by A. G. Bain, Esq., in sandstone rocks at the south-eastern extremity of Africa, referable to different species of an extinct genus of Reptilia (*Dicynodon*), and indicative of a new Tribe or Sub-order of Sauria. Transactions of the Geological Society of London 7:59–84.

252. Owen, R. 1845b. Report on the Reptilian Fossils of South Africa: Part II—Description of the skull of a large species of Dicynodon (D. tigriceps, Ow.), transmitted from South Africa by A. G. Bain, Esq. Transactions of the Geological Society of London, Series 2 7:233–240.

253. Owen, R. 1859. On some reptilian remains from South Africa. Edinburgh New Philosophical Journal 10:289–291.

254. Owen, R. 1876. Descriptive and Illustrated Catalogue of the Fossil Reptilia of South Africa in the Collection of the British Museum. Printed by order of the Trustees, London.

255. Owerkowicz, T., R. M. Elsey, and J. W. Hicks. 2009. Atmospheric oxygen level affects growth trajectory, cardiopulmonary allometry and metabolic rate in the American alligator (*Alligator mississippiensis*). Journal of Experimental Biology 212:1237–1247.

256. Owerkowicz, T., F. Andrade, R. Elsey, K. Middleton, and J. Hicks. 2010. Atmospheric hypoxia increases bone robusticity in the American alligator. Journal of Vertebrate Paleontology 30(supplement to 5):142A.

257. Pagel, M. D. 1992. A method for the analysis of comparative data. Journal of Theoretical Biology 156:431–442.

258. Payne, J. L. 2005. Evolutionary dynamics of gastropod size across the end-Permian extinction and through the Triassic recovery interval. Paleobiology 31:269–290.

259. Peters, R. 1983. The Ecological Implications of Body Size. Cambridge University Press, Cambridge: 344 pp.

260. Ranivoharimanana, L., C. F. Kammerer, J. J. Flynn, and A. R. Wyss. 2011. New material of *Dadadon isaloi* (Cynodontia, Traversodontidae) from the Triassic of Madagascar. Journal of Vertebrate Paleontology 31:1292–1302.

261. Ray, S., and A. Chinsamy. 2004. *Diictodon feliceps* (Therapsida, Dicynodontia): bone histology, growth and biomechanics. Journal of Vertebrate Paleontology 24:180–194.

262. Ray, S., J. Botha, and A. Chinsamy. 2004. Bone histology and growth patterns of some nonmammalian therapsids. Journal of Vertebrate Paleontology 24:634–648.

263. Ray, S., A. Chinsamy, and S. Bandyopadhyay. 2005. *Lystrosaurus murrayi* (Therapsida; Dicynodontia): bone histology, growth and lifestyle adaptations. Palaeontology 48:1169–1185.

264. Ray, S., S. Bandyopadhyay, and D. Bhawal. 2009. Growth patterns as deduced from bone microstructure of some selected neotherapsids with special emphasis on dicynodonts: Phylogenetic implications. Palaeoworld 18:53–66.

265. Ray, S., S. Bandyopadhyay, and R. Appana. 2010. Chapter 5: Bone histology of a kannemeyriid dicynodont *Wadiasaurus*: palaeobiological implications: Pp. 73–89 *in* S. Bandyopadhyay (ed.) New Aspects of Mesozoic Biodiversity (Lecture Notes in Earth Sciences 132). Springer, Berlin.

266. Ray, S., J. Botha-Brink, and A. Chinsamy-Turan. 2012. Dicynodont growth dynamics and lifestyle adaptations: Pp. 121–146 *in* A. Chinsamy-Turan (ed.) Forerunners of Mammals: Radiation, Histology, Biology. Indiana University Press, Bloomington.

267. Rego, B. L., S. C. Wang, D. Altiner, and J. L. Payne. 2012. Within- and among-genus components of foraminiferan size evolution during mass extinction, recovery, and background intervals. Paleobiology 38:627–643.

268. Reid, R. E. H. 1984. The histology of dinosaurian bone, and its possible bearing on dinosaurian physiology. Zoological Symposium 52:629–663.

269. Reid, R. E. H. 1985. On supposed Haversian bone from the hadrosaur *Anatosaurus*, and the nature of compact bone in dinosaurs. Journal of Paleontology 59:140–148.

270. Retallack, G. 2013. Permian and Triassic greenhouse crises. Gondwana Research 24:90–103.

271. Retallack, G. J., R. M. H. Smith, and P. D. Ward. 2003. Vertebrate extinction across the Permian-Triassic boundary in the Karoo Basin of South Africa. Bulletin of the Geological Society of America 115:1133–1152.

272. Retallack, G. J., N. D. Sheldon, P. F. Carr, M. Fanning, C. A. Thompson, M. L. Williams, B. G. Jones, and A. Hutton. 2011. Multiple Early Triassic greenhouse crises impeded recovery from Late Permian mass extinction. Palaeogeography, Palaeoclimatology, Palaeoecology 308:233–251.

273. Ricqlès, A. de. 1969. Recherches paléohistologiques sur les os longs des Tétrapodes II—Quelques observations sur la structure des os longs des Thériodontes. Annales de Paléontologie (Vertébrés) 55:1–52. [in French]

274. Ricqlès, A. de. 1974a. Evolution of endothermy: histological evidence. Evolutionary Theory 1:51–80.

275. Ricqlès A. de. 1974b. Recherches paléohistologiques sur les os longs des Tétrapodes IV—Eothériodontes et pélycosaures. Annales de Paléontologie (Vertébrés) 60:3–39. [in French]

276. Ricqlès, A. de. 1976. On bone histology of fossil and living reptiles, with comments on its functional and evolutionary significance: Pp. 123–150 *in* A. d'A. Bellairs and C. B. Cox (eds.) Morphology and biology of reptiles. Academic Press, London.

277. Ricqlès, A. de, K. Padian, F. Knoll, and J. R. Horner. 2008. On the origin of high growth rates in archosaurs and their ancient relatives: complementary histological studies on Triassic archosauriforms and the problem of a "phylogenetic signal" in bone histology. Annales de Paléontologie 94:57–76.

278. Romer, A.S. 1966. Vertebrate Paleontology, 3rd ed. The University of Chicago Press, Chicago and London: 468 pp.

279. Romer, A. S. 1969. The Chañares (Argentina) Triassic reptile fauna. V. A new chiniquodontid cynodont, *Probelesodon lewisi*—cynodont ancestry. Breviora 333:1–24.

280. Romer, A. S. and L. I. Price. 1940. Review of the Pelycosauria. Geological Society of America Special Paper 28:1–538.

281. Ronquist, F., P. van der Mark, and J. P. Huelsenbeck. 2009. Bayesian phylogenetic analysis using MrBayes. *In* A. M. Vandamme, M. Salemi, and P. Lemey (eds.) The Phylogenetic Handbook 2nd Edition. Cambridge University Press, Cambridge.

282. Roopnarine, P. D., and K. D. Angielczyk. 2012. The evolutionary palaeoecology of species and the tragedy of the commons. Biology Letters 8:147–150.

283. Roopnarine, P. D., K. D. Angielczyk, S. C. Wang, and R. Hertog. 2007. Trophic network models explain instability of Early Triassic terrestrial communities. Proceedings of the Royal Society of London B 274:2077–2086.

284. Roth, J. J, E. C. Roth, and N. Hotton III. 1986. The parietal foramen and eye: their function and fate in therapsids: Pp. 173–184 *in* N. Hotton, P. D. MacLean, J. J. Roth, and E. C. Roth (eds.) The Ecology and Biology of Mammal-like Reptiles. Smithsonian Institution Press, Washington, D.C.

285. Rowe, T. 1986. Osteological Diagnosis of Mammalia, L. 1758, and its Relationship to Extinct Synapsida. Unpublished Ph.D. dissertation. University of California, Berkeley.

286. Rowe, T. 1988. Definition, diagnosis and origin of Mammalia**.** Journal of Vertebrate Paleontology 8:241–264.

287. Ruben, J. A., W. J. Hillenius, T. S. Kemp, and D. E. Quick. 2012. The evolution of mammalian endothermy: Pp. 273–286 *in* A. Chinsamy-Turan (ed.) Forerunners of Mammals: Radiation, Histology, Biology. Indiana University Press, Bloomington.

288. Rubidge, B. S. 1988. A palaeontological and palaeoenvironmental synthesis of the Permian Ecca-Beaufort contact in the southern Karoo between Prince Albert and

Rietbron, Cape Province, South Africa. Unpublished Ph.D. dissertation, University of Port Elizabeth.

289. Rubidge, B. S. 1995. Biostratigraphy of the Beaufort Group (Karoo Supergroup). South African Committee for Stratigraphy Biostratigraphic Series 1, Geological Survey of South Africa: 46 pp.

290. Rubidge, B. S. 2005. Reuniting lost continents – Fossil reptiles from the ancient Karoo and their wanderlust. South African Journal of Geology 108:135–172.

291. Rubidge, B. S., and J. A. Hopson. 1990. A new anomodont therapsid from South Africa and its bearing on the ancestry of Dicynodontia. South African Journal of Science 86:43–45.

292. Rubidge, B. S., and J. A. Hopson. 1996. A primitive anomodont therapsid from the base of the Beaufort Group (Upper Permian) of South Africa. Zoological Journal of the Linnean Society 117:115–139.

293. Rubidge, B. S., and C. A. Sidor. 2001. Evolutionary patterns among Permo-Triassic therapsids. Annual Review of Ecology and Systematics 32: 449–480.

294. Rubidge, B. S., J. W. Kitching, and J. A. van den Heever. 1983. First record of a therocephalian (Therapsida: Pristerognathidae) from the Ecca of South Africa. Navorsing Nasionale Museum, Bloemfontein 4:229–235.

295. Rubidge, B. S., D. H. Erwin, J. Ramezani, S. A. Bowring, and W. J. de Klerk. 2013. High-precision temporal calibration of Late Permian biostratigraphy: U-Pb constraints from the Karoo Supergroup, South Africa. Geology 41:363–366.

296. Russell, G. A., E. L. Rezende, and K. A. Hammond. 2008. Development partly determines the aerobic performance of adult deer mice, *Peromyscus maniculatus*. Journal of Experimental Biology 211:35–41.

297. Ruta, M., D. Pisani, G. T. Lloyd, and M. J. Benton. 2007. A super-tree of Temnospondyli: cladogenetic patterns in the most species-rich group of early tetrapods. Proceedings of the Royal Society B 274:3087–3095.

298. Rybczynski, N. 2000. Cranial anatomy and phylogenetic position of *Suminia getmanovi*, a basal anomodont (Amniota: Therapsida) from the Late Permian of Eastern Europe. Zoological Journal of the Linnean Society 130:329–373.

299. Sahney, S., and M. J. Benton. 2008. Recovery from the most profound mass extinction of all time. Proceedings of the Royal Society of London B 275:759–765.

300. Secord, R., J. I. Bloch, S. G. B. Chester, D. M. Boyer, A. R. Wood, S. L. Wing, M. J. Kraus, F. A. McInerney, and J. Krigbaum. 2012. Evolution of the earliest horses driven by climate change in the Paleocene-Eocene thermal maximum. Science 335:959–962.

301. Seeley, H. G. 1889. Researches on the Structure, Organization, and Classification of the Fossil Reptilia. VI. On the Anomodont Reptilia and their Allies. Philosophical Transactions of the Royal Society B 180:215–296.

302. Seeley, H. G. 1894. Researches on the Structure, Organization, and Classification of the Fossil Reptilia. IX, Section 1. On the Therosuchia. Philosophical Transactions of the Royal Society B 185:987–1018.

303. Seeley, H. G. 1895. Researches on the Structure, Organization, and Classification of the Fossil Reptilia. IX, Section 5. On the skeleton in new Cynodontia from the Karroo rocks. Philosophical Transactions of the Royal Society B 186:59–148.

304. Sereno, P. C. 2007. Logical basis for morphological characters in phylogenetics. Cladistics 23:565–587.

305. Shen, S.-Z., J. L. Crowley, Y. Wang, S. A. Bowring, D. H. Erwin, P. M. Sadlet, C.-q. Cao, D. H. Rothman, C. M. Henderson, J. Ramezani, H. Zhang, Y. Shen, X.-d. Wang, W. Wang, L. Mu, W.-z. Li, Y.-g. Tang, X.-l. Liu, L.-j. Liu, Y. Zeng, Y.-f. Jiang, and Y.-g. Jin. 2011. Calibrating the end-Permian mass extinction. Science 334:1367–1372.

306. Sidor, C. A. 2001. Simplification as a trend in synapsid cranial evolution. Evolution 55:1419–1442.

307. Sidor, C. A. 2003. Evolutionary trends and the origin of the mammalian lower jaw. Paleobiology 29: 605–640.

308. Sidor, C. A., and P. J. Hancox. 2006. *Elliotherium kersteni*, a new tritheledontid from the lower Elliot Formation (Upper Triassic) of South Africa. Journal of Paleontology 80:333–342.

309. Sidor, C. A., and J. A. Hopson. 1998. Ghost lineages and "mammalness": assessing the temporal pattern of character acquisition in the Synapsida. Paleobiology 24:254–273.

310. Sidor, C. A., and R. M. H. Smith. 2004. A new galesaurid (Therapsida: Cynodontia) from the Lower Triassic of South Africa. Palaeontology 46:535–556.

311. Sidor, C. A., R. M. H. Smith, A. K. Huttenlocker, and B. R. Peecook. In press. New Middle Triassic tetrapods from the upper Fremouw Formation of Antarctica and their depositional setting. Journal of Vertebrate Paleontology 34.

312. Sidor, C. A., D. A. Vilhena, K. D. Angielczyk, A. K. Huttenlocker, S. J. Nesbitt, B. R. Peecook, J. Sébastien Steyer, R. M. H. Smith, and L. A. Tsuji. 2013. Provincialization of terrestrial faunas following the end-Permian mass extinction. Proceedings of the National Academy of Sciences 110:8129–8133.

313. Sigogneau, D. 1963. Note sur une nouvelle espece de Scaloposauridae. Palaeontologia Africana 8: 13–37. [in French]

314. Sigogneau, D. 1970. Révision systématique des Gorgonopsians Sud-Africains. Cahiers de Paléontologie, Paris: 414 pp.

315. Sigogneau, D., Tchudinov, P.K. 1972. Reflections on some Russian eotheriodonts (Reptilia, Synapsida, Therapsida). Palaeovertebrata 5:1–30.

316. Sigogneau-Russell D. 1989. Theriodontia I. Encyclopedia of Paleoherpetology 17B. Gustav Fischer Verlag, Stuttgart: 127 pp.

317. Sigurdsen, T. 2006. New features of the snout and orbit of a therocephalian therapsid from South Africa. Acta Palaeontologica Polonica 51:63–75.

318. Sigurdsen, T. A. K. Huttenlocker, S. P. Modesto, T. Rowe, and R. Damiani. 2012. Reassessment of the morphology and paleobiology of the therocephalian

Tetracynodon darti (Therapsida), and the phylogenetic relationships of Baurioidea. Journal of Vertebrate Paleontology 32:1113–1134.

319. Smith, R. M. H. 1995. Changing fluvial environments across the Permian-Triassic boundary in the Karoo Basin, South Africa and possible causes of tetrapod extinctions. Palaeogeography, Palaeoclimatology, Palaeoecology 117:81–104.

320. Smith, R. M. H., and J. Botha. 2005. The recovery of terrestrial vertebrate diversity in the South African Karoo Basin after the end-Permian extinction. Comptes Rendus Palevol 4:623–636.

321. Smith, R. M. H., and P. D. Ward. 2001. Pattern of vertebrate extinctions across an event bed at the Permian-Triassic boundary in the Karoo Basin of South Africa. Geological Society of America 29:1147–1150.

322. Smith, R., B. Rubidge, and M. van der Walt. 2012. Therapsid biodiversity patterns and paleoenvironments of the Karoo Basin, South Africa: Pp. 31–62 *in* A. Chinsamy-Turan (ed) Forerunners of Mammals: Radiation, Histology, Biology. Indiana University Press, Bloomington.

323. Snyder, L. R. G. 1981. Deer mouse hemoglobins: is there genetic adaptation to high altitude? BioScience 31:299–304.

324. Song, H., J. Tong, and Z. Q. Chen. 2011. Evolutionary dynamics of the Permian-Triassic foraminifer size: Evidence for Lilliput effect in the end-Permian mass extinction and its aftermath. Palaeogeography, Palaeoclimatology, Palaeoecology 308:98–110.

325. Sookias, R. B., R. J. Butler, and R. B. J. Benson. 2012a. Rise of dinosaurs reveals major body-size transitions are driven by passive processes of trait evolution. Proceedings of the Royal Society B 279:2180–2187.

326. Sookias, R. B., R. B. J. Benson, and R. J. Butler. 2012b. Biology, not environment, drives major patterns in maximum tetrapod body size through time. Biology Letters 8:674–677.

327. Stanley, S. M. 1973. An explanation for Cope's rule. Evolution 27:1–26.

328. Stearns, S. C. 1992. The Evolution of Life Histories. Oxford University Press, Oxford: 249 pp.

329. Stein, K., and E. Prondvai. 2013. Rethinking the nature of fibrolamellar bone: an integrative biological revision of sauropod plexiform bone formation. Biological Reviews of the Cambridge Philosophical Society 2013. doi: 10.1111/brv.12041

330. Sun, A. 1981. Reidentification of *Traversodontoides wangwuensis* Young. Vertebrata Palasiatica 19:1–4.

331. Sun, A. 1991. A review of Chinese therocephalian reptiles. Vertebrata Palasiatica 29:85–94.

332. Sun, A., and L. Hou. 1981. *Hazhenia*, a new genus of Scaloposauria. Acta Palaeontologica Sinica 20:297–311.

333. Swofford, D. 1999. PAUP* phylogenetic analysis using parsimony, Version 4.0 beta 10. Sinauer Associates, Sunderland, MA.

334. Tatarinov, L. P. 1963. A new Late Permian therocephalian. Paleontological Journal 4:76–94. [in Russian]

335. Tatarinov, L. P. 1968. New Theriodonts from the Upper Permian of the USSR: Pp. 32–46 *in* Verkhnepaleozoiskie i mezozoiskie zemnovodnye i presmykayushchiesya SSSR (Upper Paleozoic and Mesozoic Amphibians and Reptiles of the USSR). Moscow. [in Russian]

336. Tatarinov, L. P. 1973. Cynodonts of Gondwanan appearance in the Middle Triassic of the USSR. Paleontological Journal (1973) no. 2:83–89. [in Russian]

337. Tatarinov, L. P. 1974. Theriodonts of the USSR. Trudy Paleontologicheskogo Instituta, Akademii Nauk SSSR 143:1–240. [in Russian]

338. Tatarinov, L. P. 1977. A new Theriodont from the Lower Triassic of the Orenburg Region. Paleontological Journal (1977) no. 4:88–100. [in Russian]

339. Tatarinov, L. P. 1995a. *Viatkosuchus sumini*, a new Late Permian therocephalian from the Kirov region. Paleontological Journal 29:111–128.

340. Tatarinov, L.P. 1995b. A new ictidosuchid *Karenites ornamentatus* (Theriodontia) from the Upper Permian of the Kotel'nich Locality in the Kirov Region. Russian Journal of Herpetology 2:18–33.

341. Tatarinov, L. P. 1997. A new Scaloposaurid (Reptilia, Theriodontia) with an extraordinary sensory system from the Upper Permian of the Kirov Region. Paleontological Journal 31:669–676.

342. Tatarinov, L. P. 1999. The first Scaloposaurid (Reptilia, Theridontia) from Russia (Upper Permian, Kirov Region). Paleontological Journal 33:278–288.

343. Tatarinov, L. P. 2000. New material on Scaloposaurians (Reptilia, Theriodontia) from the Upper Permian of the Kotelnich Locality, Kirov Region. Paleontological Journal 34:179–186.

344. Thomason, J. J., and A. P. Russell. 1986. Mechanical factors in the evolution of the mammalian secondary palate: a theoretical analysis. Journal of Morphology 189:199–213.

345. Tverdokhlebov, V. P., G. I. Tverdokhlebova, A. V. Minikh, M. V. Surkov, and M. J. Benton. 2005. Upper Permian vertebrates and their sedimentological context in the South Urals, Russia. Earth-Science Reviews 69:27–77.

346. Twitchett, R. J. 2007. The Lilliput effect in the aftermath of the end-Permian extinction event. Palaeogeography, Palaeoclimatology, Palaeoecology 252:132–144.

347. Twitchett, R. J., and C. G. Barras. 2004. Trace fossils in the aftermath of mass extinction events: Pp. 397-418 *in* D. McIlroy (ed.) The Application of Ichnology to Palaeoenvironmental and Stratigraphic Analysis, Geological Society Special Publications 228. Geological Society of London, London.

348. Twitchett, R. J., C. V. Looy, R. Morante, H. Visscher, and P. B. Wignall. 2001. Rapid and synchronous collapse of marine and terrestrial ecosystems during the end-Permian biotic crisis. Geology 29:351–354.

349. Urbanek, A. 1993. Biotic crises in the history of Upper Silurian graptoloids: a paleobiological model. Historical Biology 7:29–50.

350. VandenBrooks, J. M. 2007. The effects of varying partial pressure of oxygen on vertebrate development and evolution. Unpublished Ph.D. dissertation. Yale University, New Haven.

351. Ward P. D., J. Botha, R. Buick, M. O. De Kock, D. H. Erwin, G. H. Garrison, J. L. Kirschvink, and R. Smith. 2005. Abrupt and gradual extinction among Late Permian land vertebrates in the Karoo Basin, South Africa. Science 307:709–714.

352. Vjuschkov, B. P. Therocephals of the Soviet Union: Pp. 128-175 *in* I. A. Efremov (ed.) Materials of the Permian and Triassic Terrestrial Vertebrates of the USSR. Trudy Paleontologicheskogo Instituta, Akademii Nauk SSSR, 1955, vol, 49. [in Russian]

353. Wall, P. W. 1983. The correlation between high limb-bone density and aquatic habitats in recent mammals. Journal of Paleontology 57:197–207.

354. Ward, P. D., J. Botha, R. Buick, M. O. Dekock, D. H. Erwin, G. Garrison, J. Kirschvink, and R. M. H. Smith. 2005. Abrupt and gradual extinction among Late Permian land vertebrates in the Karoo Basin, South Africa. Science 307:709–714.

355. Watson, D. M. S. 1914. The zones of the Beaufort beds of the Karroo system of South Africa. Geological Magazine 1:203–208.

356. Watson, D. M. S. 1931. On the skeleton of a bauriamorph reptile. Proceedings of the Zoological Society of London 1931:1163–1205.

357. Watson, D. M. S., and A. S. Romer. 1956. A classification of therapsid reptiles. Bulletin of the Museum of Comparative Zoology, Harvard 111:37–89.

358. Wilson, G. P. 2013. Mammals across the K/Pg boundary in northeastern Montana, U.S.A.: dental morphology and body-size patterns reveal extinction selectivity and immigrant-fueled ecospace filling. Paleobiology 39:429–469.

359. Wilson, G. P., A. R. Evans, I. J. Corfe, P. D. Smits, M. Fortelius, and J. Jernvall. 2012. Adaptive radiation of multituberculate mammals before the extinction of dinosaurs. Nature 483:457–460.

360. Wilson, J. W. 1994. Histological techniques: Pp. 205–234 *in* P. Leiggi and P. May, (eds.) Vertebrate Paleontological Techniques. Cambridge University Press, New York.

361. Woodward, H. N., J. R. Horner, and J. O. Farlow. 2011. Osteohistological evidence for determinate growth in the American alligator. Journal of Herpetology 45:339–342.

362. Woods, H. A., and R. I. Hill. 2004. Temperature-dependent oxygen limitations in insect eggs. Journal of Experimental Biology 207:2267–2276.

363. Young, C.-c. 1952. On a new therocephalian from Sinkiang, China. Acta Scientia Sinica 1:152–165.

364. Young, C.-c. 1961. A new cynodont from NW Shansi. Vertebrata Palasiatica 2:109–113. [in Chinese]

365. Young, C.-c. 1974. A new traversodont from Jiyuan, Henan. Vertebrata Palasiatica 12: 203–206. [in Chinese]

APPENDIX 2. Specimens and sources for phylogenetic analysis.

Taxon:	Source:
Akidnognathus parvus	SAM-PK-4021 (holotype); BP/1/499 ('*Proalopecopsis'* type); BP/1/641 (cast); Brink, 1960
Alopecodon priscus	SAM-PK-920 (holotype); AMNH 5569
Annatherapsidus petri	Tatarinov, 1974; Ivakhnenko, 2011 (PIN 2005/1993)
Anomodontia	AMNH 5536 (*Galeops whaitsi*); AMNH 5541 (*Galepus jouberti*); Brinkman, 1981; Rubidge and Hopson, 1990, 1996; Modesto et al., 1999; Rybczynski, 2000; Liu et al., 2010
Antecosuchus ochevi	Tatarinov, 1974; Ivakhnenko, 2011 (PIN 1579/53; 2865/595, 596)
Bauria cynops	SAM-PK-1333 (holotype); SAM-PK-5875 ('*Aelurosuchus*' type); AMNH 5622; NHMUK R4095 ('*Baurioides'* type); UCM 39522 (cast); UCMP 42804; Brink, 1963
Biarmosuchus tener	Sigogneau and Tchudinov, 1972; Sigogneau-Russell, 1989
Cerdosuchoides brevidens	RC 58 (*'Cerdops'* type); AM 4208 ('*Hewittia*' type); CGS CM86-778
Charassognathus gracilis	SAM-PK-10364 (holotype); Botha et al., 2007
Chthonosaurus velocidens	PIN 521/1 (holotype); Tatarinov, 1974; Ivakhnenko, 2011
Dvinia prima	UCMP 177307 (cast of type PIN 2005/2465); Tatarinov, 1974
Ericiolacerta parva	AMNH 9542; Watson, 1931; Mendrez 1975; Colbert and Kitching, 1981; Hopson and Barghusen, 1986
Euchambersia mirabilis	NHMUK R5696 (holotype); BP/1/4009; Boonstra, 1934; Brink, 1988
Glanosuchus macrops	SAM-PK-637 (holotype); AMNH 5559; UCMP 42669; BP/1/6228; NMQR 2908; SAM-PK-K7808; SAM-PK-K7809; Boonstra, 1954a; van den Heever, 1994; Abdala et al., 2008
Gorgonopsia	AMNH 5515, UCM 23384 (*Gorgonops torvus*); AMNH 5537 (*Lycaenops angusticeps*); Kemp, 1969; Sigogneau-Russell, 1989; Laurin, 1998
Hazhenia concava	Sun and Hou, 1981; Sun, 1991 (IVPP V5866)

Taxon:	Source:
Hofmeyria atavus	TM 254 (holotype); RC 639; BP/1/4401; BP/1/4404; Broom, 1935; Hopson and Barghusen, 1986; Brink, 1988; Sidor 2001, 2003
Ictidochampsa platyceps	RC 69 (holotype)
Ictidosaurus angusticeps	SAM-PK-630 (holotype); NMQR 2910; Abdala et al., 2008
Ictidostoma hemburyi	AMNH 5520 (holotype); AMNH 5521; BP/1/3052; SAM-PK-K6731; Broom, 1932; Boonstra, 1935; Brink, 1960; Hillenius, 2000
Ictidosuchoides longiceps	NHMUK R5744 (holotype); CGS CM86-655; BP/1/4092; SAM-PK-K8659, K10423; UCMP 42702; Boonstra, 1934; Brink, 1960, 1988; Mendrez, 1975; Sidor, 2003
Ictidosuchops rubidgei	RC 6 (holotype); CGS CM86-486
Ictidosuchus primaevus	AMNH 5529 (holotype); SAM-PK-K10650; Broom, 1932; Boonstra, 1935; Hopson & Barghusen, 1986; Brink, 1988
Karenites ornamentatus	Tatarinov, 1995b, 1999; Ivakhnenko, 2011 (PIN 2212/60, 93, 97)
Lycideops longiceps	NHMUK R5695 (holotype); CGS JNN10-0-02; RC 646; Boonstra, 1934; Mendrez, 1975; Brink, 1988; Hopson and Barghusen, 1986
Lycosuchidae indet.	UCMP 42395 (unidentified lycosuchid); van den Heever, 1994: figs. 4, 5, 7 (GS C60, Lycosuchidae indet.)
Lycosuchus vanderrieti	SAM-PK-12185 (‘*Zinnosaurus*’ type); SAM-PK-9084; SAM-PK-K9012; van den Heever, 1994
Microgomphodon oligocynus	NHMUK R3305 (holotype); NMQR 3189, 3596; SAM-PK-K10160
Mirotenthes digitipes	UCMP 40467 (holotype); CGP-1-1264; SAM-PK-K6511; Attridge, 1956; Cys, 1971
Moschorhinus kitchingi	NHMUK R5698 (holotype); BP/1/4227; BP/1/4636; NMQR 3351; Mendrez, 1974a; Hopson and Barghusen, 1986; Durand, 1991; Sidor, 2003
Moschowhaitsia vjuschkovi	PIN 1100/20 (holotype); Kemp, 1972a; Tatarinov, 1974; Brink, 1986; Hopson and Barghusen, 1986; Ivakhnenko, 2011
new *Cistecephalus* AZ akidnognathid	USNM PAL412421
new *Cistecephalus* AZ hofmeyriid	SAM-PK-K8516

APPENDIX 1. List of institutional abbreviations.

AM, Albany Museum, Grahamstown; **AMNH**, American Museum of Natural History, New York; **BP**, Evolutionary Studies Institute (previously Bernard Price Institute for Palaeontological Research), University of Witwatersrand, Johannesburg; **CAMZM**, University Museum of Zoology, Cambridge; **CGP**, Council for Geoscience Palaeontology Collection, Pretoria; **CGS**, Council for Geoscience, Pretoria (former Geological Survey field numbers); **GSN**, Geological Survey of Namibia, Windhoek; **FMNH**, Field Museum of Natural History, Chicago; **IVPP**, Institute of Vertebrate Paleontology and Paleoanthropology, Chinese Academy of Sciences, Beijing; **MCN,** Museu de Ciências Naturais, Fundação Zoobotânica do Rio Grande do Sul, Porto Alegre; **MCZ**, Harvard University Museum of Comparative Zoology, Cambridge; **MGB**, Museo Guido Borgomanero, Mata; **MVP**, Museu Vicente Pallotti, Santa Maria; **NHCC**, National Heritage Conservation Commission, Lusaka; **NHMUK**, Natural History Museum, London; **NMQR**, National Museum, Bloemfontein; **PIN**, Paleontological Institute, Moscow; **PKUP**, Peking University Paleontology Collections, Beijing; **PULR**, Universidad Nacional de La Rioja; **PVL**, Fundación Miguel Lillo, Tucumán; **PVSJ**, Museo de Ciencias Naturales, Universidad Nacional de San Juan, San Juan; **RC**, Rubidge Collection, Wellwood, Graaff-Reinet; **SAM**, Iziko South African Museum, Cape Town; **TM**, Ditsong National Museum of Natural History (former Transvaal Museum), Pretoria; **UCM**, University of Colorado Museum of Natural History, Boulder; **UCMP**, University of California Museum of Paleontology, Berkeley; **UFRGS**, Universidade Federal do Rio Grande do Sul, Porto Alegre; **USNM**, National Museum of Natural History, Washington, D.C.

Taxon:	Source:
new *Tropidostoma* AZ whaitsiid	SAM-PK-K10990, K10984
new Zambian chthonosaurid	NHCC LB36, 38
new Zambian karenitid	NHCC LB44
Nothogomphodon danilovi	Tatarinov, 1974; Ivakhnenko, 2011 (PIN 2865/1)
Olivierosuchus parringtoni	BP/1/3849 (holotype); BP/1/3973; NMQR 62, 3605; SAM-PK-K117; Brink, 1965; Findlay, 1968; Sidor, 2001, 2003; Botha-Brink and Modesto, 2011
Ordosiodon youngi	Hou, 1979; Sun, 1991 (IVPP V4786)
Pardosuchus whaitsi	SAM-PK-1077 (holotype)
Perplexisaurus foveatus	Tatarinov, 1997; Ivakhnenko, 2011 (PIN 2212/15, 19, 90)
Pristerognathus polyodon	NHMUK R2581 (holotype); SAM-PK-11942 (‘*Ptomalestes’* type); Boonstra, 1954; Mendrez, 1975; van den Heever, 1994
Procynosuchus delaharpeae	AMNH 8220; Kemp, 1979
Promoschorhynchus platyrhinus	BP/1/484 (holotype); CGS K85 (reported as ‘R85’ by Mendrez, 1974b); RC 116; SAM-PK-K10014; Mendrez, 1974b; Huttenlocker et al., 2011b
Regisaurus jacobi	BP/1/5394 (holotype); BP/1/5895; CGS AK86-7; SAM-PK-K10613; Mendrez, 1972
Scaloposaurus constrictus	NHMUK R1723 (holotype); SAM-PK-K10023, K10403; Mendrez-Carroll, 1979
Scylacosaurus sclateri	SAM-PK-634 (holotype); SAM-PK-11888 (‘*Therioides’* type)
Silphedosuchus orenburgensis	Battail and Surkov, 2000; Ivakhnekno, 2011 (PIN 951/100)
Tetracynodon tenuis	RC 89
Tetracynodon darti	BP/1/2710 (holotype); BP/1/6026; NMQR 3756; UCMP 42869; UCMP 78394–96; Sigogneau, 1963; Sigurdsen et al., 2012
Theriognathus microps	NHMUK R47065 (holotype); BP/1/182 (‘*Aneugomphius*’ type); BP/1/512; BP/1/785; BP/1/844; BP/1/4008; UCM 23381; UCM 39524 (cast); UCMP 42675; UCMP 42676; Kemp, 1972a, 1972b; Brink, 1956, 1957, 1980
Titanophoneus potens	King, 1988

Taxon:	Source:
Traversodontoides wangwuensis	Sun, 1981; Sun, 1991 (IVPP V4068)
Urumchia lii	Young, 1952; Sun, 1991
Viatkosuchus sumini	PIN 2212/13 (holotype); Tatarinov, 1995a; Sidor, 2001, 2003

APPENDIX 3. List of 135 craniodental and postcranial characters scored for phylogenetic analysis of 56 therapsid taxa (including 49 therocephalians). Characters are from Sigurdsen et al. (2012) and references cited therein. Characters 4 and 53 of Sigurdsen et al. (2012) were deemed redundant and omitted accordingly; characters 130–135 in the present analysis are new.

(1) Premaxilla: does not overhang incisor region (0); anterodorsal most tip of premaxilla forms a rostral process, overhanging incisors (1).

(2) Septomaxilla shape: long, narrow and moderately well exposed on facial region (0); enlarged and well exposed outside of external naris, broadly overlapping premaxilla anteriorly (1). (From Botha et al., 2007)

(3) External nare shape: moderately large and face anterolaterally (0); enlarged, close-set, and face more anteriorly (1).

(4) Dorsal profile of antorbital region: convex (0); relatively straight (1). (From Sidor and Hopson, 1998)

(5) Constriction of snout directly behind caniniform(s): absent (0); present (1). (From van den Heever, 1994)

(6) Preorbital depression: absent (0); present anterior to a thickened ridge on anterior margin of orbit, extending from lacrimal to canine buttress of maxilla (1).

(7) Maxilla facial plate (or 'dorsal lamina') shape: high (0); low with a height less than 40% its length (1).

(8) Maxilla facial plate concave ventral step: present between anterior-most maxillary teeth and incisors (0); absent (1).

(9) Broad excavation or pit in the maxilla immediately posterior to the dominant canine: absent (0); present (1).

(10) Posterior region of maxillary facial plate folded inward onto palatal region, so that maxilla is well exposed in ventral view just anterior to orbit: absent (0); present (1).

(11) Suborbital bar depth: shallow (0); deep (1). (From van den Heever, 1994)

(12) Suborbital bar lateral expansion: absent (0); slightly expanded and extends from jugal onto posterior part of maxillary facial plate, contributing to a pronounced degree of orbital convergence (i.e., orbits facing forward and appearing more triangular than oval in dorsal view) (1).

(13) Long, low rostrum just anterior to orbital region: absent (0); present (1).

(14) Anterior border of orbit location: posterior half of skull (0); anterior half of skull (1); near transverse midline (2). (Modified from van den Heever, 1994)

(15) Jugal postorbital process: present (0); absent (1).

(16) Postorbital bar: moderately well-built (0); extremely slender (1); absent/unossified (2).

(17) Ventral edge of zygomatic arch shape (behind orbit): distinct posteroventral orientation (0); relatively straight / horizontal (1); curved, having a concave ventral margin throughout its length (2).

(18) V-shaped, posterior border of nasals: absent (0); present, pointing toward occiput (1). (Modified from van den Heever, 1994)

(19) Median frontonasal crest: absent (0); present (1).

(20) Postfrontal: present (0); absent (1). (From Hopson and Barghusen, 1986; Sidor, 2001; Botha et al., 2007)

(21) Parietal (= pineal) opening: present irrespective of ontogenetic stage (0); absent or extremely reduced (1). (Modified from Rubidge and van den Heever, 1997; Botha et al., 2007)

(22) Temporal fenestra size in adults: fenestra and orbit subequal in size (0); fenestra larger than orbit (1). (Modified from Rubidge and Kitching, 2003)

(23) Zygomatic arch shape: moderately deep (0); very slender (1). (From Hopson and Kitching, 2001)

(24) Participation of parietal in temporal fenestra dorsal border: absent (0); present (1). (From Hopson and Barghusen, 1986)

(25) Parietal expanded posteriorly on the midline behind the region of parietal foramen: absent (0); present (1). (From Hopson and Barghusen, 1986)

(26) Parietal crest length: moderately long, just over half temporal fenestra length (0); short, less than half temporal fenestra length (1).

(27) Posterodorsal inclination of the temporal region reaching its maximum height where parietal crest meets lambdoidal (= occipital) crest: present (0); absent (1).

(28) Intertemporal width in adults: wide (0); narrow with vertical lateral faces (1). (Modified from Kemp, 1972a; Hopson and Barghusen, 1986)

(29) Temporal fenestra anteroposterior enlargement: absent (0); present (1). (From Sidor and Hopson, 1998)

(30) Squamosal posteroventral process: absent (0); present (1). (From Rybczynski, 2000)

(31) Medially directed process of squamosal contacting prootic: absent (0); present, enclosing pterygoparoccipital foramen (1). (From Kemp, 1972a, 1982)

(32) Parietal crest: short in adults, located posteriorly (0); extends forward to include parietal foramen (1). (From Hopson and Kitching, 2001.) Note: due to the ontogenetic development of this feature, we have not included an "absent" character state, but several taxa are instead coded "?" (i.e., the crest may or may not develop later).

(33) Nasal-lacrimal contact: absent (0); present (1). (From Hopson and Kitching, 2001; Botha et al., 2007)

(34) Prefrontal-postorbital contact in adults: absent (0); present only on dorsomedial wall of orbit (1); present dorsally, excluding frontal from orbit margin (2). (From Hopson and Kitching, 2001; Botha et al., 2007)

(35) Level of greatest width of zygomatic arches: toward middle (0); at back of arch (1). (From Hopson and Kitching, 2001)

(36) Upturning of alveolar margin of premaxilla: moderate to pronounced (0); absent or horizontal (1). (Adapted from Rubidge and van den Heever, 1997)

(37) Interorbital width: approximately 20% or more of total skull length (0); less than 20% of total skull length (1).

(38) Jugal anterior extent: extends anteriorly beyond anterior margin of orbit (0); restricted to anterior margin of orbit (1).

(39) Palatal fenestra for lower caniniform: absent (0); present and confluent with internal naris (1); a separate palatal housing for the lower canine is created by an extension of

premaxilla and maxilla from the primary palate (2); a fossa for the lower canine is present where maxilla and premaxilla meet on the ventral surface of the secondary palate (3). (Modified from Hopson and Barghusen, 1986; van den Heever, 1994)

(40) Maxilla palatal processes: absent (0); form a well developed crista choanalis with a ridge extending posteriorly onto the palatine (1); contact or nearly contact the ventrally extending vomer at a shallow angle with no sutural connection (2); contact vomer with a strong but short sutural connection (3); contact vomer at a strong angle creating a concave anteromedial surface on the crista choanalis, and bearing a moderately long sutural connection with the lateral margins of the vomer (4); meet at midline, sharing a sutural connection and obscuring anterior portion of vomer on palatal surface (5); small anteriorly located processes contact transverse processes of vomer (6). (Modified from Hopson and Barghusen, 1986; van den Heever, 1994; Botha et al., 2007)

(41) Vomer shape between choanae: slightly bulbous, narrowing toward its contact with premaxilla (0); expands anteriorly and is widest at its contact with premaxilla (1); bears specialized transverse processes at level of upper caniniform(s) (2). (From Hopson and Barghusen, 1986; van den Heever, 1994)

(42) Vomer anteriormost contact with premaxilla: short contact with vomerine process of premaxilla (0); broadly overlaps ventral surface of premaxilla vomerine process (1). (From Hopson and Barghusen, 1986)

(43) Vomer fusion: paired (0); fused anteriorly (1); completely fused (2). (From Rubidge and Kitching, 2003)

(44) Vomer ventromedian crest between palatines: absent (0); present (1). (Modified from Kemp, 1972a; van den Heever, 1994)

(45) Palatine teeth: present (0); absent (1). (Modified from Sidor and Hopson, 1998; Rubidge and Kitching, 2003)

(46) Large suborbital vacuities bound by palatine, pterygoid, and ectopterygoid: absent in adults (0); present throughout ontogeny (1). (Modified from Hopson and Barghusen, 1986)

(47) Pterygoid median tubercle/crest: absent (0); ventromedian tubercle/crest is present anterior to interpterygoid vacuity (1). (Modified from van den Heever, 1994; Botha et al., 2007)

(48) Teeth on transverse processes of pterygoids: present (0); absent (1). (From van den Heever, 1994)

(49) Teeth on pterygoid boss: present (0); absent (1). (From van den Heever, 1994)

(50) Pterygoid transverse flange expansion: moderate (0); reduced (1); having sharp, posteriorly projecting wings with slight posterolateral extension (2).

(51) Pterygoid transverse flange position: anterior to center of orbit (0); posterior to center of orbit (1).

(52) Palatal exposure of maxilla behind canine: less than 20% distance from canine to anterior palatine suture (0); greater than 20% distance from canine to anterior palatine suture (1). (modified from Hopson and Kitching, 2001)

(53) Formation of (rudimentary) secondary palate: occurs such that posterior portions of the maxillae and palatines approach at midline, but are slightly open anteriorly, thus creating an incipient incisive fissure or foramen (0); anterior portion is more closed than the posterior, leaving no indication of an incisive foramen or fissure in forms with a complete secondary palate (1). *Biarmosuchus*, *Titanophoneus*, Gorgonopsidae, Anomodontia, and *Lycosuchus* are coded '?' for this character

because basal representatives lack any indication of a secondary palate or crista choanalis. (Based on Maier, 1999)

(54) Parasagittal ridges on pterygoid: absent (0); present, running from medial posterior flare of transverse flanges to basioccipital (1). (Modified from van den Heever, 1994 and Rubidge and Kitching, 2003)

(55) Vomer anterior vault: present (0); absent (1). (Modified from Sidor and Hopson, 1998)

(56) Epipterygoid-parietal contact: separate from parietal (0); contacts parietal (1). (From Modesto et al., 1999)

(57) Epipterygoid ascending process: appears as a thin rod (0); slightly expanded anteroposteriorly (1); greatly expanded, the greatest dorsal anteroposterior length being almost equal to dorsal height (2). (Modified from Kemp, 1972a; Hopson and Barghusen, 1986; Botha et al., 2007)

(58) Posterior apophysis of epipterygoid contacting or nearly contacting the prootic: absent (0); present, enclosing an aperture presumably for trigeminal nerve (1). (From Kemp, 1972a; Hopson and Barghusen, 1986)

(59) Laterally directed processes of the prootic: absent (0); present, participating in pterygoparoccipital foramen (1). (From Hopson and Barghusen, 1986.)

(60) Basal tuber: small (0); large, ca. 1/3 occipital breadth (1). (From van den Heever, 1994)

(61) Dorsal surface of paroccipital process: relatively smooth or straight (0); deeply hollowed in floor of posttemporal fenestra (1). (From Hopson and Barghusen, 1986)

(62) Paroccipital process of opisthotic orientation: strongly posteroventral (0); moderately posteroventral (1); transverse relative to horizontal (2). (From Rubidge and Kitching, 2003)

(63) Opisthotic dorsolateral process: absent (0); present and contacts tabular and/or squamosal, thus excluding supraoccipital from post-temporal fenestra (1). (Modified from Botha-Brink and Modesto, 2011)

(64) 'Mastoid process': absent or poorly developed (0); squamosal and paroccipital process of opisthotic form a distinct, posteriorly projecting 'mastoid process' (1). (Based on Crompton, 1955)

(65) Tabular-opisthotic contact: present (0); tabular is withdrawn from contact with opisthotic (1). (From Modesto et al., 1999)

(66) Tabular contribution to post-temporal fenestra: extends below fenestra (0); just barely contacts post-temporal fenestra (1). (Modified from Sidor and Hopson, 1998)

(67) Trigeminal nerve exit: located between prootic incisure and epipterygoid (0); via a foramen between prootic and epipterygoid (1). (From Hopson and Kitching, 2001)

(68) Epipterygoid-prootic overlap: absent (0); present (1). (From Hopson and Kitching, 2001)

(69) Epipterygoid-frontal contact: absent (0); present (1). (From Hopson and Kitching, 2001)

(70) Occipital condyle: single (0); double (1). (From Hopson and Kitching, 2001; Botha et al., 2007)

(71) Tabular dorsal contribution to lambdoidal crest: low and broad with little or no contribution (0); high, nearly contacting dorsal margin of interparietal with significant contribution to lambdoidal crest (1).

(72) Quadrate and quadratojugal size: relatively large (0); reduced in height (1). (From Hopson and Barghusen 1986)

(73) Quadrate and quadratojugal situated in a depression on the anterior face of the squamosal: absent (0); present (1). (From Hopson and Barghusen, 1986; Sidor and Hopson, 1998)

(74) Stapes dorsal process: present (0); reduced/absent (1).

(75) Posteroventral process on quadrate in posterior notch (quadrate recess) of squamosal: absent (0); present (1). (From Hopson and Kitching, 2001; Botha et al., 2007)

(76) Stapedial foramen: oriented posteroventrally (0); dorsoventrally (1); absent (2). (Modified from Hopson and Kitching, 2001)

(77) Overall dentary shape: deep/robust (0); short and banana-shaped (1); long, slender, and relatively straight with a smooth ventral edge (2). (Modified from Hopson and Barghusen, 1986; Sidor, 2003)

(78) Dentary anterior portion: deepens anteriorly (0); continuously tapers to a narrow anterior edge (1). (Modified from Sidor, 2003)

(79) Specialized boss on posteroventral portion of dentary: absent (0); present (1).

(80) Dentary symphyseal region: only moderately expanded mediolaterally with a low mentum angulation in ventral view (0); anteroposteriorly thickened with strong suture (1). (Based on Mendrez, 1974b)

(81) Dentary lateral surface near canine: relatively smooth (0); bears a marked constriction behind lower canine where upper canine rests in dorsal and ventral views (1). (Based on Mendrez, 1974b)

(82) Dentary angle anterolateral to reflected lamina: shallow, smoothly rounded (0); moderate or sharp (1); pronounced, protruding with an angle < 120º (2).

(83) Coronoid process posterodorsal terminal margin: straight (0); rounded (1); comes to a sharp point (2). (Modified from Sidor, 2003)

(84) Coronoid process dorsal extent: terminates below middle of orbit (0); or in upper half of orbit (1). (From Sidor, 2003)

(85) Dentary height increased posteriorly and postdentary bones reduced so that dentary forms a free standing coronoid process: absent (0); present (1). (Modified from Sidor and Hopson, 1998; Rubidge and Kitching, 2003)

(86) Postdentary bones height relative to total dentary height: equal (0); between 1/2 and equal (1). (Modified from Sidor and Hopson, 1998)

(87) Ventral margins of angular and dentary: confluent (0); angular (= tympanic) positioned dorsal to ventral margin of dentary (1). (From Hopson and Barghusen, 1986; Sidor and Hopson, 1998)

(88) Splenial: exposed laterally near symphysis (0); obscured laterally by dentary (1). (From Sidor and Hopson, 1998; Sidor, 2003)

(89) Mandibular fenestra: absent (0); penetrating mandible and visible laterally (1); surangular above and prearticular below a small fenestra on medial surface of mandible (2). (Modified from Kemp, 1972a; Gauthier et al., 1988; Sidor and Hopson, 1998)

(90) Reflected lamina shape and ventral extent: rounded, projecting below ventral margin of dentary at about the level of the second groove (0); slightly anteroposteriorly elongate (spade-shaped) and does not appear to extend below dentary (1); reduced and spoon-shaped (2).

(91) Dentary masseteric fossa in adults: absent (0); present, high on coronoid process (1). (From Hopson and Kitching, 2001; Botha et al., 2007)

(92) Reflected lamina of angular (= tympanic) size: large (0); reduced (1). (Modified from Hopson and Kitching, 2001)

(93) Area between left and right dentaries: widens greatly posteriorly (0); remains relatively long and narrow (almost slit-like) just posterior to symphyseal region (1).

(94) Dentary ramus lateral groove: absent (0); present (1). ('Longitudinal depression' of Botha et al., 2007)

(95) Interlocking incisors: present (0); absent (1). (Modified from Rubidge and Kitching, 2003; Sidor and Welman, 2003)

(96) Upper incisors: few, up to five (0); six (1); seven or more (2).

(97) Upper incisor longitudinal facets or fluting: absent (0); present (1). (From Hopson and Barghusen, 1986)

(98) Incisor shape: relatively straight and conical (0); spatulate, concave lingually with mesiolingual and distolingual crests (1). (From Hopson and Barghusen, 1986)

(99) Functional upper precanine maxillary teeth in adults: absent (0); present (1). (Modified from Hopson and Barghusen, 1986; van den Heever, 1994; Botha et al., 2007)

(100) Upper dominant canine size: large relative to maxillary height (0); medium (1); reduced even in adults (2). (From Rubidge and van den Heever, 1997)

(101) Deep groove running vertically along the anterior surface of the dominant canine: absent (0); present (1).

(102) Upper postcanines in adults: numerous, more than five (0); few, five or less (1); absent (2). (Modified from Kemp, 1972b; van den Heever, 1994)

(103) Lower canine: large (0); medium (1); reduced, even in adults (2). (Modified from Botha et al., 2007)

(104) Postcanine teeth in lower jaw: present (0); absent (1).

(105) Incisor cutting margins: serrated (0); unserrated/smoothly ridged (1). (From Hopson and Kitching, 2001)

(106) Postcanine shape (if applicable): tall, sharp apices (0); bear two or more cusps in line (1); short, fat cones (2).

(107) Lower incisors number: four (0); less than four (1); more than four (2).

(108) Relative length of maxillary tooth row: > 50% of total maxillary length (0); approximately 50% or less (1).

(109) Caudal vertebrae: more than fifteen (0); fifteen or less (1).

(110) Scapular blade shape: short and broad (0); moderate breadth (1); delicate and narrow (2).

(111) Procoracoid foramen position: bound within procoracoid (0); between procoracoid-coracoid suture (1); between procoracoid-scapula suture (2).

(112) Ossified cleithrum: present (0); absent (1).

(113) Interclavicle shape: long and thin (0); short and broad anterior to sternum (1).

(114) Humerus shape: short and robust (0); long and slender (1).

(115) Ectepicondylar foramen of humerus: present (0); absent (1).

(116) Manual digit III second phalanx: short or disc-like but present (0); absent (1).

(117) Manual digit IV phalangeal number: 5 (0); 4 (1); 3 (2).

(118) Sharp anterior process of the dorsal iliac plate: absent (0); present below an anterodorsal concavity (1). (Based on Kemp, 2005)

(119) Pubis and ischium orientation: relatively vertical (0); more horizontal, forming a broad puboischiatic plate (1). (Based on Kemp, 2005)

(120) Obturator foramen size: small (0); moderately enlarged (1); extremely large opening (2). (From Sidor and Hopson, 1998)

(121) Obturator foramen position: situated completely within pubis (0); bound by pubis and ischium (1).

(122) Femur bears distinct trochanter minor: absent (0); present (1). (Based on Kemp, 2005)

(123) Clavicle shape medially: broad (0); narrow (1). (Gauthier et al., 1988)

(124) Humeral head: convex articular surface extends broadly across head (0); articular surface bulbous and inflected (1). (Gauthier et al., 1988)

(125) Radius width relative to ulna distally: equal, or radius narrower (0); radius broader (1). (Gauthier et al., 1988)

(126) Femoral head shape: elongate to subspherical (0); oblong and spherical (1). (Gauthier et al., 1988)

(127) Calcaneal tuber (tuber calcis): absent (0); present and oriented posteriorly (1). (Gauthier et al., 1988)

(128) Premaxillary foramina on palate: two small foramina (0); two enlarged foramina (1); medially positioned premaxillary fossa present (2).

(129) Angle of incidence between adjoining processes of maxilla and vomer on surface of secondary palate: shallow so that anterior portion of choana rapidly narrows (0); smoothly arching along anterior border of choana (1) in ventral view.

(130) Parietal crest fusion at midline: forms narrow sagittal crest joined tightly around or behind a bulbous pineal housing (0); weak such that parasagittal contributions of left and right parietals are continuous with temporal line and bound a narrow fissure (1).

(131) Maxillary postcanine alveolar margin in ventral view: straight to slightly concave along buccal margin, bowing inward toward the midline (0); buccally convex at anterior extent, bowing outward away from the midline (1).

(132) Upper postcanine diastema immediately behind dominant caniniform: present, greater than the spacing between successive postcanines (0); absent (1).

(133) Lacrimal pits/foramina exposed ventrolaterally outside orbital wall in separate anteorbital fossa: absent (0); present (1).

(134) Suborbital vacuity shape: suboval, about as long as wide (0); elongated and D-shaped (or subtriangular) with straight medial margins (1); broad, anteroposteriorly shorter than wide due to anterior truncation by scalloped webbing (2).

(135) Premaxilla vomerine process contacts maxilla on medial border of lower canine fossa: absent (thereby permitting vomer to contact anterior choana) (0); present (restricting vomer from contact with anterior choana).

APPENDIX 4. Character matrix for phylogenetic analysis (characters listed in Appendix 3). '?' missing character; '-' not applicable.

	10	20	30	40
Biarmosuchus_tener	0000000000	0000000000	00000--000	0?00000000
Titanophoneus_potens	0000000000	1000002?00	01000--000	0?00001000
Gorgonopsia	0000000000	0000000000	01000--010	0?00000010
Anomodontia	1 0000010?00	0001002000	00100--011	0?00000?0
Charassognathus_gracilis	?0?1?00000	0101001001	011110?111	0?1200?1??
Dvinia_prima	0001100100	0101001001	1111100111	011201013-
Procynosuchus_delaharpeae	0001100100	0101001001	0111100111	011201013-
Lycosuchus_vanderrieti	0001000000	1001002100	0101100111	0000100010
Alopecodon	?001?10100	000?002??0	??????????	??00?1?0??
Glanosuchus_macrops	0001110000	0002002000	0111100111	1000110011
Ictidosaurus_angusticeps	0001110000	00020?2??0	?111??11?	??00?1??11
Pardosuchus	?0011?0000	000???????	??????????	?????????1
Pristerognathus_polyodon	0001110000	0002002000	0111100111	1000?10?11
Scylacosaurus	0001110000	000?002000	???1???1??	??00?10?11

Scylacosuchus	0001010100	??02???0?0	01?1100111	?00011??11
Annatherapsidus	?001000?00	000200201?	0111100111	1000110011
USNM_PAL_412421	?001?00100	0002002011	0111100111	1000110021
Akidnognathus_parvus	1111100100	0002002011	0111100111	1000110021
Euchambersia_mirabilis	0111-00110	00010?2001	1111100111	1002110121
SAM_PK_K8516	???1000?01	0101012001	0111110111	?0011?011?
Promoschorhynchus	1111100100	0002002011	0111110111	1100110121
Olivierosuchus_parringtoni	1111100100	0002002011	0111100111	1100100121
Cerdosuchoides	0111100000	0001002011	0111100111	1 ?100100121
Moschorhinus_kitchingi	0111100000	2 0001002011	0111100111	1100100121
Chthonosaurus	???1?00?00	000?002011	011110?111	?1001??0??
Zambian_chthonosaurid	???1?0??0?	0?0?0??001	?1?11??11?	1?00???0?6
Ictidostoma_hemburyi	1001100001	010?01?001	0111110111	?001110111
Tropidostoma_AZ_whaitsiid	1001000001	110?002001	??????????	??00?1?111
Hofmeyria_atavus	1001000001 1	0101012000 1	0111110111	1001110111
Mirotenthes_digitipes	1001100001	0101012001	0111110111	1001110111
Ictidochampsa_platyceps	1?01000101	01?1012??1	11111?0111	1?0?110?1?
Viatkosuchus_sumini	1001000101	1101002011	1111110111	1100110116

Moschowhaitsia_vjuschkovi	1001000101	11?1002011	1111???11?	?100110126
Theriognathus_microps	1001000101 1	1101002011	1111100111	1100110026 1
Ictidosuchus_primaevus	?001101000	001?012001	0111110111	10001?1?12
Ictidosuchoides_longiceps	1001101000	0012012001	0111110111	1000111012
Perplexisaurus	???1?0?000	???????001	01?110011?	?100????11
Ictidosuchops_rubidgei	1001101000	001?012001	01111??11?	?000?1?012
Regisaurus_jacobi	1001101100	0012012001	1011110111	1?00111113
Urumchia	1??11??100	?0?????????	??????????	??001???13
Choerosaurus_dejageri	??01-01100	0010111?01	11111-1111	??10111?1?
Lycideops_longiceps	1001101000	0010011001	1111111111	??10111014
Karenites_ornamentatus	??01101000	0012011001	0111110111 1	10001111??
Zambian_karenitid	???1101000	0012011001	1111110111	?000111?4
Tetracynodon_tenuis	?001001000	0010?21001	1?111-1?11	1?10111014
Tetracynodon_darti	1001001000	0010121001	1?111-1?11	1?10111014
Scaloposaurus_constrictus	1001101000	0002???001	0?11111?11	1?00111013
Ericiolacerta_parva	?001-01100	0002??1001	1?111-1?11	??001100-5
Silphedosuchus	?001-01100	0002??1001	1?111-1?1?	??00?1?0-5
Nothogomphodon	?001100100	010?01?001	1??1??11??	?100?1?023

Ordosiodon	1001100101	010???????	??????????	??0??1?125
Hazhenia	1001100001	0101121001	1111101111	110?110125
Antecosuchus	????100101	??????????	??????????	????????25
Bauria_cynops	1001100101	0101122001	1111101111	1100110025
Traversodontoides	???1100?01	010?122001	0101100111	?0001??0?5
Microgomphodon_oligocynus	1001100101	0101002001 1	0111101111	1000110025

	50	60	70	80
Biarmosuchus_tener	0??0000000	00-000?000	0000000000	0000000001
Titanophoneus_potens	0000000000	00-0000000	0000000000	0000000000
Gorgonopsia	0020000000	00-0110000	0100000000	0110000001
Anomodontia	00001?00?1	1?-00?0000	0100110000	1010010001
Charassognathus_gracilis	??????????	?????120??	??????1101	?11?1?2100
Dvinia_prima	0021100111	1100?1201?	02?0001111	?110102100
Procynosuchus_delaharpeae	0021100111	1100012017	0200001111	1110102100
Lycosuchus_vanderrieti	1000111012	10-10110?1	??100?0000	0111?10000
Alopecodon	??????????	??????????	??????????	??????0000
Glanosuchus_macrops	1001111102	1010111010	02?0110000	?111110000
Ictidosaurus_angusticeps	1?????????	???0??????	??????????	??????0000
Pardosuchus	???????10?	??1???????	??????????	??????0000
Pristerognathus_polyodon	1001111102	1010111010	02?0110000	?11???00?0
Scylacosaurus	100011?102	?0101?????	??????????	??????????

Scylacosuchus	??????????	?01??11???	?21001??00	??1?1?0000
Annatherapsidus	1021111102	1011111?0	1210010000	011?1?000?
USNM_PAL_412421	1021111102	10111????0	121011??00	111???????
Akidnognathus_parvus	1021111112	1011111??0	121????000	111?1?0001
Euchambersia_mirabilis	1111101111	1011111?10	12?0??0000	?11???????
SAM_PK_K8516	?????1?1?2	1011?????0	??????????	??????1?0?
Promoschorhynchus	1111111112	10111110101	1211110000	111?1?0001
Olivierosuchus_parringtoni	1111111112	1011111110	1211110000	011???0001
Cerdosuchoides	1111111112	10111?????	??????????	?11?1?0001
Moschorhinus_kitchingi	1111111112	1011111110	1210110000	111???0001
Chthonosaurus	??21111102	1?11111??0	12????0000	?11????1??
Zambian_chthonosaurid	2?21111?2	1?1111111?	??????000?	??????????
Ictidostoma_hemburyi	1011111?2	10111?????	?????????0	??????1100
Tropidostoma_AZ_whaitsiid	101111????	?01???????	??????????	??????1100
Hofmeyria_atavus	1011111102	1011111?10	1210000?00	0111?11100
Mirotenthes_digitipes	1?11111102	1??1111?10	1210000?00	0111?11100
Ictidochampsa_platyceps	????11?1?2	10111????0	1210?????0	011?1?????
Viatkosuchus_sumini	2021111102	1011111010	1210??1?00	0111?11100

Moschowhaitsia_vjuschkovi	2021111?2	101?1?????	?????????0	??????????
Theriognathus_microps	2011101102	1111112110	1210001100	0111110100
	2 1			1
Ictidosuchus_primaevus	1??111?1?2	1111111010	121101???0	011???2100
Ictidosuchoides_longiceps	1011111112	1111111010	1211?10?00	1111?12100
Perplexisaurus	????11??02	1011??????	??????????	??????000?
Ictidosuchops_rubidgei	1001111102	11111?????	??????????	??????????
	1			
Regisaurus_jacobi	1011111102	1111111110	1211?10100	111?1?2100
Urumchia	10?1111?2	1?111?????	??????????	???????1??
Choerosaurus_dejageri	????1111??	1?????????	??????????	?11???2110
Lycideops_longiceps	1011111102	11111?????	???1?????0	??????2100
Karenites_ornamentatus	1?01111102	1111011010	1211010100	1111112110
Zambian_karenitid	1?21111?2	11111?1??0	1211????00	1111112110
Tetracynodon_tenuis	??21111112	1111111010	??1010?00	111???2100
Tetracynodon_darti	1021111112	1110111010	1211010100	1111?12100
Scaloposaurus_constrictus	1011111112	1111111010	1211?10100	111???2100
Ericiolacerta_parva	1?2111?112	1?111????0	??100???0	?11???2100
Silphedosuchus	1?21111112	1?1?1?????	??????????	??????2100
Nothogomphodon	1021111112	111?1?????	??????????	??????000?

Ordosiodon	???1111112	1111??????	??????????	??????0000
Hazhenia	??21111112	1111?????0	12?100???0	111?1?0000
Antecosuchus	??????????	?11???????	??????????	??????0101
Bauria_cynops	1?21111112	1111111110	1211000100	111???0101
Traversodontoides	???1111112	11111????0	?????????0	???????10?
Microgomphodon_oligocynus	1?21111112	1111111110	1211000100	1111?10101

	90	100	110	120
Biarmosuchus_tener	00--000000	0000000000	0000000000	0?00100000
Titanophoneus_potens	00--000000	0000000000	0000000000	0000012001
Gorgonopsia	0020100000	0000?00000	0000000?0	0000001000
Anomodontia	?02?100010	0000?00001	0010?01001	0?01012001
Charassognathus_gracilis	0100111?22	?1?01?0101	0000111?0?	??????????
Dvinia_prima	0100111?22	1100110101	000011?0??	???????002
Procynosuchus_delaharpeae	0100111022	1100110101	0000110000	0??0001002
Lycosuchus_vanderrieti	0200111120	0001100000	0100010?0	00?00?????
Alopecodon	?2??1111??	0??1120010	00?00010??	??????????
Glanosuchus_macrops	0100111120	0001110000	0000001010	0?00112111
Ictidosaurus_angusticeps	0200111120	0001110010	000000?0??	??????????
Pardosuchus	02??1111??	0?01110010	0???00????	??????????
Pristerognathus_polyodon	0100111120	0001120000	000000?0??	????1?????
Scylacosaurus	?2?????????	?????20010	00??00?0??	????1?????

Scylacosuchus	01????????	???1101010	0000102???	??????????
Annatherapsidus	0100111111?	0001101010	000010?0??	??????????
USNM_PAL_412421	??????????	?????01010	01??10?0??	??????????
Akidnognathus_parvus	0100111111?	0001101010	000010000??	??????????
Euchambersia_mirabilis	??????????	000??00100	12??1-?-??	??????????
SAM_PK_K8516	01111111??	0?11??????	?000?0?0??	??????????
Promoschorhynchus	0100111110	0001101110	0000100?1 1 1	01111?????
Olivierosuchus_parringtoni	0100111110	0001100110 1	0100100?1?1	0111112???
Cerdosuchoides	1100111110	0001100100	0100100?1?1	?0????????
Moschorhinus_kitchingi	1100111110	0001100100	010010001??	???01?????
Chthonosaurus	??????????	??????????	?00??2?0??	??????????
Zambian_chthonosaurid	??????????	??????????	?0???2????	??????????
Ictidostoma_hemburyi	001011111?	0?10101000	000010000??	??????????
Tropidostoma_AZ_whaitsiid	0111111111?	0?1010?000	010010000??	??????????
Hofmeyria_atavus	0011111111 1	0010101000	000010000?? 1	????1?????
Mirotenthes_digitipes	0011111111	0010101?10	0001100011	011111211?
Ictidochampsa_platyceps	??????????	?????????0	?0?????0??	??????????
Viatkosuchus_sumini	01?0111111	0010101?10	01??10?0??	??????????

Moschowhaitsia_vjuschkovi	??????????	?????0??0?	?0?????0??	??????????
Theriognathus_microps	0010111111	0010100000	02011-01?1	0111112111
	1	1		
Ictidosuchus_primaevus	00111?????	0??11?1011	00?0?????1	??????????
Ictidosuchoides_longiceps	0011111111	0001110011	0010100???	???1112???
		1		
Perplexisaurus	000?1?11??	0??1???000	0010?110??	??????????
Ictidosuchops_rubidgei	??????????	?????11011	00??10?0??	??????????
Regisaurus_jacobi	001?111111	??00110001	00?01000?1	1111112111
Urumchia	0?????????	????110001	0010100???	??????????
Choerosaurus_dejageri	0010111111	01?1???011	001010?0?2	0??11??111
Lycideops_longiceps	0010111111	0100?10001	001010?0??	??????????
			1	
Karenites_ornamentatus	0010111111	01011???11	001011?0??	??????????
Zambian_karenitid	0010111111	0101????11	0010?020??	??????????
Tetracynodon_tenuis	0010111111	0?0?1200??	00?0102???	??????????
Tetracynodon_darti	0010111111	010112000?	00?01020?2	0111112111
				1
Scaloposaurus_constrictus	0010111111	01011?00?1	0010110?2	???1112???
Ericiolacerta_parva	0010111111	010111?0?2	-020110?2	10111??111
Silphedosuchus	0?101?11??	0?011??0?2	-020110??	??????????
Nothogomphodon	01111?11??	0??1100001	0000110???	??????????

Ordosiodon	0011111?1	0101100001	0010110?2	???1??????
Hazhenia	0011111111	0101100?01	0010?110??	??????????
Antecosuchus	111?1?11??	0?01????01	0010?1?0??	??????????
Bauria_cynops	1111111111	0001100001	0010111???	?????12???
Traversodontoides	?1111?1???	0??1?????1	0010?1?0??	??????????
Microgomphodon_oligocynus	1111111111	0001100001	0010110?2	1?01112???

```
                            .........130     ....135

Biarmosuchus_tener          ?00000??--       000--

Titanophoneus_potens        ?0?0000?--       000--

Gorgonopsia                 ?0000000--       000—
                              1  1
Anomodontia                 ?0111000--       010?-
                                 1
Charassognathus_gracilis    ?0??????00       000??

Dvinia_prima                ?0?????200       010-0

Procynosuchus_delaharpeae   ?011110000       010-0

Lycosuchus_vanderrieti      ?111?1?0-0       1000-

Alopecodon                  ????????-?       000?-

Glanosuchus_macrops         ?11101?0-0       0000-
                                1
Ictidosaurus_angusticeps    ????????-?       000?-

Pardosuchus                 ????????-?       000?-

Pristerognathus_polyodon    ???????0-0       00?0-

Scylacosaurus               ????????-0       0000-
```

Scylacosuchus	????????-0	000?-
Annatherapsidus	???????0-0	1100-
USNM_PAL_412421	???????0-0	11000
Akidnognathus_parvus	???????0-0	10000
Euchambersia_mirabilis	???????0-0	1 --0-0
SAM_PK_K8516	????????-0	00000
Promoschorhynchus	???1???0-0	11000
Olivierosuchus_parringtoni	?1111?0-0	11000
Cerdosuchoides	????????-0	11000
Moschorhinus_kitchingi	?1?111?0-0	11000
Chthonosaurus	?????????0	0?02?
Zambian_chthonosaurid	????????1?	0?02?
Ictidostoma_hemburyi	???????0-0	0000-
Tropidostoma_AZ_whaitsiid	????????-?	001?-
Hofmeyria_atavus	??111??0-0	0010-
Mirotenthes_digitipes	?111110?-0	0000-
Ictidochampsa_platyceps	?????????0	1 00?2-
Viatkosuchus_sumini	????????10	00020

Moschowhaitsia_vjuschkovi	????????10	00020
Theriognathus_microps	?111110010	--0-0 1
Ictidosuchus_primaevus	????????-0	0000-
Ictidosuchoides_longiceps	?11111?0-0	0000-
Perplexisaurus	????????-0	0100?
Ictidosuchops_rubidgei	???????000	00000 1
Regisaurus_jacobi	1111111100	00001 1
Urumchia	????????0?	00?0?
Choerosaurus_dejageri	11?1?1????	0101?
Lycideops_longiceps	???????111	00011
Karenites_ornamentatus	????????01	0001?
Zambian_karenitid	????????01	0001?
Tetracynodon_tenuis	????????1?	0101?
Tetracynodon_darti	111111?11?	01011
Scaloposaurus_constrictus	?111111?10	0000?
Ericiolacerta_parva	????????0?	0?001
Silphedosuchus	????????0?	0?00?
Nothogomphodon	???????010	01001

Ordosiodon	??????101?	01001
Hazhenia	????????10	00011
Antecosuchus	????????1?	00??1
Bauria_cynops	???????010	00001
Traversodontoides	????????10	0000?
Microgomphodon_oligocynus	?1?1111010	00001

APPENDIX 5. List of character states supporting the monophyly of Therocephalia and its subclades (from Appendices 3 and 4). All sampled characters (unambiguous and ambiguous) are listed with ambiguous character state transformations optimized using delayed transformation, DELTRAN.

THEROCEPHALIA (9 characters)

35. Zygomatic arch greatest width at back of arch, forming a triangular dorsal skull profile (0→1).

41. Vomer premaxillary process expands anteriorly and is widest at its contact with the premaxilla (0→1).

46. Suborbital vacuities bound by palatine, pterygoid, and ectopterygoid present throughout ontogeny (0→1). [Reversal in *Euchambersia* and *Theriognathus* in which the sutures are closed.]

47. Pterygoid ventromedian tubercle/crest anterior to interpterygoid vacuity present (0→1).

50. Pterygoid transverse flange expanded with sharp posterolateral extension (1→2). (Reversal in *Euchambersia* as in cynodonts.)

63. Opisthotic dorsolateral process present, contacting tabular/squamosal, thus excluding supraoccipital from post-temporal fenestra (0→1).

74. Stapes dorsal process reduced/absent (0→1).

76. Stapedial foramen absent (0→1). [Conv. in anomodonts.]

94. Dentary ramus lateral groove present (0→1). [Reversal in Hofmeyriidae+Whaitsiidae, *Regisaurus*, and *Lycideops*.]

122. Femur bears distinct trochanter minor (0→1).

SCYLACOSAURIA (11 characters)

14. Anterior border of orbit located on transverse midline of skull (1→2). [Reversed in *Euchambersia*+(*Cerdosuchoides*+*Moschorhinus*), Hofmeyriidae, Whaitsiidae, and *Nothogomphodon*+Ordosiidae+Bauriidae.]

31. Squamosal medial process contacting prootic present, enclosing the pterygo-paroccipital foramen (0→1).

36. Premaxilla alveolar margin horizontal/straight (0→1). [Conv. in cynodonts; reversal in *Cerdosuchoides* and *Moschorhinus*.]

40. Maxilla palatal processes present, forming a well developed crista choanalis with a ridge extending posteriorly onto the palatine (0→1).

44. Vomer ventromedian crest between palatines present (0→1). [Conv. in cynodonts; absent in *Scylacosaurus*.]

48. Pterygoid transverse flange teeth absent (0→1). [Conv. in cynodonts.]

55. Vomer anterior vault absent (0→1).

99. Functional upper precanine maxillary teeth in adults present (0→1). [Reversal in some scylacosaurids, akidnognathids, hofmeyriids, whaitsiids, and baurioids.]

115. Humerus ectepicondylar foramen absent (0→1).

118. Iliac dorsal plate bears sharp anterior process below an anterodorsal concavity (0→1). [Ambiguous, condition uncertain in *Lycosuchus*.]

119. Pubis and ischium orientation more horizontal, forming a broad puboischiatic plate (0→1). [Ambiguous, condition uncertain in *Lycosuchus*.]

Scylacosauridae (2 characters)

6. A shallow antorbital depression anterior to a thickened ridge on the anterior margin of the orbit is present, extending anteroventrally from the lacrimal to the canine buttress of the maxilla (0→1).

96. Upper incisors number six or more (0→1). [Conv. in cynodonts and Baurioidea.]

EUTHEROCEPHALIA (3 characters)

1. Anterodorsal most tip of premaxilla forms a rostral process, overhanging incisors (0→1). (Reversed in *Euchambersia* and adult specimens of *Moschorhinus.*)

97. Upper incisor longitudinal fluting/striae present (0→1). [Modified into large, flat facets in *Cerdosuchoides* and smooth in *Moschorhinus*; Reversal in most non-ictidosuchid baurioids (although *Regisaurus* and *Scaloposaurus* may exhibit faint striae on canines).]

105. Incisor cutting margins unserrated (0→1). [Conv. in cynodonts.]

non-*Scylacosuchus* EUTHEROCEPHALIA (7 characters)

20. Postfrontal absent (0→1). [Conv. in cynodonts; polymorphic in the holotype of *Hofmeyria*, being present on only one side of the skull.]

43. Vomers unpaired and either fused anteriorly (0→1) or completely fused (0→2). [Conv. in cynodonts; condition uncertain in *Scylacosuchus.*]

61. Paroccipital process dorsal surface deeply hollowed in floor of post-temporal fenestra (0→1). [Ambiguous, condition uncertain in *Scylacosuchus* and *Perplexisaurus*.]

89. Mandibular fenestra present, penetrating the mandible and visible laterally (1→2). [Ambiguous, condition uncertain in *Scylacosuchus*, *Perplexisaurus*, and Chthonosauridae]

107. Lower incisors number four (1→0). [Modified in Karenitidae+Lycideopidae which bear more than four, and

Scaloposaurus+(Ericiolacertidae+(*Nothogomphodon*+Ordosiidae+Bauriidae)) which bear fewer than four.]

113. Interclavicle shape short and broad anterior to sternum (0→1). [Ambiguous, condition uncertain in *Scylacosuchus*, *Perplexisaurus*, and Chthonosauridae]

121. Obturator foramen position bound by pubis and ischium (0→1). [Ambiguous, condition uncertain in *Scylacosuchus*, *Perplexisaurus*, and Chthonosauridae]

Akidnognathidae (4 characters)

19. Median frontonasal crest present (0→1). [Absent in *Euchambersia*; Conv. in *Chthonosaurus* and some whaitsiids.]

80. Dentary symphysis anteroposteriorly thickened with strong suture (0→1). [Conv. in Bauriidae.]

131. Maxillary postcanine alveolar margin in ventral view buccally convex at anterior extent, bowing outward away from the midline (0→1). [Conv. in *Lycosuchus*.]

132. Upper postcanine diastema immediately behind dominant caniniform absent (0→1). [Conv. in some cynodonts and some baurioids where the tooth row is continuous.]

non-*Annatherapsidus* (African) Akidnognathidae (2 characters)

39. Palatal housing for lower caniniform formed as separate fossa by premaxillary and maxillary extensions from primary palate (1→2). [Conv. in some whaitsiids and *Nothogomphodon*+Ordosiidae+Bauriidae.]

65. Tabular-opisthotic contact withdrawn (0→1). [Conv. in Scylacosauridae.]

***Akidnognathus* + (*Olivierosuchus* + *Promoschorhynchus*) + (*Euchambersia* + (*Cerdosuchoides* + *Moschorhinus*))** (3 characters)

2. Septomaxilla is enlarged and well-exposed outside of the external naris, broadly overlapping the premaxilla anteriorly (0→1).

3. External nares are enlarged, close-set, and face anteriorly (0→1).

49. Pterygoid boss teeth absent (0→1). [Conv. in cynodonts, *Theriognathus*, *Tetracynodon*, and *Scaloposaurus*+(Ericiolacertidae +(*Nothogomphodon*+Ordosiidae+Bauriidae)).]

(*Olivierosuchus* + *Promoschorhynchus*) + (*Euchambersia* + (*Cerdosuchoides* + *Moschorhinus*)) (6 characters)

32. Parietal crest extends forward in adults to include the pineal enclosure (0→1). [Conv. in cynodonts, Whaitsiidae, and *Nothogomphodon*+Ordosiidae+Bauriidae.]

38. Jugal anterior extent restricted to anterior border of orbit (0→1). [Conv. in cynodonts, Hofmeyriidae+Whaitsiidae, Regisauridae, Karenitidae, and Ordosiidae.]

42. Vomer anteriormost contact with premaxilla has broad overlap on ventral surface of premaxilla vomerine process (0→1).

98. Incisor shape spatulate, concave lingually with mesiolingual and distolingual crests (0→1). [Conv. in cynodonts.]

102. Upper postcanines number five or fewer (0→1). [Conv. in *Lycosuchus* and some whaitsiids; polymorphic in *Promoschorhynchus*.]

108. Maxillary tooth row approximately 50% or less total length of maxilla (0→1). [Conv. in *Theriognathus* due to loss of postcanine teeth.]

***Euchambersia* + (*Cerdosuchoides* + *Moschorhinus*)** (2 characters)

14. Anterior border of orbit located on anterior half of skull (2→1). [Conv. in cynodonts, *Lycosuchus*, Hofmeyriidae, Whaitsiidae, and *Nothogomphodon*+Ordosiidae+Bauriidae.]

81. Dentary lateral surface near canine bears marked constriction where upper canine rests behind lower canine (0→1). [Ambigous; condition uncertain in *Euchambersia*.]

NON-AKIDNOGNATHID 'WHAITSIOIDS' + BAURIOIDEA (5 characters)

16. Postorbital bar extremely slender (0→1). [Reversal in some whaitsiids; bar is absent in some baurioids.]

26. Parietal (sagittal) crest short, less than half the anteroposterior length of the temporal fenestra (0→1). [Reversal in *Theriognathus*, Ordosiidae and Bauriidae where it is longer than the anteroposterior length of the temporal fenestra.]

78. Dentary continuously tapers to a narrow anterior edge (0→1). [Conv. in cynodonts; Reversal in *Nothogomphodon* and Ordosiidae.]

83. Coronoid process posterodorsal terminal margin rounded (0→1).

90. Reflected lamina shape elongated (spade-shaped), does not extend ventrally below dentary (0→1).

Non-akidnognathid 'whaitsioids' (Hofmeyriidae + Whaitsiidae) (9 characters)

10. Posterior region of the maxillary facial plate is folded inward onto the palatal region, so that the maxilla is well exposed ventrally just anterior to the orbit (0→1). [Conv. in *Nothogomphodon*+Ordosiidae+Bauriidae.]

12. Suborbital bar is laterally expanded, contributing to a pronounced degree of orbital convergence (i.e., orbits facing forward and appearing more triangular than oval in dorsal view) (0→1). [Conv. in cynodonts and *Nothogomphodon*+Ordosiidae+Bauriidae.]

14. Anterior border of orbit located on anterior half of skull (2→1). [Conv. in cynodonts, *Lycosuchus*, *Euchambersia*+(*Cerdosuchoides*+*Moschorhinus*), and *Nothogomphodon*+Ordosiidae+Bauriidae.]

38. Jugal anterior extent restricted to anterior border of orbit (0→1). [Conv. in cynodonts, some akidnognathids, Regisauridae, Karenitidae, and Ordosiidae.]

66. Tabular extends below post-temporal fenestra (1→0). [Reversal; Conv. in Ericiolacertidae+(*Nothogomphodon*+Ordosiidae+Bauriidae).]

71. Tabular dorsal extent low and broad (1→0). [Conv. in some akidnognathids.]

77. Dentary overall shape, short and banana-shaped (0→1).

93. Area between left and right dentaries remains relatively long and narrow just posterior to symphyseal region (0→1).

94. Dentary ramus lateral groove absent (1→0). [Reversal; Conv. in *Regisaurus* and *Lycideops.*]

Hofmeyriidae (1 character)

34. Prefrontal-postorbital contact present in orbit dorsomedial wall (0→1).

Whaitsiidae, incl. *Viatkosuchus* (6 characters)

11. Suborbital bar deep (0→1). [Conv. in *Lycosuchus.*]

19. Median fronto-nasal crest present (0→1). [Conv. in *Chthonosaurus* and Akidnognathidae.]

16. Postorbital bar moderately well-built (1→0).

21. Parietal (=pineal) opening in adults absent/extremely reduced (0→1). [Conv. in *Dvinia*, *Euchambersia*, and most non-ictidosuchid baurioids.]

32. Parietal crest extends forward in adults to include the pineal enclosure (0→1). [Conv. in cynodonts, some akidnognathids, and *Nothogomphodon*+Ordosiidae+Bauriidae.]

67. Trigeminal nerve exits via a foramen between the prootic and epipterygoid (0→1). [Conv. in cynodonts.]

non-*Viatkosuchus* Whaitsiidae (*Moschowhaitsia* + *Theriognathus*) (3 character)

39. Palatal housing for lower caniniform formed as separate fossa by premaxillary and maxillary extensions from primary palate (1→2). [Conv. in some akidnognathids and *Nothogomphodon*+Ordosiidae+Bauriidae.]

40. Maxilla palatal processes present with small, anteriorly located medial projection contacting transverse processes of vomer (1→6). [Conv. in some chthonosaurids.]

41. Vomer premaxillary process bears specialized transverse processes at level of upper caniniform(s) (1→2). [Conv. in some chthonosaurids.]

BAURIOIDEA (10 characters)

7. Maxilla facial plate low with a height less than 40% its length (0→1). [Reversed in *Nothogomphodon*+Ordosiidae+Bauriidae.]

13. Long, low rostrum just anterior to orbital region present (0→1). [Reversed in *Scaloposaurus*+(Ericiolacertidae +(*Nothogomphodon*+Ordosiidae+Bauriidae)).]

37. Interorbital width narrow, less than 20% basal skull length (0→1). [Reversed in Ericiolacertidae +(*Nothogomphodon*+Ordosiidae+Bauriidae).]

40. Maxilla palatal processes present and contact or nearly contact the ventrally extending vomer at a shallow angle with no sutural connection (1→2).

52. Palatal exposure of maxilla behind canine greater than 20% distance from canine to posterior end of palatine (0→1). [Conv. in cynodonts and *Theriognathus.*]

64. Squamosal and opisthotic paroccipital process form a distinct, posteriorly projecting 'mastoid process' (0→1). [Conv. in some akidnognathids.]

77. Dentary overall shape, long and slender with straight ventral edge (0→2).

82. Dentary angle anterolateral to reflected lamina shallow, smoothly rounded (1→0).

96. Upper incisors number six or more (0→1). [Conv. in cynodonts and Scylacosauridae.]

127. Calcaneal tuber (tuber calcis) present, oriented posteriorly (0→1).

Ictidosuchidae (1 character)

84. Coronoid process dorsal extent terminates in upper half of orbit (0→1). [Conv. in some hofmeyriids and *Nothogomphodon*+Ordosiidae+Bauriidae.]

Regisauridae+((Karenitidae+Lycideopidae) + (*Scaloposaurus*+(Ericiolacertidae +(*Nothogomphodon*+Ordosiidae+Bauriidae)))) (3 characters)

21. Parietal (=pineal) opening in adults absent/extremely reduced (0→1). [Conv. in *Dvinia*, *Euchambersia*, and Whaitsiidae; polymorphic in *Karenites* and present (0) in *Scaloposaurus* and some bauriids.]

40. Maxilla palatal processes present and contact vomer with a strong but short sutural connection (2→3).

135. Premaxilla vomerine process contacts maxilla on medial border of lower canine fossa, restricting vomer from contact with anterior choana (0→1).

(Karenitidae+Lycideopidae) + (*Scaloposaurus*+(Ericiolacertidae +(*Nothogomphodon*+Ordosiidae+Bauriidae))) (3 characters)

17. Zygomatic arch orientation behind orbit relatively straight (2→1). [Reversal in Bauriidae.]

92. Angular reflected lamina reduced in size (0→1). [Conv. in cynodonts; Reversal in Bauriidae.]

110. Scapula blade delicate/narrow (1→2).

Karenitidae+Lycideopidae (4 characters)

40. Maxilla palatal processes present and contact vomer at a strong angle creating a concave anteromedial surface on the crista choanalis, and bearing a moderately long sutural connection with the lateral margins of the vomer (3→4).

107. Lower incisors number more than four (0→2). [Conv. in *Scylacosuchus*.]

130. Parietal crest fusion at midline weak, such that parasagittal contributions of left and right parietals are continuous with temporal line and bound a narrow fissure (0→1).

134. Suborbital vacuity shape, elongated and D-shaped (or subtriangular) with straight medial margins (0→1).

Lycideopidae (3 characters)

14. Anterior border of orbit located on posterior half of skull (2→0).

33. Nasal-lacrimal contact present (0→1). [Conv. in cynodonts.]

128. Premaxillary foramina on palate, two enlarged foramina (0→1). [Conv. in *Regisaurus*.]

Choerosaurus* + *Tetracynodon (1 character)

15. Jugal postorbital process absent (0→1). [Conv. in Ordosiidae and some bauriids; uncertain or ambiguous in *Scaloposaurus* and Ericiolacertidae.]

***Scaloposaurus* + (Ericiolacertidae + (*Nothogomphodon* + Ordosiidae + Bauriidae))** (2 characters)

106. Postcanines bear two or more cusps in line (0→1). [Conv. in cynodonts.]

107. Lower incisors number less than four (0→1). [Conv. basal therocephalians.]

Ericiolacertidae + (*Nothogomphodon* + Ordosiidae + Bauriidae) (3 characters)

8. Maxilla facial plate concave ventral step between caniniform(s) (or anterior most maxillary teeth) and incisors absent (0→1).

40. Maxilla palatal processes present and meet at midline, sharing a sutural connection and obscuring anterior portion of vomer on palatal surface (3→5).

66. Tabular extends below post-temporal fenestra (1→0). [Reversal; Conv. in Hofmeyriidae+Whaitsiidae.]

***Nothogomphodon* + Ordosiidae + Bauriidae** (8 characters)

10. Posterior region of the maxillary facial plate is folded inward onto the palatal region, so that the maxilla is well exposed ventrally just anterior to the orbit (0→1). [Conv. in hofmeyriids and whaitsiids.]

12. Suborbital bar is laterally expanded, contributing to a pronounced degree of orbital convergence (i.e., orbits facing forward and appearing more triangular than oval in dorsal view) (0→1). [Conv. in cynodonts, hofmeyriids and whaitsiids.]

14. Anterior border of orbit located on anterior half of skull (2→1). [Conv. in cynodonts, *Lycosuchus*, *Euchambersia*, *Cerdosuchoides*, *Moschorhinus*, Hofmeyriidae, Whaitsiidae.]

32. Parietal crest extends forward in adults to include the pineal enclosure (0→1). [Conv. in cynodonts, some akidnognathids, and Whaitsiidae.]

39. Palatal housing for lower caniniform formed as separate fossa by premaxillary and maxillary extensions from primary palate (1→2). [Conv. in some akidnognathids and whaitsiids.]

77. Dentary shape, deep/robust (2→0). [Reversal.]

84. Coronoid process dorsal extent terminates in upper half of orbit (0→1). [Conv. in some hofmeyriids and ictidosuchid baurioids.]

99. Functional upper precanines in adults absent (1→0). [Conv. in some scylacosaurids, akidnognathids, hofmeyriids, and whaitsiids.]

Bauriidae (3 characters)

80. Dentary symphysis anteroposteriorly thickened with strong suture (0→1). [Conv. in Akidnognathidae.]

81. Dentary lateral surface near canine bears marked constriction where upper canine rests behind lower canine (0→1). [Conv. in *Cerdosuchoides*+*Moschorhinus*.]

92. Angular reflected lamina large (1→0). [Reversal.]

APPENDIX 6 . Therocephalian and cynodont diversity from Middle Permian through Middle Triassic rocks of the Karoo Basin, South Africa (listed by assemblage zone).

***Eodicynodon* Assemblage Zone (2)**

Therocephalians:

Glanosuchus macrops
Ictidosaurus angusticeps

***Tapinocephalus* Assemblage Zone (7)**

Therocephalians:

Alopecodon priscus
Glanosuchus macrops
Ictidosaurus angusticeps
Lycosuchus vanderrieti
Pardosuchus whaitsi
Pristerognathus polyodon
Scylacosaurus sclateri

***Pristerognathus* Assemblage Zone (5)**

Therocephalians:

Glanosuchus macrops
Hofmeyria atavus
Ictidostoma hemburyi
Ictidosuchoides longiceps
Pristerognathus polyodon

***Tropidostoma* Assemblage Zone (8)**

Therocephalians:

Choerosaurus dejageri
Hofmeryia atavus
Ictidostoma hemburyi
Ictidosuchoides longiceps
Ictidosuchus primaevus
Whaitsiidae, new sp. (SAM-PK-K10990)

Cynodonts:

Charassognathus gracilis
Procynosuchus delaharpeae

***Cistecephalus* Assemblage Zone (10)**

Therocephalians:

Akidnognathidae, new sp. (USNM PAL 412421)
Euchambersia mirabilis
Ictidosuchoides longiceps
Hofmeyria atavus

Hofmeyriidae, new sp. (SAM-PK-K8516)
Ictidostoma hemburyi
Mirotenthes digitipes
Theriognathus microps

Cynodonts:
Cynosaurus suppostus
Procynosuchus delaharpeae

***Dicynodon* Assemblage Zone (14)**

Therocephalians:
Akidnognathus parvus
Cerdosuchoides brevidens
Ictidochampsa platyceps
Ictidosuchoides longiceps
Ictidosuchops rubidgei
Lycideops longiceps
Mirotenthes digitipes
Moschorhinus kitchingi
Promoschorhynchus platyrhinus
Tetracynodon tenuis
Theriognathus microps

Cynodonts:
basal cynodont, new sp. (BP/1/6978; SAM-PK-K10702; F. Abdala, pers. comm., 2012)
Cynosaurus suppostus
Procynosuchus delaharpeae

***Lystrosaurus* Assemblage Zone (11)**

Therocephalians:
Ericiolacerta parva
Moschorhinus kitchingi
Olivierosuchus parringtoni
Promoschorhynchus cf. *P. platyrhinus*
Regisaurus jacobi
Scaloposaurus constrictus
Tetracynodon darti

Cynodonts:
Galesaurus planiceps
Platycraniellus elegans
Progalesaurus lootsbergensis
Thrinaxodon liorhinus

***Cynognathus* Assemblage Zone (10)**

Therocephalians:

Bauria cynops
Microgomphodon oligocynus

Cynodonts:

Allotheria-like teeth (Abdala et al., 2007a)
Bolotridon frerensis
Cricodon metabolus
Cynognathus crateronotus
Diademodon tetragonus
Langbergia modisei
Lumkuia fuzzi
Trirachodon berryi

APPENDIX 7. Outcrop area and sampled diversity of Karoo Basin therocephalians and cynodonts (from Appendix 6).

Karoo Biozone	Base (Ma)	Top (Ma)	Duration (Myr)	Outcrop area (km^2) (total)	Outcrop area (km^2) (productive)	# theroceph genera	# cyno genera
Cynognathus AZ	248	241.2	6.8	11,196	5,488	2	8
Lystrosaurus AZ	252.3	248	4.3	76,550	48,358	7	4
Dicynodon AZ	255	252.3	2.7	41,113	20,322	11	3
Cistecephalus AZ	257	255	2.0	41,082	31,360	8	2
Tropidostoma AZ	259.5	257	2.5	17,718	14,739	6	2
Pristerognathus AZ	262	259.5	2.5	3,857	3,857	5	--
Tapinocephalus AZ	265.8	262	3.8	21,043	15,806	7	--
Eodicynodon AZ	268	265.8	2.2	1,286	1,066	2	--

Ma, millions of years ago (mega-annum); Myr, million years; dates are estimates based on Abdala and Ribeiro (2010), Smith et al. (2012), and Rubidge et al. (2013); AZ, Assemblage Zone;
Outcrop area estimates from King (1991).

APPENDIX 8. Age and clade rank data for the therocephalian and cynodont subclades. Basal skull length measurements (BSL) are in mm.

Eutheriodontia	CR[†]	AR[‡]	MaxBSL	lnBSL	Voucher specimen/Source
Therocephalia					
Lycosuchus (CR1)	1	2	340	5.828	SAM-PK-9084
Scylacosauridae (CR2)					
Ictidosaurus	2	1	168[*]	5.123	Abdala et al., 2007b (NMQR 2910)
Glanosuchus	2	2	330	5.799	UCMP 42669
Pristerognathus	2	2	262	5.568	SAM-PK-11492
Scylacosuchus (CR3)	3	3	250[*]	5.521	Ivakhnenko, 2011 (PIN 2628/1)
Akidnognathidae (CR4)					
Annatherapsidus	4	5	250[*]	5.521	Ivakhnenko, 2011 (PIN 2005/1993)
Akidnognathidae, new sp.	4	5	218	5.384	USNM 412421
Akidnognathus	4	5	150	5.010	BP/1/499
Promoschorhynchus	4	6	125	4.828	RC 116
Olivierosuchus	4	7	122	4.804	NMQR 3605
Euchambersia	4	5	115	4.744	NHMUK R5696
Cerdosuchoides	4	6	134	4.897	RC 58
Moschorhinus	4	6	260	5.560	BP/1/3983
Unnamed clade (CR5)					
Hofmeyriidae, new sp.	5	5	60	4.094	SAM-PK-K8516
Hofmeyria	5	3	89	4.488	SAM-PK-10525
Mirotenthes	5	5	110	4.700	UCMP 40467
Ictidostoma	5	3	74	4.304	CGS CM86-258
Ictidochampsa	5	6	115	4.744	RC 69
Viatkosuchus	5	4	170	5.135	Tatarinov, 1995 (PIN 2212/13)
Moschowhaitsia	5	6	250[*]	5.521	Ivakhnenko, 2011 (PIN 1100/20)
Theriognathus	5	5	336	5.817	BP/1/4008
Ictidosuchidae (CR6)					
Ictidosuchus	6	4	150	5.010	SAM-PK-K10650
Ictidosuchoides	6	3	146	4.983	SAM-PK-K6886
Regisaurus (CR7)	7	7	123	4.812	CGS AK86/7

	CR	AR	MaxBSL	lnBSL	Voucher specimen/Source
Unnamed clade (CR8)					
Karenites	8	4	100*	4.605	Ivakhnenko, 2011 (PIN 2212/93)
Zambian karenitid	8	5	77	4.343	NHCC LB44
Lycideops	8	6	210	5.347	NHMUK R5695
Choerosaurus	8	4	89	4.488	SAM-PK-8797
Tetracynodon tenuis	8	6	63	4.143	RC 89
Tetracynodon darti	8	7	75	4.317	UCMP 42869
Scaloposaurus (CR9)	9	7	67	4.204	NMQR 3323
Ericiolacertidae (CR10)					
Ericiolacerta	10	7	59	4.077	BP/1/4794
Silphedosuchus	10	7	35*	3.555	Ivakhnenko, 2011 (PIN 951/100)
Ordosiidae (CR11)					
Ordosiodon	11	9	101	4.615	Hou, 1979 (IVPP V4786)
Hazhenia	11	8	157	5.056	Sun and Hou, 1981 (IVPP V5866)
Bauriidae (CR12)					
Bauria	12	9	130	4.867	AMNH FR 5622
Microgomphodon	12	8	87	4.465	SAM-PK-K10160
Cynodontia					
Basal cynodont, n. sp.	n/a	6	185	5.220	SAM-PK-K10702
Charassognathus (CR1)	1	4	63	4.143	SAM-PK-K10369
Dvinia (CR2)	2	6	88	4.477	PIN 2005/2469
Procynosuchus (CR3)	3	4	60	4.094	SAM-PK-K10138
Galesauridae (CR4)					
Cynosaurus	4	5	48	3.871	BP/1/1563
Galesaurus	4	7	120	4.787	NMQR 860
Progalesaurus	4	7	93	4.532	SAM-PK-K9954
Thrinaxodon (CR5)	5	7	100	4.605	SAM-PK-K1461
Platycraniellus (CR6)	6	7	84	4.430	Abdala, 2007 (TM 25)
Cynognathia (CR7)					
Cynognathus	7	8	330	5.799	SAM-PK-11484

	CR	AR	MaxBSL	lnBSL	Voucher specimen/Source
Diademodon	7	9	265	5.579	BP/1/3754
Sinognathus	7	9	121	4.795	Abdala et al., 2005 (IVPP V2339)
Beishanodon	7	8	232*	5.446	Gao et al., 2010 (PKUP V3007)
Trirachodon	7	8	105	4.653	SAM-PK-K10762
Langbergia	7	8	115	4.744	BP/1/5362
Cricodon	7	9	160	5.075	Abdala et al., 2005 (BP/1/5540)
Luangwa	7	9	142	4.955	BP/1/3731
Dadadon	7	10	143	4.962	Ranivoharimanana et al., 2011 (FMNH PR2232)
Massetognathus	7	10	204	5.318	Abdala and Giannini, 2000 (PULR11)
Protuberum	7	10	200	5.298	Reichel et al., 2009 (MGB 368-100)
Exaeretodon	7	11	400	5.991	Abdala et al., 2002 (MCZ 4486)
Lumkuia (CR8)	8	9	58	4.060	BP/1/2669
Unnamed clade (CR9)					
Ecteninion	9	11	98	4.584	Martinez et al., 1996 (PVSJ 422)
Trucidocynodon	9	11	187	5.231	Oliveira et al., 2010 (UFRGS PV1051T)
Chiniquodontidae (CR10)					
Chiniquodon	10	10	310	5.736	Abdala and Giannini, 2002 (UFRGS PV0122T)
Aleodon	10	9	156	5.049	Abdala and Smith, 2009 (GSN EN3)
Probainognathus (CR11)	11	10	83	4.418	Romer, 1970; Sidor, 2000 (MCZ 4277)
Therioherpeton (CR12)	12	11	33*	3.496	Oliveira, 2006 (MVP05.22.04)
Ictidosauria (CR13)					
Riograndia	13	12	35	3.555	Bonaparte et al., 2001; Soares et al., 2011 (MCN PV2264; UFRGS PV0569T)
Chaliminia	13	13	48	3.871	Martinelli et al., 2007 (PVL 3257)
Elliotherium	13	13	58	4.060	BP/1/6106
Brasilodontidae (CR14)					
Brasilodon	14	12	26	3.258	Bonaparte et al., 2003 (UFRGS PV0628T)

	CR	AR	MaxBSL	lnBSL	Voucher specimen/Source
Brasilitherium	14	12	27	3.295	Bonaparte et al., 2005 (UFRGS PV0929T)
Mammaliaformes (CR15)					
Sinoconodon	15	13	37	3.610	Patterson and Olson, 1961; Crompton and Sun, 1985 (IVPP 4727; IVPP 8683; IVPP 8692)
Morganucodon	15	13	26*	3.258	Kermack et al., 1981

CR, clade rank; AR, age rank;
Asterisk (*) denotes estimation of measurement from cited source;
† CR values correspond to side branches designated in Figure 3.3;
‡ AR values correspond to: 1, Wordian (Middle Permian) *Eodicynodon* AZ; 2, Capitanian (Middle Permian) *Tapinocephalus* AZ; 3, Capitanian-Wuchiapingian (Middle-Late Permian) *Pristerognathus* AZ; 4, Wuchiapingian (early Late Permian) *Tropidostoma* AZ; 5, Wuchiapingian (Late Permian) *Cistecephalus* AZ; 6, Wuchiapingian-Changxingian (Late Permian) *Dicynodon* AZ; 7, Induan-Olenekian (Early Triassic) *Lystrosaurus* AZ; 8, Olenekian (late Early Triassic) *Cynognathus* subzone A; 9, Anisian (early Middle Triassic) *Cynognathus* subzones B-C; 10, Ladinian (late Middle Triassic); 11, Carnian (early Late Triassic); 12, Norian (Late Triassic); 13, Rhaetian (latest Triassic).

APPENDIX 9. Bone tissue typology and radial periosteal bone apposition rates in long bone diaphyses of selected tetrapods.

	Species	Element	Tissue type	Est. radial growth rate µm/d	Reference
Lissamphibia	*Triturus cristatus*	humerus	LNV	0.15 - 0.25	Francillon 1979; Ricqles et al. 1991
Metatheria	*Didelphis virginiana*	femur	LSV	1.70 - 2.00	
Eutheria	*Bos primigenius*	femur	laminar FLB	2.50 - 4.50	Ricqles et al. 1991
	Cavia porcellus	humerus		30.0	Cubo et al. 2012
		femur		40.2	Cubo et al. 2012
	Microcebus murinus	humerus	reticular FLB	10.9	Cubo et al. 2012
		femur	reticular FLB	13.0	Cubo et al. 2012
		tibia	reticular FLB	13.8	Castanet et al. 2004; Cubo et al. 2012
	Mus musculus	humerus		22.2	Cubo et al. 2012
		femur		24	Cubo et al. 2012
	Neovison vison	femur	longitudinal & reticular FLB	1.80 - 2.90	
	Rattus sp.	femur	longitudinal & reticular FLB	3.20	Ricqles et al. 1991
Testudines	*Chelodina siebenrocki*	humerus	LSV	0.30	Cubo et al. 2012
		femur	LSV	0.20	Cubo et al. 2012
	Emys orbicularis	femur	LSV	0.22 - 0.25	Ricqles et al. 1991
	Pelodiscus sinensis	humerus	LSV	1.60	Cubo et al. 2012
		femur	LSV	1.50	Cubo et al. 2012
	Trachemys scripta	humerus	LSV	2.70	Cubo et al. 2012
		femur	LSV	3.50	Cubo et al. 2012
Squamata	*Lacerta viridis*	femur	LNV	0.14 - 0.56	Castanet 1985; Ricqles et al. 1991
	Lacerta vivipara	humerus	LNV	1.00	Cubo et al. 2012
		femur	LNV	1.00	Cubo et al. 2012
	Podarcis muralis	humerus		0.80	Cubo et al. 2012
		femur		1.10	Cubo et al. 2012

	Varanus exanthematicus	humerus		5.30	Cubo et al. 2012
		femur		7.50	Cubo et al. 2012
	Varanus niloticus	humerus	LPO	3.0	Buffrenil et al. 2008; Cubo et al. 2012
		femur	LPO	4.0	Buffrenil et al. 2008; Cubo et al. 2012
Crocodylia	*Crocodylus niloticus*	humerus	LPO	13.5	Cubo et al. 2012
		femur	LPO	9.5	Cubo et al. 2012
Aves	*Anas platyrhynchos*	humerus	FLB	44	Margerie et al. 2002; Cubo et al. 2012
		femur	FLB	73	Margerie et al. 2002; Cubo et al. 2012
	Dromaius novaehollandiae	humerus		26	Cubo et al. 2012
		femur		91	Cubo et al. 2012
	Streptopelia decaocto	humerus		119	Cubo et al. 2012
		femur		64	Cubo et al. 2012
	Struthio camelus	humerus		56	Cubo et al. 2012
		femur		156	Cubo et al. 2012
	Turdus merula	humerus		195	Cubo et al. 2012
		femur		102	Cubo et al. 2012

Abbreviations: FLB, fibrolamellar bone complex; LNV, lamellar bone with no vascular canals; LPO, parallel-fibered bone with primary osteons; LSV, lamellar or parallel-fibered bone with simple vascular canals;

Sources: Buffrénil, V. de, Houssaye, A., & Böhme, W. (2008). Bone vascular supply in monitor lizards (Squamata: Varanidae): influence of size, growth, and phylogeny. *Journal of Morphology*, *269*:533-543; Castanet, J. (1985). La squelettochronologie chez les reptiles. I: résultats expérimentaux sur la signification des marques de croissance squelettiques chez les lézards et les tortues. *Annales des Sciences Naturelles. Zoologie et Biologie Animale* 7:23-40; Castanet, J., Croci, S., Aujard, F., Perret, M., Cubo, J., & Margerie, E. D. (2004). Lines of arrested growth in bone and age estimation in a small primate: Microcebus murinus. *Journal of Zoology*, *263*:31-39; Cubo, J., Le Roy, N., Martinez-Maza, C., & Montes, L. (2012). Paleohistological estimation of bone growth rate in extinct archosaurs. *Paleobiology*, *38*:335-349; Francillon, H. (1979). Etude expérimentale des marques de croissance sur les humérus et les fémurs de Tritons crêtés (Tritus cristatus cristatus Laurenti) en relation avec la détermination de l'âge individuel. *Acta Zoologica*, *60*:223-232; Margerie, E. de, Cubo, J., & Castanet, J. (2002). Bone typology and growth rate: testing and quantifying 'Amprino's rule'in the mallard (*Anas platyrhynchos*). *Comptes Rendus Biologies*, *325*:221-230; Ricqlès, A. de, Meunier, F. J., Castanet, J., & Francillon-Vieillot, H. (1991). Comparative microstructure of bone. Pp. 1-78 in B. K. Hall (ed.) *Bone*, *Vol. 3*. CRC Press, Boca Raton.

APPENDIX 10. Complete list of specimens measured for basal skull length (BSL). Only skulls with complete BSL measurements are shown.

thero/ cyno	Karoo/ non-karoo	Period/Interval	Taxon	Country/Basin	Specimen no.	Basal skull length (mm)
thero	karoo	Permian/EoAZ	*Ictidosaurus angusticeps*	South Africa/Karoo Basin	NMQR 2910	168 (est. Abdala et al. 2007)
thero	karoo	Permian/TaAZ	*Glanosuchus macrops*	South Africa/Karoo Basin	SAM-PK-K07808	223
thero	karoo	Permian/TaAZ	*Glanosuchus macrops*	South Africa/Karoo Basin	SAM-PK-K07809	233
thero	karoo	Permian/TaAZ	Lycosuchidae (cf. *Lycosuchus*)	South Africa/Karoo Basin	BP/1/276	305
thero	karoo	Permian/TaAZ	Lycosuchidae (cf. *Lycosuchus*)	South Africa/Karoo Basin	CGS RMS335	288
thero	karoo	Permian/TaAZ	Lycosuchidae (cf. *Lycosuchus*)	South Africa/Karoo Basin	CGS RMS1013	228
thero	karoo	Permian/TaAZ	Lycosuchidae (cf. *Lycosuchus*)	South Africa/Karoo Basin	SAM-PK-009084	340
thero	karoo	Permian/TaAZ	Lycosuchidae (cf. *Lycosuchus*)	South Africa/Karoo Basin	SAM-PK-011843	282
thero	karoo	Permian/TaAZ	Lycosuchidae (cf. *Lycosuchus*)	South Africa/Karoo Basin	UCMP 42395	240
thero	karoo	Permian/TaAZ	*Lycosuchus vanderrieti* ("*Zinnosaurus*" type)	South Africa/Karoo Basin	SAM-PK-012185	230
thero	karoo	Permian/TaAZ	*Pristerognathus polyodon* ("*Ptomalestes*" type)	South Africa/Karoo Basin	SAM-PK-11492	262
thero	karoo	Permian/TaAZ	Scylacosauridae	South Africa/Karoo Basin	BP/1/278	210
thero	karoo	Permian/TaAZ	Scylacosauridae	South Africa/Karoo Basin	BP/1/1768	165
thero	karoo	Permian/TaAZ	Scylacosauridae (cf. *Glanosuchus*)	South Africa/Karoo Basin	BP/1/6228	156.5
thero	karoo	Permian/TaAZ	Scylacosauridae ("*Blattoidealestes*" type)	South Africa/Karoo Basin	SAM-PK-004321	50
thero	karoo	Permian/TaAZ	Scylacosauridae	South Africa/Karoo Basin	UCMP 42659	90.9
thero	karoo	Permian/TaAZ	Scylacosauridae	South Africa/Karoo Basin	UCMP 42667	324

thero	karoo	Permian/TaAZ	Scylacosauridae (cf. *Glanosuchus*)	South Africa/Karoo Basin	UCMP 42669	330
thero	karoo	Permian/PAZ	*Hofmeyria atavus*	South Africa/Karoo Basin	SAM-PK-K10525	89
thero	karoo	Permian/PAZ	Hofmeryiidae (cf. *Hofmeyria*)	South Africa/Karoo Basin	CGS RS51	71
thero	karoo	Permian/PAZ	Hofmeryiidae (cf. *Ictidostoma*)	South Africa/Karoo Basin	CGS CM86-258	74
thero	karoo	Permian/PAZ	*Ictidosuchoides longiceps*	South Africa/Karoo Basin	SAM-PK-K06886	146
thero	karoo	Permian/PAZ	Scylacosauridae (cf. *Glanosuchus*)	South Africa/Karoo Basin	SAM-PK-K10540	135
thero	karoo	Permian/TrAZ	*Choerosaurus dejageri*	South Africa/Karoo Basin	SAM-PK-008797	89.9
thero	karoo	Permian/TrAZ	*Hofmeyria atavus*	South Africa/Karoo Basin	BP/1/1399	90.3
thero	karoo	Permian/TrAZ	Hofmeryiidae (cf. *Ictidostoma*)	South Africa/Karoo Basin	BP/1/3155	99.85
thero	karoo	Permian/TrAZ	Hofmeryiidae (cf. *Ictidostoma*)	South Africa/Karoo Basin	SAM-PK-K06731	89.85
thero	karoo	Permian/TrAZ	Hofmeyriidae	South Africa/Karoo Basin	SAM-PK-K10629	155
thero	karoo	Permian/TrAZ	*Ictidosuchoides longiceps*	South Africa/Karoo Basin	SAM-PK-K06670	134
thero	karoo	Permian/TrAZ	*Ictidosuchoides longiceps*	South Africa/Karoo Basin	SAM-PK-K07784	52
thero	karoo	Permian/TrAZ	*Ictidosuchoides longiceps*	South Africa/Karoo Basin	SAM-PK-K08659	101
thero	karoo	Permian/TrAZ	*Ictidosuchus primaevus*	South Africa/Karoo Basin	AMNH 5529	130 (est)
thero	karoo	Permian/TrAZ	*Ictidosuchus primaevus*	South Africa/Karoo Basin	SAM-PK-K10650	150.5
thero	karoo	Permian/CiAZ	Akidnognathid new sp.	South Africa/Karoo Basin	USNM PAL 412421	218
thero	karoo	Permian/CiAZ	*Euchambersia mirabilis*	South Africa/Karoo Basin	BP/1/4009	83
thero	karoo	Permian/CiAZ	*Euchambersia mirabilis*	South Africa/Karoo Basin	NHMUK R5696	115
thero	karoo	Permian/CiAZ	*Hofmeyria atavus*	South Africa/Karoo Basin	RC 639	83.5
thero	karoo	Permian/CiAZ	*Hofmeyria atavus*	South Africa/Karoo	BP/1/4401	97

				Basin		
thero	karoo	Permian/CiAZ	*Hofmeyria atavus*	South Africa/Karoo Basin	BP/1/4404	67.5
thero	karoo	Permian/CiAZ	Hofmeyriidae new sp.	South Africa/Karoo Basin	SAM-PK-K8516	60
thero	karoo	Permian/CiAZ	*Ictidostoma hemburyi*	South Africa/Karoo Basin	BP/1/3052	97.5
thero	karoo	Permian/CiAZ	*Ictidosuchoides longiceps*	South Africa/Karoo Basin	BP/1/218	100
thero	karoo	Permian/CiAZ	*Ictidosuchoides longiceps*	South Africa/Karoo Basin	BP/1/223	84.78
thero	karoo	Permian/CiAZ	*Ictidosuchoides longiceps*	South Africa/Karoo Basin	BP/1/1321	129
thero	karoo	Permian/CiAZ	*Ictidosuchoides longiceps*	South Africa/Karoo Basin	BP/1/1334	99.87
thero	karoo	Permian/CiAZ	*Ictidosuchoides longiceps*	South Africa/Karoo Basin	BP/1/2125	83.53
thero	karoo	Permian/CiAZ	*Ictidosuchoides longiceps*	South Africa/Karoo Basin	BP/1/2294	90.75
thero	karoo	Permian/CiAZ	*Ictidosuchoides longiceps*	South Africa/Karoo Basin	BP/1/3506	96.77
thero	karoo	Permian/CiAZ	*Ictidosuchoides longiceps*	South Africa/Karoo Basin	BP/1/4092	200
thero	karoo	Permian/CiAZ	*Ictidosuchoides longiceps*	South Africa/Karoo Basin	UCMP 42702	99
thero	karoo	Permian/CiAZ	*Mirotenthes digitipes*	South Africa/Karoo Basin	CGS STH65	112.8
thero	karoo	Permian/CiAZ	*Mirotenthes digitipes*	South Africa/Karoo Basin	SAM-PK-K06511	87.5
thero	karoo	Permian/CiAZ	*Mirotenthes digitipes*	South Africa/Karoo Basin	UCMP 40467	110
thero	karoo	Permian/CiAZ	*Theriognathus microps*	South Africa/Karoo Basin	RC 380	240
thero	karoo	Permian/CiAZ	*Theriognathus microps*	South Africa/Karoo Basin	SAM-PK-K10981	260
thero	karoo	Permian/CiAZ	*Theriognathus microps*	South Africa/Karoo Basin	USNM 23355	109
thero	karoo	Permian/CiAZ/DAZ?	Akidnognathidae	South Africa/Karoo Basin	MCZ 8960	110
thero	karoo	Permian/CiAZ/DAZ?	Akidnognathidae	South Africa/Karoo Basin	SAM-PK-K7454	100

thero	karoo	Permian/CiAZ/DAZ?	Baurioidea (ictidosuchid?)	South Africa/Karoo Basin	SAM-PK-K07590	72
thero	karoo	Permian/CiAZ/DAZ?	Baurioidea (ictidosuchid?)	South Africa/Karoo Basin	SAM-PK-K07439	102
thero	karoo	Permian/CiAZ/DAZ?	*Ictidosuchoides longiceps*	South Africa/Karoo Basin	CGS CM86-655	92.6
thero	karoo	Permian/CiAZ/DAZ?	Lycideopidae *(*cf. *Lycideops)*	South Africa/Karoo Basin	CGS C104	75
thero	karoo	Permian/CiAZ/DAZ?	*Theriognathus microps*	South Africa/Karoo Basin	BP/1/747	141.84
thero	karoo	Permian/DAZ	*Akidnognathus parvus* ("*Proalopecopsis*" type)	South Africa/Karoo Basin	BP/1/499	150
thero	karoo	Permian/DAZ	*Akidnognathus parvus*	South Africa/Karoo Basin	SAM-PK-004021	103
thero	karoo	Permian/DAZ	*Cerdosuchoides brevidens*	South Africa/Karoo Basin	CGS CM86/778	115.5
thero	karoo	Permian/DAZ	*Cerdosuchoides brevidens*	South Africa/Karoo Basin	RC 58	134
thero	karoo	Permian/DAZ	*Ictidochampsa platyceps*	South Africa/Karoo Basin	RC69	115
thero	karoo	Permian/DAZ	*Ictidosuchoides longiceps*	South Africa/Karoo Basin	NHMUK R5744	135
thero	karoo	Permian/DAZ	*Ictidosuchoides longiceps*	South Africa/Karoo Basin	RC 105	86
thero	karoo	Permian/DAZ	*Ictidosuchoides longiceps*	South Africa/Karoo Basin	RC 106	101.5
thero	karoo	Permian/DAZ	*Lycideops longiceps*	South Africa/Karoo Basin	NHMUK R5695	210
thero	karoo	Permian/DAZ	*Lycideops longiceps*	South Africa/Karoo Basin	RC 646	155
thero	karoo	Permian/DAZ	*Mirotenthes digitipes*	South Africa/Karoo Basin	CGS JKW83-40	76
thero	karoo	Permian/DAZ	*Moschorhinus kitchingi*	South Africa/Karoo Basin	BP/1/2788	215
thero	karoo	Permian/DAZ	*Moschorhinus kitchingi*	South Africa/Karoo Basin	BP/1/3983	260
thero	karoo	Permian/DAZ	*Moschorhinus kitchingi*	South Africa/Karoo Basin	CGS GHG148	160
thero	karoo	Permian/DAZ	*Moschorhinus kitchingi*	South Africa/Karoo Basin	CGS GHG299	200
thero	karoo	Permian/DAZ	*Moschorhinus kitchingi*	South Africa/Karoo	CGS JFD32/92	225

				Basin		
thero	karoo	Permian/DAZ	*Moschorhinus kitchingi*	South Africa/Karoo Basin	NMQR 76	230
thero	karoo	Permian/DAZ	*Moschorhinus kitchingi*	South Africa/Karoo Basin	NMQR 3351	240
thero	karoo	Permian/DAZ	*Moschorhinus kitchingi*	South Africa/Karoo Basin	NMQR 3835	254
thero	karoo	Permian/DAZ	*Moschorhinus kitchingi*	South Africa/Karoo Basin	NMQR 3921	215
thero	karoo	Permian/DAZ	*Moschorhinus kitchingi*	South Africa/Karoo Basin	NMQR 3939	170
thero	karoo	Permian/DAZ	*Moschorhinus kitchingi*	South Africa/Karoo Basin	RC 32	232
thero	karoo	Permian/DAZ	*Moschorhinus kitchingi*	South Africa/Karoo Basin	RC 99	223
thero	karoo	Permian/DAZ	*Moschorhinus kitchingi*	South Africa/Karoo Basin	SAM-PK-K10015a	230
thero	karoo	Permian/DAZ	*Promoschorhynchus platyrhinus*	South Africa/Karoo Basin	RC 116	125
thero	karoo	Permian/DAZ	*Tetracynodon tenuis*	South Africa/Karoo Basin	RC 89	63
thero	karoo	Permian/DAZ	*Theriognathus microps*	South Africa/Karoo Basin	AMNH FR 8226	151
thero	karoo	Permian/DAZ	*Theriognathus microps*	South Africa/Karoo Basin	BP/1/ 100	185
thero	karoo	Permian/DAZ	*Theriognathus microps*	South Africa/Karoo Basin	BP/1/145	200.91
thero	karoo	Permian/DAZ	*Theriognathus microps*	South Africa/Karoo Basin	BP/1/ 164	132
thero	karoo	Permian/DAZ	*Theriognathus microps*	South Africa/Karoo Basin	BP/1/ 182	67
thero	karoo	Permian/DAZ	*Theriognathus microps*	South Africa/Karoo Basin	BP/1/ 512	125
thero	karoo	Permian/DAZ	*Theriognathus microps*	South Africa/Karoo Basin	BP/1/717	244.92
thero	karoo	Permian/DAZ	*Theriognathus microps*	South Africa/Karoo Basin	BP/1/ 724	150
thero	karoo	Permian/DAZ	*Theriognathus microps*	South Africa/Karoo Basin	BP/1/ 785	210
thero	karoo	Permian/DAZ	*Theriognathus microps*	South Africa/Karoo Basin	BP/1/ 844	162

thero	karoo	Permian/DAZ	*Theriognathus microps*	South Africa/Karoo Basin	BP/1/ 4008	336
thero	karoo	Permian/DAZ	*Theriognathus microps*	South Africa/Karoo Basin	CGS AF124-83	128
thero	karoo	Permian/DAZ	*Theriognathus microps*	South Africa/Karoo Basin	CGS K274	188
thero	karoo	Permian/DAZ	*Theriognathus microps*	South Africa/Karoo Basin	CGS K280	158
thero	karoo	Permian/DAZ	*Theriognathus microps*	South Africa/Karoo Basin	CGS WB261	128
thero	karoo	Permian/DAZ	*Theriognathus microps*	South Africa/Karoo Basin	NMQR 1549	300
thero	karoo	Permian/DAZ	*Theriognathus microps*	South Africa/Karoo Basin	NMQR 3375	128
thero	karoo	Permian/DAZ	*Theriognathus microps*	South Africa/Karoo Basin	SAM-PK-4006	263.14
thero	karoo	Permian/DAZ	*Theriognathus microps*	South Africa/Karoo Basin	SAM-PK-K5263	213
thero	karoo	Permian/DAZ	*Theriognathus microps*	South Africa/Karoo Basin	SAM-PK-K7511	152.6
thero	karoo	Permian/DAZ	*Theriognathus microps*	South Africa/Karoo Basin	SAM-PK-K7453	224
thero	karoo	Permian/DAZ	*Theriognathus microps*	South Africa/Karoo Basin	SAM-PK-K10429	190.6
thero	karoo	Permian/DAZ	*Theriognathus microps*	South Africa/Karoo Basin	UCM 23381	155
thero	karoo	Permian/DAZ	*Theriognathus microps*	South Africa/Karoo Basin	UCMP 42675	160
thero	karoo	Permian/DAZ	*Theriognathus microps*	South Africa/Karoo Basin	UCMP 42676	210
thero	karoo	Permian/DAZ	Whaitsiidae (cf. *Theriognathus)*	South Africa/Karoo Basin	BP/1/ 4093	125
thero	karoo	DAZ/LAZ?	*Moschorhinus kitchingi*	South Africa/Karoo Basin	BP/1/1713	262
thero	karoo	DAZ/LAZ?	*Moschorhinus kitchingi*	South Africa/Karoo Basin	CGS JFD9/94	210
thero	karoo	DAZ/LAZ?	*Moschorhinus kitchingi*	South Africa/Karoo Basin	NMQR 48	163
thero	karoo	Permian unknown	Hofmeyriidae (cf. *Ictidostoma*)	South Africa/Karoo Basin	CGS JNN10/0/01	92
thero	karoo	Permian unknown	Ictidosuchidae	South Africa/Karoo	CGS GM60	99

				Basin		
thero	karoo	Permian unknown	*Ictidosuchoides longiceps*	South Africa/Karoo Basin	SAM-PK-K07441	110.8
thero	karoo	Permian unknown	Lycosuchidae (cf. *Lycosuchus*)	South Africa/Karoo Basin	CGS S273	165
thero	karoo	Permian unknown	Scylacosauridae (cf. *Glanosuchus*)	South Africa/Karoo Basin	CGS RS330	238
thero	karoo	Triassic/LAZ	Akidnognathidae (cf. *Olivierosuchus*)	South Africa/Karoo Basin	BP/1/4283	90.12
thero	karoo	Triassic/LAZ	Akidnognathidae (cf. *Olivierosuchus*)	South Africa/Karoo Basin	SAM-PK-K00117	105
thero	karoo	Triassic/LAZ	Akidnognathidae ("*Zorillodontops*" type)	South Africa/Karoo Basin	SAM-PK-K01392	42.5
thero	karoo	Triassic/LAZ	Baurioidea	South Africa/Karoo Basin	BP/1/4583a	70
thero	karoo	Triassic/LAZ	Baurioidea	South Africa/Karoo Basin	BP/1/4583b	64
thero	karoo	Triassic/LAZ	Baurioidea	South Africa/Karoo Basin	BP/1/4583c	56
thero	karoo	Triassic/LAZ	Baurioidea	South Africa/Karoo Basin	BP/1/4583d	59
thero	karoo	Triassic/LAZ	Baurioidea	South Africa/Karoo Basin	BP/1/4583e	57
thero	karoo	Triassic/LAZ	Baurioidea	South Africa/Karoo Basin	NMQR 3578	69
thero	karoo	Triassic/LAZ	*Ericiolacerta parva*	South Africa/Karoo Basin	CAMZM R377/T369	45 (Watson 1931)
thero	karoo	Triassic/LAZ	Ericiolacertidae (cf. *Ericiolacerta*)	South Africa/Karoo Basin	BP/1/4794	59
thero	karoo	Triassic/LAZ	Lycideopidae (cf. *Tetracynodon*)	South Africa/Karoo Basin	UCMP 40499	53
thero	karoo	Triassic/LAZ	*Moschorhinus kitchingi*	South Africa/Karoo Basin	BP/1/4227	200
thero	karoo	Triassic/LAZ	*Moschorhinus kitchingi*	South Africa/Karoo Basin	CGS GHG 295	190
thero	karoo	Triassic/LAZ	*Moschorhinus kitchingi*	South Africa/Karoo Basin	CGS GHG 324	136
thero	karoo	Triassic/LAZ	*Moschorhinus kitchingi*	South Africa/Karoo Basin	NMQR 3568	198
thero	karoo	Triassic/LAZ	*Moschorhinus kitchingi*	South Africa/Karoo Basin	SAM-PK-K00118	157

thero	karoo	Triassic/LAZ	*Moschorhinus kitchingi*	South Africa/Karoo Basin	SAM-PK-K09953	155
thero	karoo	Triassic/LAZ	*Olivierosuchus parringtoni*	South Africa/Karoo Basin	BP/1/3849	103
thero	karoo	Triassic/LAZ	*Olivierosuchus parringtoni*	South Africa/Karoo Basin	BP/1/3973	96
thero	karoo	Triassic/LAZ	*Olivierosuchus parringtoni*	South Africa/Karoo Basin	CGS 426	92
thero	karoo	Triassic/LAZ	*Olivierosuchus parringtoni*	South Africa/Karoo Basin	NMQR 62	98
thero	karoo	Triassic/LAZ	*Olivierosuchus parringtoni*	South Africa/Karoo Basin	NMQR 3605	122
thero	karoo	Triassic/LAZ	*Promoschorhynchus* cf. *P. platyrhinus*	South Africa/Karoo Basin	SAM-PK-K10014	119
thero	karoo	Triassic/LAZ	Regisauridae (cf. *Regisaurus*)	South Africa/Karoo Basin	BP/1/1341	45.9
thero	karoo	Triassic/LAZ	Regisauridae (cf. *Regisaurus*)	South Africa/Karoo Basin	BP/1/5895	55.25
thero	karoo	Triassic/LAZ	Regisauridae (cf. *Regisaurus*)	South Africa/Karoo Basin	CGS S273	80
thero	karoo	Triassic/LAZ	Regisauridae (cf. *Regisaurus*)	South Africa/Karoo Basin	NMQR 597	42
thero	karoo	Triassic/LAZ	Regisauridae (cf. *Regisaurus*)	South Africa/Karoo Basin	SAM-PK-K10613	69.38
thero	karoo	Triassic/LAZ	Regisauridae (cf. *Regisaurus*)	South Africa/Karoo Basin	SAM-PK-10980	54
thero	karoo	Triassic/LAZ	Regisauridae (cf. *Regisaurus*)	South Africa/Karoo Basin	UCMP 42782	42
thero	karoo	Triassic/LAZ	*Regisaurus jacobi*	South Africa/Karoo Basin	BP/1/5394	118
thero	karoo	Triassic/LAZ	*Regisaurus jacobi*	South Africa/Karoo Basin	CGS AK86/7	123
thero	karoo	Triassic/LAZ	Scaloposauridae (cf. *Scaloposaurus*)	South Africa/Karoo Basin	BP/1/5220	58
thero	karoo	Triassic/LAZ	Scaloposauridae (cf. *Scaloposaurus*)	South Africa/Karoo Basin	SAM-PK-K10023	55.5
thero	karoo	Triassic/LAZ	Scaloposauridae (cf. *Scaloposaurus*)	South Africa/Karoo Basin	SAM-PK-K10382	45.33
thero	karoo	Triassic/LAZ	Scaloposauridae (cf. *Scaloposaurus*)	South Africa/Karoo Basin	SAM-PK-K10403	49.2
thero	karoo	Triassic/LAZ	*Scaloposaurus*	South Africa/Karoo	BP/1/5177	61

			constrictus	Basin		
thero	karoo	Triassic/LAZ	*Scaloposaurus constrictus*	South Africa/Karoo Basin	NHMUK R1723	48
thero	karoo	Triassic/LAZ	*Scaloposaurus constrictus*	South Africa/Karoo Basin	NMQR 1457	44.5
thero	karoo	Triassic/LAZ	*Scaloposaurus constrictus*	South Africa/Karoo Basin	NMQR 3323	67.5
thero	karoo	Triassic/LAZ	*Scaloposaurus constrictus*	South Africa/Karoo Basin	SAM-PK-K4638	45
thero	karoo	Triassic/LAZ	*Scaloposaurus constrictus*	South Africa/Karoo Basin	SAM-PK-K7881	61
thero	karoo	Triassic/LAZ	*Scaloposaurus constrictus*	South Africa/Karoo Basin	SAM-PK-K10604	49
thero	karoo	Triassic/LAZ	*Tetracynodon darti*	South Africa/Karoo Basin	BP/1/2710	74
thero	karoo	Triassic/LAZ	*Tetracynodon darti*	South Africa/Karoo Basin	NMQR 3597	65
thero	karoo	Triassic/LAZ	*Tetracynodon darti*	South Africa/Karoo Basin	NMQR3745a	64
thero	karoo	Triassic/LAZ	*Tetracynodon darti*	South Africa/Karoo Basin	NMQR 3756	63
thero	karoo	Triassic/LAZ	*Tetracynodon darti*	South Africa/Karoo Basin	SAM-PK-K10800	59
thero	karoo	Triassic/LAZ	*Tetracynodon darti*	South Africa/Karoo Basin	UCMP 42869	75
thero	karoo	Triassic/LAZ	*Tetracynodon darti*	South Africa/Karoo Basin	UCMP 78394	70
thero	karoo	Triassic/CyAZ-A	Bauriidae (cf. *Microgomphodon*)	South Africa/Karoo Basin	CGS JNN/99-2-3	51.2
thero	karoo	Triassic/CyAZ-B	*Bauria cynops*	South Africa/Karoo Basin	AMNH FR 5622	130
thero	karoo	Triassic/CyAZ-B	*Bauria cynops*	South Africa/Karoo Basin	BP/1/1180	114
thero	karoo	Triassic/CyAZ-B	*Bauria cynops*	South Africa/Karoo Basin	BP/1/3770	117
thero	karoo	Triassic/CyAZ-B	*Bauria cynops*	South Africa/Karoo Basin	NHMUK R4095	91
thero	karoo	Triassic/CyAZ-B/C	*Microgomphodon oligocynus*	South Africa/Karoo Basin	NHMUK R3305	63
thero	karoo	Triassic/CyAZ-B/C	*Microgomphodon oligocynus*	South Africa/Karoo Basin	NMQR 3596	69

thero	karoo	Triassic/CyAZ-B/C	*Microgomphodon oligocynus*	South Africa/Karoo Basin	SAM-PK-K10160	87.36
thero	non-karoo	Permian/PAZ-TrAZ	*Karenites ornamentatus* ("*Scalopodon*" type)	Russia/Kirov region	PIN 2212/93	100 (est.)
thero	non-karoo	Permian/PAZ-TrAZ	*Scylacosuchus orenburgensis*	Russia/Orenburg region	PIN 2628/1	250 (est.)
thero	non-karoo	Permian/PAZ-TrAZ	*Viatkosuchus sumini*	Russia/Kirov region	PIN 2212/13	170
thero	non-karoo	Permian/CiAZ	Karenitidae new sp.	Zambia/Luangwa Basin	NHCC LB44	86
thero	non-karoo	Permian/CiAZ-DAZ	*Annatherapsidus petri*	Russia/Arkhangelsk region	PIN 2005/1993	250 (est.)
thero	non-karoo	Permian/DAZ	*Moschowhaitsia vjuschkovi*	Russia/Vladimir region	PIN 1100/20	250 (est.)
thero	non-karoo	Triassic/LAZ	*Silphedosuchus orenburgensis*	Russia/Orenburg region	PIN 951/100	35 (est.)
thero	non-karoo	Triassic/CyAZ-A	*Hazhenia concava*	China/Ordos Basin	IVPP_V5866	157 (Sun and Hou 1981)
thero	non-karoo	Triassic/CyAZ-B/C	*Ordosiodon youngi*	China/Ordos Basin	IVPP_V4786	101 (Hou 1979)
cyno	karoo	Permian/TrAZ	*Charassognathus gracilis*	South Africa/Karoo Basin	SAM-PK-K10369	63.98
cyno	karoo	Permian/TrAZ	Procynosuchidae (cf. *Procynosuchus*)	South Africa/Karoo Basin	SAM-PK-K10138	60
cyno	karoo	Permian/CiAZ	*Cynosaurus suppostus*	South Africa/Karoo Basin	BP/1/47	45
cyno	karoo	Permian/CiAZ	*Cynosaurus suppostus*	South Africa/Karoo Basin	BP/1/1563	48
cyno	karoo	Permian/CiAZ	*Procynosuchus delaharpeae*	South Africa/Karoo Basin	BP/1/591	82.6
cyno	karoo	Permian/CiAZ	*Procynosuchus delaharpeae*	South Africa/Karoo Basin	BP/1/1545	85.92
cyno	karoo	Permian/CiAZ	*Procynosuchus delaharpeae*	South Africa/Karoo Basin	BP/1/3747	115
cyno	karoo	Permian/CiAZ	*Procynosuchus delaharpeae*	South Africa/Karoo Basin	BP/1/3748	142
cyno	karoo	Permian/CiAZ	*Procynosuchus delaharpeae*	South Africa/Karoo Basin	RC92	152
cyno	karoo	Permian/CiAZ	*Procynosuchus delaharpeae*	South Africa/Karoo Basin	SAM-PK-K8511	99.5

cyno	karoo	Permian/CiAZ	*Procynosuchus delaharpeae*	South Africa/Karoo Basin	SAM-PK-K5339	51
cyno	karoo	Permian/CiAZ/DAZ?	*Procynosuchus delaharpeae*	South Africa/Karoo Basin	CGS R500	53.9
cyno	karoo	Permian/CiAZ/DAZ?	*Procynosuchus delaharpeae*	South Africa/Karoo Basin	NMQR 280	86.9
cyno	karoo	Permian/DAZ	Cynodontia new sp. (pers. obsv.)	South Africa/Karoo Basin	BP/1/6978	155
cyno	karoo	Permian/DAZ	Cynodontia new sp. (F. Abdala, pers. comm.)	South Africa/Karoo Basin	CGS GHG 141	178
cyno	karoo	Permian/DAZ	Cynodontia new sp. (F. Abdala, pers. comm.)	South Africa/Karoo Basin	SAM-PK-K10702	185
cyno	karoo	Permian/DAZ	*Cynosaurus suppostus*	South Africa/Karoo Basin	BP/1/3926	114.8
cyno	karoo	Permian/DAZ	*Cynosaurus suppostus*	South Africa/Karoo Basin	BP/1/4281	88
cyno	karoo	Permian/DAZ	*Cynosaurus suppostus*	South Africa/Karoo Basin	BP/1/4469	56.7
cyno	karoo	Permian/DAZ	*Procynosuchus delaharpeae*	South Africa/Karoo Basin	BP/1/226	84.79
cyno	karoo	Permian/DAZ	*Procynosuchus delaharpeae*	South Africa/Karoo Basin	BP/1/372	87.17
cyno	karoo	Permian/DAZ	*Procynosuchus delaharpeae*	South Africa/Karoo Basin	BP/1/650	58.19
cyno	karoo	Permian/DAZ	*Procynosuchus delaharpeae*	South Africa/Karoo Basin	RC 27	43
cyno	karoo	Permian/DAZ	*Procynosuchus delaharpeae*	South Africa/Karoo Basin	SAM-PK-K10394	107
cyno	karoo	Triassic/LAZ	Galesauridae	South Africa/Karoo Basin	BP/1/4637	74
cyno	karoo	Triassic/LAZ	Galesauridae	South Africa/Karoo Basin	BP/1/4602	83.5
cyno	karoo	Triassic/LAZ	*Galesaurus planiceps*	South Africa/Karoo Basin	BP/1/472	67.61
cyno	karoo	Triassic/LAZ	*Galesaurus planiceps*	South Africa/Karoo Basin	BP/1/4597	68.55
cyno	karoo	Triassic/LAZ	*Galesaurus planiceps*	South Africa/Karoo Basin	BP/1/4714	82.9
cyno	karoo	Triassic/LAZ	*Galesaurus planiceps*	South Africa/Karoo Basin	BP/1/5064	104
cyno	karoo	Triassic/LAZ	*Galesaurus planiceps*	South Africa/Karoo	NMQR 135	96.8

				Basin		
cyno	karoo	Triassic/LAZ	*Galesaurus planiceps*	South Africa/Karoo Basin	NMQR1451	90.5
cyno	karoo	Triassic/LAZ	*Galesaurus planiceps*	South Africa/Karoo Basin	NMQR3340	104.5
cyno	karoo	Triassic/LAZ	*Galesaurus planiceps*	South Africa/Karoo Basin	NMQR 3542	108
cyno	karoo	Triassic/LAZ	*Galesaurus planiceps*	South Africa/Karoo Basin	NMQR3678	72
cyno	karoo	Triassic/LAZ	*Galesaurus planiceps*	South Africa/Karoo Basin	RC845	67.7
cyno	karoo	Triassic/LAZ	*Galesaurus planiceps*	South Africa/Karoo Basin	SAM-PK-K1119	72
cyno	karoo	Triassic/LAZ	*Galesaurus planiceps*	South Africa/Karoo Basin	SAM-PK-K8549	80
cyno	karoo	Triassic/LAZ	*Galesaurus planiceps*	South Africa/Karoo Basin	SAM-PK-K9956	73
cyno	karoo	Triassic/LAZ	*Galesaurus planiceps*	South Africa/Karoo Basin	SAM-PK-K10448	103
cyno	karoo	Triassic/LAZ	*Platycraniellus elegans*	South Africa/Karoo Basin	NMQR860	114 (Abdala 2007)
cyno	karoo	Triassic/LAZ	*Platycraniellus elegans*	South Africa/Karoo Basin	TM25	84 (Abdala 2007)
cyno	karoo	Triassic/LAZ	*Progalesaurus lootsbergensis*	South Africa/Karoo Basin	SAM-PK-K9954	93.5
cyno	karoo	Triassic/LAZ	*Thrinaxodon liorhinus*	South Africa/Karoo Basin	BP/1/1375	81.93
cyno	karoo	Triassic/LAZ	*Thrinaxodon liorhinus*	South Africa/Karoo Basin	BP/1/1737	89
cyno	karoo	Triassic/LAZ	*Thrinaxodon liorhinus*	South Africa/Karoo Basin	BP/1/2793	81.19
cyno	karoo	Triassic/LAZ	*Thrinaxodon liorhinus*	South Africa/Karoo Basin	BP/1/4263	70.6
cyno	karoo	Triassic/LAZ	*Thrinaxodon liorhinus*	South Africa/Karoo Basin	BP/1/4280	66.42
cyno	karoo	Triassic/LAZ	*Thrinaxodon liorhinus*	South Africa/Karoo Basin	BP/1/5018	92
cyno	karoo	Triassic/LAZ	*Thrinaxodon liorhinus*	South Africa/Karoo Basin	BP/1/5208	74.66
cyno	karoo	Triassic/LAZ	*Thrinaxodon liorhinus*	South Africa/Karoo Basin	BP/1/5372	37

cyno	karoo	Triassic/LAZ	*Thrinaxodon liorhinus*	South Africa/Karoo Basin	NMQR 1416	85
cyno	karoo	Triassic/LAZ	*Thrinaxodon liorhinus*	South Africa/Karoo Basin	SAM-PK-K379	89
cyno	karoo	Triassic/LAZ	*Thrinaxodon liorhinus*	South Africa/Karoo Basin	SAM-PK-K1121a	66
cyno	karoo	Triassic/LAZ	*Thrinaxodon liorhinus*	South Africa/Karoo Basin	SAM-PK-K1121b	80
cyno	karoo	Triassic/LAZ	*Thrinaxodon liorhinus*	South Africa/Karoo Basin	SAM-PK-K1461	100
cyno	karoo	Triassic/LAZ	*Thrinaxodon liorhinus*	South Africa/Karoo Basin	SAM-PK-K1468	58
cyno	karoo	Triassic/LAZ	*Thrinaxodon liorhinus*	South Africa/Karoo Basin	SAM-PK-K1498	71
cyno	karoo	Triassic/LAZ	*Thrinaxodon liorhinus*	South Africa/Karoo Basin	SAM-PK-K1499	74
cyno	karoo	Triassic/LAZ	*Thrinaxodon liorhinus*	South Africa/Karoo Basin	SAM-PK-K8004a	30
cyno	karoo	Triassic/LAZ	*Thrinaxodon liorhinus*	South Africa/Karoo Basin	SAM-PK-K10017a	41
cyno	karoo	Triassic/LAZ	*Thrinaxodon liorhinus*	South Africa/Karoo Basin	SAM-PK-K10017b	41
cyno	karoo	Triassic/LAZ	*Thrinaxodon liorhinus*	South Africa/Karoo Basin	SAM-PK-K10607	65
cyno	karoo	Triassic/LAZ	*Thrinaxodon liorhinus*	South Africa/Karoo Basin	SAM-PK-K10615	63
cyno	karoo	Triassic/LAZ	*Thrinaxodon liorhinus*	South Africa/Karoo Basin	UCMP 42865	65
cyno	karoo	Triassic/LAZ	*Thrinaxodon liorhinus*	South Africa/Karoo Basin	UCMP 42877	40
cyno	karoo	Triassic/LAZ	*Thrinaxodon liorhinus*	South Africa/Karoo Basin	UCMP 42878	42.5
cyno	karoo	Triassic/CyAZ-A	*Langbergia modisei*	South Africa/Karoo Basin	BP/1/5362	115.35
cyno	karoo	Triassic/CyAZ-A	*Langbergia modisei*	South Africa/Karoo Basin	CGP1/33	90 (Abdala 2006)
cyno	karoo	Triassic/CyAZ-A	*Langbergia modisei*	South Africa/Karoo Basin	NMQR3255	99 (Abdala 2006)
cyno	karoo	Triassic/CyAZ-A	*Langbergia modisei*	South Africa/Karoo Basin	NMQR3256	82 (Abdala 2006)
cyno	karoo	Triassic/CyAZ-B	*Cynognathus*	South Africa/Karoo	BP/1/4543	315

			crateronotus	Basin		
cyno	karoo	Triassic/CyAZ-B	*Cynognathus crateronotus*	South Africa/Karoo Basin	SAM-PK-K10497	380
cyno	karoo	Triassic/CyAZ-B	*Diademodon tetragonus*	South Africa/Karoo Basin	BP/1/2522	293
cyno	karoo	Triassic/CyAZ-B	*Diademodon tetragonus*	South Africa/Karoo Basin	BP/1/4669	179
cyno	karoo	Triassic/CyAZ-B	*Lumkuia fuzzi*	South Africa/Karoo Basin	BP/1/2669	58.58
cyno	karoo	Triassic/CyAZ-B/C	*Cynognathus crateronotus*	South Africa/Karoo Basin	BP/1/1181	308
cyno	karoo	Triassic/CyAZ-B/C	*Cynognathus crateronotus*	South Africa/Karoo Basin	BP/1/3755	265
cyno	karoo	Triassic/CyAZ-B/C	*Cynognathus crateronotus*	South Africa/Karoo Basin	SAM-PK-6235	300
cyno	karoo	Triassic/CyAZ-B/C	*Cynognathus crateronotus*	South Africa/Karoo Basin	SAM-PK-11484	330
cyno	karoo	Triassic/CyAZ-B/C	*Diademodon tetragonus*	South Africa/Karoo Basin	BP/1/2097	41.56
cyno	karoo	Triassic/CyAZ-B/C	*Diademodon tetragonus*	South Africa/Karoo Basin	BP/1/3511	52.4
cyno	karoo	Triassic/CyAZ-B/C	*Diademodon tetragonus*	South Africa/Karoo Basin	BP/1/3639	192
cyno	karoo	Triassic/CyAZ-B/C	*Diademodon tetragonus*	South Africa/Karoo Basin	BP/1/3754	265
cyno	karoo	Triassic/CyAZ-B/C	*Diademodon tetragonus*	South Africa/Karoo Basin	BP/1/3769	94.59
cyno	karoo	Triassic/CyAZ-B/C	*Diademodon tetragonus*	South Africa/Karoo Basin	BP/1/3771	94
cyno	karoo	Triassic/CyAZ-B/C	*Diademodon tetragonus*	South Africa/Karoo Basin	BP/1/3772	136.72
cyno	karoo	Triassic/CyAZ-B/C	*Diademodon tetragonus*	South Africa/Karoo Basin	BP/1/3773	118.16
cyno	karoo	Triassic/CyAZ-B/C	*Diademodon tetragonus*	South Africa/Karoo Basin	BP/1/3775	98
cyno	karoo	Triassic/CyAZ-B/C	*Diademodon tetragonus*	South Africa/Karoo Basin	SAM-PK-5716	195
cyno	karoo	Triassic/CyAZ-B/C	*Diademodon tetragonus*	South Africa/Karoo Basin	SAM-PK-K5223	190
cyno	karoo	Triassic/CyAZ-B/C	*Diademodon tetragonus*	South Africa/Karoo Basin	SAM-PK-K5266	105

cyno	karoo	Triassic/CyAZ-B/C	*Trirachodon berryi*	South Africa/Karoo Basin	AM 461	100 (Abdala et al. 2005)
cyno	karoo	Triassic/CyAZ-B/C	*Trirachodon berryi*	South Africa/Karoo Basin	BP/1/4534	44.76
cyno	karoo	Triassic/CyAZ-B/C	*Trirachodon berryi*	South Africa/Karoo Basin	BP/1/4535	46
cyno	karoo	Triassic/CyAZ-B/C	*Trirachodon berryi*	South Africa/Karoo Basin	BP/1/4658	99.26
cyno	karoo	Triassic/CyAZ-B/C	*Trirachodon berryi*	South Africa/Karoo Basin	BP/1/4661	87 (Abdala et al. 2005)
cyno	karoo	Triassic/CyAZ-B/C	*Trirachodon berryi*	South Africa/Karoo Basin	NMQR 1298	75
cyno	karoo	Triassic/CyAZ-B/C	*Trirachodon berryi*	South Africa/Karoo Basin	NMQR 1349	102 (Abdala et al. 2005)
cyno	karoo	Triassic/CyAZ-B/C	*Trirachodon berryi*	South Africa/Karoo Basin	SAM-PK-K7888	88
cyno	karoo	Triassic/CyAZ-B/C	*Trirachodon berryi*	South Africa/Karoo Basin	SAM-PK-K10761	90
cyno	karoo	Triassic/CyAZ-B/C	*Trirachodon berryi*	South Africa/Karoo Basin	SAM-PK-K10762	105
cyno	karoo	Triassic/CyAZ-C	*Cricodon* sp.	South Africa/Karoo Basin	BP/1/5540	160 (Abdala et al. 2005)
cyno	non-karoo	Permian/DAZ	*Dvinia prima*	Russia	PIN2005/2469	88
cyno	non-karoo	Triassic/LAZ	*Thrinaxodon liorhinus*	Transantarctic Mountains	SAM-PK-K10434	71
cyno	non-karoo	Triassic/CyAZ-A	*Beishanodon youngi*	China/Ordos Basin	PKUP V3007	232 (est. from Gao et al. 2010)
cyno	non-karoo	Triassic/CyAZ-B/C	*Sinognathus gracilis*	China/Ordos Basin	IVPP_V2339	121 (Abdala et al. 2005)
cyno	non-karoo	Triassic/CyAZ-B/C	*Aleodon* sp.	Namibia	GSN_EN3	156 (Abdala & Smith, 2009)
cyno	non-karoo	Triassic/CyAZ-C	*Luangwa drysdalli*	Zambia/Luangwa Basin	BP/1/3731	142
cyno	non-karoo	Ladinian	*Chiniquodon theotonicus*	Argentina	MCZ4296	50 (Abdala & Giannini 2002)
cyno	non-karoo	Ladinian	*Chiniquodon theotonicus*	Argentina	PVL4675	55 (Abdala & Giannini 2002)
cyno	non-karoo	Ladinian	*Chiniquodon theotonicus*	Argentina	PULR12	70 (Abdala & Giannini 2002)
cyno	non-	Ladinian	*Chiniquodon theotonicus*	Argentina	MCZ4100	73 (Abdala &

	karoo					Giannini 2002)
cyno	non-karoo	Ladinian	*Chiniquodon theotonicus*	Argentina	PVL4444	85 (Abdala & Giannini 2002)
cyno	non-karoo	Ladinian	*Chiniquodon theotonicus*	Argentina	PVL4674	101 (Abdala & Giannini 2002)
cyno	non-karoo	Ladinian	*Chiniquodon theotonicus*	Argentina	PULR18	110 (Abdala & Giannini 2002)
cyno	non-karoo	Ladinian	*Chiniquodon theotonicus*	Argentina	PVL4448	113 (Abdala & Giannini 2002)
cyno	non-karoo	Ladinian	*Chiniquodon theotonicus*	Argentina	PVL4167	116 (Abdala & Giannini 2002)
cyno	non-karoo	Ladinian	*Chiniquodon theotonicus*	Argentina	MCZ3779	116 (Abdala & Giannini 2002)
cyno	non-karoo	Ladinian	*Chiniquodon theotonicus*	Argentina	MCZ3777	121 (Abdala & Giannini 2002)
cyno	non-karoo	Ladinian	*Chiniquodon theotonicus*	Argentina	PULR0101	129 (Abdala & Giannini 2002)
cyno	non-karoo	Ladinian	*Chiniquodon theotonicus*	Argentina	PULR0100	134 (Abdala & Giannini 2002)
cyno	non-karoo	Ladinian	*Chiniquodon theotonicus*	Argentina	MCZ4002	137 (Abdala & Giannini 2002)
cyno	non-karoo	Ladinian	*Chiniquodon theotonicus*	Argentina	PULR0102	138 (Abdala & Giannini 2002)
cyno	non-karoo	Ladinian	*Chiniquodon theotonicus*	Argentina	MCZ3776	145 (Abdala & Giannini 2002)
cyno	non-karoo	Ladinian	*Chiniquodon theotonicus*	Argentina	NHMUK R8429	145 (Abdala & Giannini 2002)
cyno	non-karoo	Ladinian	*Chiniquodon theotonicus*	Argentina	MCZ4020	200 (Abdala & Giannini 2002)
cyno	non-karoo	Ladinian	*Massetognathus pascuali*	Argentina	PULR11	204 (Abdala & Giannini 2000)
cyno	non-karoo	Ladinian	*Probainognathus jenseni*	Argentina	MCZ_4277	83 (Romer 1970; Sidor 2000)
cyno	non-karoo	Ladinian	*Chiniquodon theotonicus*	Brazil	MCZ3035	65 (Abdala & Giannini 2002)
cyno	non-karoo	Ladinian	*Chiniquodon theotonicus*	Brazil	PV0066T	105 (Abdala & Giannini 2002)
cyno	non-karoo	Ladinian	*Chiniquodon theotonicus*	Brazil	PV0066Tg	130 (Abdala & Giannini 2002)
cyno	non-karoo	Ladinian	*Chiniquodon theotonicus*	Brazil	GPIT1050	145 (Abdala & Giannini 2002)

cyno	non-karoo	Ladinian	*Chiniquodon theotonicus*	Brazil	MCZ3615	150 (Abdala & Giannini 2002)
cyno	non-karoo	Ladinian	*Chiniquodon theotonicus*	Brazil	MCZ3614	152 (Abdala & Giannini 2002)
cyno	non-karoo	Ladinian	*Chiniquodon theotonicus*	Brazil	MCP_PV1600	164 (Abdala & Giannini 2002)
cyno	non-karoo	Ladinian	*Chiniquodon theotonicus*	Brazil	MCZ1533	224 (Abdala & Giannini 2002)
cyno	non-karoo	Ladinian	*Chiniquodon theotonicus*	Brazil	PV0274	255 (Abdala & Giannini 2002)
cyno	non-karoo	Ladinian	*Chiniquodon theotonicus*	Brazil	GPIT40	260 (Abdala & Giannini 2002)
cyno	non-karoo	Ladinian	*Chiniquodon theotonicus*	Brazil	PV0122T	310 (Abdala & Giannini 2002)
cyno	non-karoo	Ladinian	*Exaeretodon riograndensis*	Brazil	MCP3843PV	170 (Abdala & al. 2002)
cyno	non-karoo	Ladinian	*Exaeretodon riograndensis*	Brazil	MCP1522PV	223 (Abdala & al. 2002)
cyno	non-karoo	Ladinian	*Exaeretodon riograndensis*	Brazil	MCP2361PV	263 (Abdala & al. 2002)
cyno	non-karoo	Ladinian	*Protuberum cabralensis*	Brazil	MGB_368-100	200 (Reichel & al. 2009)
cyno	non-karoo	Ladinian	*Therioherpeton cargnini*	Brazil	MVP05.22.04	33 (Oliveira 2006)
cyno	non-karoo	Ladinian	*Dadadon isaloi*	Madagascar	FMNH_PR2232	143 (Kammerer et al. 2011)
cyno	non-karoo	Triassic/Carnian	*Chiniquodon sanjuanensis*	Argentina	PVSJ411	80 (Abdala & Giannini 2002)
cyno	non-karoo	Triassic/Carnian	*Ecteninion lunensis*	Argentina	PVSJ422	98 (Martinez et al.)
cyno	non-karoo	Triassic/Carnian	*Exaeretodon frenguellii*	Argentina	MCZ4486	400 (Abdala & al. 2002)
cyno	non-karoo	Triassic/Carnian	*Trucidocynodon riograndensis*	Brazil	UFRGS_PV1051-T	187 (Oliveira et al. 2010)
cyno	non-karoo	Triassic/Norian	*Chaliminia musteloides*	Argentina	PVL3257	48 (Martinelli et al., 2007)
cyno	non-karoo	Triassic/Norian	*Brasilitherium riograndensis*	Brazil	UFRGS_PV0929T	27 (Bonaparte et al. 2005)
cyno	non-karoo	Triassic/Norian	*Brasilodon quadrangularis*	Brazil	UFRGS_PV0628T	26 (Bonaparte et al. 2003)

cyno	non-karoo	Triassic/Norian	*Riograndia guaibensis*	Brazil	MCN-PV2264; UFRGS_PV0569T	35 (Bonaparte et al. 2001; Soares et al. 2011)
cyno	non-karoo	Triassic/Rhaetic	*Morganucodon watsoni*	Wales		26 (est, Kermack et al. 1981)
cyno	non-karoo	Triassic/Rhaetic	*Sinoconodon rigneyi*	China	IVPP_4727; IVPP_8683; IVPP_8692	37 (Patterson & Olson 1961; Crompton & Sun 1985)

Abbreviations: CiAZ, *Cistecephalus* Assemblage Zone; cyno, Cynodontia; CyAZ, *Cynognathus* Assemblage Zone; DAZ, *Dicynodon* Assemblage Zone; EoAZ, *Eodicynodon* Assemblage Zone; LAZ, *Lystrosaurus* Assemblage Zone; PAZ, *Pristerognathus* Assemblage Zone; TaAZ, *Tapinocephalus* Assemblage Zone; thero, Therocephalia; TrAZ, *Tropidostoma* Assemblage Zone.

Vita

Adam Keith Huttenlocker was born in Wailuku, Hawai'i and grew up in California, Washington, and Hawai'i. In 2005, he earned a Bachelor of Arts from University of Colorado at Boulder with a major in Evolutionary, Population and Organismic Biology and a minor in Geology. In 2008, he earned a Master of Science in Biology at California State University, San Bernardino, under supervision of Dr. Stuart S. Sumida. In 2013, he earned a Doctor of Philosophy in Biology from the Department of Biology at the University of Washington, Seattle, under supervision of Dr. Christian Sidor.